ADVANCED WIND ENERGY CONVERTERS USING ELECTRONIC POWER CONVERSION

ZHE CHEN

School of Engineering

University of Durham

A thesis submitted in partial fulfilment of the requirements of the Council of the University of Durham for the Degree of Doctor of Philosophy (PhD)

1997

Advanced Wind Energy Converters Using Electronic Power Conversion

ZHE CHEN

PhD 1997

Abstract

This thesis details the research work on developing the variable speed direct drive wind power generation system. Attention is focused mainly on interfacing the modular permanent magnet generator into the power network to capture optimal power, provide controllable reactive power and minimise the network harmonic pollution using efficient and economical power electronic converters.

The AC/DC/AC type of power electronic conversion system is adopted. Alternative configurations of poly phase PM generator -rectifier system are addressed. A high quality DC link is achieved by the proposed poly-phase generator and rectifier system. The diode rectifier provides cheap and reliable AC/DC power conversion. A power enhancement technique is proposed and investigated to overcome the output power limit of the generator-rectifier system so as to match the generator-rectifier power characteristics to the wind power characteristics and to enable the maximum power to be captured from the wind.

The power control, the network performance and economics of the power electronic conversion system are mainly dependent on the grid inverters. Various DC/AC power conversion systems are discussed and control strategies are proposed to control real power and reactive power. The steady state performances of inverters in a power network have been studied. The harmonic performance, an important issue of grid connection, is discussed. Several harmonic reduction methods are presented and their performance are studied.

Three typical inverter systems are chosen for detailed investigation by analysis, simulation and experimental implementation. Main attention is focused on the optimal power control, reactive power regulation, harmonic minimisation, cost and power losses of the semiconductors. Based on these studies, an appropriate DC/AC conversion system is recommended.

The proposed power electronics conversion and the control systems, combined with the modular PM generator, have demonstrated a promising advance wind energy converter for the wind power industry.

This thesis is dedicated to my parents, Ruilu CHEN, Shuyi XIE and my family.

Acknowledgements

I would like to thank:

My supervisors, Prof. E. Spooner, School of Engineering, University of Durham for his invaluable advice, support and guidance.

Dr J Bialek, Dr J Bumby, Mr G Grey, Dr S Johnson, and Prof. A Purvis, School of Engineering, University of Durham for their encouragement and advice on various occasions.

Technical and Administrative staff of School of Engineering, University of Durham for their support.

My fellow researchers for making the research environment bearable.

The School of Engineering, University of Durham for providing the facilities and financial support.

The EPSRC and Energy Technology Support Unit, DTI for providing financial support.

Yanting, My wife, for her support, endurance and help on the thesis preparation, especially the drawing of some illustrations.

Cong, my son, for his support and endurance.

List of Symbols and Abbreviations

SYMBOLS /ABBREVIATIONS	DESCRIPTION
WECS	wind energy conversion system
PM	permanent magnet
B	magnetic-flux density
B_r	remanence, residual magnetic-flux density
H	magnetic-field intensity
H_c	coercive force
C_p	wind turbine efficiency coefficient
λ	ratio of blade tip speed to wind speed ($\lambda=R\omega/v$)
R	rotor radius of the wind turbine
ω	angular speed
v	wind speed
v_{in}	cut in wind speed
v_r	rated wind speed
v_{out}	cut out wind speed
EMF	electric motive force
V_d	DC voltage mean value
I_d	DC current mean value
p_n	DC voltage pulse number
i_{coil}	stator coil current
R_g	resistance of single stator coil
L_g	inductance of single stator coil
E_g	EMF generated in stator coil $E_g = \omega E_{gb}$, where E_{gb} is constant
R_{load}	load resistance
P_{load}	power delivered to the load
C_{ac}	ac capacitor connected at rectifier ac terminal
ASVC	advanced static var compensator
HVDC	high voltage direct current
SCR	silicon-controlled rectifier
GTO	gate turn-off thyristor
BJT	bipolar junction transistor
MOSFET	Metal-Oxide-Semiconductor Field Effect Transistor
IGBT	insulated gate bipolar transistor
SOA	safe operating area
MCT	MOS-controlled thyristor
CSI	current source inverter
VSI	voltage source inverter
L_s	inductance between ac grid and VSI
L_d	DC link inductance
C_d	DC link capacitance
L_c	inductance between ac grid and SCR-CSI (commutating inductance)
P	real power

Q	reactive power
δ	power angle between VSI output and grid
K_{dv}	ratio of rectifier d.c. voltage to inverter a.c output voltage
a_t	transformer ratio
α	delay angle of SCR inverter
u	overlap period (commutation or overlap angle) of SCR inverter
γ	extinction (recovery) angle of SCR inverter
ϕ_1	displacement angle
V_s	ac system voltage
VHF	voltage harmonic factor
CHF	current harmonic factor
$V_{(1)}$	voltage fundamental component
$I_{(1)}$	current fundamental component
$V_{(n)}$	voltage nth order harmonic component
$I_{(n)}$	current nth order harmonic component
V_{dis}	voltage distortion component
I_{dis}	current distortion component
TVHD	total voltage harmonic distortion
TCHD	total current harmonic distortion
PF	power factor
DPF	displacement power factor, DPF=cos ϕ_1
PWM	pulse width modulation
SPWM	sinusoidal pulse width modulation
SHE	selective harmonic elimination
f_{sw}	switching frequency
M_a	modulation ratio of SPWM
SUR	switch utilisation ratio
$t_{on,}$	on duration of DC/DC converter switch
t_{off}	off duration of DC/DC converter switch
D	DC/DC converter switch duty ratio, $D=t_{on}f_{sw}$
I_{LB}	DC/DC converter boundary current
N_k	voltage ratio of DC/DC converter
i_{CSI}	current generated by line commutated SCR inverter,
i_c	current generated by active compensator
i_s	current injected into ac system by active compensated SCR-CSI system
E_{ci}	conduction energy loss during the ith conduction period of a cycle
E_C	total conduction energy losses in one cycle
$E_{on,i}$	turn-on energy losses at ith switching
$E_{rr,i}$	reverse recovery energy losses at ith switching
$E_{off,i}$	turn-off energy losses at ith switching
E_S	total switching energy losses in one cycle

Contents

List of Figures

List of Tables

Chapter

1. Introduction

The development of renewable energy sources is needed urgently in view of the increasing rate of depletion of fossil fuels and their associated pollution. Wind energy, the most competitive renewable energy source [71], has been developed rapidly and demonstrated to be a viable energy technology.

The cost-competitiveness of wind energy is being improved as wind power technology advances. "The future of wind-electric conversion is tied to advances in electromechanical energy conversion devices and power electronics technologies, in addition to advances in aeroturbine designs and controls" [71]. Low speed, direct drive generators, eliminating gearboxes, variable speed and power electronics grid interface are expected to be important features of the next generation wind energy conversion systems which will be built with power ratings of one megawatt and beyond.

Direct drive, eliminating the gear box and its power transfer limit can increase the system efficiency and reduce the system cost, weight and acoustic noise.

Variable speed can increase the energy capture which will expand the number of sites where electricity could be economically generated. Variable-speed operation can also alleviate mechanical stresses and reduce aerodynamic noise levels, especially in light winds. "the long-term potential for large-scale utilisation of wind energy lies with variable-speed systems integrated with power electronics subsystems to obtain utility-grade ac." [71].

In response to the wind power industry development, this thesis examines advanced wind energy converters using power electronics interface, variable-speed, direct-coupled modular PM generators.

A direct-drive wind generator requires large number of poles to operate efficiently. A low-speed, high pole-number, modular, permanent-magnet, synchronous generator has been designed to fit within a wind turbine nacelle of normal dimensions and to generate three-phase 50 Hz ac output for direct connection to the grid [82, 83]. Permanent magnet excitation avoids the field current supply or reactive power compensation facilities needed by synchronous or induction generators.

Many features of the direct-drive modular PM generator are useful for a promising variable speed generator. In addition, variable-speed operation removes the need for special synchronising equipment and for damping both of which have been found to be difficult and costly to implement. Therefore, modifying the direct-coupled, modular PM generator for variable-speed operation should provide an attractive machine for the wind energy industry. The new variable-speed generator will require an efficient power electronic interface that provides high quality power. The work reported in this thesis aims to develop an advanced wind energy converter using electronic power conversion with the modular PM generator. The main contents are as follows:

The history, development and technology of the wind energy utilisation are reviewed for providing a background for the research work.

The modular permanent-magnet generator, a promising direct drive machine, and its attractive features for variable speed wind energy conversion system are described.

AC/DC/AC power electronics conversion is identified as suitable type of system. AC/DC power conversion is addressed first. The semiconductor and circuit configurations are discussed. Various poly-phase PM generator-rectifier systems are studied.

Without excitation control, the output power of PM generator-diode rectifier system is limited so as not able to match the wind power characteristics. The power limit problem is investigated. A power enhancement technique is proposed. The significant improvement is achieved to establish the basis of optimal power capture.

With a PM generator and a diode rectifier system, power control is possible only at the grid inverter. Two type of DC/AC converters, Voltage Source Inverter (VSI) and Current Source Inverter (CSI), are discussed with attention paid to optimal power transfer and reactive power regulation. The performance of inverters in a power network are also investigated.

Harmonic pollution is an important issue with power electronics interface. The general harmonic performance of inverters are analysed. The harmonic performance of VSI and CSI following the optimal power curve are presented on the basis of the proposed control strategies. Harmonic reduction methods are discussed and their effects on the potential inverter systems are presented.

The following DC/AC converter systems are chosen for detailed investigation

- Sinusoidal pulse width modulation voltage source inverter, SPWM-VSI.
- DC/DC converter-VSI with selective harmonic elimination switching or multi-pulse circuit.
- Line commutated thyristor CSI with VSI active compensator.

Power control strategies and harmonic reduction techniques for the above converter systems are presented which allow them to deliver optimal real power captured from the wind to the grid and to produce a controllable reactive power with satisfactory harmonic performance.

The economic issues of the above inverter systems, the power losses and costs of the semiconductors, are also addressed.

Suitable systems are recommended based on the analysis of technical feasibility and economic performance.

Investigation approach

The aims of the project have been achieved by analysis, numeric computation, time domain simulation and laboratory experiment.

The numerical analysis and computation are mainly performed with high level programming language (FORTRAN) and software package MATLAB.

Time domain simulation studies are performed using circuit simulators in SPICE.

The experimental models (power converters with associated driving and control circuits) have been designed and built during the project. The controllers are developed on the basis of analogue-digital electronic circuitry and a PC/486 with C/C++ as programming languages.

Chapter

2. Wind Power Utilization Review

At present, the most widely used energy sources are finite. These include sources such as oil, natural gas, coal and nuclear with only limited storage on the earth. It is estimated that oil and natural gas may last for as little as 30-50 years, although coal and nuclear could last for several centuries at present rates of consumption [6]. Moreover, these energy source present serious environmental problems: coal requires large-scale mining operations leaving behind land that is difficult or impossible to restore to usefulness in many cases; the combustion of fossil fuel may upset the planet's heat balance; the production of carbon dioxide and sulphur dioxide may affect the atmosphere and the food production ability of the planet. Whilst waste disposal is a major difficulty of nuclear power. For these reasons, renewable energy sources, such as wind, solar, wave and tidal etc., have attracted much attention in recent years. The wind, at present the cheapest to capture of the renewable energy sources [71], is clean, inexhaustible and has been demonstrated as a viable energy source. This chapter reviews the utilisation history of wind energy, and briefly describes wind power generation technology to establish the background for the research work reported in this thesis.

2.1 Wind Electric Power Development

Humankind started to use the wind power many centuries ago. The wind has been used as almost the only source of power for ships until Watt invented the steam engine in the eighteenth century. Windmills have existed since the earliest antiquity in Persia, Iraq, Egypt and China [6]. The early machines normally had vertical axes and were used for lifting water and grinding grain.

During the Middle Ages, windmills began to appear in European countries [6]. At that time windmills were used for pumping water, sawing lumber, grinding corn and wheat, for providing mechanical power to run small factories.

In the last century, the wind has been used to generate electrical power. In the late 1860's a magneto rotated by fans was designed to produce electricity to light an incandescent bulb. In 1894, an Arctic explorer (Fridtjof Nansen) powered an electric light bulb by wind power during the search for the North Pole [6].

Major progress in wind electrical power was made in Denmark in the 1890's, the first wind tunnel in the world was built about 1895. By 1910, several hundred units with capacities of 5 to 25 kW were in operation in Denmark. The output voltage was usually 110 or 220 volts DC with batteries for storage. During World War I and World War II, Denmark relied heavily on its wind power plants for the electricity production.

About 6.5 million windmills were built between 1880 and 1930 in the United States to pump water, charge batteries, light houses, and supply the pre-transistor days' radios. Reasonably large-scale wind turbines were also constructed. A 1.2 MW machine operated in central Vermont used a turbine of 53.34m diameter, the stainless steel two bladed propeller was 3.35m wide and weighed over 15 tons! The hub height was 36.6m. The generator was a General Electric synchronous machine rated at 1250kVA at 2400V and 600rpm [6].

In the immediate post World War II years, R&D on wind-electric power was at a minimum due to the availability of cheap fossil fuel and relatively high cost of wind energy. However, the energy crisis of the 1970's led to serious attentions being paid to the development of renewable energy and interest in wind power has returned. As result, wind electric power generation has been developed rapidly in the last 20 years.

In the USA, a series of horizontal-axis wind turbines, such as MOD-0 (38 meter diameter, rated 100kW for wind speed of 6.5m/s), MOD-0A (38 meter diameter, 200kW

at 7.7m/s), MOD-1 (61 meter diameter, 2MW at 11.5m/s), MOD-2 (91 meter diameter, 2.5MW at 8.9m/s), and even higher power MOD-5A (122 meter diameter, 7.3MW), have been built during 1970's and 1980's. A number of vertical axis Darrieus wind turbines (2-bladed 17m 300kW; 3-bladed 25m 500kW; 3-bladed 50m 3MW) were also built [3].

In 1977, the UK Department of Energy funded wind energy program commenced [13]. Large horizontal axis wind turbines were developed. One of these machines has a 60m diameter with a fixed pitch, 2-bladed rotor mounted upwind of the tower. The power output is 3.7MW in a wind speed of 22m/s. A 20m diameter machine with rated output of 250kW at 17 m/s and a rotational speed of 88rpm was also developed with the intention of replacing expensive diesel electricity generation for the island systems.

Other medium and large wind turbine generators have also been built and tested in many other countries, including Sweden, Denmark, Germany, Italy, Canada, France, and Russia.

In 1992, in California, USA, there were more than 15,000 wind turbines with 1,600MW of capacity producing approximately 2.7 billion kWh of electricity every year, meeting approximately 1.2 percent of California's electrical energy needs. With the advance of the technology, the cost of the wind energy is falling, it was $.07 to $.09 per kWh in 1992 and is expected to be $.04 to $.05 per kWh by 2000 [71].

In 1993, there was 1400MW installed capacity of wind power generation in 12 EC countries. In Denmark the wind turbines produced approximately 2.4 percent of the Danish electrical energy consumption. In 1993, twenty-two wind farms were operational or are under construction in the UK. They have a total installed capacity of approximately 140MW and will generate about 360GWh in a full year (the total electrical energy consumption is about 300TWh/year), saving the emission of about 400,000 tonnes of CO_2. It is estimated that wind farms in the UK could provide about 20TWh/year by the year 2005 at a cost of about 4p/kWh (8% discount rate) [59].

Clearly, wind energy is a viable technology and a rapidly developing industry. It is moving steadily, according to scale, location and application, towards or beyond cost competitiveness with conventional sources.

2.2 Wind Energy Source

Wind results from the expansion and convection of air as solar radiation is absorbed on earth. The total solar energy reaching the earth and its atmosphere is almost 5.2×10^{24} J per year (average power 1.65×10^{11} MW). A small fraction (about 9×10^{22} J per year) is converted into air movement. On a global scale these thermal effects combine with dynamic effects from the earth's rotation, the local geographical and environmental factors to produce prevailing wind patterns. The classical estimates of the maximum extractable from the 0-100m layer by land based plant are at about 3.6×10^{18}J per year (10^{12}kWh/year).

Countries and regions with the richest wind source are mostly in coastal areas, and include UK, Eire, Iceland, Newfoundland, New Zealand, Greenland, Argentina (southern extremity) and Chile (southern extremity). A second group would include Japan, Malagasy Republic, Norway, Tasmania, and certain maritime areas of North and South America, Denmark, France, Spain and north eastern former USSR.

The UK has the largest wind resource in Europe. Some 20% of the UK land area has the annual mean wind speeds considered necessary for the economic generation of electricity. In practice, however, due to many constraints on the use of land for wind farm, such as towns, lakes, roads, railways, rivers, National Parks and the distance requirements from buildings, roads, power lines, microwave communication path and between wind turbines, the accessible wind energy from the sites on land in the UK is about 300 terrawatt hours per year (TWh/y). However, this slightly exceeds the current UK total electricity consumption [25], and is far larger than the assessed accessible potential of any other renewable energy source in the UK.

2.3 Wind Energy Conversion

2.3.1 Features of wind power

The kinetic energy (E), in an air mass (M) moving with a speed, v(m/s), can be expressed as

$$E = \frac{1}{2} M v^2 \qquad (J)$$

The mass of air intercepted by a turbine which sweeps out an area A is the product of the air density (ρ) and the air volume which is $A \times v \times t$. Therefore the kinetic energy in the air is

$$E = \frac{1}{2} (\rho A v t) v^2 \qquad (J)$$

and the wind power, W, is

$$W = \frac{1}{2} \rho A v^3 \qquad (W) \qquad (2.1)$$

The above equation indicates that the available wind power is proportional to the cube of the wind speed. But not all the available energy is extractable, the actual captured amount will be

$$W_{turbine} = \frac{1}{2} C_p \rho A v^3 \qquad (W) \qquad (2.2)$$

Where C_p, being known as the power coefficient, is dependent on the types and operations of the wind turbine. The theoretical upper limit for C_p is 59.3% and is known as the Betz limit.

The main features of wind power are:

- Its globally widespread availability;
- The relatively small land occupancy of plant (almost all of this land (98%) could still be used for agricultural purposes);
- The possibility of low environmental impact (careful attention to design can improve acceptability);

However, wind also is a very complex and variable source of energy. Wind is intermittent, with it's speeds varying with geographic location, land form, height above

sea level, season and time of day. The main characteristics of wind as an energy source are as follows:

- It is a low density fluid, so that the physical dimension of any device to convert its kinetic power to a usable form is large in relation to the power produced;
- It is random in magnitude and direction, except that at any site average wind speed and direction distribution on an annual basis is repeatable within moderate limits;
- Generally, it increases in magnitude and becomes less turbulent with height above the ground;
- It cannot be stored before conversion, i.e. it must be applied, as it occurs, to the load that can be provided at that time, or to storage in secondary form; a firm power requirement calls for an alternative source in parallel.

Wind driven plant has a different balance of costs to conventional thermal plant because the fuel cost is zero and the capital cost relatively high.

2.3.2 Wind turbines

A wind turbine is a device to convert energy from the kinetic form of wind to rotational mechanical form. Geometrically, there are two basic types of wind turbine, horizontal axis and vertical axis.

Horizontal Axis Machines where the axis of rotation is horizontal and the wind turbine plane is vertical facing the wind. A schematic diagram of a modern horizontal wind turbine-power conversion system is shown in figure 2.1, where the rotating rotor blades of the wind turbine change the wind power into the mechanical power on the shaft, then the gear box located between the wind turbine and the generator increases the rotation speed to suit the generator. The power produced by the generator is sent to the load or/and grid through the transformer located on the ground.

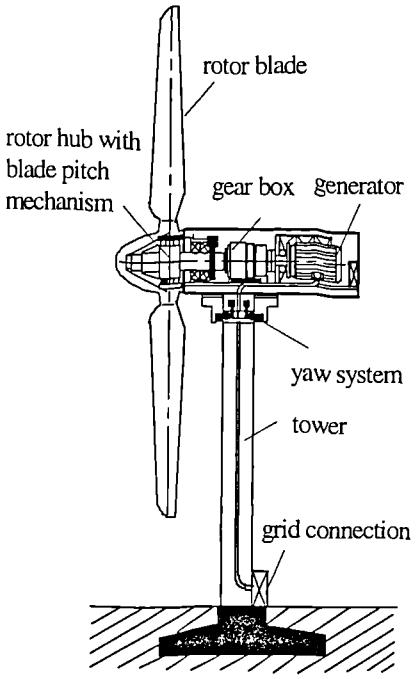

Figure 2.1 Schematic horizontal high speed wind power conversion system

Blade construction must be matched to turbine size. In smaller plant, solid blades (made of plastic, alloy or even wood) are sufficient. Larger blades necessitate materials and construction techniques having a high strength/density ratio. There are several types of wind turbine blades, e.g. sails, planes, and aerodynamic surfaces based on the aircraft wing cross section. Early windmills were based on the first two types; The modern high speed machines have propeller type blades with aerodynamic surfaces, two and three-bladed rotors are common for electricity generation. The rotor may be in front of (upwind) or behind (downwind) the tower.

Horizontal axis wind turbines can be divided into two categories: low and high speed. Low speed turbines usually rely on drag forces to extract the kinetic energy from the wind. Drag devices move slower than the wind. The American multi-blade wind turbines used for pumping water are commonplace examples of the low speed horizontal type. High speed wind turbines rely on lift forces and their speed is several times faster than that of the wind. The ratio of the power extracted by a lift device to that of a drag device is usually greater than 3:1 for the same swept area.

The wind turbine may be regulated by various methods: based on aerodynamic stall, adjusting the pitch of the blades, or turning the turbine out of the wind using the yaw drive. With stall regulation, the power increases smoothly with wind speed, until it reaches some limiting value then the blades stall. At still higher wind speeds the drag associated with fully stalled airfoil sections actually reduces the power taken by the wind turbine. The advantage of stall regulation is its simplicity and strength in the turbine and blade design and it is therefore, potentially a low cost technology. On the other hand, a variable pitch system can adjust pitch within operating range to regulate output and can feather the blades to stop the turbine. In large machines, wind and other sensors controlling pitch angle through electrical/mechanical/hydraulic systems are used. Pitch control implies substantially increased costs. However, the pitch system also performs other tasks such as preventing an excessive over speed in the case where the machine loses connection with the grid and bringing the rotor to a standstill when required. The fixed pitch, stall regulated machine does not have this facility and hence must be provided with a separate braking system.

Variation of the relative surface of the blades by changing the direction of the rotor axis with the wind, thus changing the effective area presented to the wind, could also adjust the power output of the wind turbine. The variation can be carried out by the yaw drive which is fitted to most turbines. A further method, coning , also allows the area presented to the wind to vary by mounting the blades separately on hinges so that rotation of the turbine causes the blades to sweep out a cone of adjustable angle instead of a disc.

There are several types of braking system for wind turbine, such as aerodynamic brakes, mechanical brakes, and electrical brakes. Aerodynamic brakes operate directly on the rotor so that large forces are not required to overcome the rotor torque and they can easily be made fail-safe by use of centrifugal activation. The disadvantages are that they cannot usually bring the machine to a complete standstill and so a mechanical brake of some sort is always required. Mechanical disc brakes are also widely used especially on stall-regulated wind turbines. They are commonly located on the high speed shaft to act

as the operational and/or parking brake in conjunction with airbrakes. They are more expensive than the airbrakes. Electrical dynamic brake is another alternative, where an electrical load is switched onto the generator to absorb the kinetic energy of the turbine. (for an induction generator, a capacitor is normally connected with a resistor to provide the field requirement of the generator). In this case, a parking brake is also needed.

Vertical Axis Machines: A schematic vertical axis wind power generation system (Darrieus) is shown in figure 2.2. Other typical vertical axis wind turbines are Savonius and Musgrove machines.

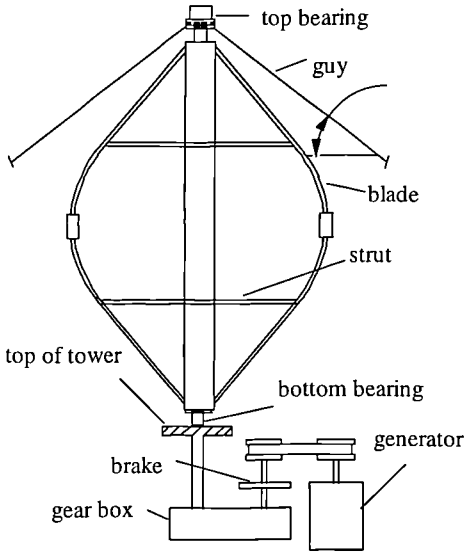

Figure 2.2 Schematic vertical axis (Darrieus) wind power conversion system

The vertical machine can accept wind from any direction and so avoids the cost of a yaw mechanism. The generator and gearing machinery might be situated at ground level for easy access, maintenance, and simplicity of the structure. The overall weight of the turbine might be less than that of horizontal systems, because of the small amount of material involved in relation to the swept area resulting in lower cost.

The Darrieus has been used for electricity generation, its rotor has two or three thin curved blades with an airfoil section and fixed geometry. No simple means of pitch variation is available. These high speed vertical axis turbines are not normally self

starting, therefore rotation must be initiated with the electrical generator used as a motor.

The Savonius rotor offers a simple and inexpensive vertical axis wind turbine. The high solidity produces high starting torque, so it is suitable for water pumping.

Musgrove straight-bladed vertical-axis wind turbines were developed in the UK. It was reported that the Musgrove machine has an efficiency fully comparable with a good modern horizontal axis wind turbine and has many advantages over the Darrieus vertical axis design. Though vertical-axis wind turbines have some attraction, the majority of commercial wind turbines are horizontal axis machines at present and the claimed cost advantages of vertical-axis design have yet to be realised.

2.3.3 Efficiency of the wind turbines

The wind turbine efficiency, the power coefficient, C_p, is sketched in figure 2.3 [6, 53], where λ is the ratio of blade tip speed to wind speed ($\lambda=R\omega/v$), R is the rotor radius of the wind turbine and ω is the angular speed.

It can be noted that power coefficients have rather large differences between various kinds of turbines. Savonius and American Multi-Blade are obviously intended for low speed operation and have relatively high starting torque. The modern two blade type and Darrieus rotor type are more suitable for high speed operation and are suitable for generating electric power. The classical Dutch blade is intermediate. The modern two blade horizontal-axis wind turbine has the highest peak power coefficient.

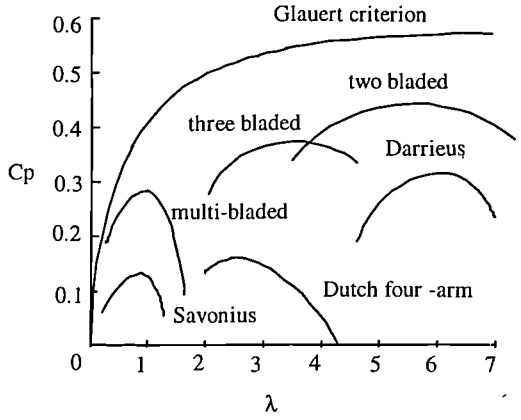

Figure 2.3 Power coefficient C_p as a function of tip speed ratio λ

2.3.4 Generator for wind turbines

Various electric machines have been used for wind power generation. DC generators (shunt type) with battery storage were used in early small systems. They have commutators and brushes required regular maintenance. Synchronous or asynchronous ac generators are now universally employed, with inexpensive diode rectifiers used to convert the ac power into dc if needed.

synchronous generator

A further advantage of a synchronous generator compared with a DC generator is its higher efficiency. When directly connected to the grid, the synchronous machine requires synchronising equipment. The damping of oscillations in power angle is especially important owing to the constant presence of wind gusts.

With controllable excitation current, a synchronous generator can carry out automatic voltage regulation and maintain high power factor operation, but it requires field control equipment and hence is more expensive than an induction generator.

Permanent Magnet (PM) generators do not require field excitation control facilities, however the generated internal voltage is proportional to the machine speed, and so the power factor is not controllable by the machine itself.

Induction machine

The squirrel cage induction generator is generally simpler, cheaper and more reliable than the synchronous generator. Its stator may be similar to that of a PM generator. An induction generator is likely to be cheaper than a PM generator by perhaps a factor of 2 [53]. However, the grid-connected induction generator draws reactive magnetising current from the utility and would normally require reactive power compensation equipment. Starting means (e.g. soft start) are also often required to avoid heavy inrush currents. The cage induction generator can also be operated as an isolated ac generator by supplying the necessary exciting current from capacitors or var compensators connected at its terminals.

The slip-ring, wound-rotor induction machine has a similar structure to a synchronous generator therefore is more expensive than a cage induction machine. It is attracting some attention for variable speed operation by means of slip power recovery equipment in the rotor circuit.

2.3.5 Energy captured by wind power conversion system

A normal wind turbine power curve (power transfer curve) is shown in figure 2.4 (a) with respect to the wind speed. Below the cut in speed (v_{in}), the wind turbine is incapable of meeting fixed losses and so is not operated. As wind speed increases beyond v_{in}, electrical power output rises rapidly. When the wind reaches the speed (v_r), the generator output reaches the rated value. For wind speeds beyond the rated speed, turbine controls act to limit the output power to a constant value either by mechanical control (turbine pitch angle control and/or stall regulation) or by electrical reaction torque control. Thus the power curve is flat up to wind speed v_{out} where the turbine blades are furled, rotation stops, and the power output drops to zero. It is necessary to furl the machine at very high wind speed to avoid potential irreversible structural damage.

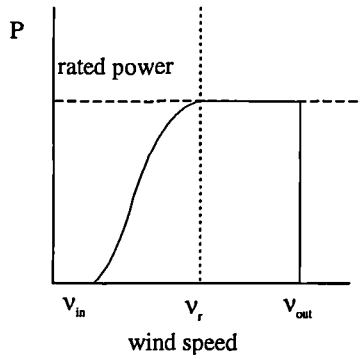

(a) Machine power transfer curve

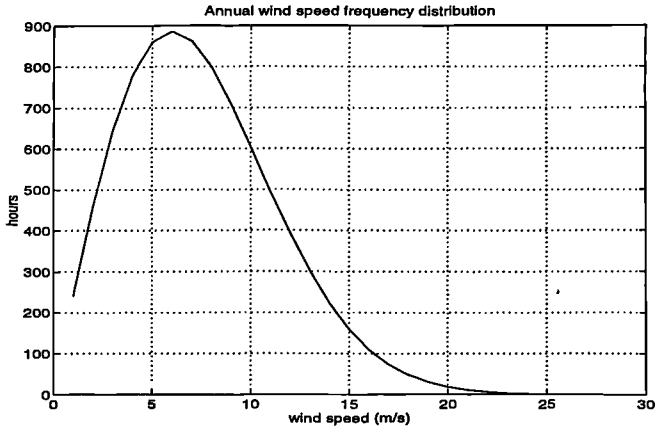

(b)Annual wind speed frequency distribution

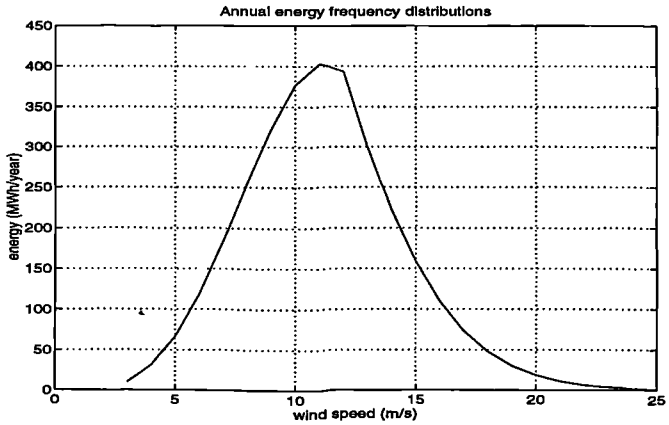

(c) Annual energy frequency distribution

Figure 2.4 Wind power curves

A wind speed frequency distribution curve is shown in figure 2.4 (b). The annual captured energy distribution figure 2.4 (c) of a wind energy conversion system (WECS) can be found by using the power transfer curve in figure 2.4 (a) and the wind speed frequency distribution curve. The annual captured mechanical energy is the summation

of the energy on the annual captured energy frequency distribution curve. It is clear from the above procedure that the annual electrical energy output from a WECS generator is strongly dependent on site wind statistics, machine design, and the control strategy of the wind turbine.

2.4 Wind Electric Power Systems

Although some wind power has been used for pumping water and heating, most modern wind turbines are used for electricity generation. A wind electric conversion system may be connected to a large electrical network or it may operate in an autonomous system; it can operate at constant speed or variable speed. Some typical system configurations and their features are briefed in this section. Due to the limited application of DC generators, only the synchronous and induction generator systems are discussed.

2.4.1 Autonomous operation

These systems could be stand alone DC systems or ac systems. The dc is normally used for small systems such as power supply for communication repeaters, navigational beacons, weather stations and similar self-contained unmanned installations in remote locations. The basic systems are shown in figure 2.5, where the synchronous generator (alternator or PM generator) or capacitor self-excited cage induction generator can be used. The rectified generator output may be in parallel with a storage battery to supply the load. The dc voltage can be controlled to keep a constant value, either by the excitation control (alternator case) or by means of controllable rectifier (PM generator or induction generator cases).

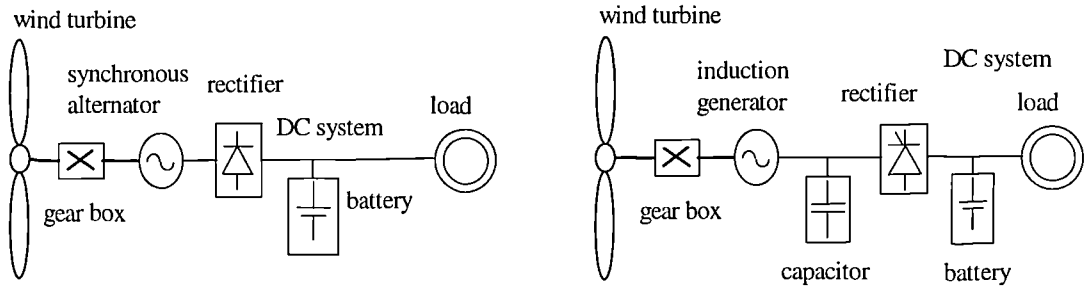

(a) (b)

Figure 2.5 Stand alone DC systems

(a) synchronous alternator dc system (b) induction generator dc system

An ac supply at constant voltage and frequency may be required for loads located remotely from power network, e.g. rural enterprises, island systems etc. In order to keep a constant voltage and frequency, a battery and inverter back up is often used. Other power sources (solar, diesel etc.) can also be used in parallel in such systems. Such a system is shown in figure 2.6.

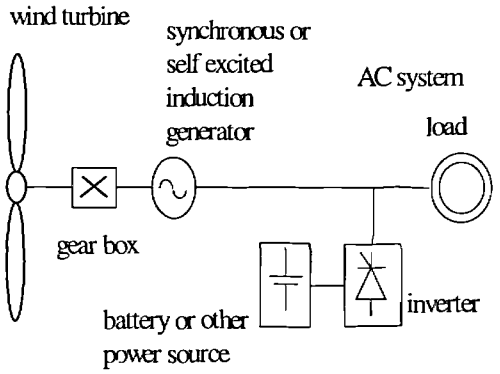

Figure 2.6 Stand alone AC system

2.4.2 Network connection operation

For fully utilising the capacity of the WECS, most medium and large wind generators are connected to relatively large power networks. There are basically two types of wind power conversion systems: constant speed system and variable speed system. The majority of turbines currently installed operate at constant speed.

2.4.2.1 Constant speed operation

In this case, the generator produces power at the grid frequency while the wind turbine and generator maintain constant speed. This arrangement is shown in figure 2.7 and has the great merit of extreme simplicity. The system consists of a field excited or permanent magnet synchronous generator, or a squirrel cage induction generator, connected to the power network. The turbine control system need to regulates the power captured from the wind and if a field-excited synchronous generator is used, excitation control regulates reactive power.

Squirrel cage induction generators, are lighter, more robust and cheaper than equivalent synchronous generators. Because of the load increasing with slip, induction generators intrinsically provide damping. Also an induction machine may be motored up to speed. For these reasons, induction generators are more widely used as modern wind power generators. However, they do have a reactive power requirement , typically 75% of the kW rating, and a charge is usually levied for reactive power drawn. Reactive power compensation equipment is thus normally installed.

Synchronous generators have field excitation systems which enable reactive power to be regulated. The transient currents on paralleling (connecting to grid) are small, although the auto synchronising equipment is required. Since the generator is normally solidly coupled through a gearbox to the wind turbine, the wind turbine and generator act as an undamped mass-spring system, and some damping equipment is required to deal with the power oscillations.

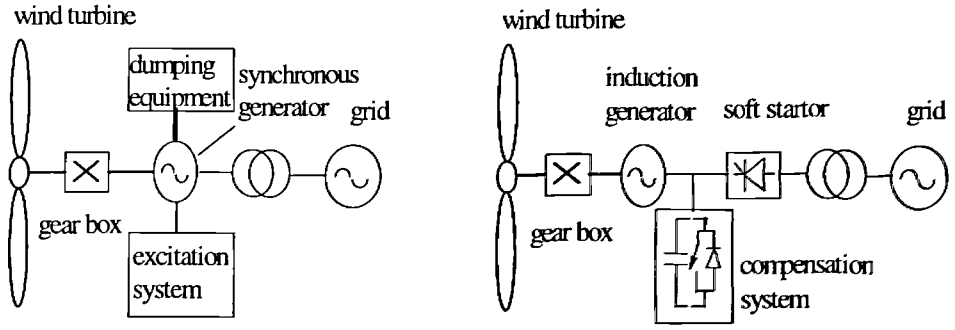

Figure 2.7 Constant speed AC system connection

(a) synchronous generator constant speed grid connection operation

(b) induction generator constant speed grid connection operation

2.4.2.2 Variable Speed operation

Due to its greater power capture and its ability to absorb loads caused by sudden wind speed changes without undue mechanical stresses, the variable speed system is becoming more and more popular. Various variable-speed wind power generator systems are being studied. The features of variable speed systems and some typical configurations are briefly presented in this section.

An important advantage of a broad of range variable speed operation is the increased energy capture. From the wind turbine characteristics (figure 2.3), it can be seen that operation at the maximum performance coefficient C_p (max.) requires the turbine speed to be proportional to the wind speed. The general torque-wind speed characteristics of a wind turbine are illustrated in figure 2.8. It can be seen that optimal power capture is achieved with variable-speed operation by tracking the wind speed and maintaining the optimal C_p value, where the wind speed is used as parameter.

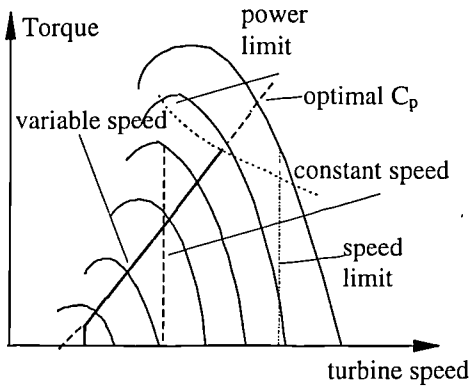

Figure 2.8 Wind turbine characteristics for variable and constant operation

The wind turbine may be pitch controlled or a fixed pitch variable speed machine may be regulated by controlling the reaction torque of the generator to induce stall. One typical strategy is to keep the optimal tip speed ratio by adjusting the rotor speed for maximum energy capture below rated wind speed. Above rated wind speed the rotor speed is adjusted to maintain power generation at the rated value. As the wind speed reaches cut off speed, the rotor speed is decreased to induce stall. In variable speed operation, the cut-in speed of the turbine can also be reduced to increase the energy capture, as mechanical losses are smaller at lower rotational speed.

The ability to operate at reduced rotational speed in low wind speeds has the advantage of reduced noise which is important because there is less wind noise to mask the turbine noise.

With continuously variable speed, power fluctuations are reduced, since part of the power variation in the wind is taken up by acceleration and deceleration of the rotor, which can act as a flywheel and store short term variations as the kinetic energy changes. This is especially important for connection to a weak grid. In gear box coupling case, the torque fluctuations passed on to the gearbox are correspondingly reduced, which may allow the gearbox cost to be reduced.

The disadvantage of variable speed operation is that this scheme usually involves power electronic frequency conversion equipment which cause power losses and makes the system more expensive than a constant speed system. These costs partly offset the benefit of increased energy capture. However, constant-speed system often use slipping devices such as high-slip induction generators or fluid couplings to provide compliance, and these also have substantial losses which are eliminated in variable speed system.

Some variable systems

Synchronous generator system

field controlled alternator

This scheme can use a plain diode bridge rectifier to converter the variable frequency machine power to DC at unity displacement power factor as shown in figure 2.9. The scheme has the merit that several generators with their associated diode bridges may feed into one inverter and that any unit may be taken out of service merely by reducing its excitation, so terminating current flow through the diode bridge. The DC link voltage can be regulated by field control. If power is needed to start the turbine, a rectifier able operate as an inverter is required at the generator terminal.

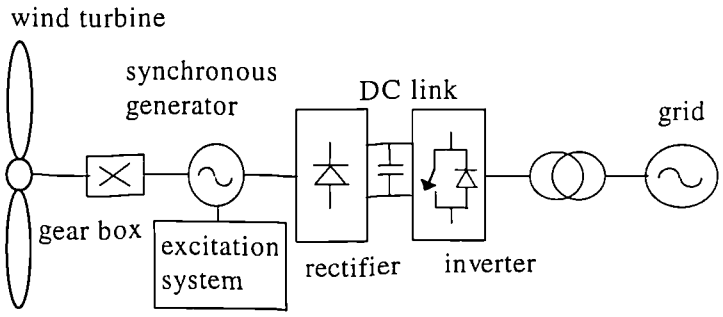

Figure 2.9 Variable speed AC alternator grid connection system

Permanent Magnet (PM) generator

A PM machine has fixed field excitation, which does not require a power supply, but the output voltage magnitude, and therefore the dc link voltage vary with the turbine speed. A significant feature of the PM machine is that it is suitable for the development of a direct drive system without a gear box as will be further described in the following chapter.

Induction machine system

The cage induction generator requires a source of reactive power for magnetising which can be done by a self commutated rectifier at the generator side of the dc link. Figure 2.10 shows such a system, similar pulse-width-modulation (PWM) inverters, employing modern high-speed switching devices such as insulated-gate bipolar transistors (IGBTs), can be used for both generator and grid converter. Inverters of this type can be designed to provide a good sinusoidal current waveform which is necessary for quiet operation of the generator and for eliminating harmonic pollution to the network. However, this type of power electronic system is quite expensive and power losses are significant.

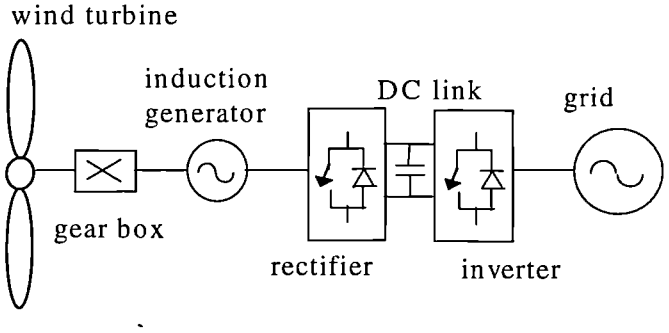

Figure 2.10 Variable speed grid connection cage induction generator system

Self-excited induction machine system:

The reactive power required by a induction machine may be about 70% of the rated power, consequently, resulting in a highly rated machine-side power electronics converter. This reactive power can be provided by capacitors or a static var compensator connected at the generator terminals. One such scheme is shown in figure 2.11. The desired level of magnetisation is maintained by the reactive power compensation

equipment. In this case a diode rectifier may be used as the machine rectifier if no power needs to be transferred to machine side.

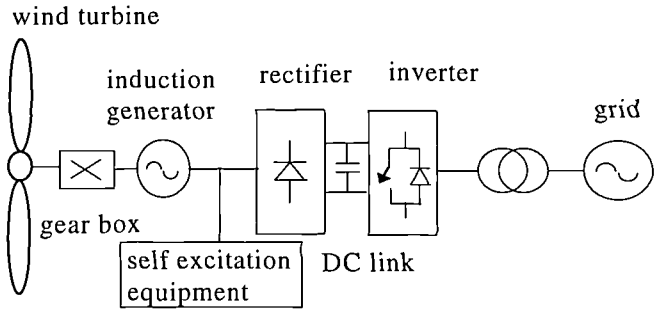

Figure 2.11 Variable speed self excited induction generator grid connection system

double output induction machine

A slip-ring, wound-rotor induction generator can also be used for variable speed operation, it is possible to connect either the stator or the rotor winding (usually the stator) directly to the grid. The other winding then gives variable frequency AC which can be converted in to grid frequency through a frequency converter. A schematic variable-speed, grid-connected, double-output, induction generator wind power conversion system is shown in figure 2.12. The frequency converter, either an AC/DC/AC converter, or a cycloconverter, could be controlled to regulate the speed of the induction generator for optimal operation. The frequency converter handles only a fraction of the total power and the allowable speed range is restricted in the same proportion, it may also be used for reactive power compensation which requires the converters to be correspondingly rated.

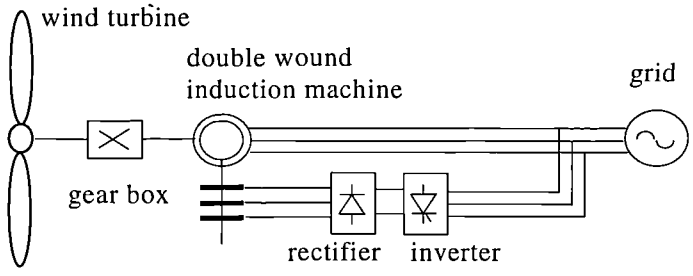

Figure 2.12 Variable speed double output induction generator grid connection system

The regulation and reactive power performance of the system is dependent on the frequency converter. A simple diode rectifier and line commutated inverter system is

capable of extracting energy from the rotor slip-rings and returning it to the supply system.

If a force-commutated inverter is used at the rotor slip-rings terminal, then power may be either extracted from or injected into the rotor slip-rings. By controlling the injected current in relation to rotor position, the induction machine can be made to behave as a synchronous machine where the power factor is controllable.

The disadvantage of the scheme is the requirement for brushes which increases the system cost and gives rise to the requirement for supervision or some kind of monitoring as well as regular planned maintenance, starting means are required to ensure that standstill rotor voltage is not impressed on the solid state equipment at starting and inrush currents and torque are restricted.

2.5 Discussions

This chapter has briefly described the history of wind power utilisation, the basic principles of wind energy conversion and present and developing technology.

Most systems discussed above include a gear box. The economic optimum turbine size has increased continuously and is expected to reach the MW level soon with turbine diameters exceeding 50m. Larger diameters are accompanied by lower rotational speeds and hence the shaft torque increases faster than the power and the gearbox, which increases the speed for driving the generator, now limits development. Furthermore, the gearbox incurs penalties of cost, loss, weight and acoustic noise emission. The latter, particularly if tonal components exist, is a sensitive planning issue restricting deployment of turbines. In addition to variable speed system, another important development which may assist the future of wind electrical power is direct-drive. (eliminating the gear box). A promising direct-drive modular PM generator has been designed and will be described in the next chapter.

Chapter

3.

Permanent Magnet Generator and AC/DC Converter

3.1 Introduction

The power electronics interface is the key component in variable speed wind energy conversion system. Its specification is subjected to the requirements related not only to the wind turbine generator but also to the power system, especially where wind power consists of a significant part of the total system capacity. In addition to frequency conversion, an ideal power electronics interface should be able to:

- optimise the wind power conversion and transmission,
- control reactive power,
- minimise harmonic distortion,
- have good economic performance (cost, efficiency).

There are boardly two types of the power electronics frequency converter systems: cycloconversion system and AC/DC/AC (rectifier-DC link-inverter) system. The cycloconversion system is a one stage frequency changer with direct conversion of ac input power at one frequency to output power at a different frequency by normally synthesising a low-frequency wave from appropriate sections of the input waveform. A cycloconverter can be considered to be composed by two converters connected back to back as shown in figure 3.1 where the semiconductors could be divided into two groups, P and N which are conducted for positive and negative waveform respectively.

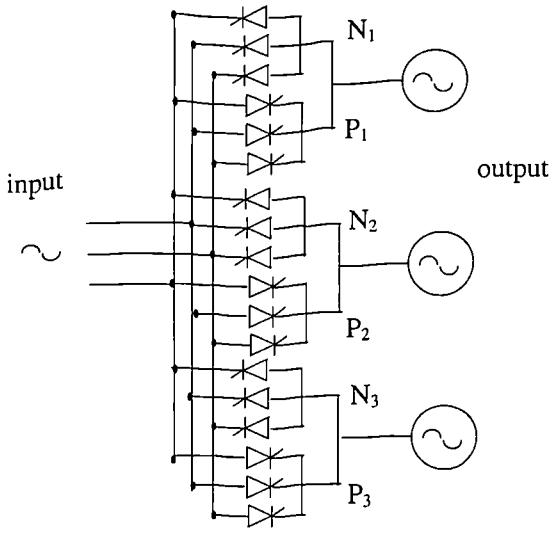

Figure 3.1 Three phase input - three phase output cycloconverter

In this system, each input phase needs at least a pair of devices to connect to each output phase. Therefore, for a 3 phase output system, the minimum number of required devices is 2×3×m, where m is the number of the input phases. For multiple phase input system, the large number of the devices will be required.

Phase angle delay (thyristor cases) could be used to control the output voltage and to synthesise a waveform close to the sinewave. In order to avoid the short circuit, the P group and N group devices of the same input phase should not conduct at the same time (blocked group operation) or the inter group reactor is required to limit the current and carried the current ripple (circulating current mode). The thyristor cycloconverter are commutated naturally, therefore the reactive power needs to be supplied. The harmonic pattern is complex. In practice, the output frequency is limited to about 1/2 -1/3 of the input frequency, the higher pulse number configuration is possible, which can improve the harmonic performance therefore permit the higher frequency limit. The PWM version of cycloconverters constructed by the self-commutated semiconductor could synthesise variable sinusoidal voltage at variable frequency and could control the power factor to generate leading or lagging reactive power.

The required multiple devices and relative complex control make the cycloconverter system a more lossy and uneconomic choice, especially, when a multi-phase input is considered. On the other hand, in the AC/DC/AC conversion system, the variable frequency power is firstly converted into DC power by rectifier and then converted into grid frequency ac power by the inverter. The frequency de-couple by the DC link provides the flexibility of power control and harmonic minimisation. Therefore, this project will focus on developing an AC/DC/AC power conversion system.

The generator with AC/DC power conversion is the first stage of the electrical power system. Desired features include: high efficiency, high reliability, low weight and low cost. This chapter discusses the modular PM generator and the poly-phase modular rectifier system. The different polyphase generator-rectifier configurations are analysed and simulated. Based on the obtained system characteristics, a simple equivalent circuit model is presented which can be used for steady state analysis and control of the power electronics energy conversion system.

3.2 Permanent Magnet Generator

In order to eliminate the heavy and noisy gearbox, direct-drive generators need a large number of poles to operate efficiently. Permanent-Magnet excitation is necessary to construct such a machine with a reasonable diameter. This section introduces the permanent magnet material and PM machines. Particularly, the novel modular PM generator [81,82,83], a promising generator for the next generation of wind power conversion systems, is discussed.

3.2.1 Permanent magnet material and PM electric machine

Permanent magnet materials

On the basis of the magnetisation characteristics, all materials fall into two main categories:

1. Non-magnetic material such as dielectric and metals with permeability equal to μ_0;
2. Magnetic material known as ferromagnetic material.

The magnetisation characteristic is a plot of magnetic-flux density (B) versus the magnetic-field intensity (H) or the B-H curve. The magnetisation characteristics for the first group of materials are straight lines because of their constant permeability. However, the permeability of ferromagnetic materials are much higher and are non-linear. The typical magnetisation characteristic of a ferromagnetic material is shown in figure 3.2. Varying a externally applied field H changes the flux density B which follows the hysteresis loop along the direction shown by arrows. When H is reduced to zero, a residual flux density, B_r exists known as remanence. To reduce the flux density in the magnetic material to zero, the applied field has to be reversed. The value of H that brings B to zero is called the coercive force H_c. The shape of the hysteresis loop depends on the type of magnetic material. On the basis of the hysteresis loop, magnetic materials can be further classified as hard or soft. Hard magnetic materials exhibit high remanence and large coercive force. These materials are capable of maintaining a magnetic field without any excitation mmf provided to it and therefore can be used for permanent magnets.

The demagnetisation characteristic, the magnetic behaviour of a material in the second quadrant of the hysteresis loop, defines the working region of a permanent magnet and is used to aid the design of the magnetic circuit for proper utilisation of a permanent magnet. In addition, the B×H or energy product curve is also often used. The typical demagnetisation and the energy-product curves are plotted in figure 3.3. The optimum use of magnetic material can be achieved by operating the magnet at its maximum energy-product point, which is shown by the horizontal line in figure 3.3.

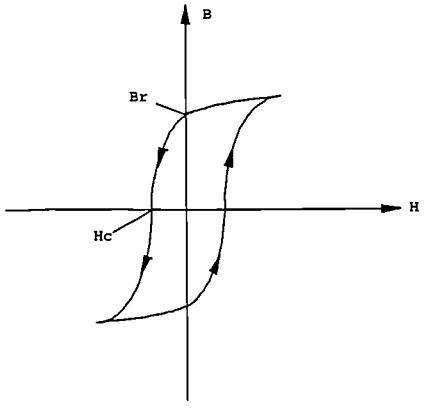

Figure 3.2 Magnetisation characteristic of ferromagnetic material

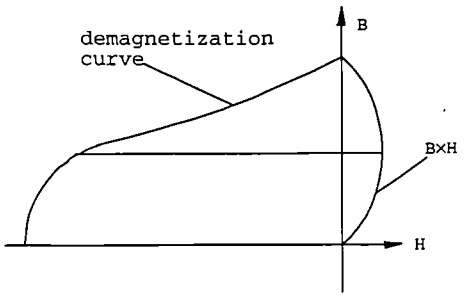

Figure 3.3 Demagnetisation characteristics and B×H or energy product curve

Many magnet materials are deliberately given a high degree of anisotropy during manufacture. Each crystal has a magnetically favourable axis and the crystals are aligned so that these axes are parallel. Devices are designed to take advantage of the superior magnetic characteristic in this direction. For such anisotropic materials, the characteristic, which is of particular reluctance to the designer, is the one relating to the preferred magnetic axis, and most published data refers implicitly to the preferred axis. Isotropic and anisotropic versions of the same material are often available at similar cost. For electrical machinery, the anisotropic version would normally be used.

Table 3.1 Magnet Properties [78]

	Alnico 5-7	Ceramic	Sm2Co17	NdFeB
B_r (T)	1.35	0.405	1.06	1.12
$\mu_0 H_c$ (T)	0.074	0.37	0.94	1.06
$(BH)_{max}$ (MGOe)	7.5	3.84	26.0	30.0
μ_{rec}	1.9	1.1	1.03	1.1
Specific gravity	7.31	4.8	8.2	7.4
Resistivity ρ (μΩ-cm)	47	>10	86	150
Thermal expansion (10^{-6} / °C)	11.3	13	9	3.4
Temperature coefficient (%/ °C)	-0.02	-0.2	-0.025	-0.1
Saturation H (kOe)	3.5	14.0	>40	>30

A family of alloys called alnico, aluminium-nickel-cobalt in various proportions with 50-60% iron, has been used for permanent magnets since the 1930s and has a high remanence. Ferrites (ceramic) materials have been used since the 1950s. These materials are mixtures of iron with other metallic oxides and have very high coercive force but relatively low remanence. Since 1960, a new class of permanent magnets known as rare-earth permanent magnets has been developed. These materials are compounds of transition elements (iron, nikel, cobalt) with rare-earth elements, important examples are Sm2Co17, SmCo5, Nd2Fe14B. Rare-earth, permanent-magnet materials have remenence similar to the Alnico materials but have much higher coercivity and energy product. Several production routes are available leading to magnets with alternative physical properties. The highest remanence and coercivity are achieved by sintering powdered material but such magnets are extremely brittle and susceptible to corrosion. Polymer bonded magnets are cheaper, easier to form to desired shape and immune to corrosion but are magnetically inferior.

The typical properties of magnets are given in Table 3.1. Obviously, the electrical machine designer has a wide choice. The high remanence of alnico type materials with greater coercivity than the ferrite. The latest addition is neodymium-iron-boron (NdFeB). The high remanence and coercivity of NdFeB have enabled designers to achieve much higher power/weight ratios for small electrical machines than were previously possible with Ferrites. However, it is considerably more expensive. For lowest cost, anisotropic sintered ferrite magnets are still the universal choice. This class of magnet materials has been steadily improved and is now available with remanence approximately 0.4T and almost straight demagnetisation characteristic throughout the second quadrant [78].

PM electrical machine

Permanent magnets can provide loss free excitation for DC and synchronous electric machines to replace electromagnetic excitation and are used in all brushless dc machines and most small dc machines. Brushless DC machines can be regarded either as d.c. machines with static commutators, or synchronous machines with a variable frequency

supply automatically governed by the shaft speed, sensed in each case by a shaft-position detector. The general arrangement looks like a three phase a.c. machine supplied through an inverter. Permanent magnets are used to replace a field winding to eliminate the electromagnetic excitation. Many permanent-magnet d.c. machines are brushless, sometimes with the power electronics incorporated in the machine itself and with mounting and external connections similar to commutator machines.

The behaviour of permanent-magnet d.c. machines is similar to the separately-excited case with constant excitation. For many years, permanent magnets have been used for small d.c. motors, e.g. toys, motor vehicle auxiliary drives, robot actuators, office and computer equipment, offering simplicity and low cost. Larger machines have not used permanent magnet excitation since at large scales, field winding are able to create stronger field and so create machines of greater power /weight ratio. In large machines, the cost of permanent magnet material, perceived assembly problem, and the possibility of demagnetisation have been the barrier. However, eliminating excitation control field coils, brushes and the excitation power loss is significant benefit, particularly for large multipole synchronous machines.

Continued advances in the development of new materials have increased the usage of permanent-magnet machines considerably. Magnets can now be smaller, lighter, readily moulded into desired shapes and can retain their magnetism under much more severe conditions. Consequently, several novel arrangements have been devised; such as "torus PM generator" [80] and "multistaked PM generator" [9] etc.

Due to the requirement for a multi-pole, reasonable size machine for direct coupling to wind turbines, PM electric generators have been developed quickly in the wind energy industry. In the US, a 20 kW PM generator has been tested and a 300 kW PM generator has been designed [39]. It now appears that the next stage in the evolution of wind energy technology will be the electronically commutated variable-speed, permanent-magnet generator.

A novel direct-drive, grid-connected modular PM generator has been presented by Spooner etc. [81, 82, 83] which has many features for the new generation of the wind generator and will be introduced in the following section.

3.2.2 Modular PM generator[81, 82, 83]

3.2.2.1 General design considerations of wind energy conversion generator

In order to match the wind speed and normal electric frequency, the generator needs a large number of poles, typical 150 which results in a big rotor diameter unless the pole pitch is made small. However, the overall diameter of the generator cannot be too large in relation to the diameter of the turbine for reasons of aesthetic appearance and obstruction of the airflow. If the pole pitch is 150 mm, the lowest value found in normal field synchronous or induction machines, the rotor diameter of a 150 poles would be more than 6 m which is unacceptable.

An acceptable ratio of diameters between wind generator and turbine would be 0.05 to 0.07. Wind turbines operate typically with tip speeds of about 60 m/s. The peripheral speed of the rotor would therefore be about 4 m/s and the pole pitch about 40 mm for 50 Hz operation. Designs limited to 60 m/s turbine tip speed and having a pole pitch of 40 mm have convenient length and diameter combined with excellent efficiency over the range of nominal wind speed 8 to 18 m/s. Only permanent magnet excitation can make such small pole pitch.

The rotor diameter will lie in the range 1 to 3 m for most applications i.e. turbines of 20 to 60 m diameter with ratings from 100 kW to several MWs. Because of the effects of slotting and the finite permeability of iron, the effective magnetic airgap will be somewhat greater than the physical clearance between rotor and stator. A 2mm physical clearance is considered the minimum in practical machines of this size. Only permanent magnet excitation can provide the necessary high magnetic flux density in such a wide airgap where the pole pitch is so small.

Ferrite magnets are preferred for the PM generator, since a lower material cost design could be achieved by using ferrite magnets in rather larger quantity and a more complex arrangement.

3.2.2.2 Modular construction

The large pole numbers involved lead to designs having large diameter and very thin back iron. The stator diameter exceeds the maximum available width of electrical steel sheet and so a modular alternative arrangement using a common lamination shape for all applications is adopted.

Modular stator core

The high pole numbers of the proposed machines make a modular approach feasible. One consequence of the high pole number is that the flux paths within the core are localised. It is permissible therefore to divide the core into a very large number of separate units without disturbing the flux distribution greatly. If the divisions between segments occur frequently, then each segment can present a flat surface to the stator bore and each segment may be a simple E shape as shown in figure 3.4.

Modular stator winding

A single-layer modular stator winding can be formed by a number of coils each occupying two adjacent slots. The coils can be wound on pre-formed bobbins and be fitted into an E-core lamination pack prior to assembly of the machine.

The interconnection of the coils to form a 3 phase output can be determined by the emf phasor diagram shown in figure 3.5. All coils with emf phasors in the band 0-60^{o} and 180^{o}-240^{o} being connected in series to form say phase A.

Modular rotor

The most economical form for ferrite magnets is the 25×100×150 mm block which can conveniently be used in pairs as the basis for a module 300 mm long and spanning

between the centres of two adjacent poles as illustrated in figure 3.4. The rotor should be subdivided axially into sections which correspond with the stator modules.

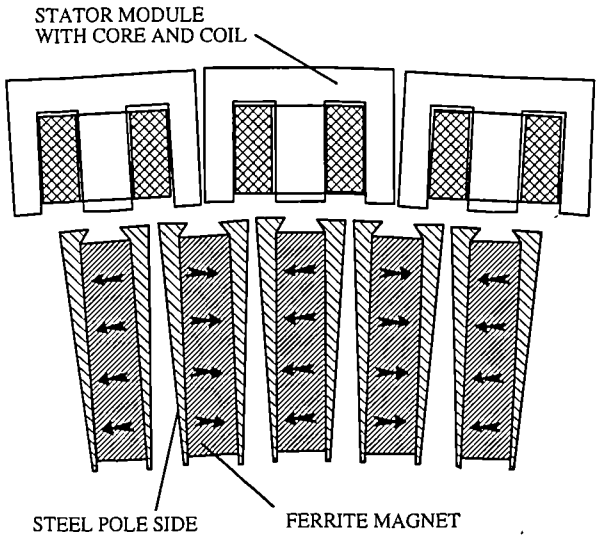

Figure 3.4 Modular stator and rotor arrangement

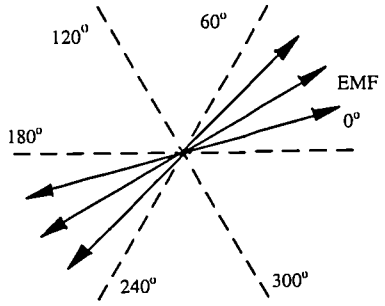

Figure 3.5 Coil EMF phase diagram

Modular structure

The outline arrangement is shown in figure 3.6. The stator core and coil modules are mounted on hollow steel beams which are fixed longitudinally between two stator end discs. Hollow beams are needed to resist the radial, tangential and torsion loads created by the magnetic forces between rotor and stator. The hollow beams can also be used as duck for cooling air. The rotor modules should be constructed on a jig to maintain a consistent geometrical relationship between the mounting holes and the pole faces and then are to be assembled into rings. The rings can be accurately pre-drilled to ensure that

when the magnet modules are attached, they present a smooth cylindrical outer surface. The rings of rotor magnets are then attached to discs of steel plate which are clamped to the shaft. This arrangement is considered suitable for machines in the power range up to about 1 MW where machine lengths are less than about 2m.

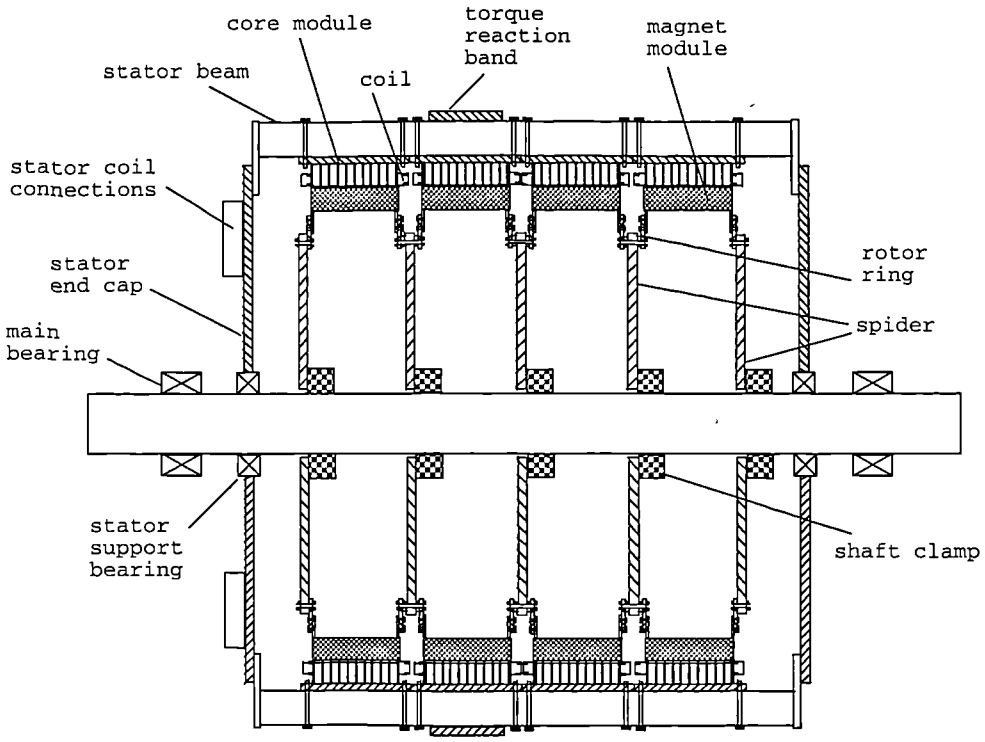

Figure 3.6 Modular structure outline arrangement

3.2.3 **Features of modular PM generator**

Large numbers of stator modules with identical laminations can be produced under ideal conditions for later assembly on all generator designs. Therefore, modular arrangement has the potential for high-speed automated manufacture of subassemblies. The machines of any pole number and any power rating can be constructed from a common set of module designs.

Notable features of the modular PM generator with respect to development towards MW scale machines include:

- Light weight,

- Simple structural parts using plate or beams,
- Use of standard magnet blocks,
- Use of simple stator laminations,
- Common rotor and stator modules for all specifications,
- Ease of assembly of magnetised rotor with stator,
- Simple cooling.

3.3 Polyphase Modular PM Generator and AC/DC Conversion

For variable speed operation, the outputs of a poly-phase generator are ideal to generate a smooth DC link waveform. Therefore each coil can be used as a single phase winding and the modular PM generator with q stator coils will produce q alternating EMFs of different phase. The phase difference between adjacent coils is $p \times 2\pi/q$ where p is the number of pole pairs. p and q can be chosen to ensure that the coil outputs are all of different phase or occur in a large number of phase groups. Provided that p and q do not share many common factors, then a suitable polyphase output is obtained. Each coil must generate an emf similar to the dc link voltage and will require many turns of thin wire. This is an inexpensive form of coil. By contrast, in the three-phase case, the coils need to be connected in series groups so that each coil generates a fairly small voltage and carries a high current. Then the coil must have a small number of turns of thick conductor. The connecting cables are therefore rather thick, cumbersome, heavy and expensive.

Rectifier circuits are power converters which perform ac to dc power conversion. A rectifier circuit could be constructed by various type of semiconductors. Diodes or thyristors are often used in normal rectifier circuit and self commutated semiconductors are normally used in PWM switching rectifiers.

Diodes are relatively cheap components and simple to use, though diode rectifiers possess no means of varying the ratio of the input ac voltage to the output dc voltage and is non-reversible, i.e. power can only flow from the ac side to dc side.

Thyristors have a means of varying the output dc voltage with respect to the input ac voltage (reduction of a ratio) and thyristor rectifiers are also reversible, i.e. they can be operated as inverters. But they are more expensive than diodes and more complex to use since control circuits are involved. They operate in reactive power consumption mode.

Self-commutated semiconductors, such as IGBT and MOSFET, can be used to construct a converter which could work as both rectifier and inverter. They can provide a controllable voltage (reduction of a ratio) and can present a unity power factor to the ac side. High frequency switching techniques can be implemented to minimise harmonic distortion. However, this type of rectifier needs more semiconductor component (anti-parallel diodes) and control circuits and presents higher power losses, therefore this type of circuit tends to be relatively complex and expensive.

In the proposed variable speed wind energy conversion system, it is not necessary to reverse the power flow direction in the main power circuit, the poly-phase connection could provide a smooth dc link voltage and harmonic distortion at dc link rectifier side is not a serious problem. Then power inversion and harmonic minimisation functions are no needed. Therefore the diodes are chosen to construct the rectifier circuit. Hereafter, in this thesis "rectifiers" is implies diode rectifiers.

3.3.1 Polyphase rectifier circuit configuration

The stator coils of the modular generator could be connected in different ways to achieve appropriate characteristics. For example, series connection for high voltage, parallel for high current. However, in order to obtain a smooth DC link voltage, a high phase number is preferred. Therefore the q phase configuration is assumed for a modular generator with q stator coils.

In order to rectify q phase alternating voltages V_1, V_2,..., V_q, one or more groups of q rectifiers should be used. Although the half way rectifier circuit (figure 3.7) needs fewer

diodes, the circuit presents lower power output than bridge rectifier circuits because each coil conducts for only alternate half cycle. Therefore only bridge rectifier configurations are considered and the following stator coil rectifier circuits are investigated in this chapter.

- single phase bridge rectifier-single stator coil connection
- bridge rectifier-star stator coil connection
- bridge rectifier-mesh stator coil connection

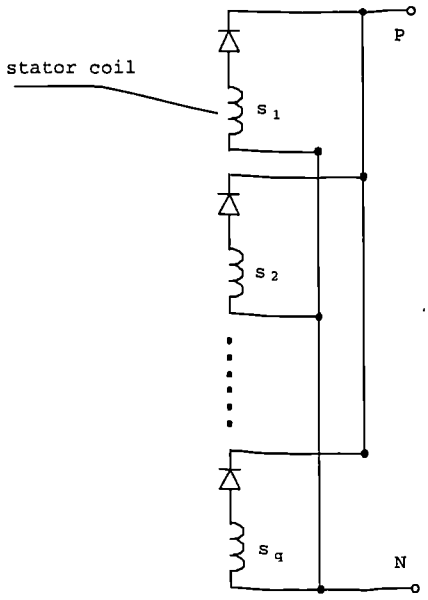

Figure 3.7 Half-way arrangement of AC/DC power conversion

In this section these rectifier circuits are presented and their performance is discussed briefly for ideal conditions where the impedance is ignored. Detailed simulation studies are presented in the following section.

The operating characteristics of a rectifier system depend on the characteristics of the source supplying it and the load connected to it. In order to characterise poly-phase PM generator-rectifier systems, following assumptions are made:

- The EMFs generated in q stator coils are sinusoidal, balanced and uniformly distributed on the phasor diagram (spaced $360^{\circ}/q$ electrical degree apart),
- A pure resistive load is connected to the DC link,

- All stator coils have identical impedance and any mutual inductance between stator coils is ignored.

The following terms and symbols are used:

V_d, rectified DC voltage mean value.

I_d, rectified DC current mean value.

p_n, DC voltage pulse number, when diode rectifier is used to produce rectified voltage from sine wave ac voltage sources, the DC voltage is formed by a number of sine wave crests per cycle T. This number is called the pulse number of the rectifier. The larger the pulse number, the lower the ripple harmonic content of the rectified voltage.

$V_{diode,max}$ and $I_{diode,RMS}$ *voltage across the diode and diode current,* These values specify the rating of the semiconductor and are related to the cost of the rectifiers.

I_{gs}, stator coil current, is the RMS value of the stator coil current and specifies the rating of the winding and the operating point of the PM generator.

Circuit 1 - single phase rectifier-single stator coil connection (modular)

The AC/DC power conversion could be completed by a modular electrical arrangement in which each stator coil of the modular PM generator is connected with a single phase bridge rectifier, the output of these single phase rectifiers are parallel connected to form a DC link. The schematic diagram of the system is shown in figure 3.8.

In this arrangement, 4q diodes are required. In the idealised case, a single phase bridge rectifier conducts when the absolute value of the EMF in the connected stator coil is the highest among the q EMFs and the rectified voltage V_d obtained between P and N is equal, at each instant, to the largest voltage among the q input voltages. The maximum voltage across the diode terminals is the peak value of EMF.

If q is odd, only one single phase bridge rectifier conducts at a time, each diode conducts for a period of $\frac{T}{2q}$ in a cycle whose total period is T. The DC current is carried by only

one coil at a time. If q is even then two bridge rectifier will conduct simultaneously. Each single phase bridge rectifier conducts twice in a cycle and each diode conducts for a period T/q.

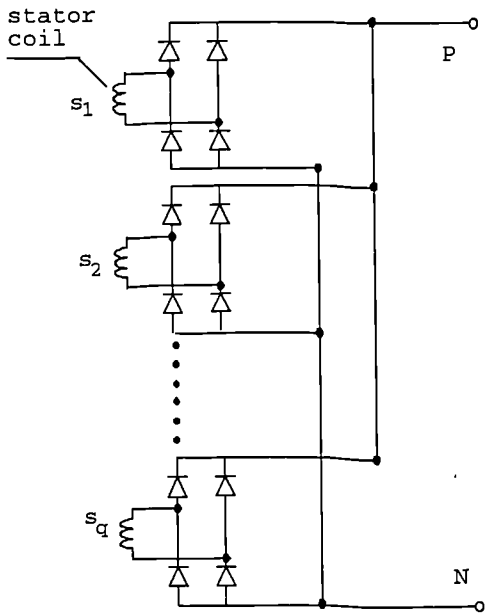

Figure 3.8 Modular electrical arrangement of AC/DC power conversion

Circuit 2 - multiple phase bridge rectifier-star stator coil connection

Figure 3.9 shows the circuit configuration, the q stator windings providing the q alternating voltages are connected in star, and 2q diodes are used for rectification.

The upper group diodes of bridge legs forms a 'most positive' commutating group and connected to DC link positive terminal P. The bottom group diodes forms a 'most negative' commutating group and connected to DC link negative terminal N.

The rectified voltage V_d obtained between P and N is equal, at each instant, to the largest difference between the input voltages. Therefore the D.C. link voltage and the maximum voltage across the terminals of each diode are higher than for the single-phase bridge configuration.

The relationship between the pulse number p_n and the phases q differs depending on whether q is even or odd. If q is even, the commutations of the upper- diode group coincide with those of the bottom group, the rectified voltage is made up of q sinusoidal crests per cycle T. If q is odd, diode groups commutate alternately and the rectified voltage has 2q sinusoidal crests per cycle.

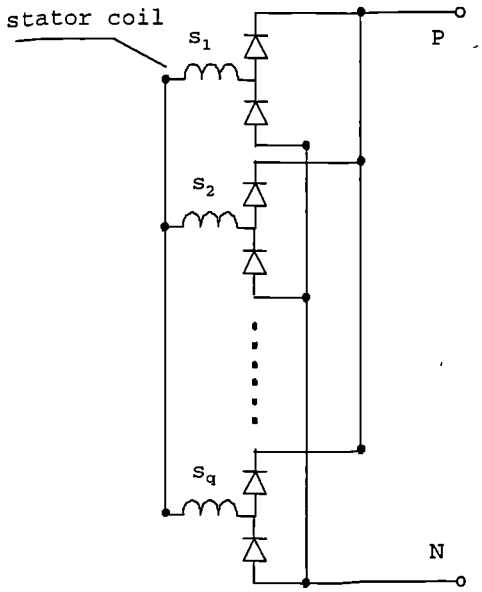

Figure 3.9 Star connection of AC/DC power conversion

Each diode has a conduction period of *T/q* during each cycle *T*. DC current is carried by two stator coils at any instant.

Circuit 3 - multiple phase bridge rectifier-mesh stator coil connection

Figure 3.10 gives the general circuit configuration of a poly-phase bridge rectifier supplied from a mesh-connected stator coils. There are q stator windings and 2q diodes. The only difference between the diagram and figure 3.9 is that the stator coils are mesh connected instead of star connected.

The rectified voltage V_d obtained between P and N is equal, at each instant, to the voltage difference between the most positive vertex of the polygon and the most negative. This type of rectifier does not operate by comparison but by addition: the

rectified voltage is at each instant equal to the sum of the positive voltages which is equal to the sum of the negative voltage.

The operation of the mesh connection is the same as star connection if the voltages at their input terminals 1,2,..., q were in the form of line-to-neutral voltages rather than being supplied as line-to-line voltages.

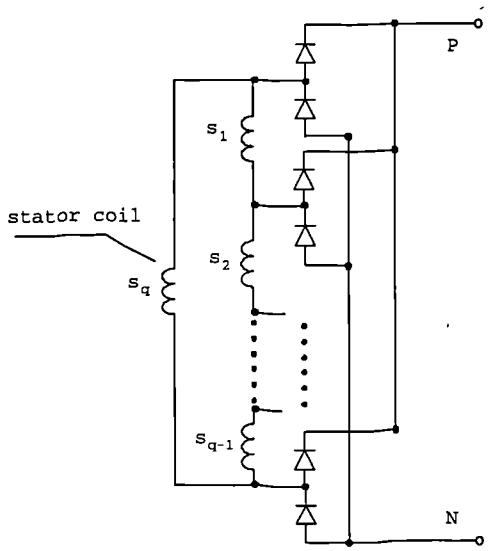

Figure 3.10 Mesh connection of AC/DC power conversion

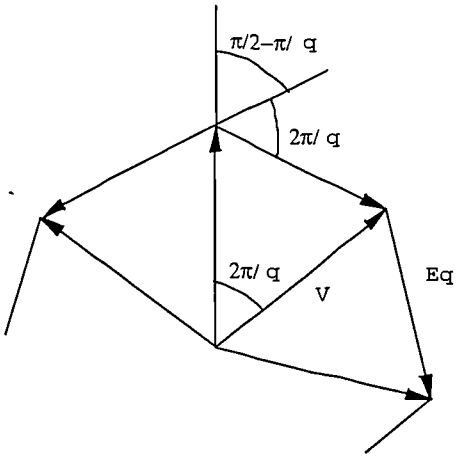

Figure 3.11 Phasor diagram of Mesh Connection

The equivalent line-to-neutral voltages V_1, V_2,..., V_q of the mesh connection are shown in the vector diagram of figure 3.11. These equivalent voltages allow the analysis in the star case be used, provided that a suitable value is taken for the individual voltages,

i.e. E_g is replaced by the RMS value of the line-to-neutral voltages V and the relation between E_g and V is

$$V = \frac{E_g}{2\sin(\pi / q)}$$

From the above expression, for a q > 6, V > E_g. Therefore the mesh connection will have a higher output voltage than star connection when q is high. For a given q, the pulse number is same as star connection. Each diode in this connection has the same conduction period as the star connection. DC current I_d leaves the polygon via the most positive vertex, returning via the most negative vertex. Within the polygon, it is divided between the two paths joining these two vertices. The first path includes all the stator coils in which the voltage is positive, the second includes all the stator coils in which the voltage is negative. I_d is shared between the two paths.

3.3.2 Comparison of different circuit configurations

A simple comparison of different circuit configurations has been made in the Table 3.2. where q is the phase number (>6).

Table 3.2 Comparison of different circuit configurations

	number of diodes	V_d and $V_{diode,max}$	p_n
modular even	4q	low	q
modular odd	4q	low	2q
star even	2q	medium	q
star odd	2q	medium	2q
mesh even	2q	high	q
mesh odd	2q	high	2q

From Table 3.2, it can be seen that for a given q all three circuits have the same pulse number and the same harmonic performance is expected. But an odd value of q leads to higher pulse number than a similar even q. Star and Mesh circuits use the same number of diodes which is half of that required by the Modular circuit. To deliver the same

amount of d.c. power, it appears that the modular circuit has the highest dc link current and lowest dc link voltage, on the other hand the mesh connection has the lowest dc link current and highest d.c. voltage.

However, the effects of the internal impedance of the stator coil have not been included in this section. The impedance could affect the behaviour of all these circuit configurations therefore will be studied in the following section.

3.4 Simulation Study of Polyphase Modular PM Generator Rectifier System

The dc link voltage is proportional to the induced EMF less the voltage drop across the stator coil impedance and rectifier. As the wind speed and the generator speed increase, the reactance also increases in proportion to the speed and the voltage drop on the stator coil increases rapidly with speed to compensate for the increasing EMF.

The DC link voltage will be lower than the ideal case discussed in the above section and therefore more diodes than that in the ideal case may be in the conduction state at the same time. This could make the circuit analysis very complicated. Therefore time domain simulation rather than analytical method is adopted to investigate the performance of the poly-phase modular PM generator rectifier system. The circuit simulator HSPICE is used.

3.4.1 Simulation circuit model

The equivalent circuit diagram of one stator coil unit is shown in figure 3.12 where R_g and L_g are the resistance and inductance of the single stator coil respectively. E_g is the EMF generated in the stator coil and a sinusoidal waveform is assumed.

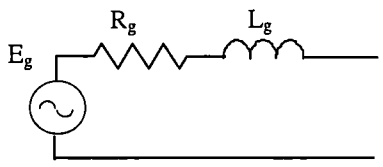

Figure 3.12 Circuit model of one stator coil

As the analysis in the above section shows that odd phase number has better harmonic performance, a 15 coil system is chosen for study. The simulation circuit models are shown in figure 3.13, figure 3.14 and figure 3.15 respectively.

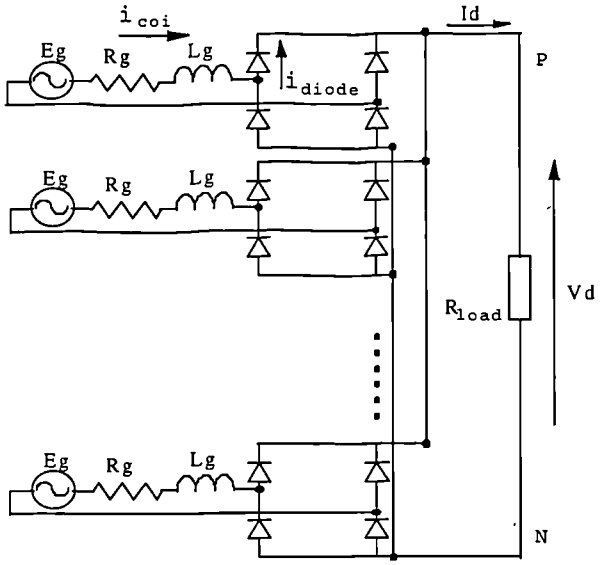

Figure 3.13 Modular connection simulation model

The following parameters are used which are the same as for the test rig:

E_g(rms)=25.2 V at 50 Hz; R_g = 0.7 Ω; L_g =10.28mH,

and the mutual inductance between the stator coils is ignored. The simulation results are presented in the following sections.

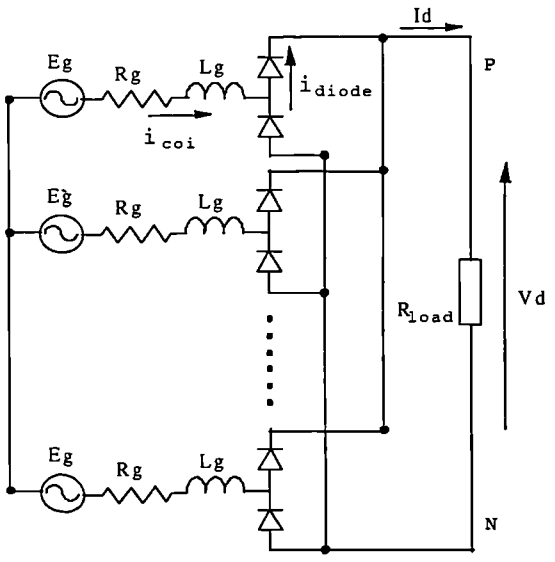

Figure 3.14 Star connection simulation model

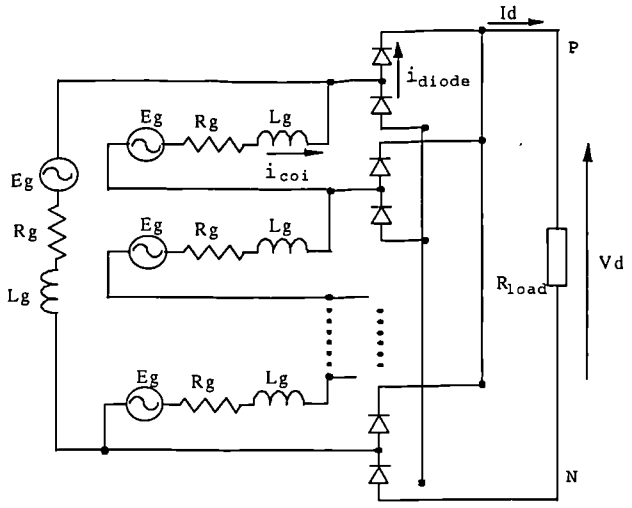

Figure 3.15 Mesh connection simulation model

3.4.2 Waveforms and characteristics of polyphase generator-rectifier system

The different operating conditions are studied by varying the frequency and magnitude (which is proportional to the frequency) of EMF and varying the load resistance. The waveforms of generator-rectifier systems are shown in figure 3.16, 3.17 and 3.18, and are proceed downward in the following sequence:

V_d dc link voltage,

E_g stator coil EMF,

I_d dc link current,

i_{coil} stator coil current,

i_{diode} diode current.

The coil current harmonic spectra are shown in figure 3.19, 3.20 and 3.21, for the frequency of 40Hz, dc power output 370W. Figure 3.22, 3.23 and 3.24 show the following six system characteristics in the sequence of 60 Hz, 50 Hz, 40 Hz, 30 Hz, 20 Hz proceed downward.

(a) d.c. voltage (V) - load resistance (Ω)

(b) d.c. power (W) - load resistance (Ω)

(c) d.c. power (W) - d.c. voltage (V)

(d) d.c. current (A) - d.c. voltage (V)

(e) stator coil current RMS value (A) - d.c. voltage (V)

(f) diode current RMS value (A) - d.c. voltage (V)

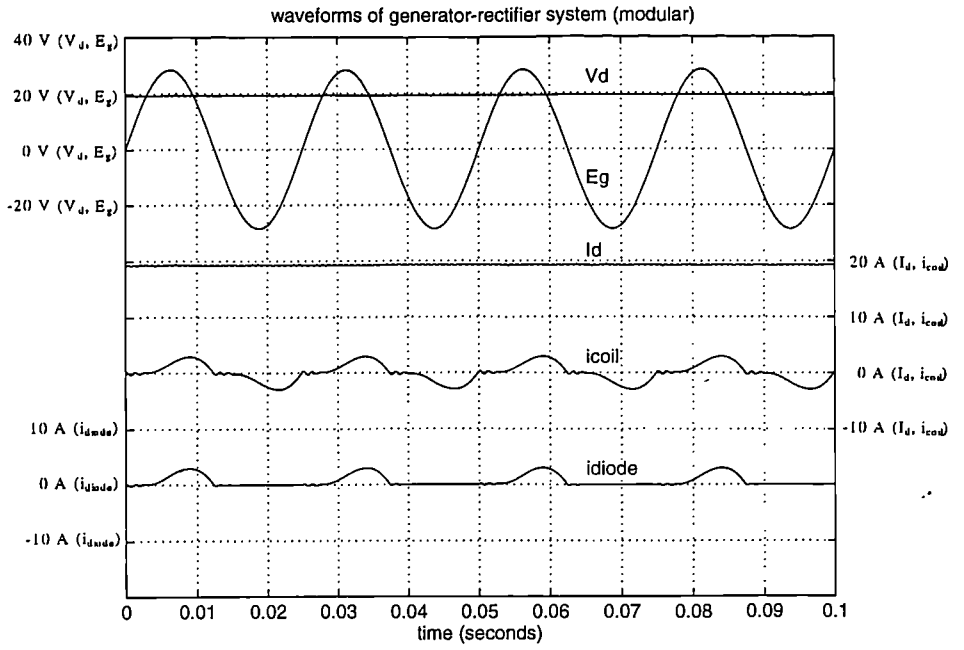

Figure 3.16 Poly-phase generator-rectifier system waveforms (modular)

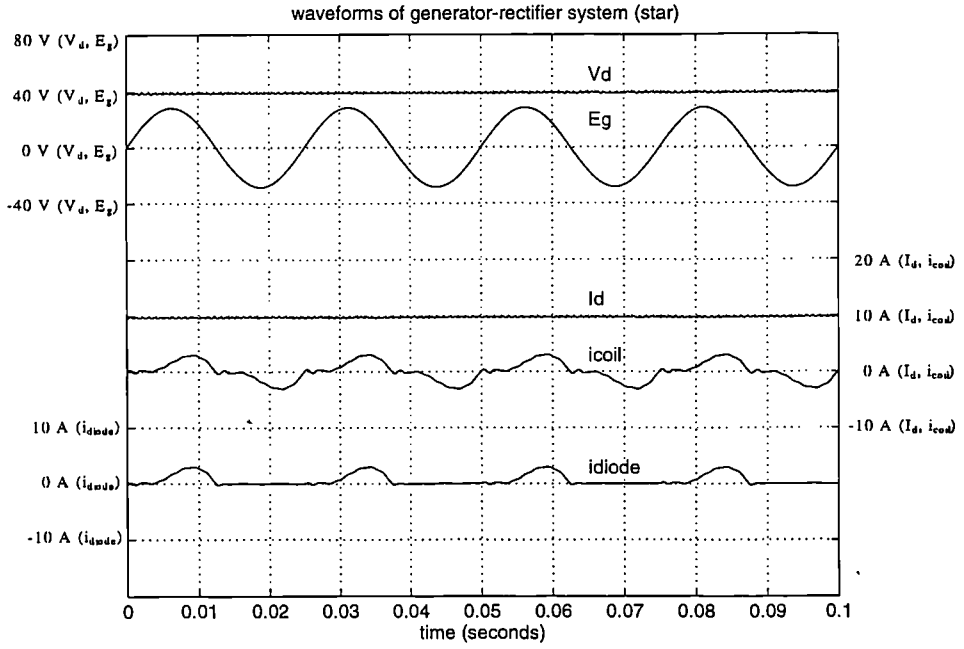

Figure 3.17 Poly-phase generator-rectifier system waveforms (star)

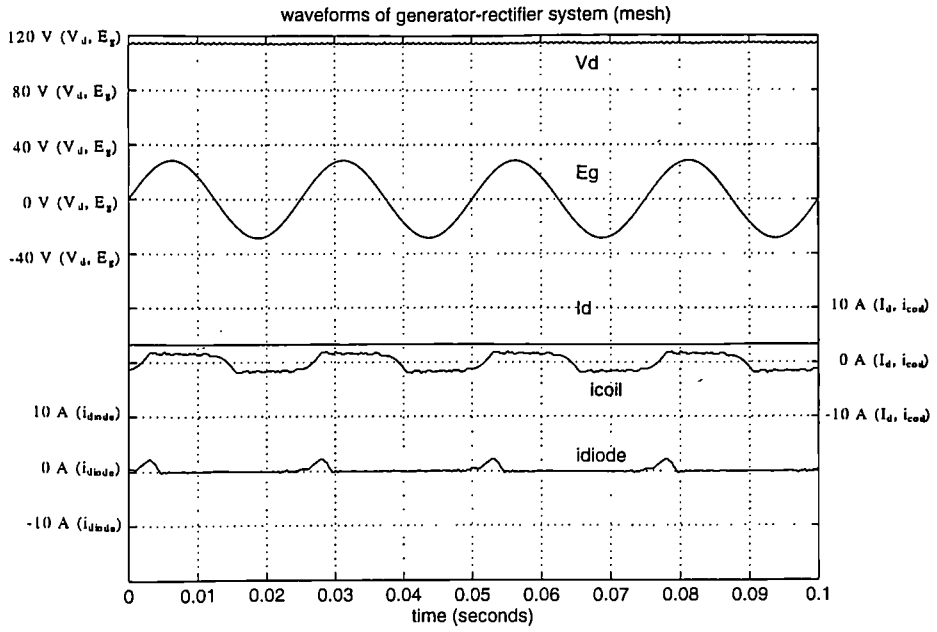

Figure 3.18 Poly-phase generator-rectifier system waveforms (mesh)

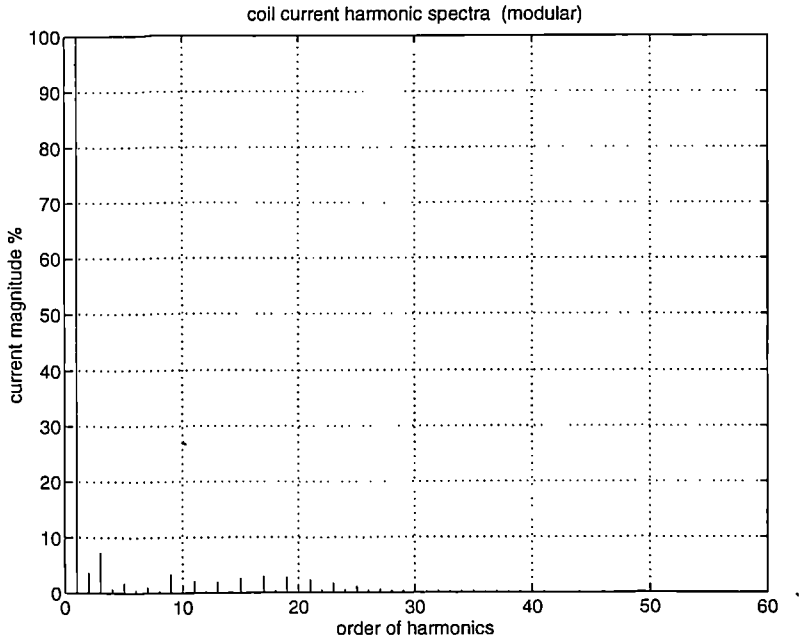

Figure 3.19 Stator coil current harmonic spectra (modular)

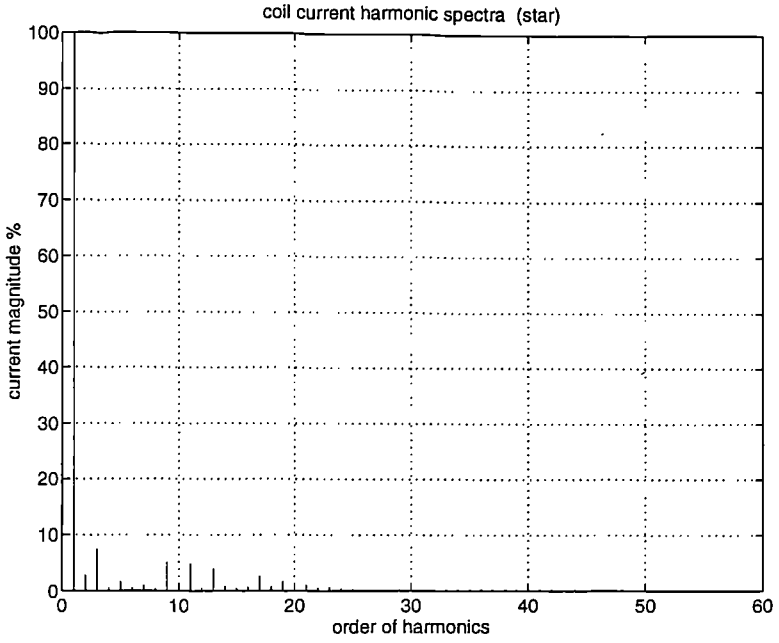

Figure 3.20 Stator coil current harmonic spectra (star)

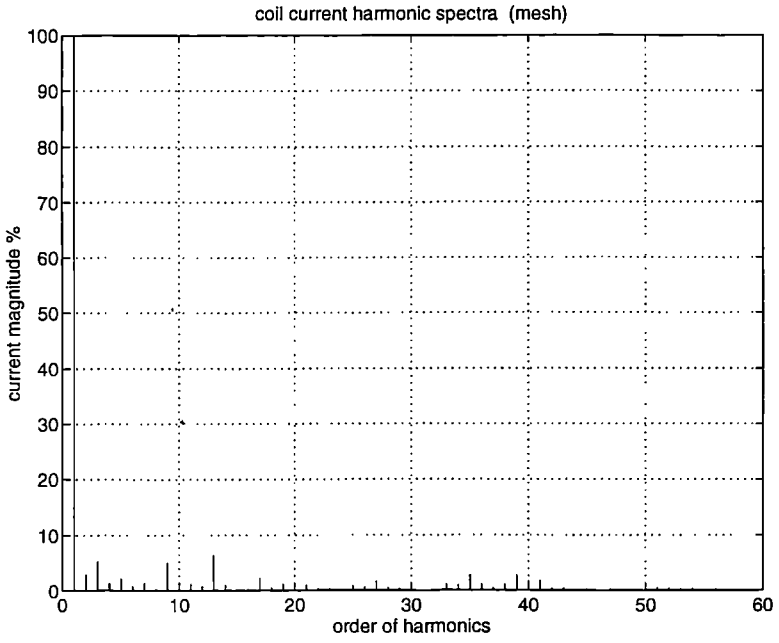

Figure 3.21 Stator coil current harmonic spectra (mesh)

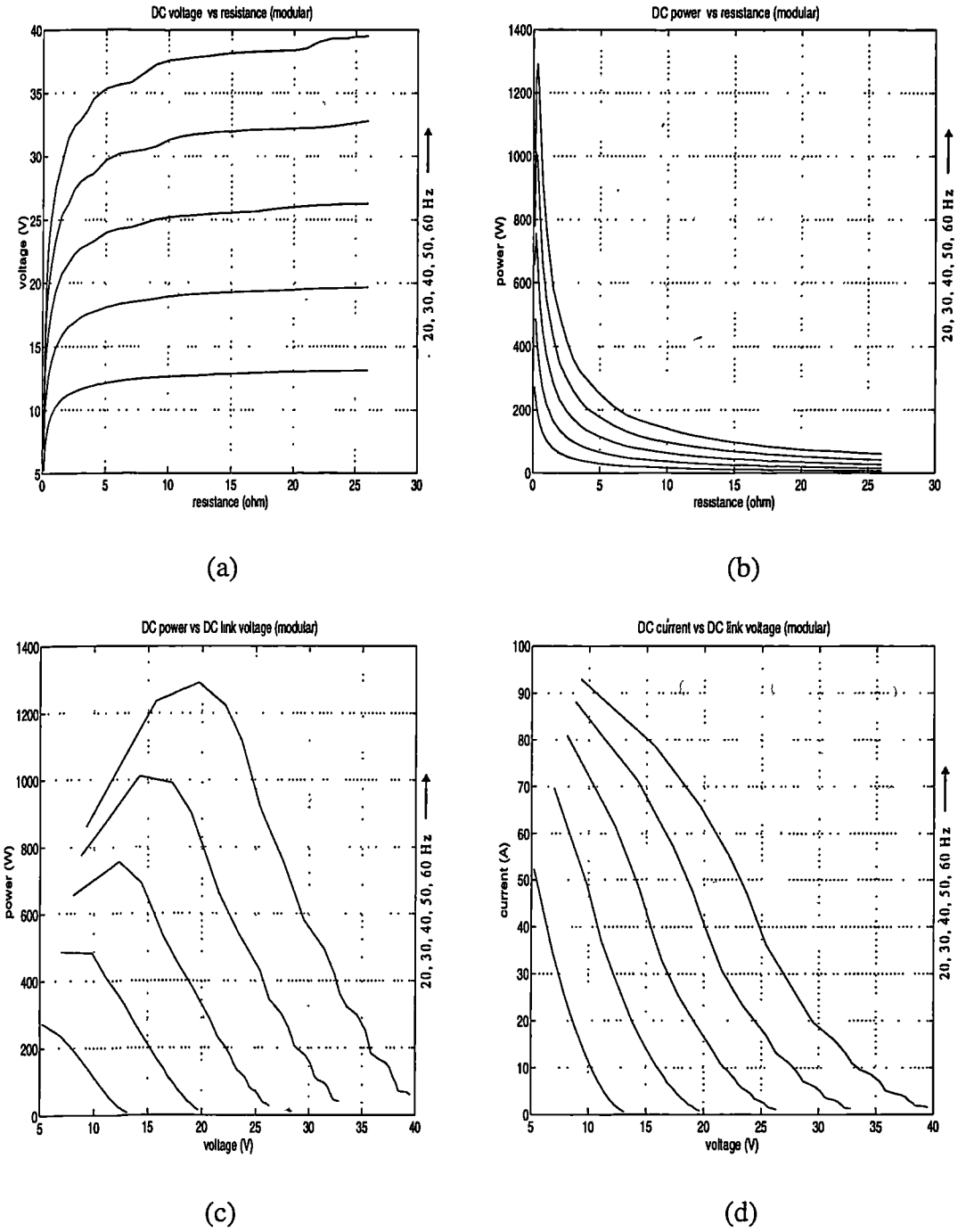

Figure 3.22 Poly-phase generator-rectifier system characteristic (modular) (a) (b) (c) (d)

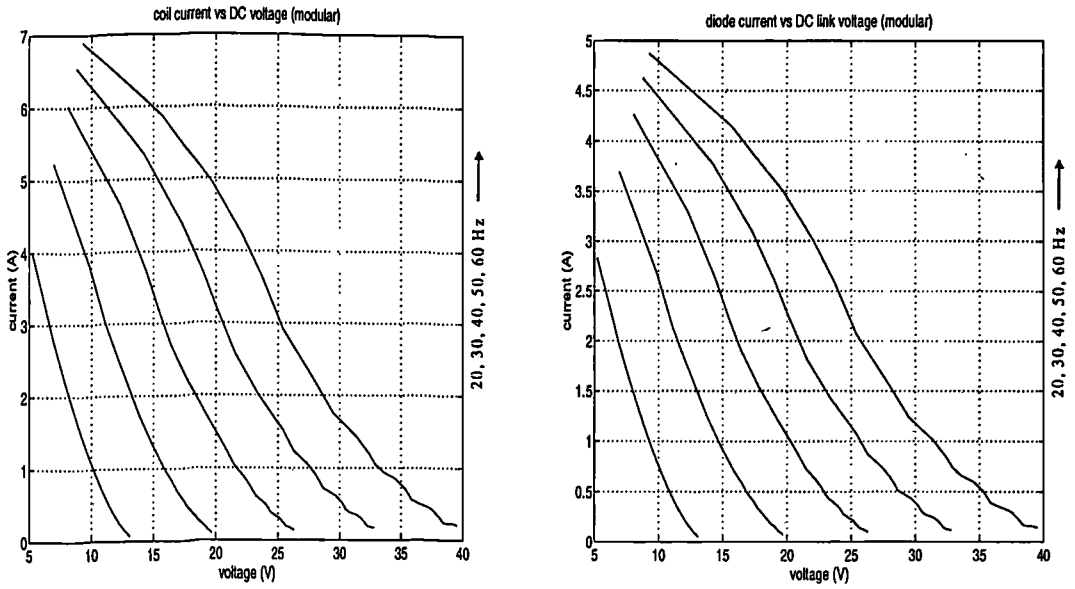

(e) (f)

Figure 3.22 Poly-phase generator-rectifier system characteristics (modular) (e) (f)

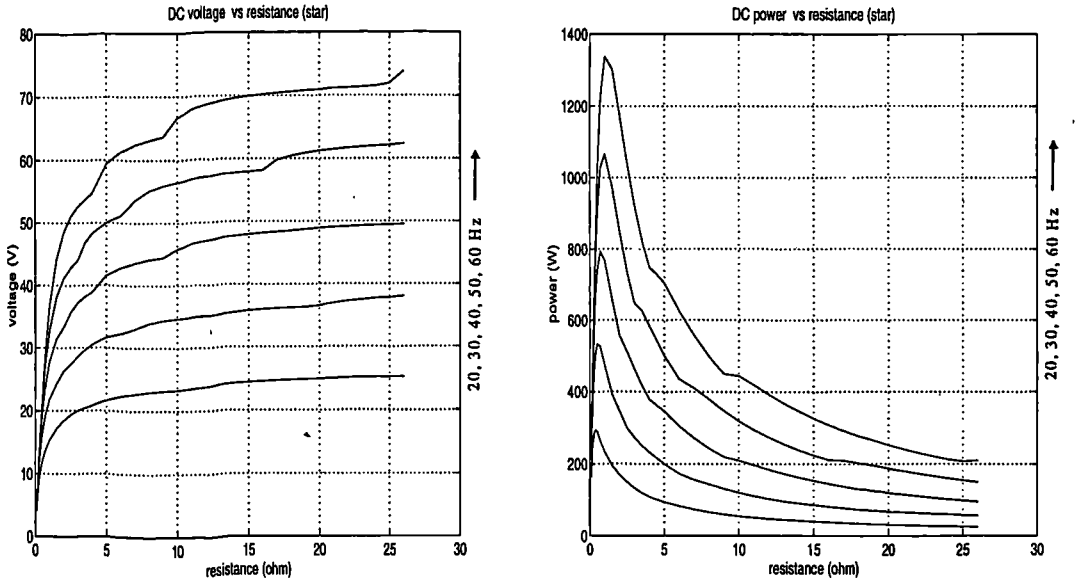

(a) (b)

Figure 3.23 Poly-phase generator-rectifier system characteristics (star) (a) (b)

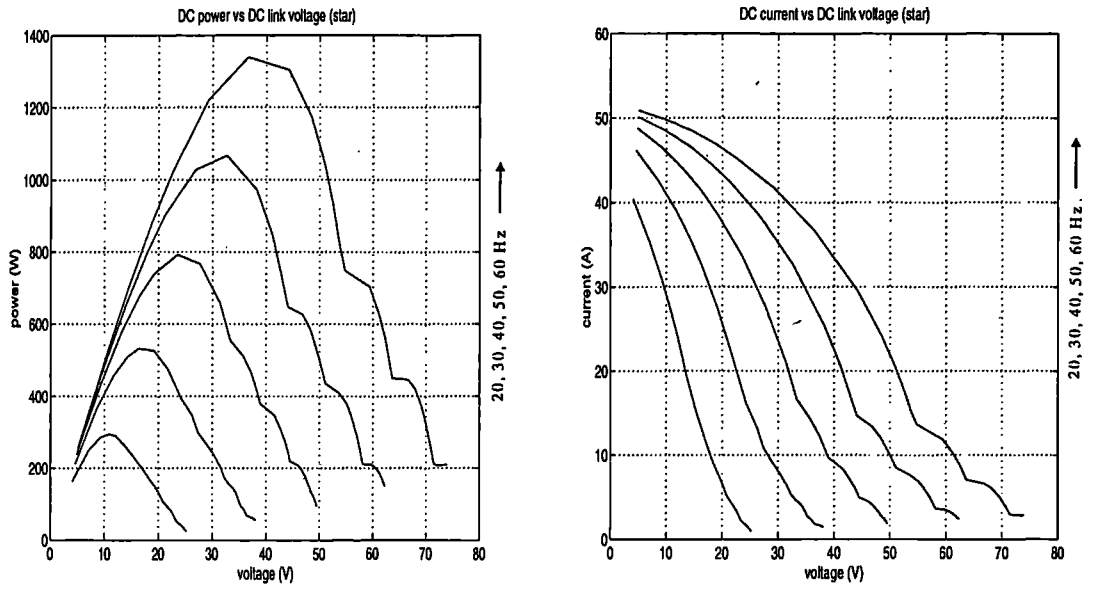

(c) (d)

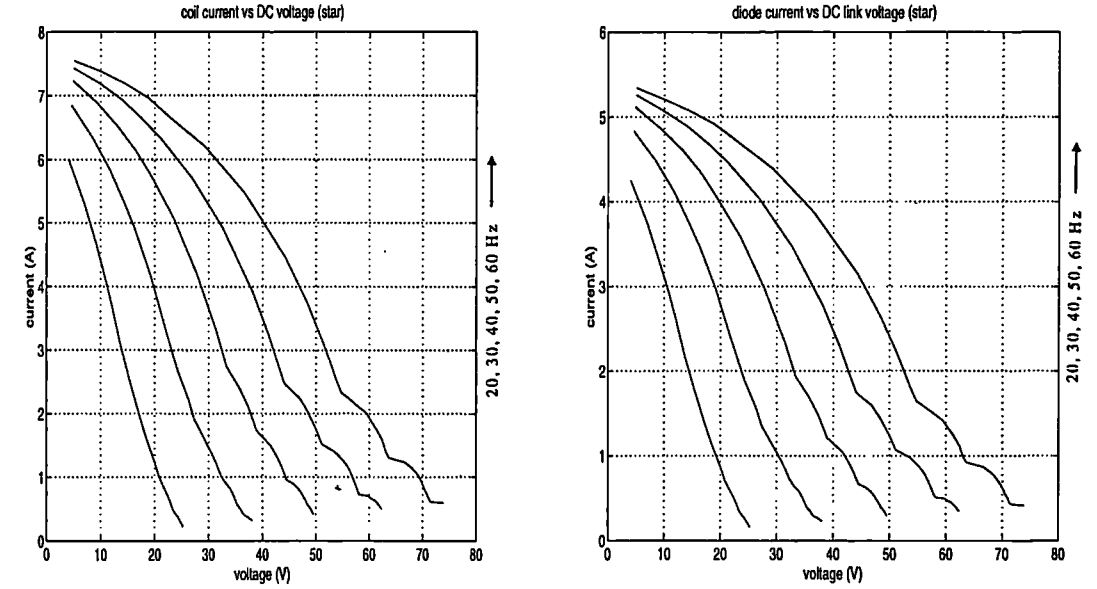

(e) (f)

Figure 3.23 Poly-phase generator-rectifier system characteristics (star) (c) (d) (e) (f)

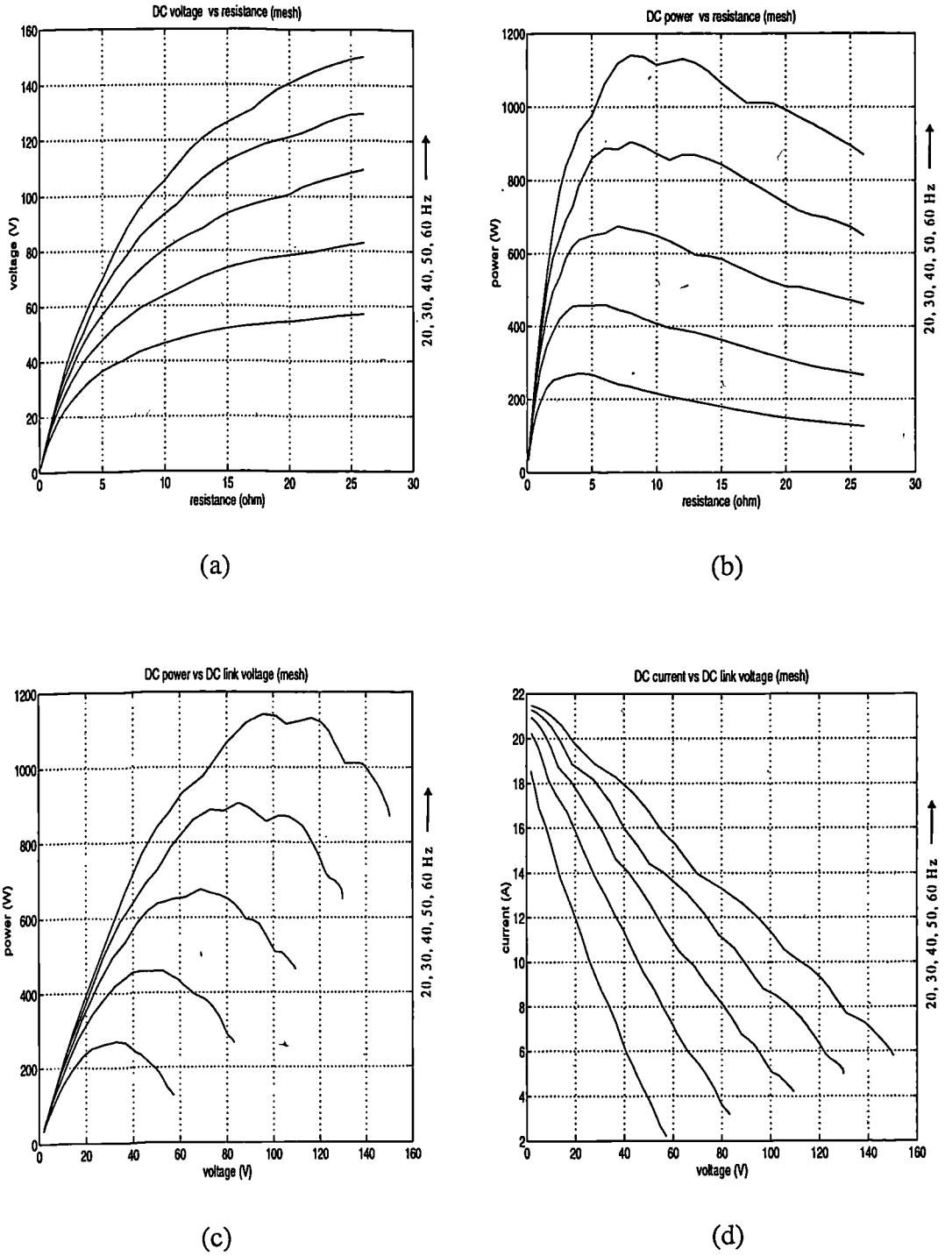

Figure 3.24 Poly-phase generator-rectifier system characteristics (mesh) (a) (b) (c) (d)

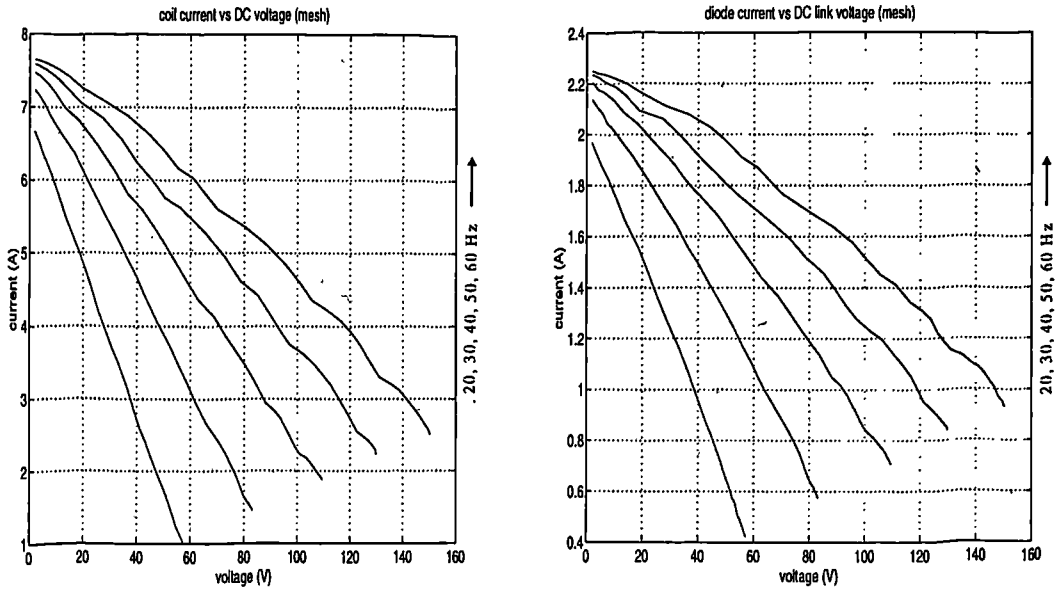

(e) (f)

Figure 3.24 Poly-phase generator-rectifier system characteristics (mesh) (e) (f)

3.4.3 Analysis and comparison of rectifier circuit simulation results

From the waveforms presented, it can be seen that all three circuits provide smooth d.c. link voltage. The requirement for a filter at the generator side of d.c. link is eliminated. Due to the existence of the coil internal impedance, more diodes conduct simultaneously than in the ideal case. This also means that the individual diodes have longer conduction periods than in the ideal case. All the three circuits give the same level coil current harmonics (total current harmonic distortion is about 12%).

From the system characteristics, the following features can be found:

(1) The three studied circuits deliver nearly the same maximum power (The mesh circuit is slightly lower).

(2) The mesh circuit operates at highest d.c. voltage and lowest d.c. current, the modular circuit operates at highest d.c. current and lowest d.c. voltage and the star circuit has intermediate values.

(3) The effect of the internal impedance can be also observed from the power -resistance characteristics, there is a maximum power transfer between a power source and the

connected external circuit, which occurs when the absolute values of the external circuit and the internal circuit equivalent impedance are equal. Therefore it can be seen that the modular circuit presents the lowest internal impedance and the mesh circuit the highest impedance.

(4) The internal impedance is obviously increased with the generator frequency, since the maximum power transfer point moves to higher load resistance with increasing frequency.

(5) The ratios of current (RMS) carried by the diode to the current in the stator coil have no significant difference between these three circuits.

3.5 Experimantal Study of Polyphase Modular PM Generator Rectifier System

3.5.1 Modular PM generator -rectifier test rig

Construction

A prototype PM generator was constructed with both stator and rotor based upon the modular concept. The rotor of 300mm diameter and 26 poles is constructed around ferrite magnets of dimensions 60mm×63mm×19mm (DOM). Each magnet carries an assembly of laminations, bonded to either side, to form laminated pole pieces. Each magnet is then bonded into radially slotted, aluminium end rings bolted to the rotor hub. The stator consists of 15 cores, each welded to a steel beam and each core is wound with a coil of 140 turns. Each stator coil is connected to a single phase diode rectifier bridge. The outputs of these rectifiers are parallel connected to form a dc link and to feed the resistor load.

Parameters of the modular PM generator

The resistance of each stator coil is 0.7 Ω at room temperature. All tests were of short duration and so the coil temperature and resistance were unchanged. The inductance of the stator coil varies slightly with the position of the rotor (9.947mH at q axis and 10.610mH at d axis). The stator coil mutual inductances are relatively small. The most significant mutual inductance (immediately next coil) is about 5% of the coil self inductance and the mutual inductances other than to the immediately next coil are less

than 0.8% of the coil self inductance. Therefore the mutual inductances between the stator coils are confirmed to be negligible.

The magnitude of the EMF of the stator coil is proportional to the frequency and is 25.4 V at 50 Hz. The waveform of the EMF of the stator coil is shown in figure 3.25. The harmonic spectrum analysis shows the fundamental component has the value of 25.2 V at 50 Hz, 3rd and 5th harmonics are the most significant harmonics at 5.94% and 6.58 % of the fundamental component respectively.

3.5.2 Circuit waveforms and characteristics from experimental study

Figure 3.26 and 3.27 show a group of the test circuit waveforms: rectifier bridge ac terminal voltage (1: 530), stator coil current (2 A/10 mV) and output dc current of stator coil-rectifier unit (2 A/10 mV). The operating condition is at 1 Ω load resistor and 40 Hz (modular circuit).

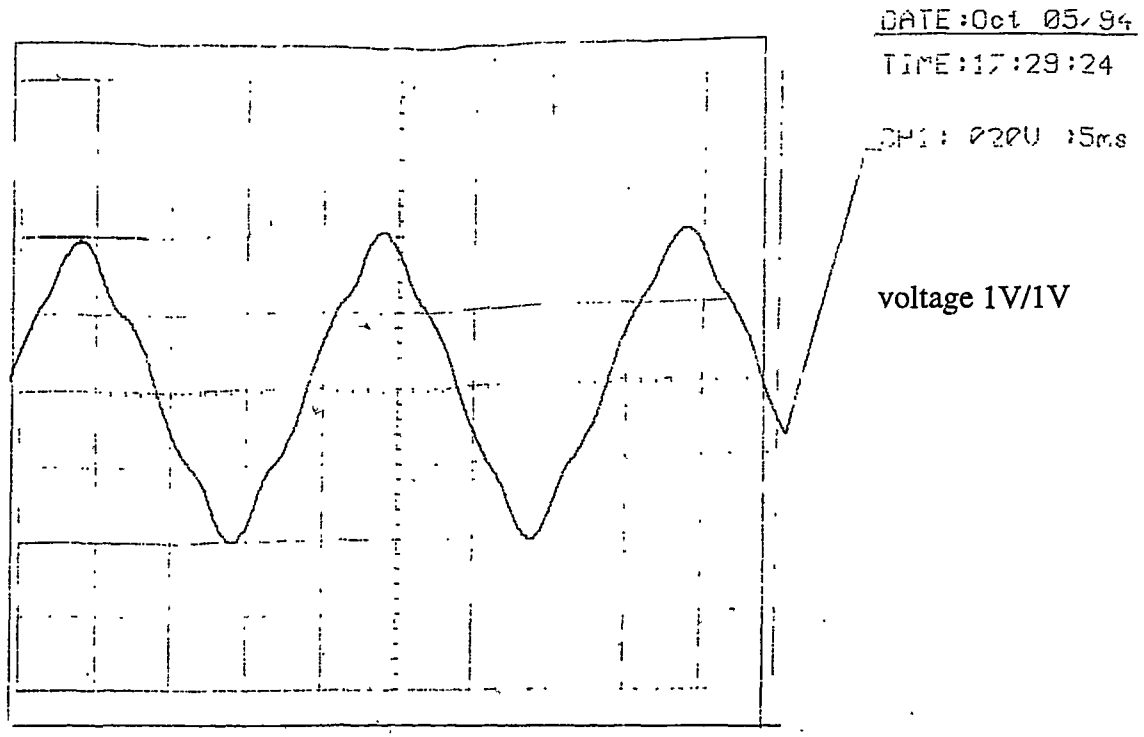

Figure 3.25 Open circuit voltage waveform of stator coil (50 Hz)

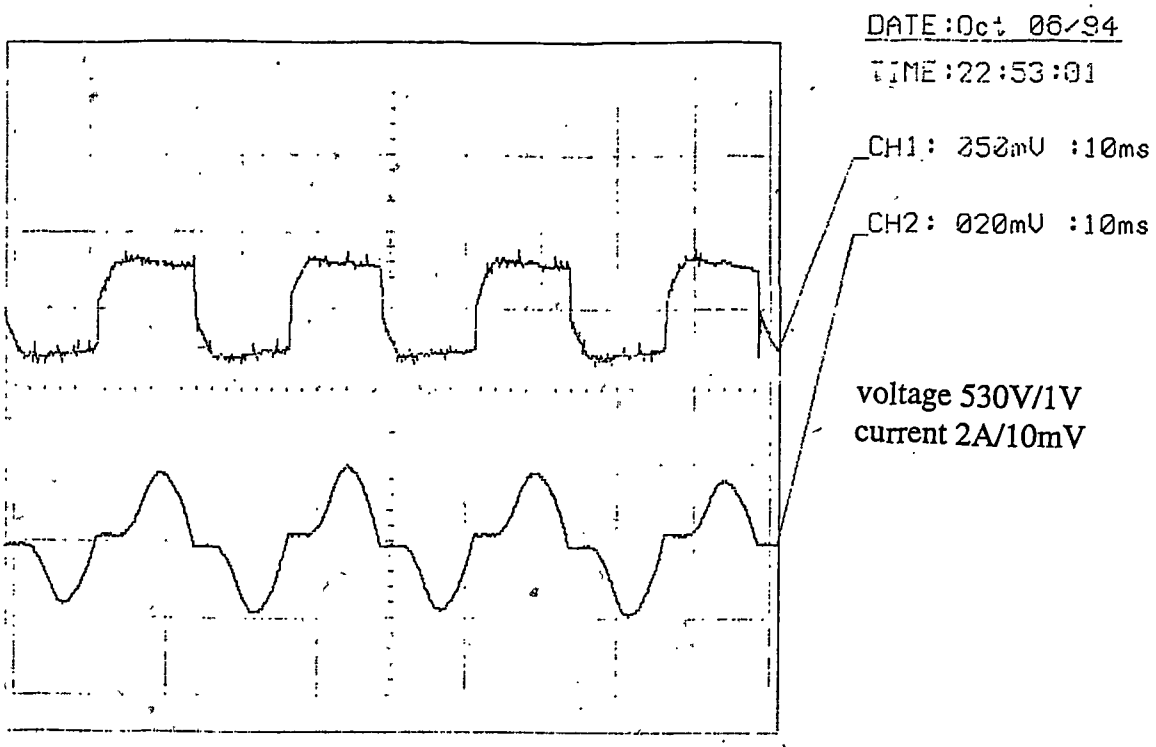

Figure 3.26 Rectifier ac terminal voltage (ch1) and coil current (ch2)
(40 Hz Rload=1Ω Modular)

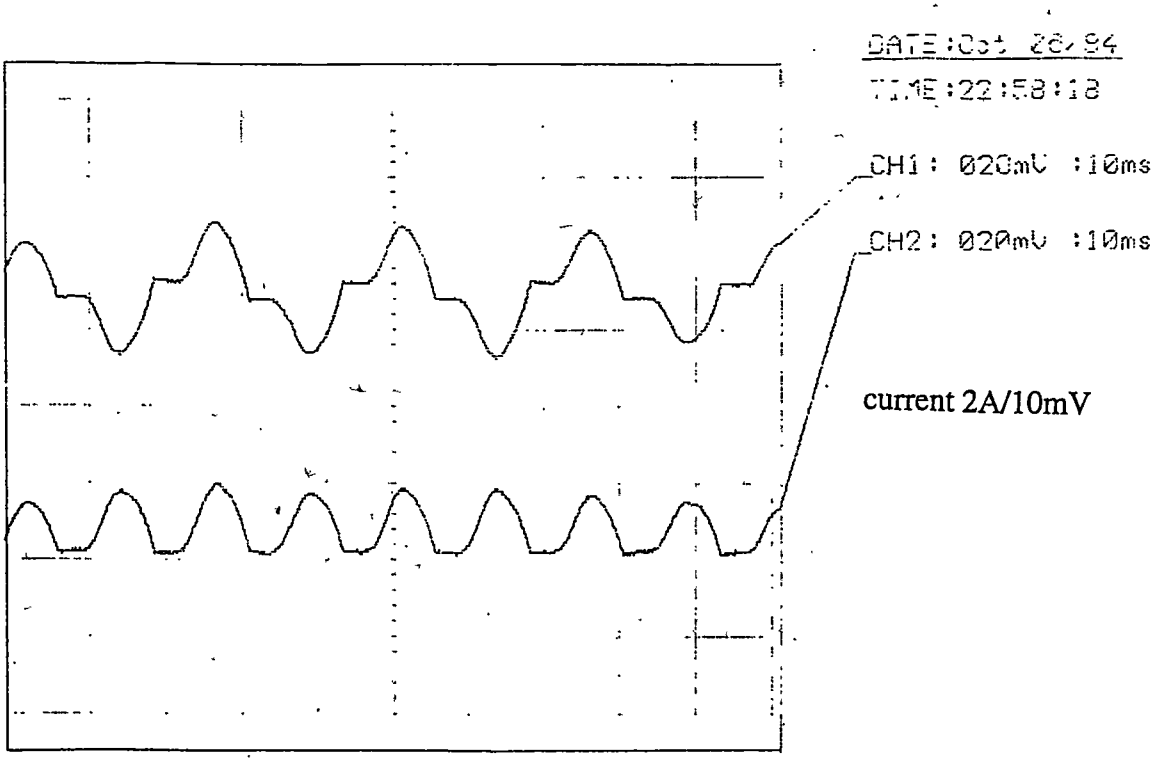

Figure 3.27 Coil current (ch1) and bridge rectifier output current (ch2)
(40 Hz Rload=1Ω Modular)

The power-frequency characteristics from the experimental studies are plotted in figure 3.28 where simulation results are also presented for comparison. It can be seen clearly that the results of simulation and experiment are in good agreement.

A simulation using three voltage sources (1st, 3rd and 5th) rather than only one sinusoidal voltage source to represent each stator coil EMF was also carried out. The EMF waveforms used for simulation are shown in figure 3.29. The power -frequency characteristics (R_{load}=0.5 Ω and R_{load}=1.0 Ω) are also presented in figure 3.28. It is clear that a single sinusoidal voltage source gives predicted characteristics of good accuracy and that the inclusion of harmonic emfs brings negligible improvement.

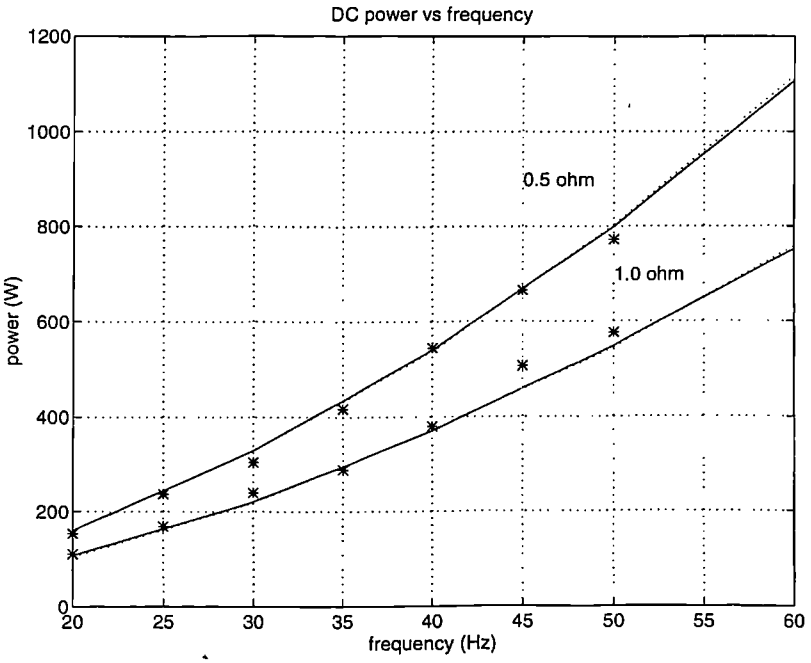

simulation (1st, 3rd and 5th harmonic emf) .....
simulation (sine wave emf) ——————
test results ******

Figure 3.28 Power-frequency characteristics (modular)

It is also noticed that the EMF is proportional to the frequency. The idealised power-frequency characteristic is a parabola, however due to the internal impedance, the output power is seriously limited by the internal impedance, resulting in almost a straight line characteristic.

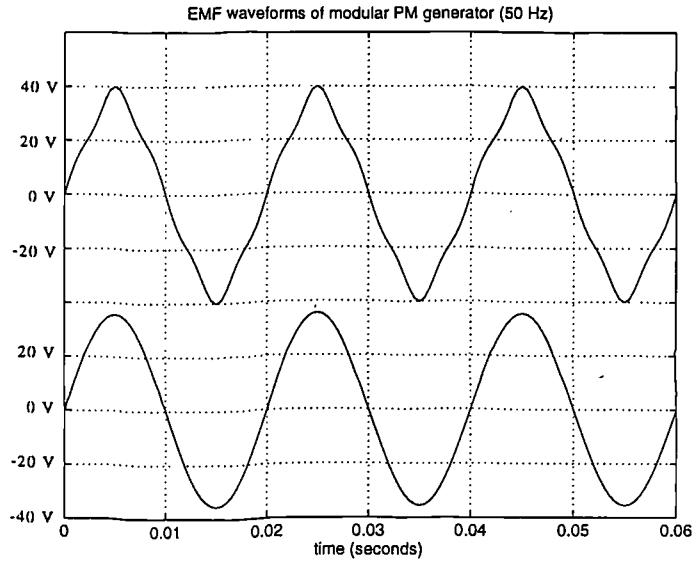

Figure 3.29 EMF waveforms for simulation study
(upper: 1st, 3rd and 5th harmonic emf; lower: sine emf only)

3.6 A Steady State Model of Polyphase Modular PM Generator - Rectifier System

In order to study the steady state performance and to select an operating trajectory for the whole power electronics energy conversion system, it is preferred to represent the generator-rectifier system with a simple circuit model such as a Thevenin equivalent circuit as shown in figure 3.30 where the generator-rectifier system is modelled by a DC voltage source (E_{eg}) and an internal resistor (R_{eg}). The d.c. link voltage V_d and current I_d can be related by $V_d = E_{eg} - R_{eg} I_d$

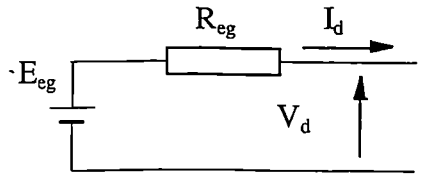

Figure 3.30 Circuit model of poly-phase generator and rectifièr

Comparing with the system characteristic presented in the above sections, it is obvious that E_{eg} and R_{eg} are frequency dependent and also R_{eg} is non-linear.
By assuming a polynomial relation between V_d and I_d

$$V_d = C_1 + C_2 I_d + C_3 I_d^2 + C_4 I_d^3 + \cdots$$

Using the characteristics obtained in simulation studies, (with simulation results V_{di} and $I_{di,}$ i=1..n), a least square curve fitting technique is used to find the coefficients C_1, C_2 .... It is found that a cubic curve can fit these characteristics quite well. Therefore for a certain frequency, E_{eg} is a constant and R_{eg} is a function of I_d.

$$E_{eg} = C_1$$

$$R_{eg} = C_2 + C_3 I_d + C_4 I_d^2$$

The resulting characteristics for such an equivalent circuit is shown in figure 3.31, 3.32 and 3.33 for modular, star and mesh circuits respectively where solid lines are the results of equivalent circuit and dashed lines are the simulation results. Again from top to bottom, 60 Hz , 50 Hz, 40 Hz, 30 Hz, 20 Hz respectively. It can be seen that the results from the equivalent circuit model are very close to the simulation results. The simple circuit model could be conveniently used for system steady state analysis.

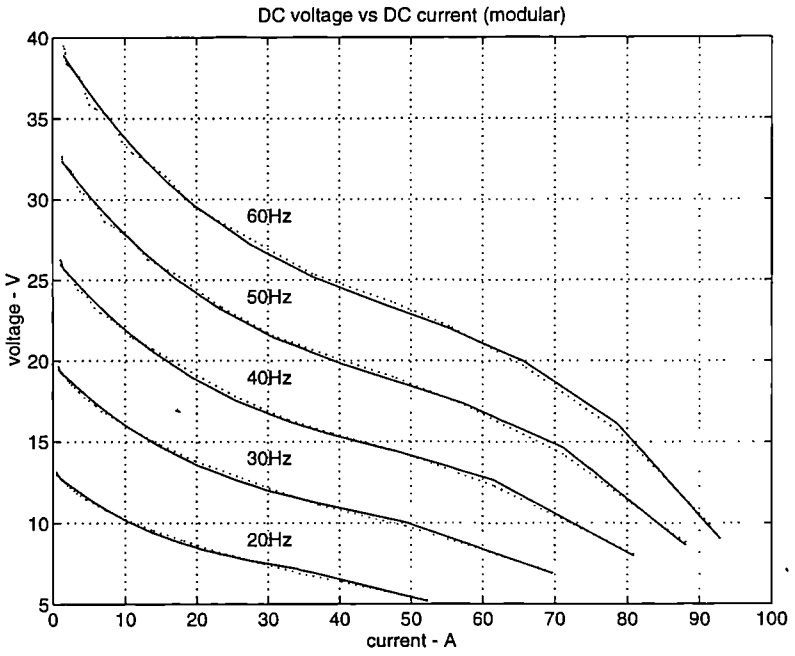

Figure 3.31 V_d - I_d characteristics (modular)

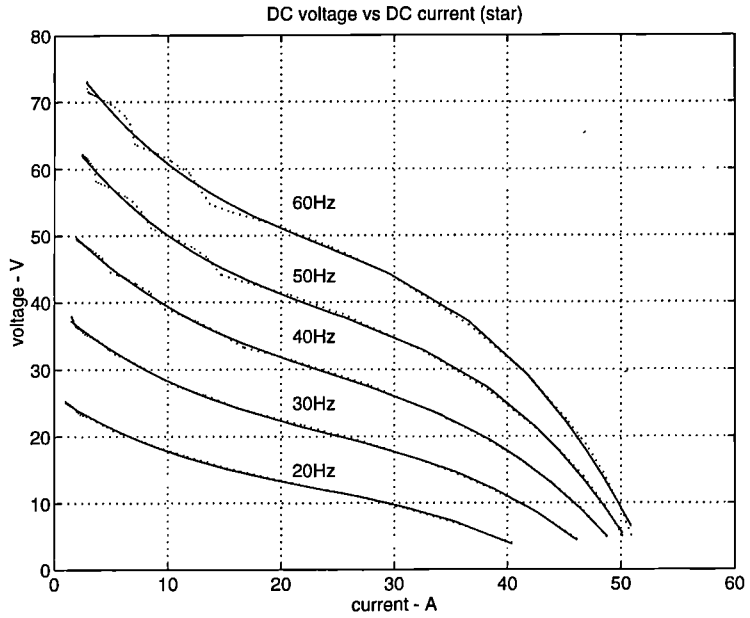

Figure 3.32 V_d - I_d characteristics (star)

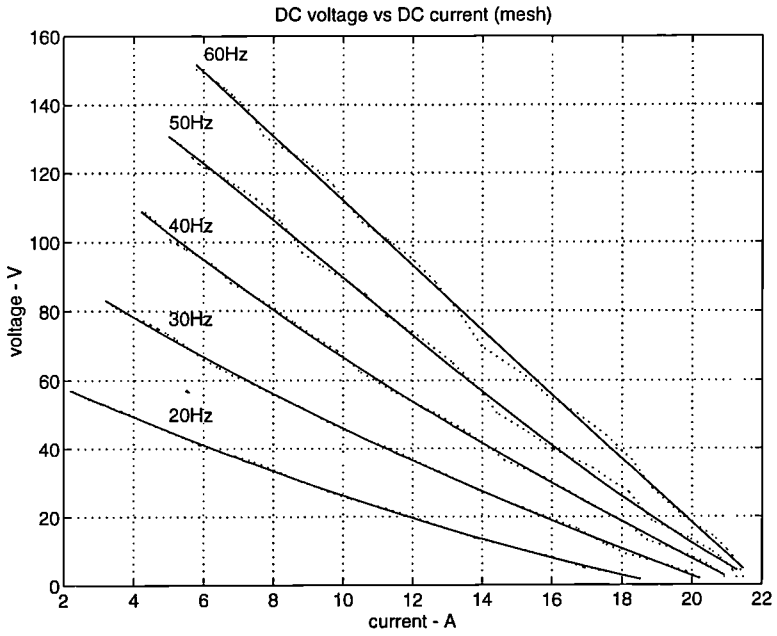

Figure 3.33 V_d - I_d characteristics (mesh)

3.7 Conclusions

The study has shown that a direct-drive, modular, permanent-magnet synchronous generator has many features which would be attractive for a variable speed wind energy conversion system.

A poly-phase modular generator system could simplify the variable speed system where each stator coil module forms one phase winding. The rather complex loom of wiring needed to establish the correct connection of coils for a three-phase output would be unnecessary.

The output of the poly phase generator can be conveniently rectified to generate a high quality DC link. The ripple voltage of the DC link is fairly small due to the uniform distribution of the poly-phase EMFs.

The diodes are cheap and reliable semiconductor components. Without any control circuit involved, the diode rectifier can operate at high efficiency.

The system simulation model has been developed and verified by the experiments. The different rectifier circuits have been analysed and simulated, the system characteristics are investigated. It is found that the star stator coil- bridge rectifier configuration offers good performance and operates at medium d.c. link voltage and current among the studied cases.

It is noticed that the internal impedance of the stator coil significantly effects the power output, therefore it will be further studied in the next chapter.

A simple circuit model is proposed to represent the generator -rectifier system. The parameters of the circuit model are obtained by polynomial fitting technique. This equivalent circuit model could significantly simplify the system steady state analysis.

Chapter

4.

Power Transfer Improvement of the PM Generator-Rectifier System

Chapter 3 has discussed the polyphase direct-drive modular PM generator and rectifier system which provides a high quality dc link. However, the impedance of the stator coils could restrict the power output capacity of the generator -rectifier system and prevent the full rating of the wind turbine being reached. In this chapter, one technique, the use of an ac capacitor connected at the stator coil terminals, is presented for enhancing the output power capability.

First, the a.c. capacitor connection technique is analysed in detail with a simple circuit, then the polyphase PM generator-rectifier system is investigated. The characteristics of different circuit connections are presented. Experimental and simulation results show that a significant increase of power transfer capability has been achieved.

The simple equivalent circuit models of the generator rectifier system discussed in Chapter 3 are also extended to include the effects of the ac capacitor connection.

4.1 Simple Circuit Studies

The characteristics of power transfer between a power source and a load are dependent on both the parameters of the power source (stator coil) and the characteristics of the load. In this section, a simple circuit is adopted for the purpose of discussing the effects of the ac capacitor connection.

4.1.1 Simple AC circuit analysis

A simple ac circuit is shown in figure 4.1 where a source with EMF E_g, resistance R_g and inductance L_g, is loaded with a resistor R_{load}. E_g is assumed to be sinusoidal. The load resistor is a simplified representation of the rectifier and the dc link.

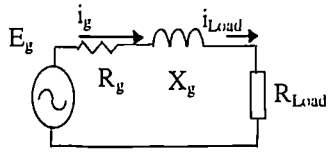

Figure 4.1 Simple ac circuit

In this circuit, the load current, being equal to the power source current, is

$$|I_{load}| = \frac{|E_g|}{|R_{load} + Z_g|} \tag{4.1}$$

the power delivered to the load (R_{load}) is

$$P_{load} = \frac{|E_g|^2 R_{load}}{|R_{load} + Z_g|^2} \tag{4.2}$$

and power loss in the power source is

$$P_{loss} = \frac{|E_g|^2 R_g}{|R_{load} + Z_g|^2} \tag{4.3}$$

the efficiency of the circuit is

$$Efficiency = \frac{P_{load}}{P_{load} + P_{loss}} \% \tag{4.4}$$

where

$$Z_g = R_g + j\omega L_g$$

and since the excitation is by permanent magnet, the emf is proportional to frequency $E_g = \omega E_{gb}$, where E_{gb} is constant.

The power delivered by the voltage source is

$$P_g = \frac{|E_g|^2 (R_g + R_{load})}{(R_g + R_{load})^2 + (\omega L_g)^2}$$

The maximum power which can be extracted from the turbine is obtained by maximising P_g against R ($R = R_g + R_{load}$).

let

$$\frac{\partial P_g}{\partial R} = |E_g|^2 \frac{\left(R^2 + (\omega L_g)^2\right) - R(2R)}{\left(R^2 + (\omega L_g)^2\right)^2} = 0$$

we have the P_g maximum condition $R = \omega L_g$

$$P_{g,\max} = \frac{|E_g|^2}{2\omega L_g} = \frac{\omega^2 E_{gb}^2}{2\omega L_g} = \frac{E_{gb}^2}{2L_g}\omega$$

The maximum power which the generator can produce is proportional to the turbine speed. Considering torque, $T_g = P_g/\omega$, therefore the torque which the generator can react at the maximum power is $E_{gb}^2/2L_g$. However, the wind power increases with ω^3 and turbine torque with ω^2. The above derivation shows a serious power and torque restriction which can be overcome either by increasing E_{gb} or reducing L_g. The approach adopted is to use a capacitor to modify the circuit to figure 4.2. It's effect can be considered as either forming a turned circuit to reduce the effective inductance, or alternatively to draw current, which flowing in the stator coil, with the correct phase for supplementing the mmf created by the magnets and so increasing E_{gb}.

ac capacitor connection case

In figure 4.2 (a), an ac capacitor is connected to the power source in parallel with the load. The circuit parameters viewed by the load are changed from E_g and Z_g into E_{eq} and Z_{eq}, the equivalent values for a Thevenin source. The equivalent circuit is shown in figure 4.2 (b).

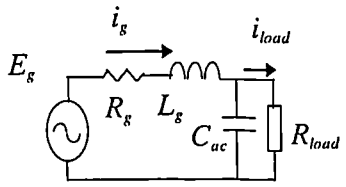

(a) ac capacitor connection to the power source

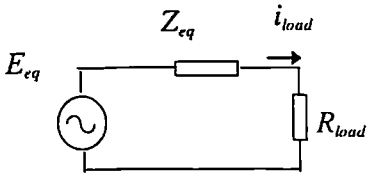

b) *Thevenin* equivalent circuit

Figure 4.2 Simple ac circuit (ac capacitor connection)

E_{eq} and Z_{eq} can be found by using *Thevenin's Theorem,* (Appendix A)

$$E_{eq} = K_c E_g \tag{4.5}$$

$$Z_{eq} = K_c Z_g \tag{4.6}$$

where

$$K_c = \frac{1}{1-\omega^2 L_g C_{ac} + jR_g \omega C_{ac}} \tag{4.7}$$

Consequently,

$$|I_{load}| = \frac{|E_{eq}|}{|R_{load} + Z_{eq}|} \tag{4.8}$$

$$V_{load} = R_{load} I_{load} \tag{4.9}$$

$$|I_g| = \frac{|E_g - V_{load}|}{Z_g} \tag{4.10}$$

$$|I_c| = |V_{load} \omega C_{ac}| \tag{4.11}$$

the power delivered to the load (R_{load}) is

$$P_{load(c)} = \frac{|E_{eq}|^2 R_{load}}{|R_{load} + Z_{eq}|^2} \tag{4.12}$$

$$= \frac{|E_g|^2 R_{load}}{\left|\frac{R_{load}}{K_c} + Z_g\right|^2} \tag{4.13}$$

and power loss in the power source is

$$P_{loss(c)} = |I_g|^2 R_g \tag{4.14}$$

The efficiency of the circuit can be calculated with $P_{load(c)}$ and $P_{loss(c)}$ using equation 4.4. To find the value of C_{ac} which makes $|K_c|$ reach its maximum for a fixed load and frequency from equation 4.7, let

$$f_1 = (1-\omega^2 L_g C_{ac})^2 + (R_g \omega C_{ac})^2$$

and

$$\frac{\partial f_1}{\partial C_{ac}} = 0$$

which gives

$$\frac{\partial f_1}{\partial C_{ac}} = 2(1-\omega^2 L_g C_{ac})(-\omega^2 L_g) + 2(R_g \omega C_{ac}) R_g \omega = 0$$

$$(1-\omega^2 L_g C_{ac})(-L_g) + R_g{}^2 C_{ac} = 0$$

therefore

$$C_{ac} = \frac{L_g}{\omega^2 L_g{}^2 + R_g{}^2} \tag{4.15}$$

The C_{ac} value calculated by equation 4.15 will make $|K_c|$, and therefore $|E_{eq}|$ and $|Z_{eq}|$ be maximum. If equation 4.7 is substituted in to equation 4.13, we have

$$P_{load(c)} = \frac{|E_g|^2 R_{load}}{\left|\frac{R_{load}}{K_c} + Z_g\right|^2} = \frac{|E_g|^2 R_{load}}{\left|R_{load}((1-\omega^2 L_g C_{ac}) + jR_g \omega C_{ac}) + R_g + j\omega L_g\right|^2}$$

$$= \frac{|E_g|^2 R_{load}}{\left|R_{load}(1-\omega^2 L_g C_{ac}) + R_g + j\omega(R_{load} R_g C_{ac} + L_g)\right|^2}$$

$$= \frac{|E_g|^2 R_{load}}{\left(R_{load}(1-\omega^2 L_g C_{ac}) + R_g\right)^2 + \omega^2 (R_{load} R_g C_{ac} + L_g)^2} \tag{4.16}$$

To find C_{ac} which makes $P_{load(c)}$ reach its maximum for a fixed load and frequency, let

$$\frac{\partial P_{load(c)}}{\partial C_{ac}} = 0$$

Again, we have (Appendix B)

$$C_{ac} = \frac{L_g}{\omega^2 L_g{}^2 + R_g{}^2}$$

That indicates that the capacitor value which obtains the maximum increase of equivalent $|E_{eq}|$ and $|Z_{eq}|$ gives the maximum output power.

It is noticed that the denominator of equation 4.16 consists of two parts. The ac capacitor connection could reduce the first part while increasing the second part. If the second part is dominated by inductance L_g and the ac capacitor connection may not increase this part significantly. On the other hand, the first part could be significantly

reduced if a suitable ac capacitor is chosen. Therefore a higher power output could be obtained.

Based on the above analytical formulae, the characteristics of the simple circuit are produced with following parameters: (which correspond to the values for the small laboratory machine)

E_g = (rms) 25.2 V at 50 Hz, R_g = 0.7 Ω, L_g =10.28mH.

Varying capacitance and load resistance

Figure 4.3 presents the relations of load power to a.c. capacitance and load resistance at the power source frequency of 50 Hz. The capacitance is presented with per unit value and the base value is C_b which is calculated using equation 4.15. The capacitance is varying between 0-1.5 per unit values and the load resistance is changing from 1.5 Ω to 26 Ω.

As expected the maximum power transfer points are located on the 1.0 p.u. capacitance curve. A higher capacitance than 1.0 p.u. will result in reduction of the power output. Since $|Z_{eq}|$ is proportional to $|K_c|$ which is varied with capacitance, therefore the load resistance corresponding the maximum power transfer points are also varied with different capacitance.

Figure 4.4 presents the following characteristics of the studied circuit for varying capacitance (0, 0.1, ..., 1.0 C_b).

load current (A) - load resistance (Ω)

source (coil) current (A) - load resistance (Ω)

a.c. capacitor current (A) - load resistance (Ω)

load voltage (V)- load resistance (Ω)

load power (W) - load resistance (Ω)

load power (W) - load voltage (V)

power loss (W) - load resistance (Ω)

efficiency (%)- load resistance (Ω)

The curves in each figure represent the 1.0, 0.9 ...0 C_b cases downwards respectively except efficiency figure 4.4 (h) where the sequence is upward. From figure 4.4, it can been seen:

The load power can be increased by connecting an a.c. capacitor to the power source in parallel. The larger the capacitance (up to 1.0 C_b), the higher power transfer can be reached.

The capacitance current, power source current and power loss are increasing, and therefore efficiency is reducing with capacitance increasing. For C_{ac} >0.6 C_b, the efficiency drops below 80%. The choice of capacitor therefore presents a conflict between the need to achieve high power transfer and the need for high efficiency.

With load resistance increasing, load current is reducing and load voltage is increasing. At certain load resistance, where $R_{load}=|Z_{eq}|$, the maximum load power is achieved.

Varying capacitance and power source frequency and magnitude

A group of characteristics of the circuit under varying frequency and magnitude of E_g condition is shown in figure 4.5. The capacitance are calculated with equation 4.15 using frequencies of 20 Hz, 30 Hz, 40 Hz, 50 Hz and 60 Hz respectively and are given in the Table 4.1.

Figure 4.5 shows that a larger capacitance will result in higher power output before its power peak value is reached, but the power output will drop quickly after the peak value. The maximum power occurs near the frequencies used for capacitance calculation (Appendix C).

Table 4.1 Capacitance of figure 4.5

curve	1	2	3	4	5	6
frequency (Hz) for C_{ac} calculation		20	30	40	50	60
capacitance (μF)	0	4761.9	2421.8	1434.7	941.4	662.8

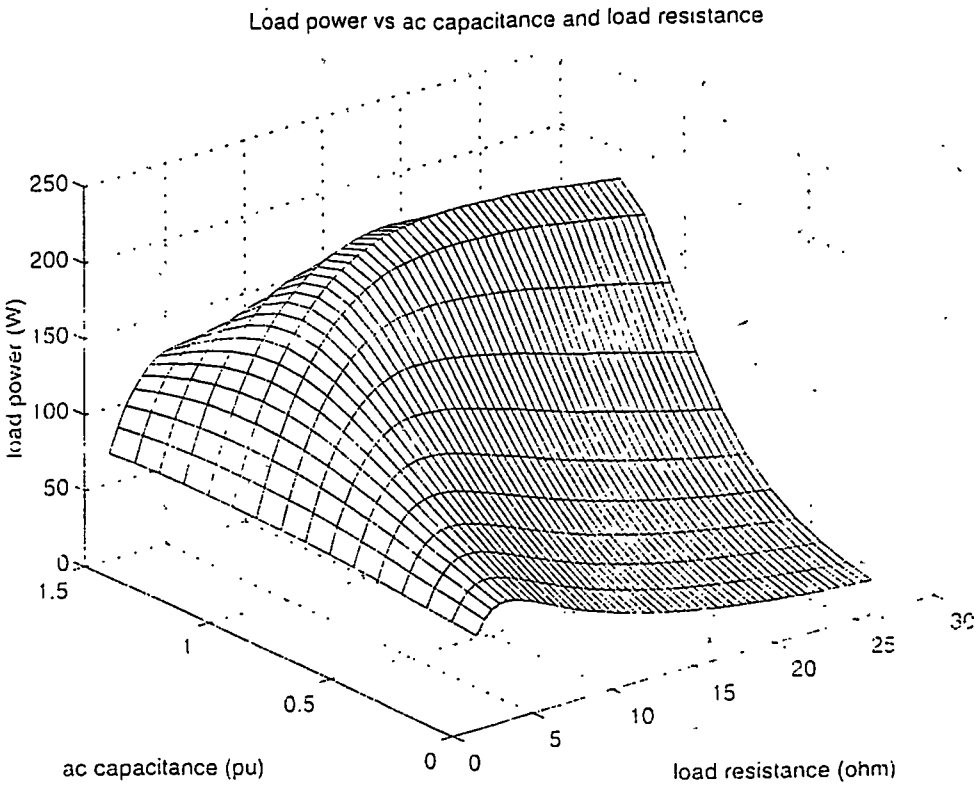

Figure 4.3 Power vs. capacitance and resistance (simple circuit)

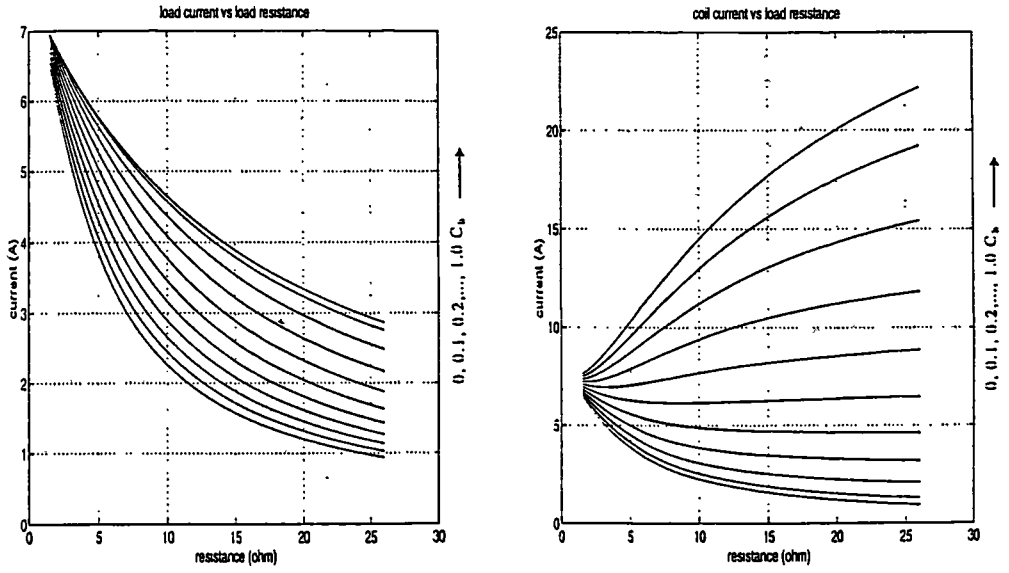

(a) (b)

Figure 4.4 Simple circuit characteristics (a) (b)

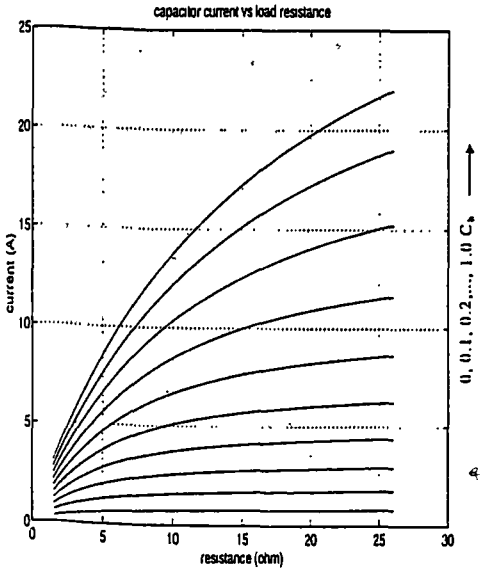

(c)

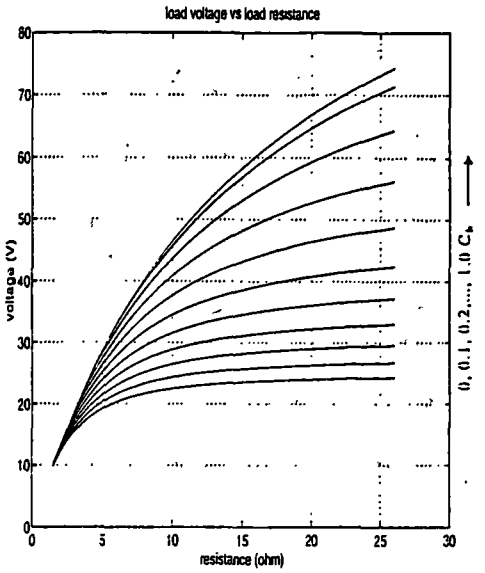

(d)

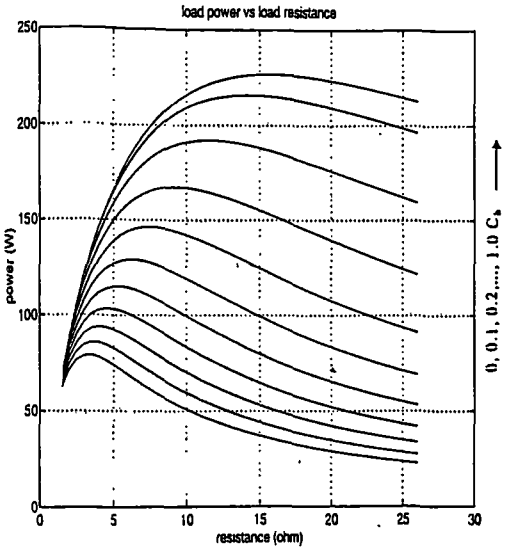

(e)

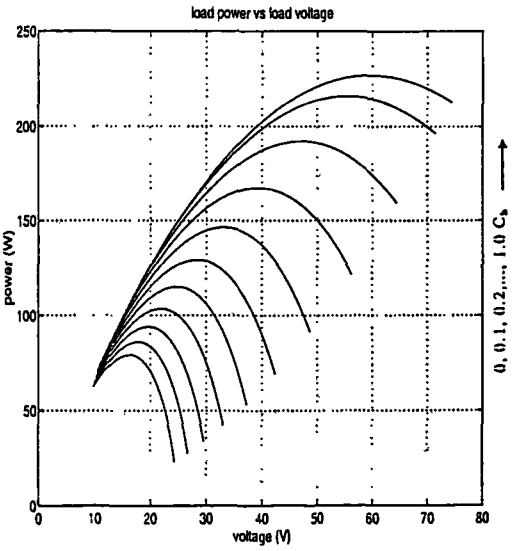

(f)

Figure 4.4 Simple circuit characteristics (c) (d) (e) (f)

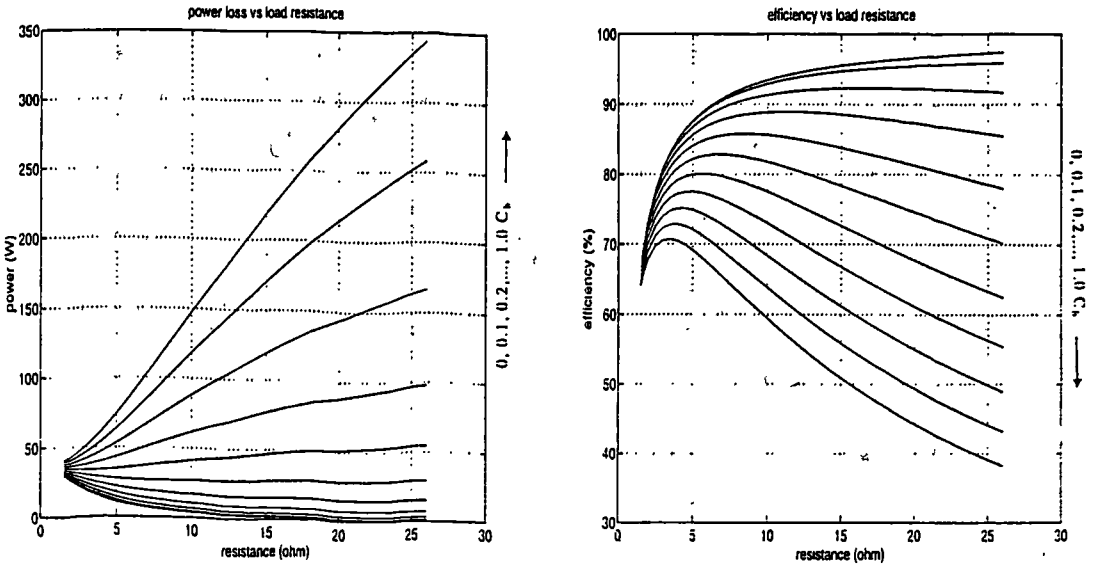

(g) (h)

Figure 4.4 Simple circuit characteristics (g) (h)

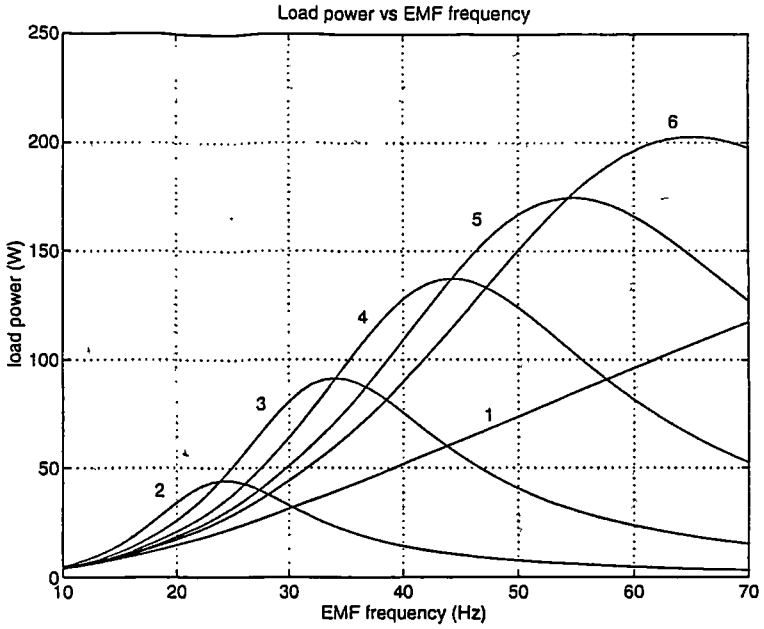

Figure 4.5 Power vs. frequency characteristics of simple ac circuit (R_{load} =5Ω)

4.1.2 Simple rectifier circuit

Figure 4.6 shows a simple rectifier circuit, the power source is directly connected to a single phase bridge rectifier and the ac capacitor is connected at the ac terminal of the rectifier.

An ideal switch characteristic is assumed for the diode to simplify analysis. In the case shown in figure 4.6 with a single ac circuit feeding the dc load, the load viewed by the power source is the same as the case discussed in section 4.1.1. Therefore the same characteristic will be obtained with a.c. capacitor connection except that a rectified current rather than an alternating current flows through the resistive load. The principle and formulas in the section 4.1.1 apply to this case.

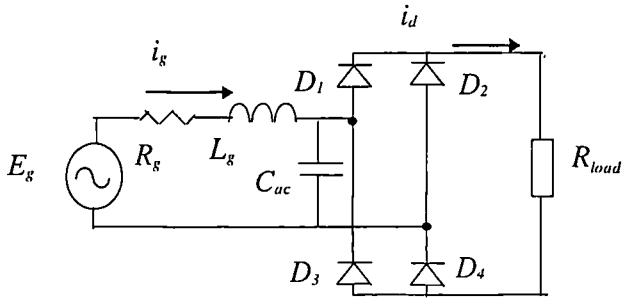

Figure 4.6 Equivalent circuit of the simple rectifier circuit

4.1.3 Summary of ac capacitor connection in the simple circuit

From the above studies, following conclusions can be drawn:

1. The ac capacitor connected at ac voltage source terminal changes the equivalent EMF and internal impedance with the same rate.
2. In the studied simple circuit, for a certain power source frequency, if ac capacitor is chosen as $C_{ac} = \frac{L_g}{\omega^2 L_g^{\,2} + R_g^{\,2}}$, the power transfer and the $|K_c|$ will reach their maximum.
3. The capacitance could be chosen to make maximum power transfer happen around the desired frequency. The higher the frequency, the smaller is the required capacitor. For the output power enhancement propose, the frequency used for C_b calculation should not be lower than the highest possible working frequency. If R_g

$<<\omega L_g$, the condition will be approximate to the circuit resonant condition ($\omega L_g = \frac{1}{\omega C_{ac}}$).

4. Since the ac capacitance connection changes the equivalent impedance of the power source, the maximum power transfer point moves to the load resistance point which is equal to $|K_c|\ |Z_g|$.
5. The efficiency of the circuit may be low if too large a capacitor is used, which results in high power source current.

4.2 Poly-Phase Circuit Studies

In poly-phase PM generator-rectifier system, a power enhancement ac capacitor could be connected separately to each stator coil. The coils may be connected in star or mesh prior to rectification or the modular system may be used where each coil has its own single phase bridge.

In order to simplify the analysis, only the modular case is analysed in the next section. However, all three type circuits are simulated and the results are presented in the following sections.

4.2.1 Analyses of ac capacitor effects in modular circuit

In polyphase system, each stator coil can be represented by the equivalent circuit of the power source in the simple ac circuit discussed in section 4.1. The stator coils and the rotor poles are such arranged so that the EMFs are evenly distributed in phases and the DC voltage can be considered as ripple free because of the large number of phases. In electrical modular arrangement, these stator coil single-phase rectifier modules may be analysed separately since mutual inductance between coils is negligible and coils are almost electrically independent.

When the ac terminal voltage of a particular bridge rectifier becomes higher than the DC link voltage, it will begin to conduct and will cease when the current drops to zero.

The power transferred to the d.c. side is dependent on the current provided by the module and the d.c. voltage. A higher d.c. voltage will result in a shorter conduction period, and lower d.c current. An optimal dc voltage exists for maximum power.

Once the rectifier conducts, its ac capacitor voltage is fixed by the constant DC link voltage. Thereafter there is no current though the ac capacitor. This module then behaves as if the capacitor were absent except that the stator coil has a non-zero initial current when rectifier begins to conduct so that both the EMF and energy storing inductor provide energy to the d.c. side.

The a.c. capacitor mainly effects the circuit behaviour in the non-conduction period. When the rectifier is blocking, the stator coil and capacitor form a RLC circuit as shown in figure 4.7 (a).

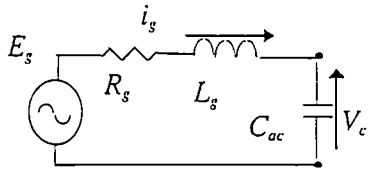

(a) Equivalent circuit of non-conduction period

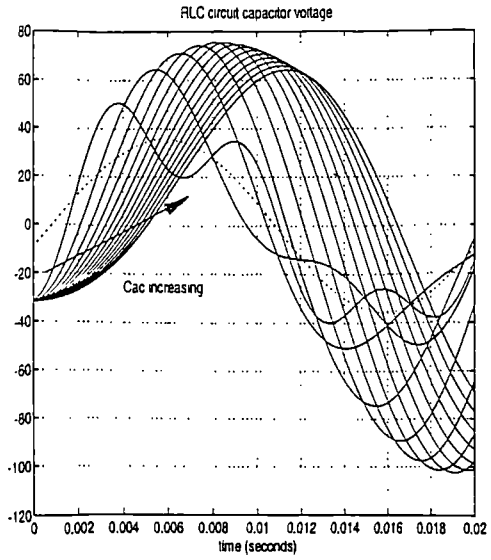

(b) capacitor voltage waveforms

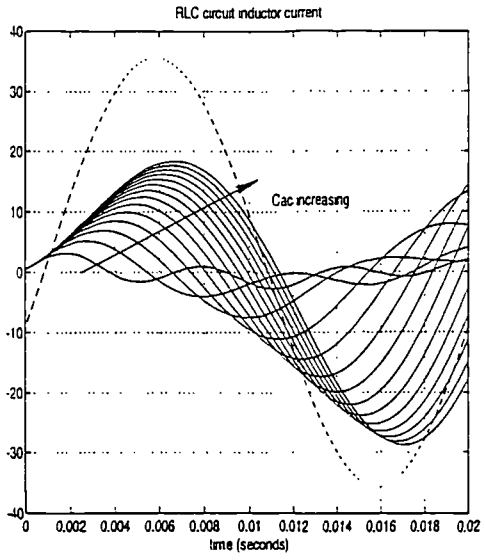

(c) inductor current waveforms

Figure 4.7 RLC circuit analysis

In the case with zero capacitance, during the blocking period, the ac terminal voltage of the rectifier will be the EMF and the current in the inductor will be zero, however, with the capacitor present, current provided by the stator coil may pass through the ac capacitor until the voltage of the ac capacitor is charged to the DC link voltage, at which time rectifier will conduct again.

The inductor current and capacitor voltage of the RLC circuit shown in figure 4.7 (a) with initial values of $i_L(0)=0$ and $V_c(0)=-V_d$ are shown in figure 4.7 (b) (c) for a given initial value of the EMF, where the parameters of the simple circuit in section 4.1 are used and C_{ac} is varied from 0.1-1.4 C_b. the dashed line represents the EMF which is at 50Hz.

Increasing the ac capacitance would increase the inductor current and therefore the energy stored giving a higher initial current when the rectifier starts to conduct. The voltage of the a.c. capacitor also increases with capacitance (up to 0.6 C_b) boosting the d.c. link voltage. It is also noticed that a larger capacitor takes longer to charge to a certain voltage thus reducing the rectifier conduction period.

It is hoped the founding in section 4.1 could serve as a guide for analysis of the polyphase case. A series of simulations has been carried out to investigate the behaviour of the poly-phase PM generator -rectifier system and the results are presented in the following sections.

4.2.2 Modular circuit simulation

In this section, the simulation results of modular circuit are presented to study the similarity of the capacitor connection effects in the modular circuit and the simple ac circuit in section 4.1. The simulation circuit model of modular configuration is shown in figure 4.8 where a.c. capacitor is connected in parallel with stator coil in each module. There are 15 modules together in this circuit.

The same parameters as section 4.1 are used for this study. The system characteristics are presented in Figure 4.9, Figure 4.10 and Figure 4.11.

In figure 4.9, the characteristics of power vs. capacitance and resistance are presented with varying capacitance (0 C_b, 0.1 C_b, , ... 1.2 C_b) where C_b is calculated with a frequency of 50Hz and resistance varying from 1.5 Ω to 26 Ω.

Figure 4.10 presents the same characteristics of figure 4.4 for varying capacitance (0, 0.1, ..., 1.0 C_b) and the same sequence is used for figure (a)-(h). Again, the curves in each figure represent the 1.0, 0.9 ...0 C_b cases downwards respectively except efficiency figure 4.10 (h) where the sequence is upward. Figure 4.11 shows the characteristics of power to frequency where the identifiers and capacitance shown in Table 4.1 are used.

Comparing figure 4.9, figure 4.10 and figure 4.11 with figure 4.3, figure 4.4 and figure 4.5, it can be clearly seen that the simple circuit and the 15 modular coil circuit present quite similar characteristics, although they have different output power.

In figure 4.9, the similar relation of power vs. capacitance is observed. In the polyphase case, the stator coil-rectifier units are paralleled connected to the DC link, then demonstrate a smaller internal equivalent impedance therefore the power peak in the power-resistance relation moves to lower resistance point.

Figure 4.10 has the similar pattern with figure 4.4. The load voltage is increasing with the increasing of capacitance (up to 1.0) in both cases, although in polyphase case, the higher power points move to lower resistance range and the voltage curves tend to be flatten and also the a.c. capacitor current. Similarly, the power losses are significant high with the ac capacitance ≥ 0.7 C_b, though the percentage of the polyphase case is not as high as that of the simple circuit case, which results in a higher efficiency of the polyphase.

Again, the similarity can be seen very clearly by comparing figure 4.11 with figure 4.5, the peak power for a particular capacitance case occurs at a higher frequency than the capacitor calculation frequency.

The results of this study show that the principle founding of the simple circuit study (C_b calculation, frequencies for maximum power generation, etc.) could be used for guiding polyphase system study.

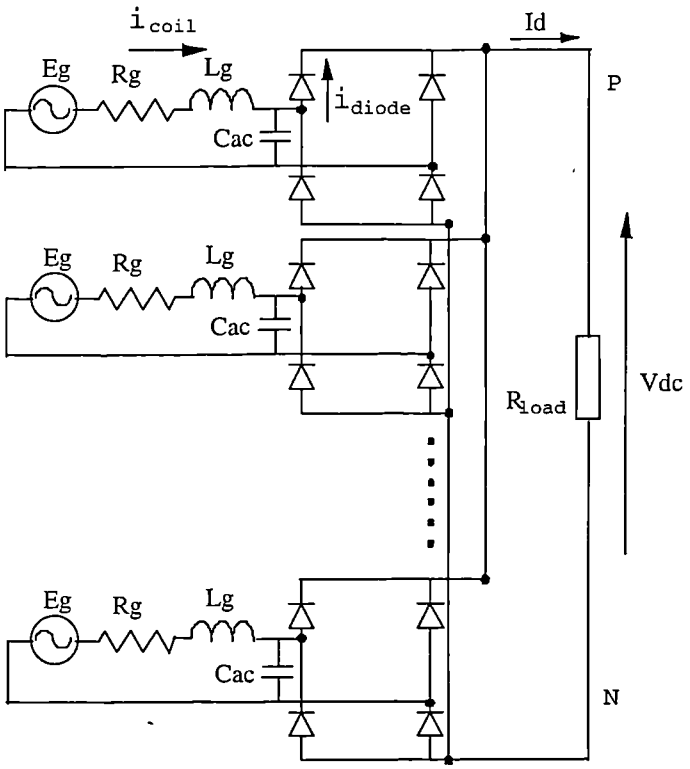

Figure 4.8 Modular connection simulation model

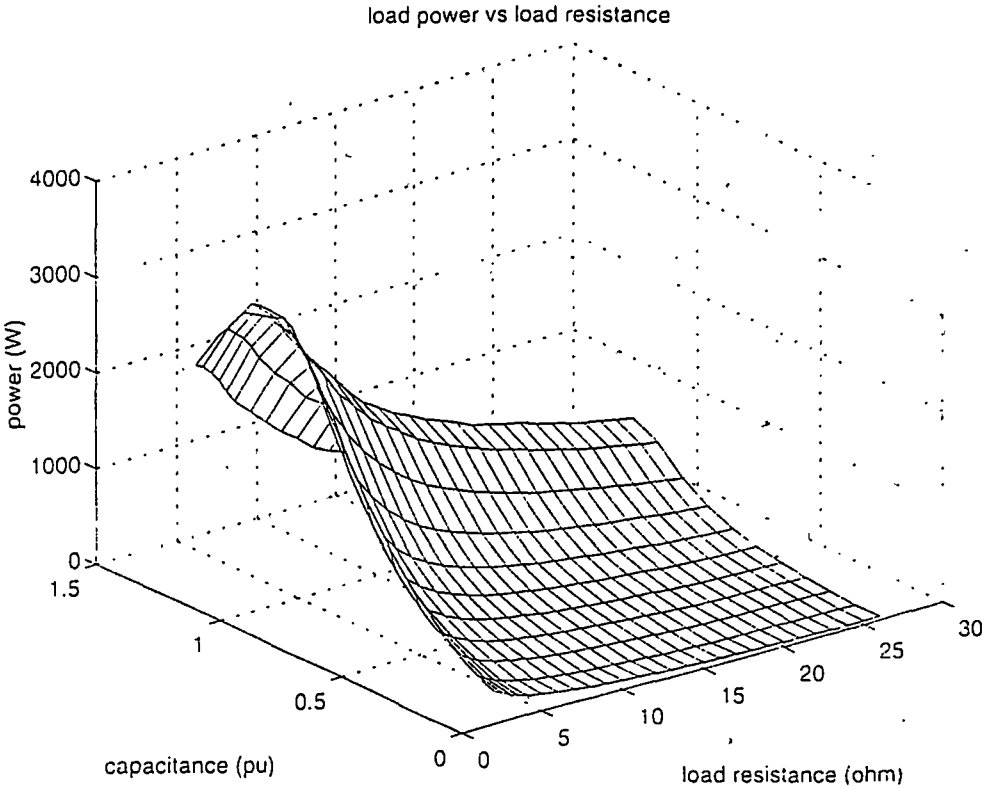

Figure 4.9 Characteristics of modular system simulation 1

(power vs. capacitance and resistance f=50 Hz)

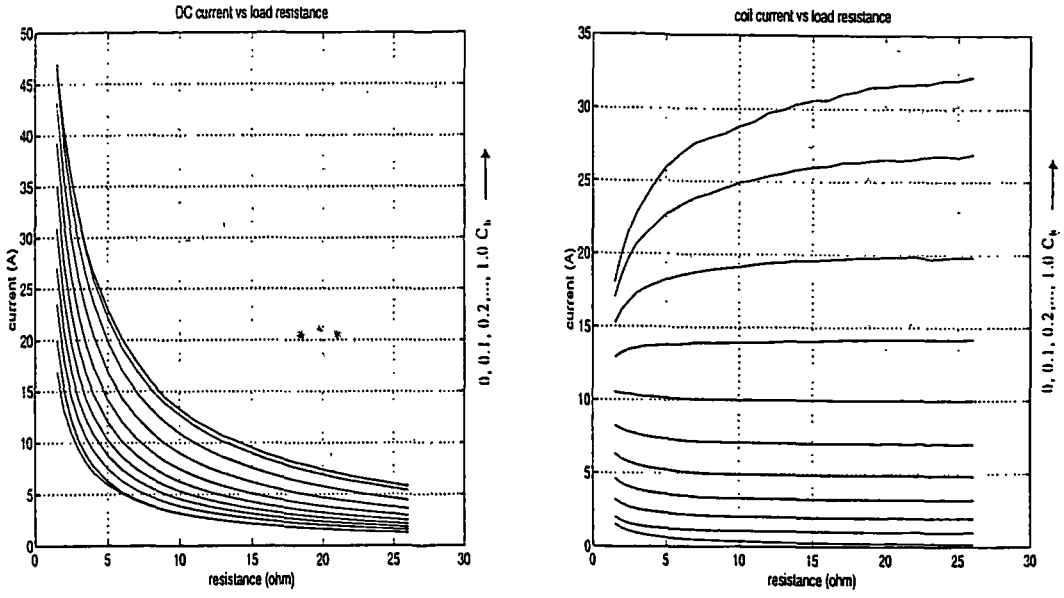

(a) (b)

Figure 4.10 Characteristics of modular system simulation 1 (a) (b)

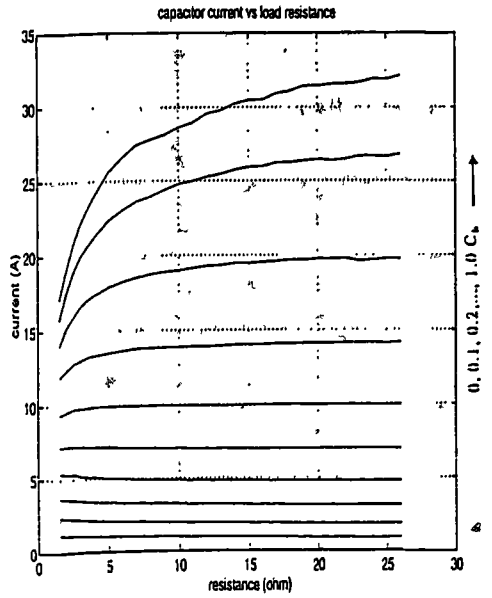

(c)

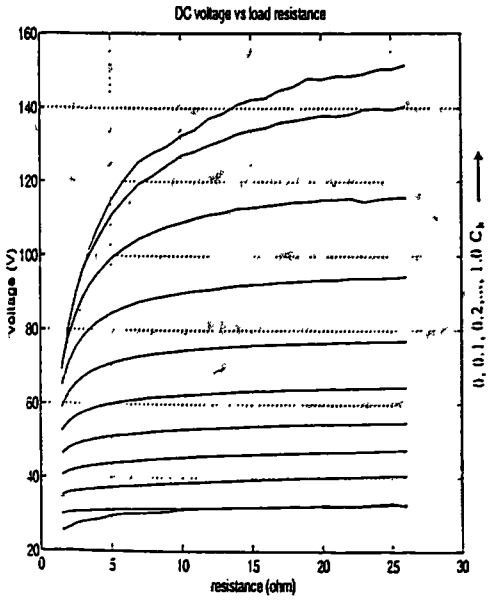

(d)

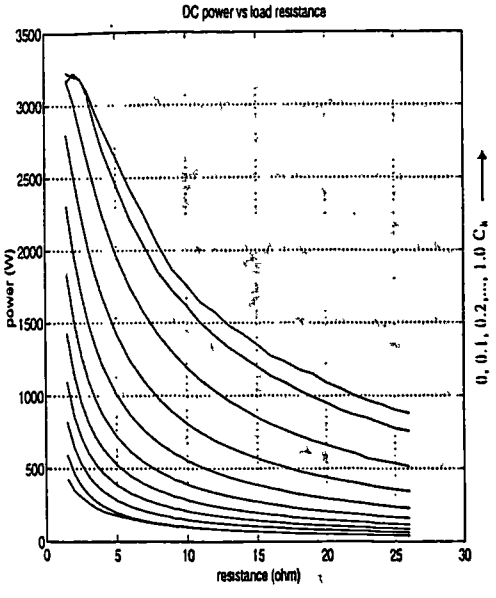

(e)

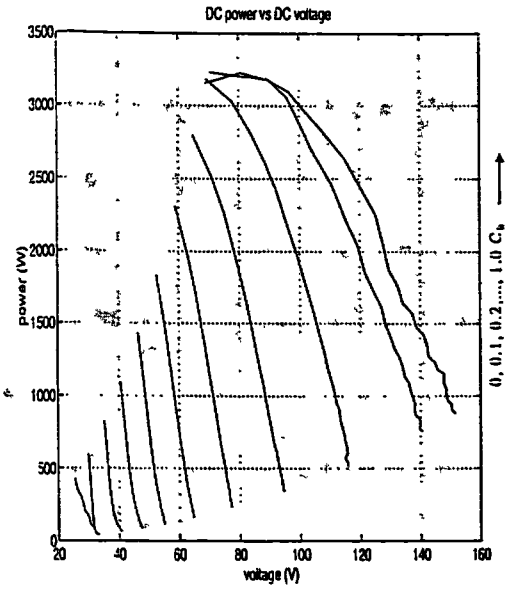

(f)

Figure 4.10 Characteristics of modular system simulation 1 (c) (d) (e) (f)

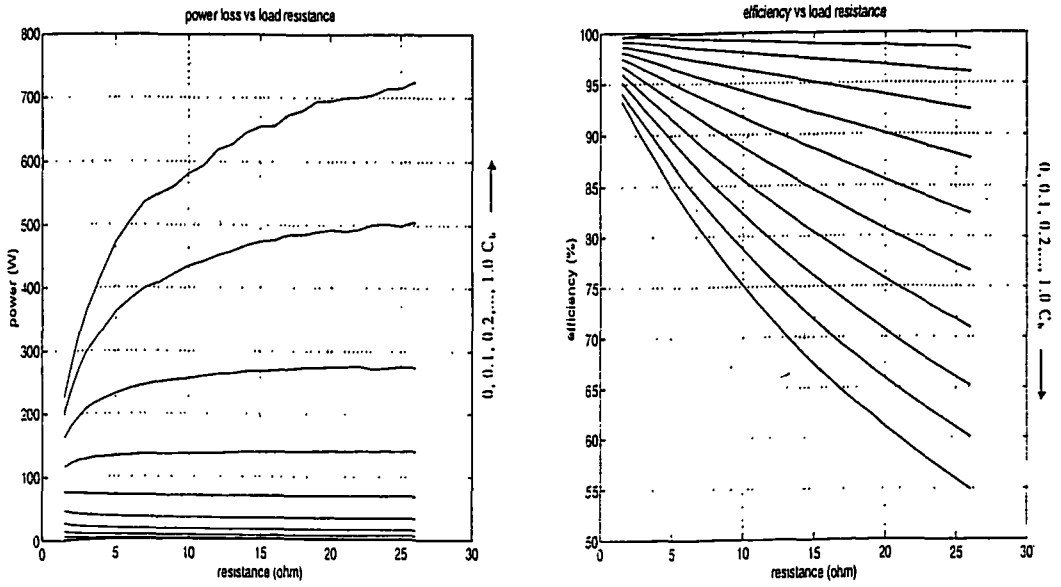

(g) (h)

Figure 4.10 Characteristics of modular system simulation 1 (g) (h)

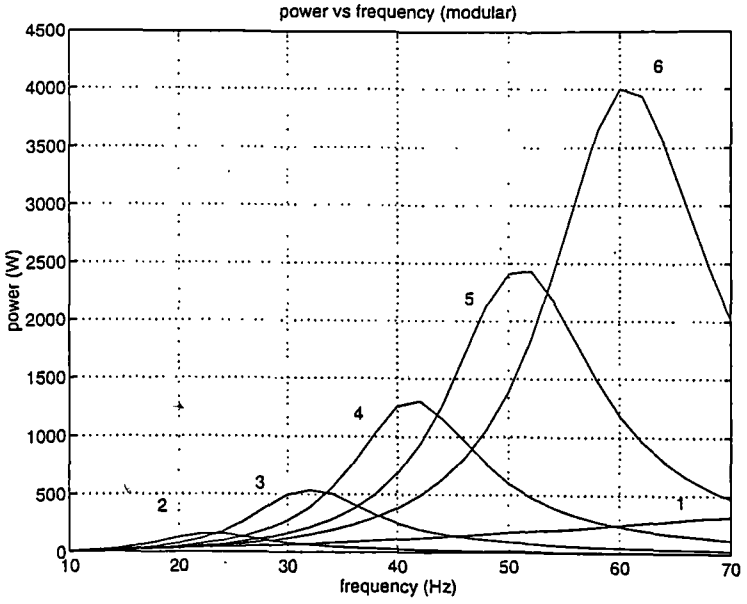

Figure 4.11 Characteristics of modular system simulation

(power vs. frequency R_{load}=5Ω)

4.2.3 Polyphase circuits simulation

In this section, all three polyphase circuits discussed in Chapter 3 are simulated and compared. Considering the founding of the above sections, a capacitor larger than 0.7 C_b would not be considered as a suitable choice, therefore the more practical capacitance will be chosen for the simulation studies.

Simulation circuit models

The circuit models shown in figure 4.8, 4.12 and 4.13 are used for simulation studies of Modular, Star and Mesh circuit configurations. The parameters are:

E_g = (rms) 25.2 V at 50 Hz, R_g = 0.7 Ω, L_g =10.28mH,

and the mutual inductance between the stator coils is ignored. The capacitance values used for this study are 100 μF , 200 μF and 400μF respectively corresponding to 0.106 C_b, 0.213 C_b and 0.425 C_b. for 50Hz (0.1509 C_b, 0.3017 C_b, and 0.6035 C_b for 60Hz). The simulation results are presented in the following sections.

Circuit waveforms

Figures 4.14 to 4.16 show the simulation circuit waveforms (40 Hz, C_{ac}=200μF 600W). In these figures, a reduction ratio of 1.0 is used for presenting all current waveforms, 0.5 for the voltage waveforms in Modular and Star circuit and 0.25 for the voltage waveforms in Mesh circuit. The curves are presented from top to bottom in the following sequence:

d.c. link voltage,
stator coil EMF,
ac capacitor voltage,
d.c. link current,
diode current,
a.c. capacitor current,
stator coil current.

The zero lines are:

coil current: 10; capacitor current: 20; diode and d.c. current: 30; voltages of Star and Mesh circuits: 60; voltages of Modular circuit: 80.

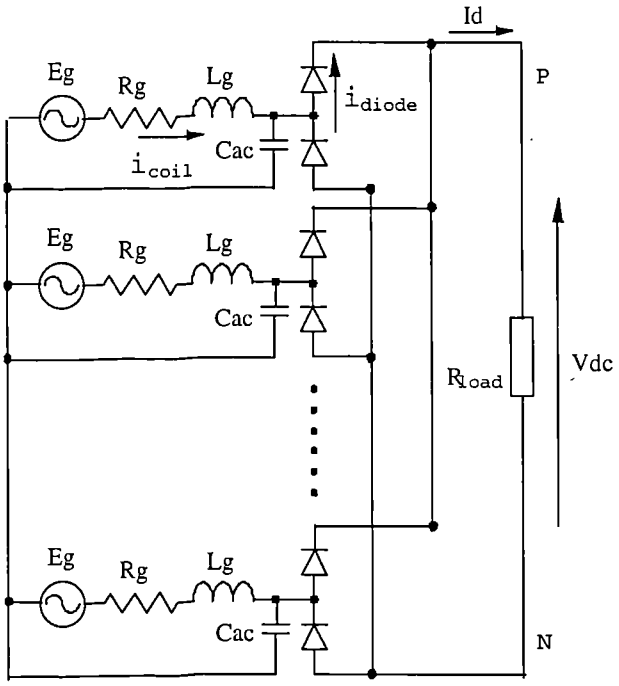

Figure 4.12 Star connection simulation model

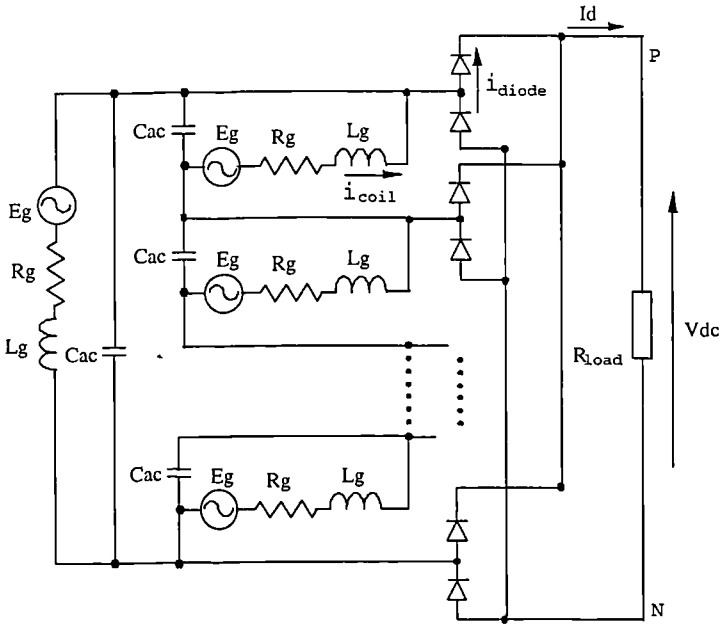

Figure 4.13 Mesh connection simulation model

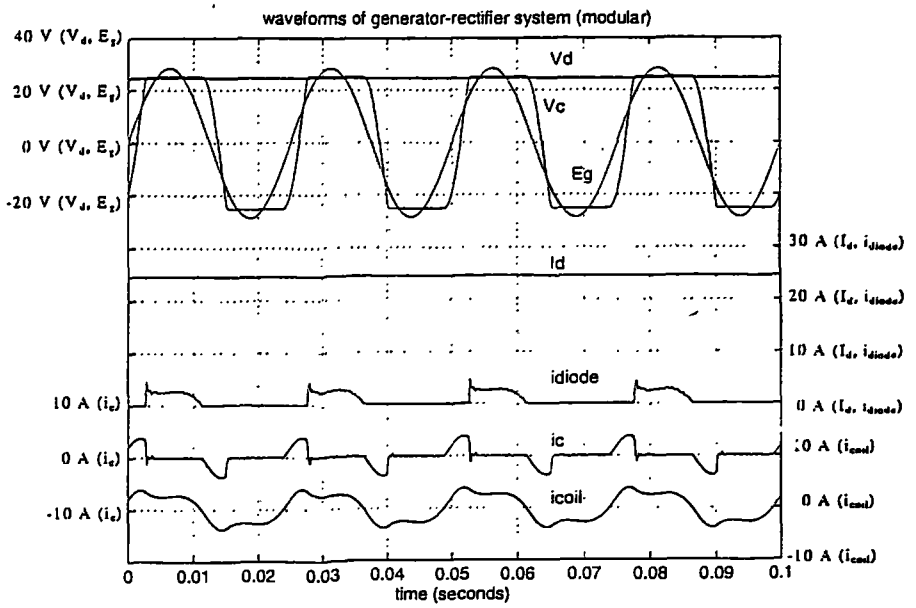

Figure 4.14 Modular circuit simulation waveforms

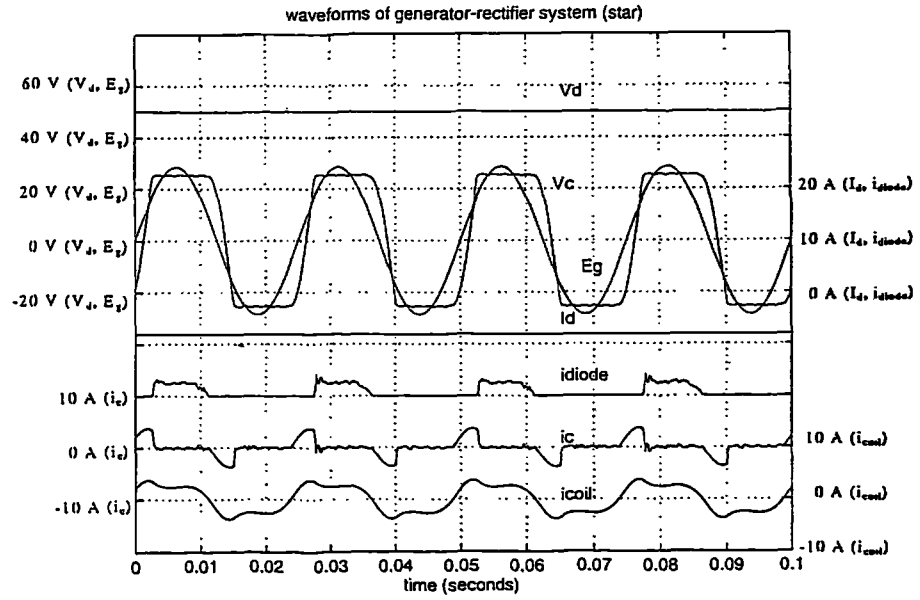

Figure 4.15 Star circuit simulation waveforms

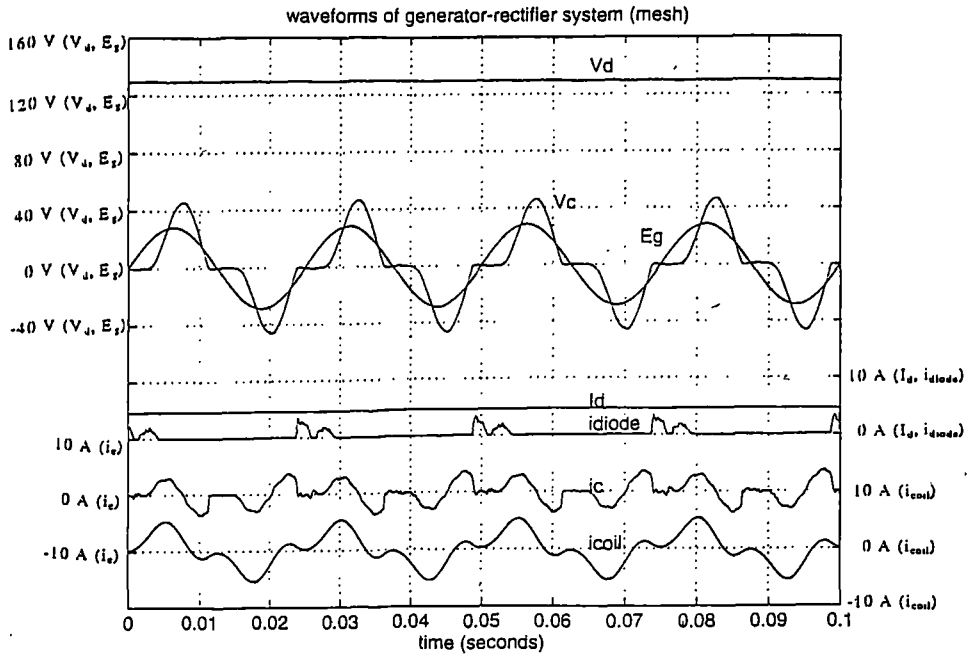

Figure 4.16 Mesh circuit simulation waveforms

Circuit characteristics

Figures 4.17 to 4.19 show the circuit characteristics (C_{ac}=200μF). They are

d.c. voltage (V) - load resistance (Ω)

d.c. power (W) - d.c. voltage (V)

d.c. current (A) - d.c. voltage (V)

stator coil current RMS (A) - d.c. voltage (V)

diode current RMS (A) - d.c. voltage (V)

a.c. capacitor current RMS (A) - d.c. voltage (V)

power loss(W) - d.c. voltage (V)

efficiency (%) - load resistance (V)

Each figure has five curves corresponding to the different EMF frequencies, form top to bottom 60 Hz, 50 Hz, 40 Hz, 30 Hz, 20 Hz respectively in figures (a)-(g). For the efficiency curves, figures (h), the sequence is reversed.

The power-d.c. voltage characteristics are given in figure 4.20, 4.21 and 4.22 for 50 Hz and different capacitance (0μF, 100μF, 200μF, 400μF).

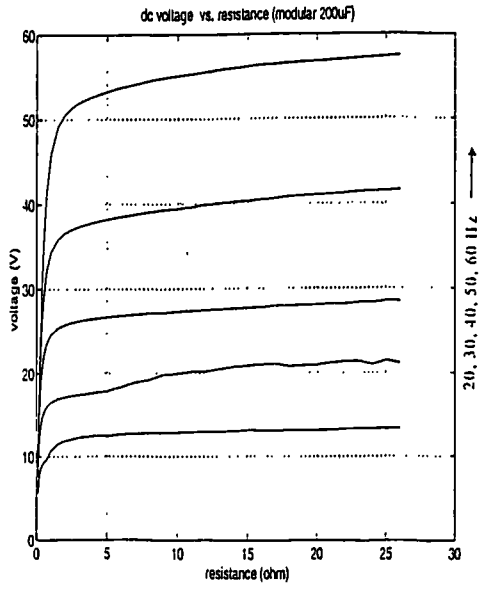

(a)

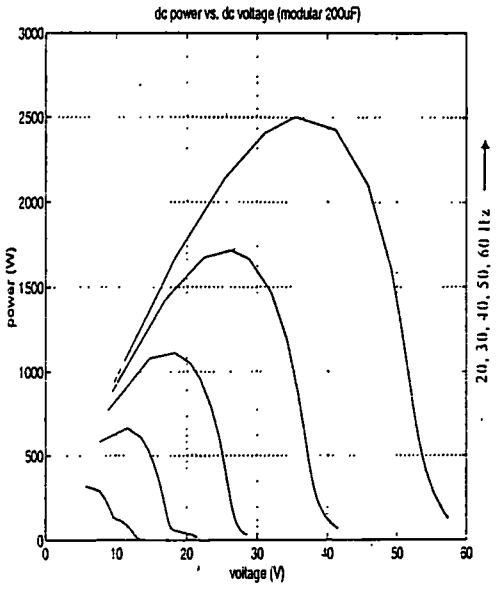

(b)

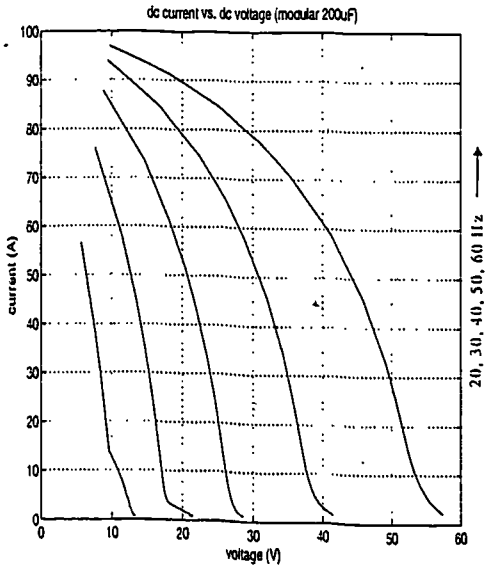

(c)

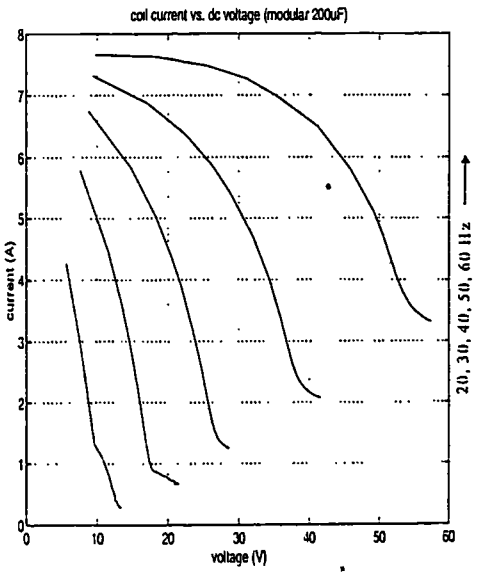

(d)

Figure 4.17 Modular circuit characteristics (a) (b) (c) (d)

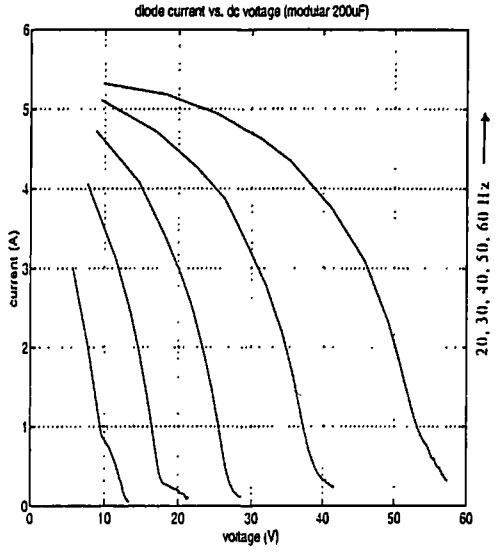

(e)

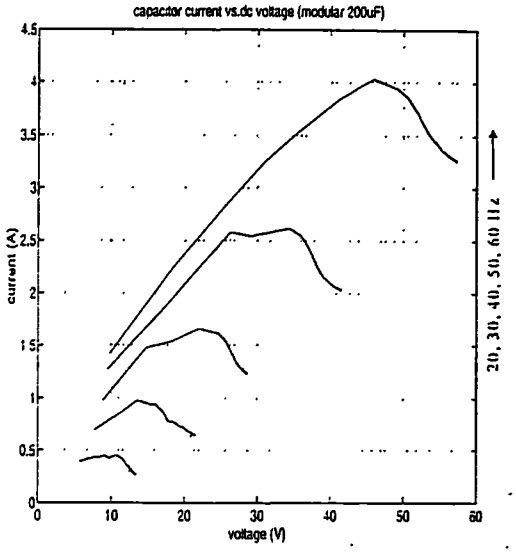

(f)

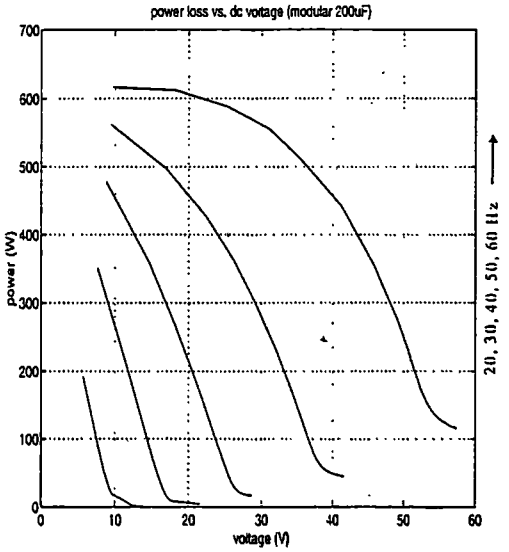

(g)

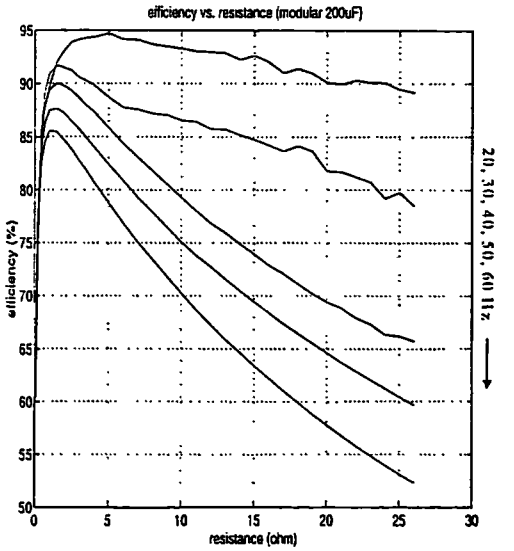

(h)

Figure 4.17 Modular circuit characteristics (e) (f) (g) (h)

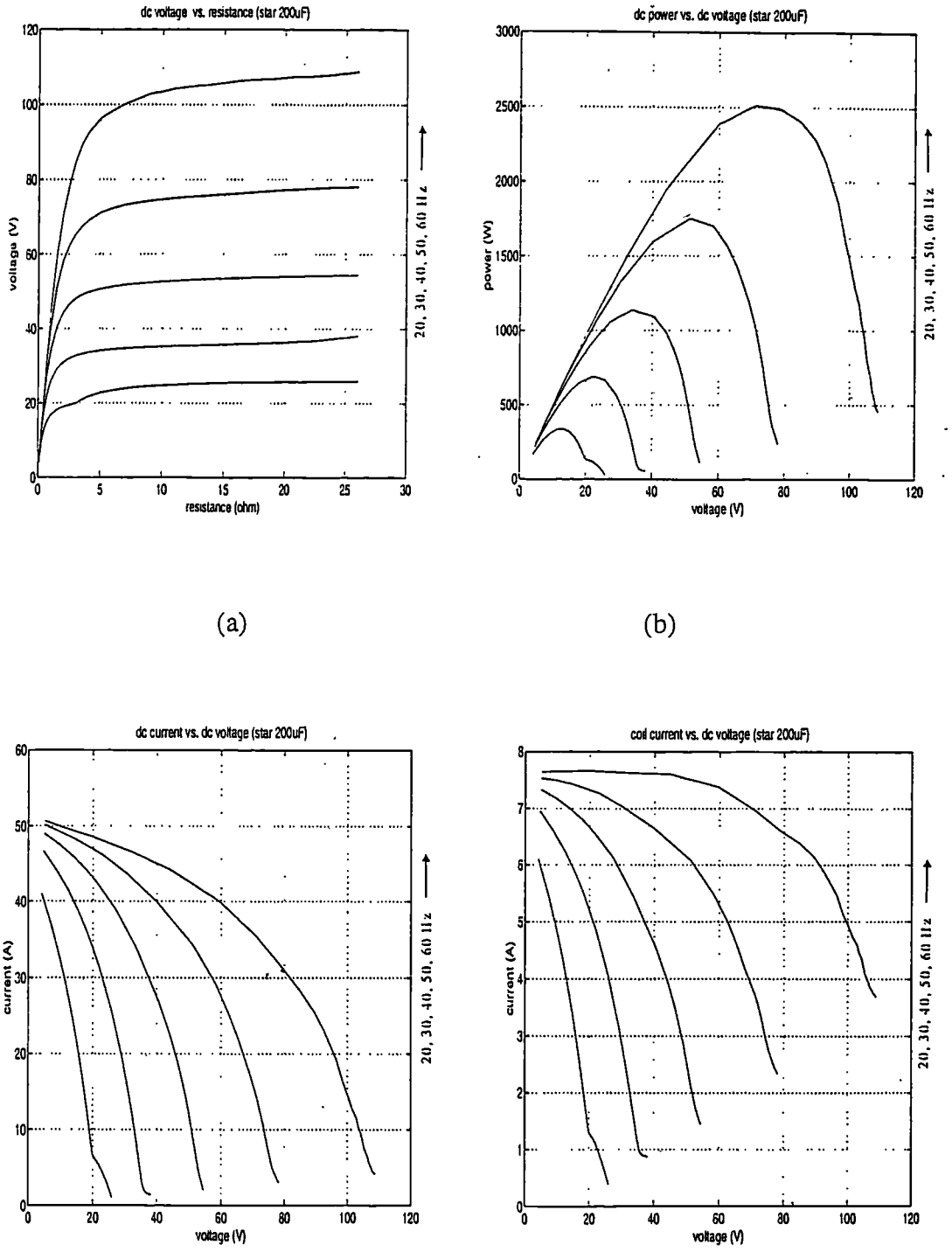

(a) (b)

(c) (d)

Figure 4.18 Star circuit characteristics (a) (b) (c) (d)

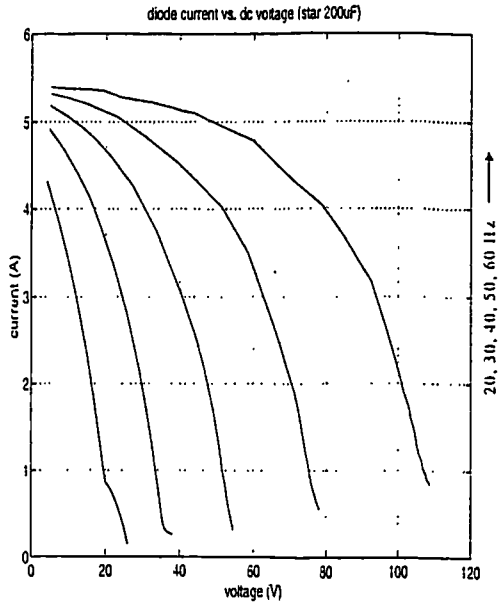

(e)

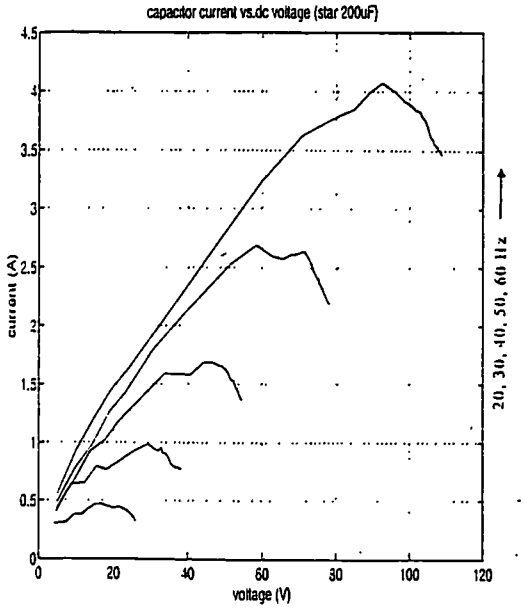

(f)

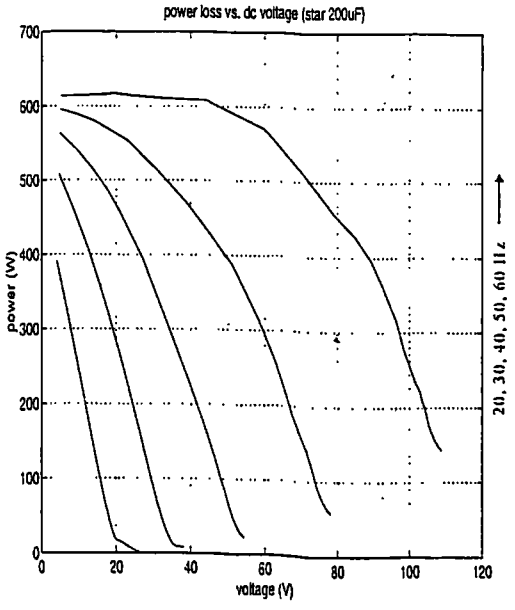

(g)

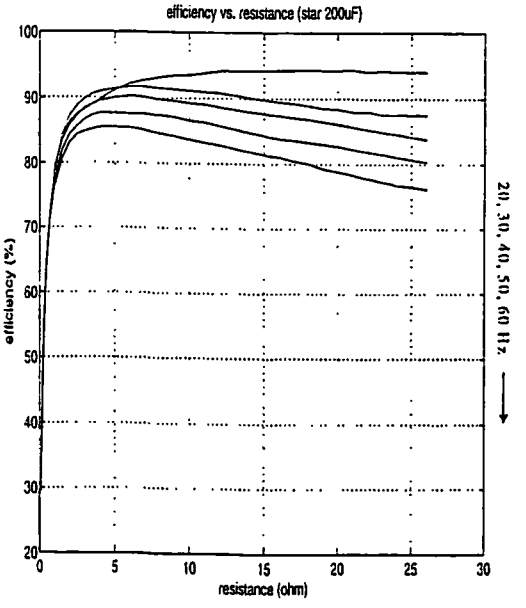

(h)

Figure 4.18 Star circuit characteristics (e) (f) (g) (h)

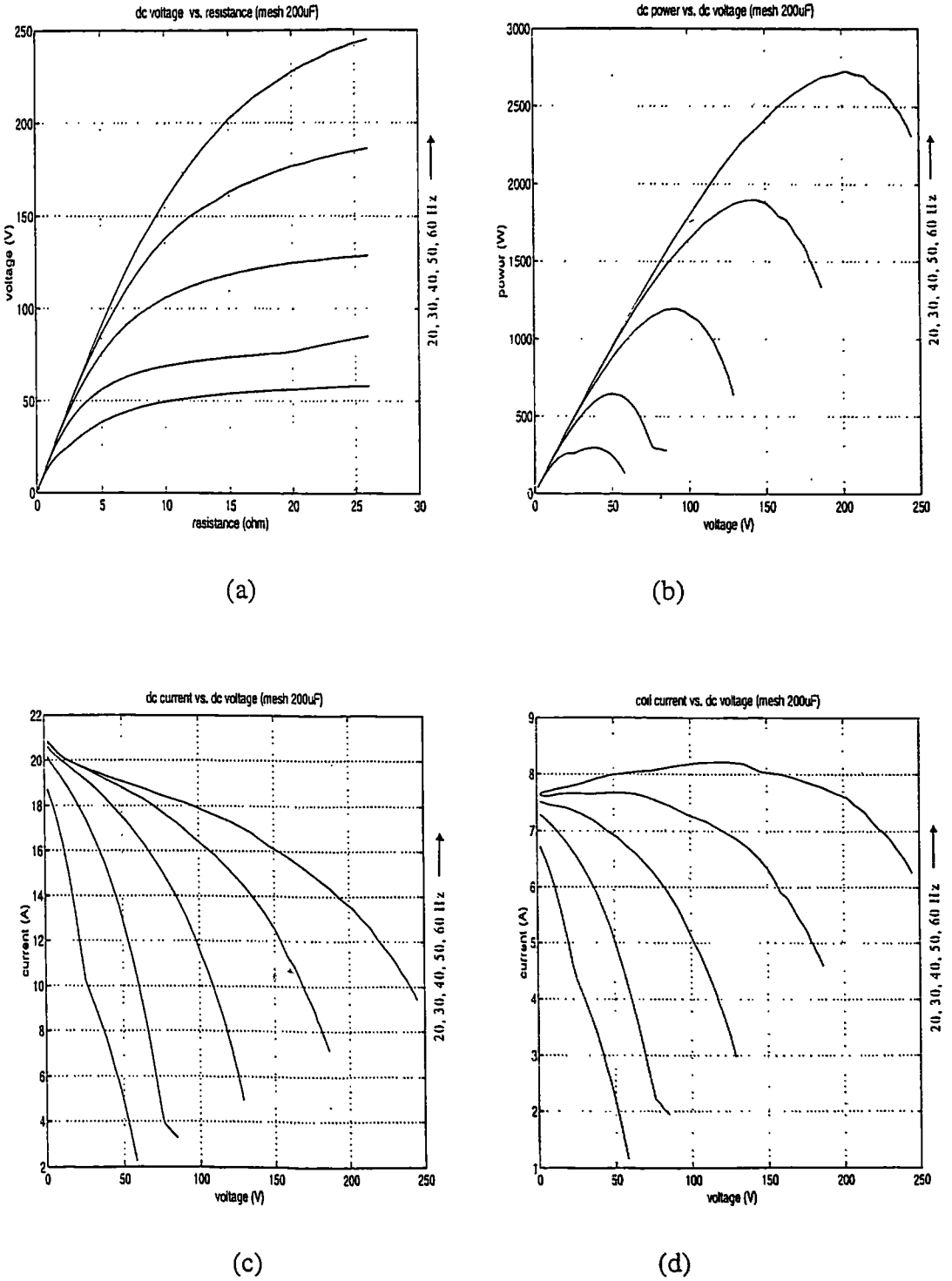

(a) (b)

(c) (d)

Figure 4.19 Mesh circuit characteristics (a) (b) (c) (d)

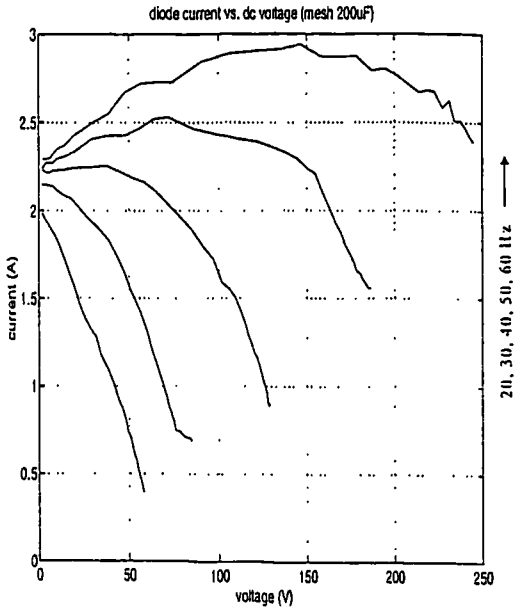

(e)

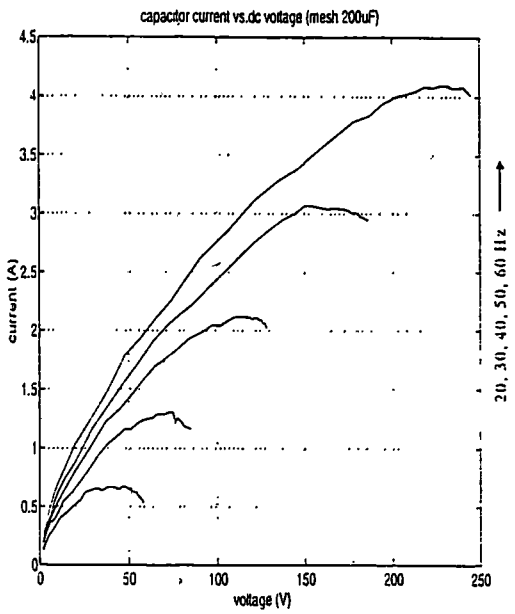

(f)

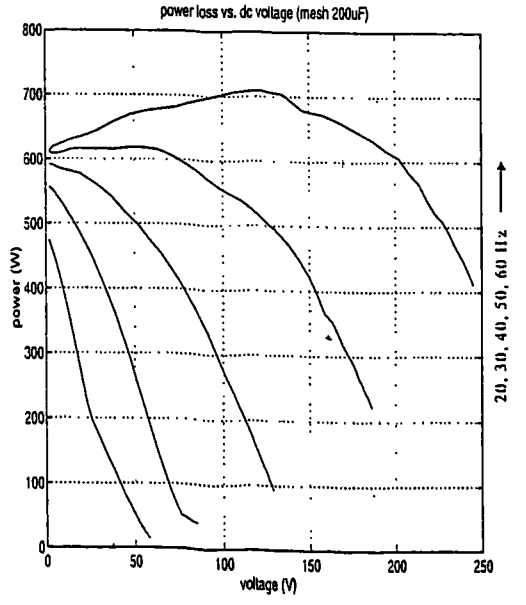

(g)

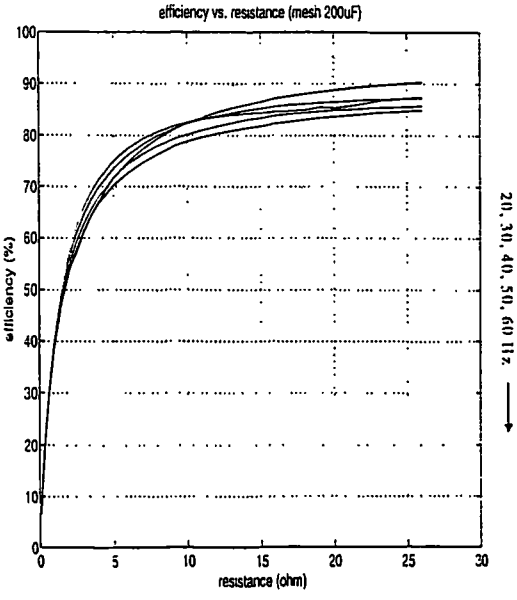

(h)

Figure 4.19 Mesh circuit characteristics (e) (f) (g) (h)

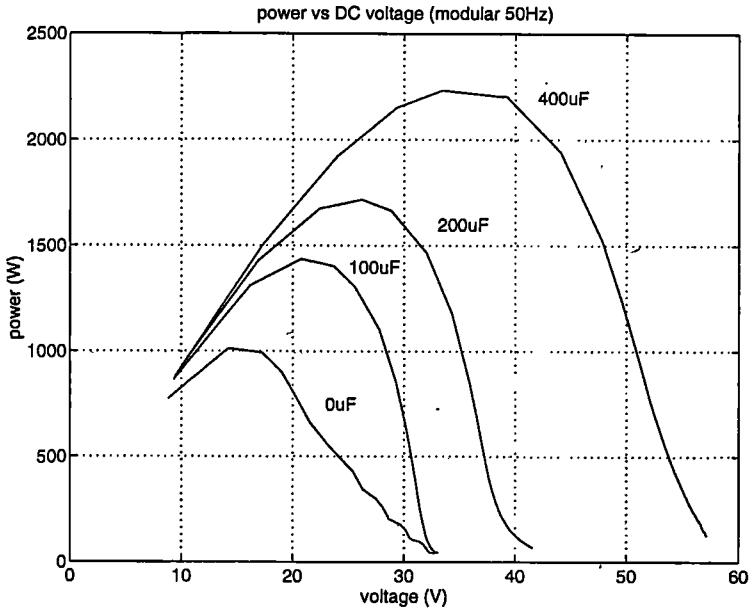

Figure 4.20 Modular circuit power-d.c. voltage characteristics

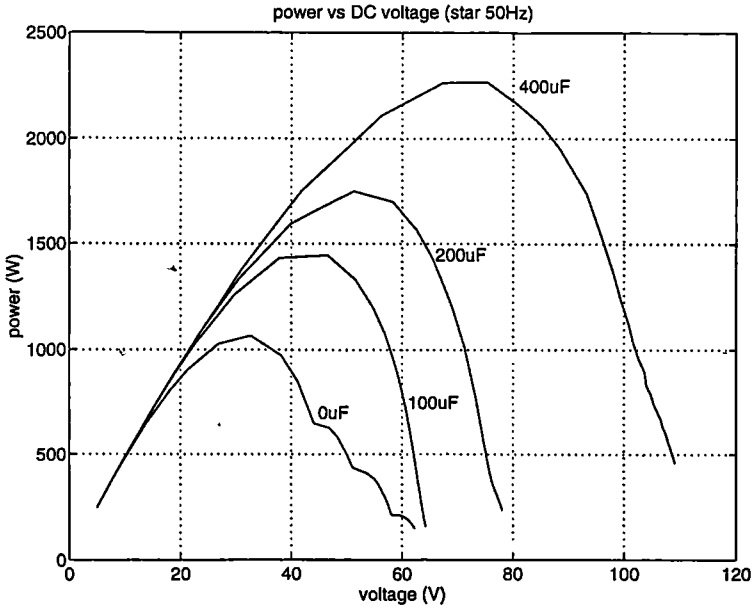

Figure 4.21 Star circuit power-d.c. voltage characteristics

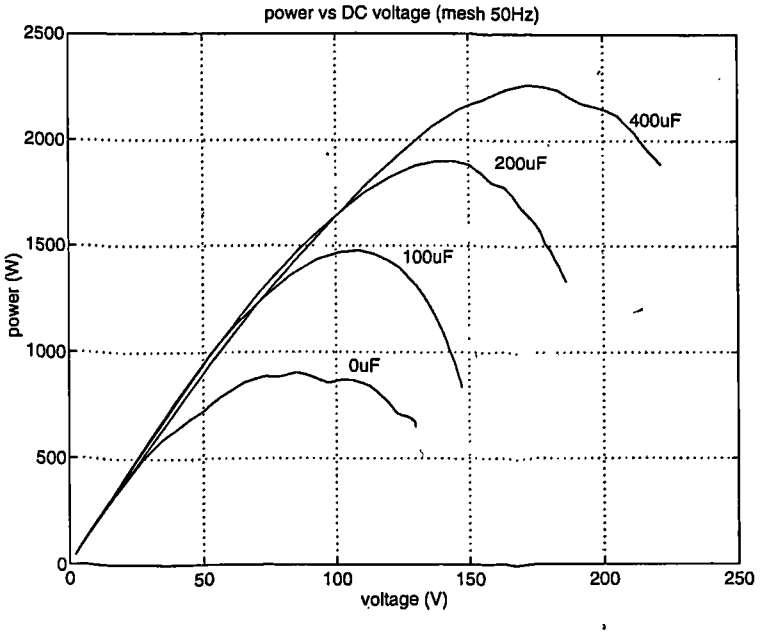

Figure 4.22 Mesh circuit power-d.c. voltage characteristics

4.2.4 Comparison of circuit behaviour

Circuit waveform analysis

From the simulated waveforms, it can be seen that all three circuits provide smooth d.c. link waveforms. The requirement for the filter at generator side of d.c. link is thus eliminated. Comparisons based on the same output power level follow.

The a.c. side, the stator coil and capacitor, has similar voltage and current waveforms in the modular and star connections, therefore the same rating of the components (a.c. capacitor and wire of the stator coil) is required. Compared with the modular circuit, the star circuit has double the d.c. voltage and half the d.c. current.

In the mesh circuit, the waveforms for the stator coil and the rectifier are quite different from the other two circuits. The a.c. capacitor experiences a higher voltage. The a.c. capacitor current waveforms are also different, since the capacitor is connected across two diode legs whose switching instants are influenced by other modules. When both upper diodes or both bottom diodes of the two legs conduct, the voltage of the capacitor

is zero. The current carrying period of the a.c. capacitor is longer. The diode current is provided by two stator coil and capacitor units as can be observed from the waveform. The mesh circuit presents the highest d.c. voltage and lowest d.c. current of the three considered circuits.

Circuit characteristic analysis

From the system characteristics, following features can be found:

The power output of the three circuits can be increased by connecting a.c. capacitor with the stator coil in parallel.

The maximum enhanced power outputs of these circuits have no significant difference. Still, the mesh circuit operates at highest d.c. voltage and lowest d.c. current, the modular circuit operates at highest d.c. current and lowest d.c. voltage. The d.c. voltage and d.c. current of the star circuit are between those two circuits.

For the studied case, the coil current, diode current and a.c. capacitor current in modular and star circuit have no significant difference. Mesh circuit has a slightly higher coil current and lower diode current.

All of the three circuits can be operated in the relative high efficiency range.

4.2.5 Summary of polyphase circuit studies

From the above simulation results, it can be concluded that

The system characteristics of a.c. capacitor connection in the polyphase stator coil rectifier systems have the similar pattern to that of the simple circuit discussed in section 4.1. Therefore the main conclusion from the simple circuit study could be used as a guide in polyphase system for power output enhancement technique implementation.

A larger capacitor will result in a lower maximum power which takes place at a lower frequency, though the higher power transfer before its output power peak is achieved.

By choosing the capacitance, the power-frequency characteristics can be changed, therefore, a suitable ac capacitor may result in the desired power -frequency curve in the practical frequency range. Then the system operation could be optimised based on the modified characteristics.

The modular circuit needed more diode components than star and mesh circuits, the a.c. capacitor in mesh circuit may experience higher voltage than star circuit and therefore the cost may be higher. However, a complete system design would be to a specified d.c. link voltage and appropriate module designs for the three circuits would have different numbers of turns and hence voltage and current ratings. An overall evaluation would be based on the requirements of the practical system.

4.3 Experimental Studies

4.3.1 Experimental model

Tests have been carried out using the laboratory model described in Chapter 3. The modular electrical arrangements are adopted where ac capacitors are connected at ac terminals of stator coils. The schematic diagram of the system for capacitor connection test is shown in figure 4.23.

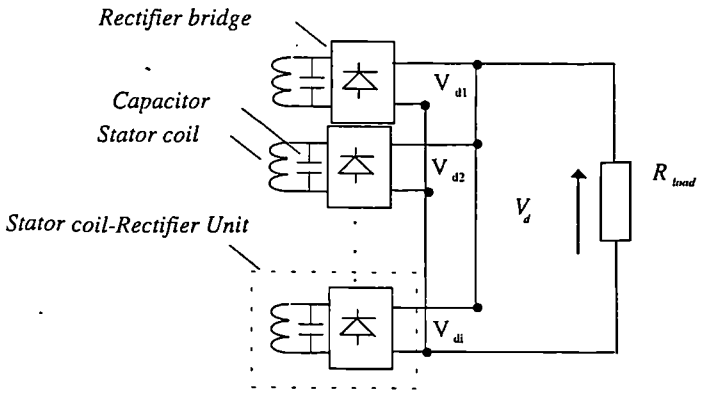

Figure 4.23 Experimental system schematic diagram

4.3.2 Experimental study

The experiment was performed by varying the generator speed to produce varying frequency EMF (20, 25, 30, 35, 40, 45 and 50 Hz) at various resistance and different capacitance (400, 200 and 100 μF) under the power rating limit of the driving system. The stator coil current, output dc current of single stator coil-rectifier unit, capacitor current, DC link voltage and DC link current were measured. The typical waveforms and system characteristics are presented as follows.

Circuit waveform

Figure 4.24 shows a group of the test circuit waveforms, they are at 1 Ω load resistor and 40 Hz operating condition and plotted with the following ratio:

rectifier bridge ac terminal voltage, (1: 530)

stator coil current, (2 A/10 mV)

output dc current of stator coil-rectifier unit, (2 A/10 mV)

ac capacitor current, (2 A/10 mV)

It can be seen that the experimental waveforms are in good agreement with simulation waveforms (figure 4.14).

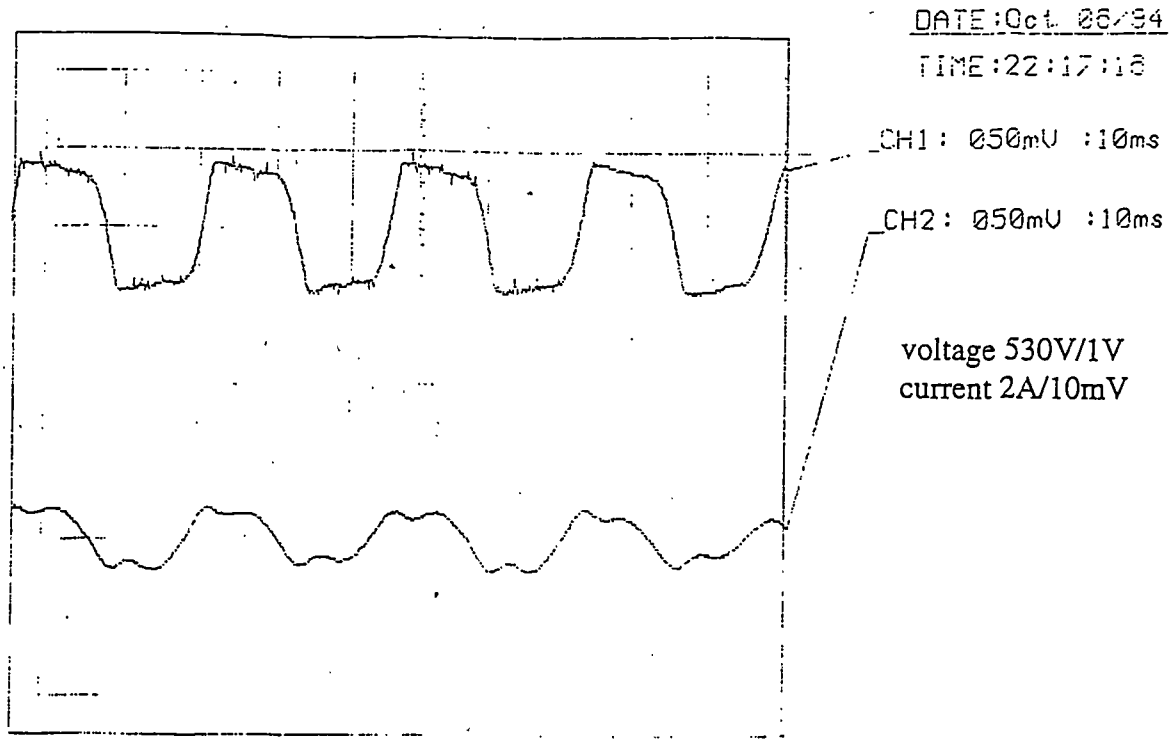

(a) rectifier ac terminal voltage (ch1) and coil current (ch2)

Figure 4.24. experimental waveform (Modular 40 Hz R_{load}=1.0 Ω, C_{ac}=200μF) (a)

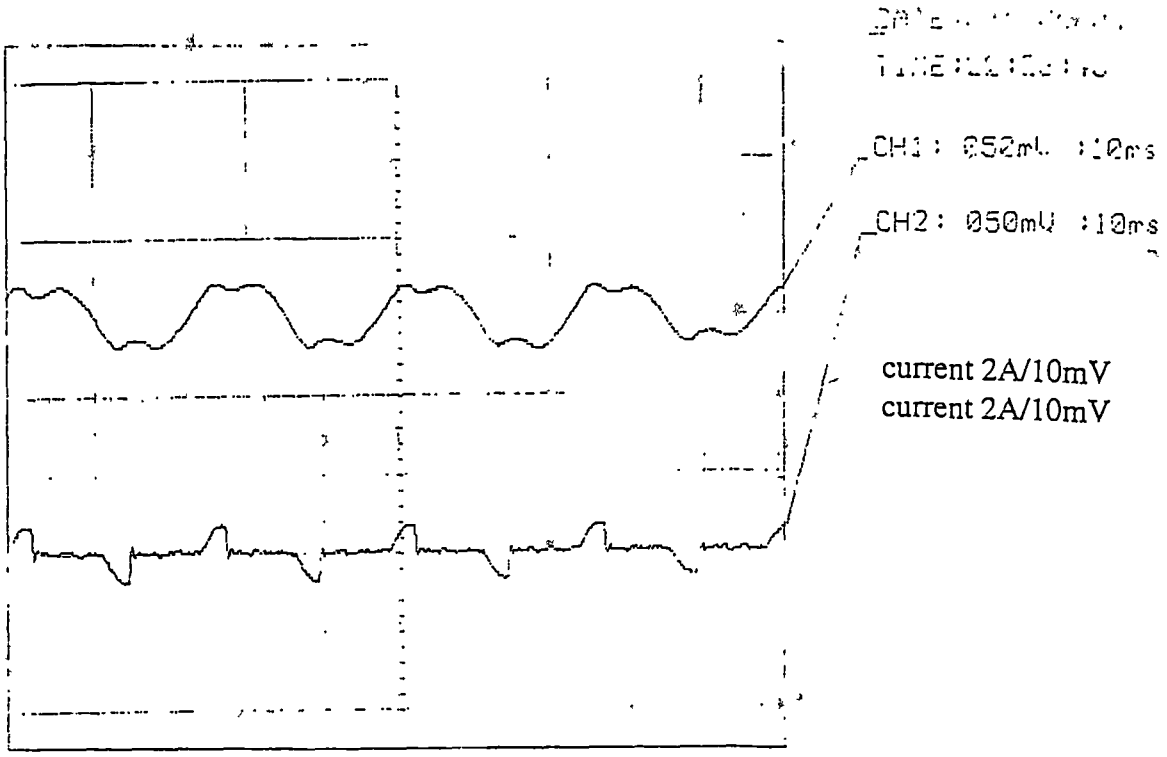

(b) Coil (ch1) and capacitor (ch2) currents

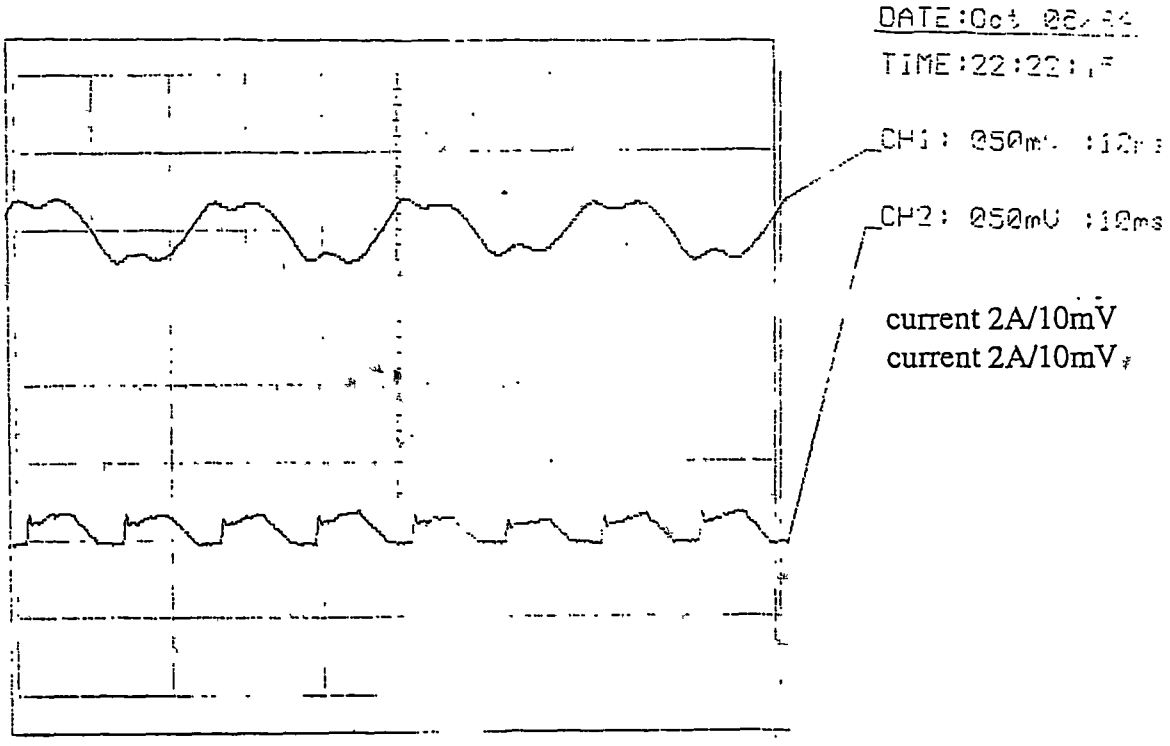

(c) Coil (ch1) and rectifier output (ch2) currents

Figure 4.24. experimental waveform (Modular 40 Hz R_{load}=1.0 Ω, C_{ac}=200μF) (b) (c)

System characteristics

The power-frequency characteristics (R_{load}=1.0 Ω and 2.5 Ω) are presented in figure 4.25 and figure 4.26 where the curves correspond to at 400 μF, 200 μF, 100 μF, and no capacitor. The experiment results are marked by symbols (o, x, + and *).

The results show that the relation between power and frequency is nearly a linear curve without a capacitor in circuit. With the capacitor present, the power transfer is increased particularly at higher frequency. Therefore it is possible in principle for the wind turbine to match the wind power characteristics by following the maximum energy capture curve.

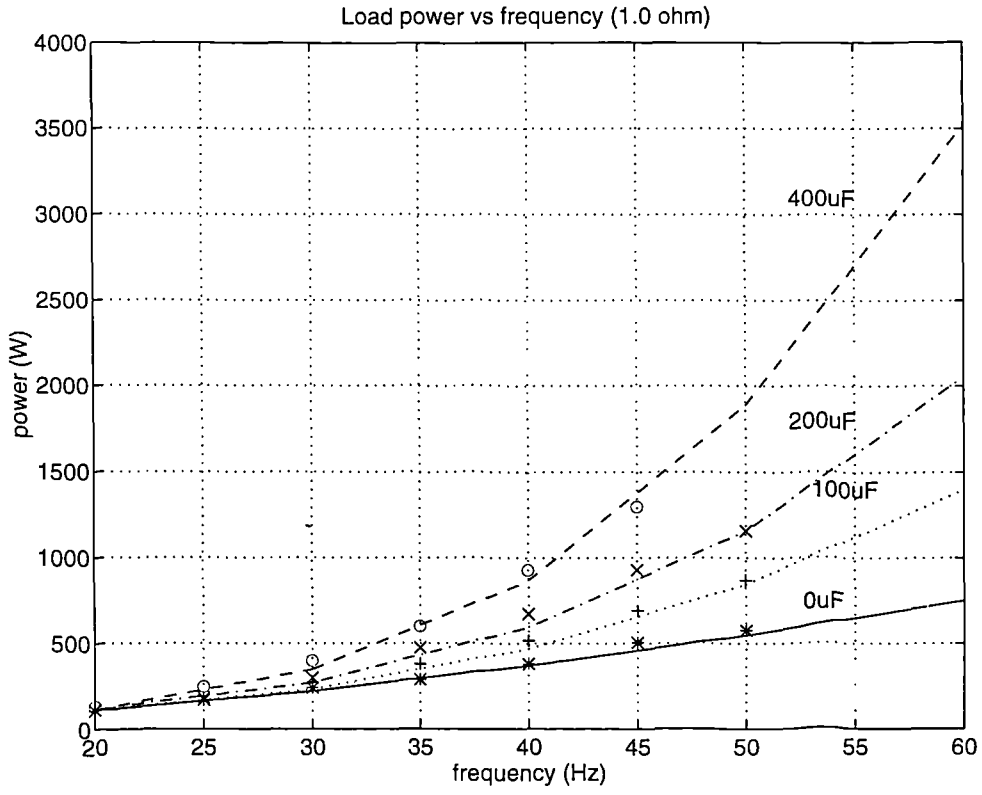

Figure 4.25 power -frequency characteristic (Modular R_{load}=1.0 Ω)

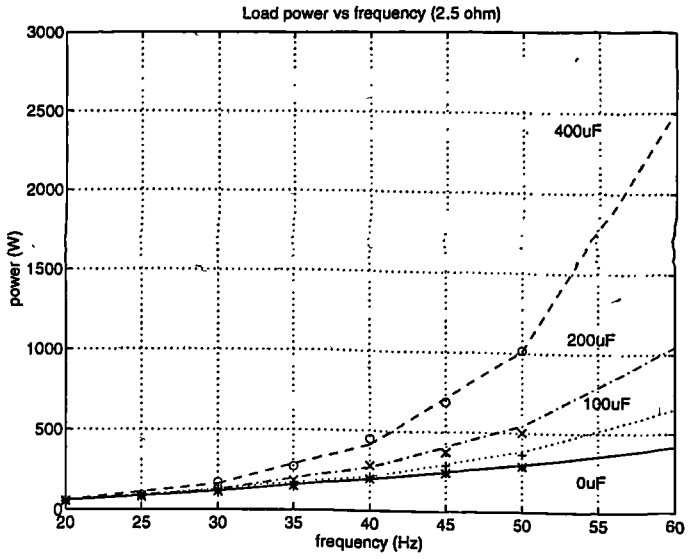

Figure 4.26 power -frequency characteristic (Modular R_{load}=2.5 Ω)

4.4 The Steady State Model Of Polyphase Modular PM Generator-Rectifier System (Including AC Capacitor)

It is hoped that the Thevenin equivalent circuit shown in figure 3.23 can still be used for simplified steady state performance analysis in the a.c. capacitor connection case.

Comparing the system characteristic in section 4.2 with that in Chapter 3, it can be found that the V_d - I_d curves have similar patterns, therefore the polynomial fitting technique is used to find the parameters of the equivalent circuit. Again, it is found that the cube curve can fit these characteristics quite well. Therefore for a certain frequency, E_{eg} is a constant and R_{eg} is a function of I_d.

The resulting characteristics of such an equivalent circuit is shown in figure 4.27, 4.28 and 4.29 for Modular, Star and Mesh circuits respectively where solid lines are the results of equivalent circuit and dash lines are the simulation results from top to bottom, corresponding to 60 Hz , 50 Hz, 40 Hz, 30 Hz, 20 Hz respectively. It can be seen that the results from the equivalent circuit model are very close to the simulation results. Therefore the simple circuit model shown in figure 3.23 can replace the poly-phase PM generator-rectifier system for steady system analysis.

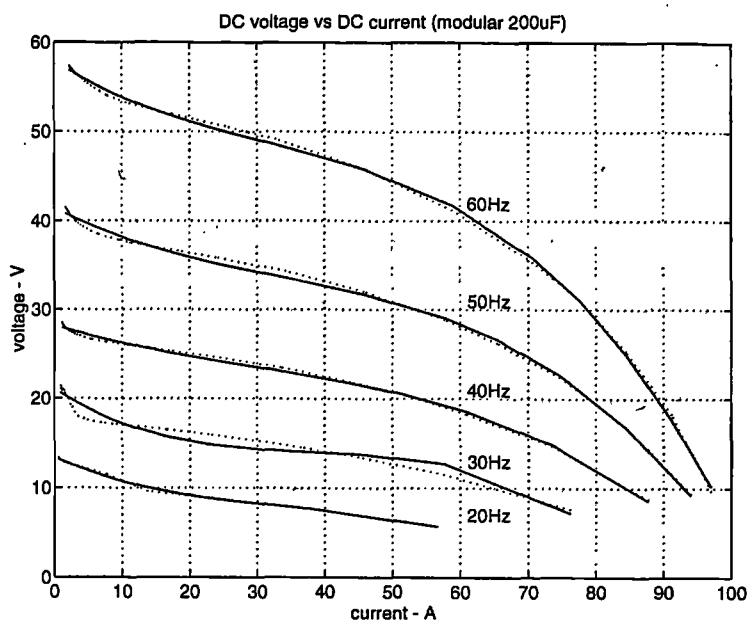

Figure 4.27 V_d - I_d characteristics (Modular 200 μF ac capacitor)

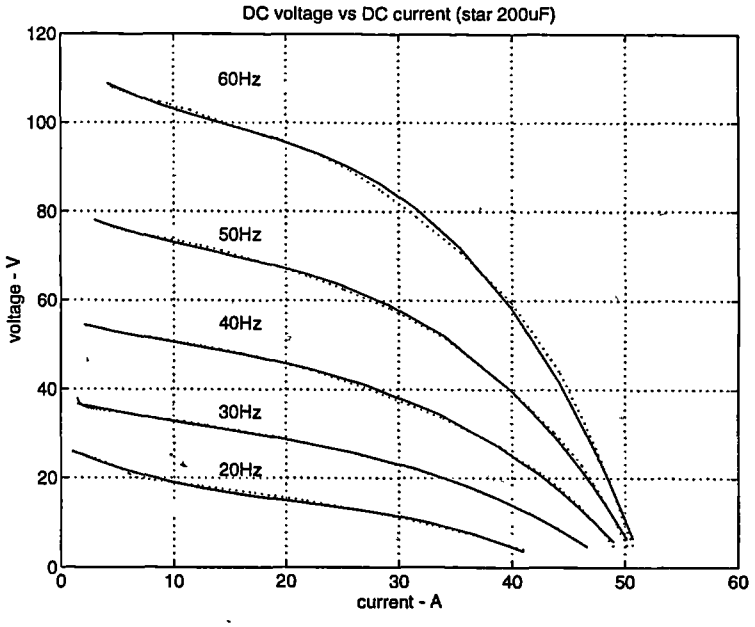

Figure 4.28 V_d - I_d characteristics (Star 200 μF ac capacitor)

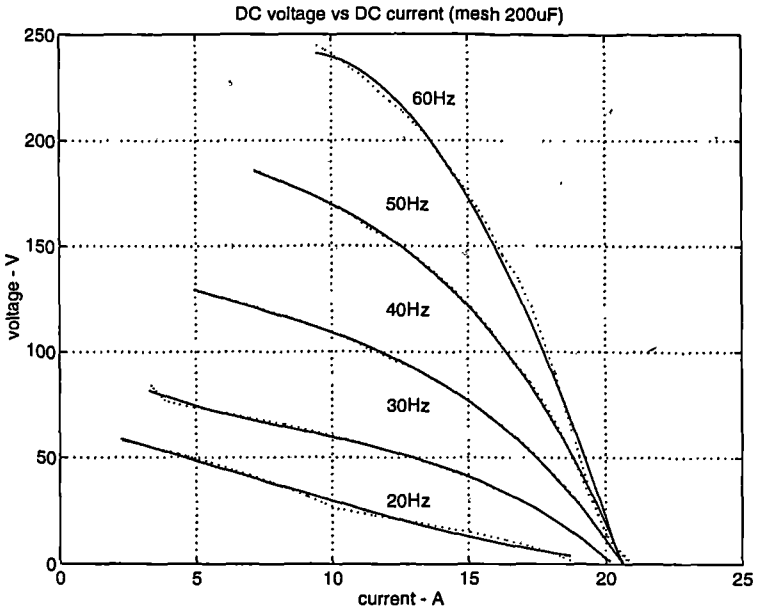

Figure 4.29 V_d - I_d characteristics (Mesh 200 μF ac capacitor)

4.5 Discussions

The a.c. capacitor connection technique for increasing the power output of a power source have been detailed as above. Some considerations of this technique are discussed and a procedure to implement this technique is suggested in this section.

A.C. capacitance

It is not desirable to choose a capacitor larger than the value which makes the $|K_C|$ reach the maximum at the highest possible operating frequency. Otherwise, the maximum possible power transfer could occur at a frequency below the highest maximum operating frequency. Consequently, an oversized capacitor will result in reduction of the power transfer at high frequency. From efficiency considerations, it is preferred that the capacitor is less than 0.7 C_b calculated at the maximum operating frequency.

Internal inductance of stator coil

The a.c. capacitor connection aims to compensate the effect of internal inductance in the power source. If the internal inductance is high, a small a.c. capacitor can have significant effect on the power transfer capacity. On the other hand, should the internal

inductance be very small, only a big ac capacitor may effectively result in the power transfer increasing (Equation 4.15 and section 4.1) but the capability may be adequate without capacitance. Therefore the economic feasibility of the technique should be studied by taking the particular circumstances into account.

Possible design procedure

Followings are suggested steps to design the modular PM generator-rectifier system with ac capacitor connection:

1. decide the capacity, maximum power output and the operating frequency of the generator.
2. carry out the generator design, obtain the machine parameters (R_g, L_g and E_g).
3. choose a capacitor based on the calculation of C_b.
4. calculate the power-frequency characteristics based on the above design particulars and compare with design specifications.
5. calculate the operating loss, efficiency and cost.

The step 2 to step 5 may be repeated by redesigning the generator and/or adjusting the capacitance until an optimal design is obtained.

4.6 Conclusions

The power delivery capability of the modular PM generator could be limited due to the internal inductance, especially at higher frequencies. However, capacitors connected at the ac terminal of the rectifier could compensate this effect and increase the power output capability.

In this chapter, the a.c. capacitor compensation technique has been discussed. The principles of power transfer improvement have been analysed. The results of the experimental and simulation are in good agreement and have demonstrated significantly increased output power.

The similarity of the characteristics of the simple a.c. circuit and poly-phase rectifier system using a.c. capacitor connection technique has been shown. Therefore, the results

obtained from the simple a.c. circuit may be used as a guide to implement this technique and design the system for both a.c power source and a.c. power source-rectifier circuit if output power limited by internal reactance needs to be enhanced.

Different stator coil circuit connections have been simulated, for given module emf and impedance, similar power transfer has been observed, where mesh circuit operates at highest d.c. voltage and lowest d.c. current and modular circuit at highest d.c. current and lowest d.c. voltage, star circuit between these two for given module emf and impedance.

The equivalent circuit of whole generator -rectifier system has been developed further to include the ac capacitor's effects.

Based the a.c. capacitor connection, the desired power-frequency characteristic could be obtained, and therefore an optimal operation trajectory could be decided to capture the maximum power from the wind.

Based on the obtained characteristics, the system can also be evaluated on the capital investment and operating cost for the optimal system design.

Chapter

5.

Voltage Source Inverter for Grid Connection

The grid side inverter is a very important device in the power conversion system. Firstly, the PM generator and diode rectifier system have no active control ability, the dc link voltage and current have to be varied over a wide range with the wind speed for maximising power capture, which can only be realised by regulating the loading of the rectifier through control of the inverter. Secondly, it is desirable for the power conversion system to send the optimal power in to the network with controllable power factor or voltage and to have a harmonic performance satisfying the system requirement. Finally, the high efficiency and low capital cost which is vital for the economic viability of the entire system. The grid side inverter, as a major component, must possess the above features.

In this chapter and the next, power electronics inverters and their relevant operation characteristics are discussed. The power control principles and strategies are presented, and effects on the network are investigated. The voltage source inverter (VSI) is addressed in this chapter and the next chapter is devoted to current source inverter (CSI). Promising types of inverters are chosen for the further investigations.

5.1 Power Electronics Semiconductor Devices

The first thyristor, or silicon-controlled rectifier (SCR), was developed in late 1957. Until 1970, the conventional thyristor has been exclusively used for power control in industrial applications. Since 1970, various types of power semiconductor devices have been developed and became commercially available. In this section, the major power electronics semiconductors are briefly discussed.

A conventional thyristor (SCR) is a turn on only device. It can be turned on by a positive gate current pulse, but once the device is on, the turn-off is only possible by reducing the load current to zero, using the ac line voltage in the load, or by an auxiliary transient circuit (commutation networks). SCRs were used in the earliest developed inverters because they were the only device available and are exclusively used in high voltage direct current (HVDC) transmission systems. Various types of SCR are commercially available, such as phase-control SCR, inverter-grade SCR and light-activated SCR etc. and can be chosen on the basis of the application requirement for the power rating, switching speed and triggering methods.

Semiconductors which can be turned on and turned off are also called controllable or self-commutated switches. Commonly used controllable switches include:

A gate turn-off thyristor (GTO) can be triggered into conduction by a small positive gate-current pulse and also has the capability of being turned off by a negative gate-current pulse (a 1:3-1:5 ratio of gate current to load current), it requires more complex gating circuitry than an SCR and has a slightly higher on-state voltage (2-3V). Currently, GTOs have the highest power capacity in the self commutated semiconductor family.

The bipolar junction transistor (BJT) is a two-junction self-controlled device with asymmetrical voltage blocking. BJTs can be switched much faster than SCRs, but they are current controlled devices therefore require continuous base current during the conduction period, the base current has to be carefully controlled in magnitude to keep the transistor just into saturation. The Darlington arrangement of the transistor considerably reduces the base drive requirements at the expense of slightly increasing the switching times and higher on-state voltage.

The Metal-Oxide-Semiconductor Field Effect Transistor (MOSFET) is a voltage-controlled, majority carrier device. If the gate voltage is positive and beyond a threshold

value, the device will conduct. No gate current flows except during transitions. The MOSFET is a fast switching device and is used in inverters at the lower power ratings due to its higher conduction voltage drop. Being a voltage-controlled device, the gate firing controls of power MOSFET are simple and it is possible to implement the gating controls directly from microelectronics circuits.

The insulated gate bipolar transistor (IGBT) is a MOS-gated turn on/off bipolar transistor. Being minority carrier devices, IGBTs have superior conduction characteristics, while sharing many of the appealing features of power MOSFETs, such as ease of drive, wide safe operating area (SOA), peak current capability and ruggedness. The IGBT has a power handing capability comparable to that of BJT and more attractive control features than the thyristor family. With higher switching speed than the BJT and higher power capacity than the MOSFET, this device is being increasingly used in inverters.

An MOS-controlled thyristor (MCT) can be turned on or off by a pulse on the high impedance MOS gate. The device has asymmetric voltage blocking capability. It has comparable switching speed to IGBT, but has a lower conduction drop. The high voltage MCTs require much simple gate drive and have faster switching speed than GTOs and hence are being developed as a direct replacement of high voltage GTOs. However, it has not yet become widely available commercially.

Although the semiconductors could be connected in series and parallel to handle the high power, the multi-device connections need the additional circuitry to ensure correct sharing of voltage and/or current. At present, the SCR is normally used for the high power, line commutated converters, the GTO for high power, self commutated converters, the IGBT and BJT for medium power and frequency applications and the MOSFET for low power, high frequency converters.

For the present application, SCR, GTO, IGBT and BJT may be considered. However, the choices also depend on the inverter circuit configuration which can be basically classified into voltage source inverters (VSIs) and current source inverters (CSIs).

5.2 Typical VSI Circuits And Switching Modes

5.2.1 Circuit configuration

The basic structure of a six pulse three phase voltage source inverter is shown in figure 5.1 where, for simplicity, snubber circuits are not shown. There are three inverter legs, each consists of two valves. Each valve includes one self-commutated semiconductor or the combination of several such devices and the inverse parallel connected diode. The term 'voltage source inverter' implies that, over the time period of one cycle of the a.c. waveform, the voltage change at the inverter d.c. side is negligible. The d.c. voltage is usually supported by a capacitor placed across the d.c. link. The capacitor is a reservoir of electric energy, charging or discharging as necessary to ensure that transient and switching events within the inverter do not significantly change the d.c. link voltage.

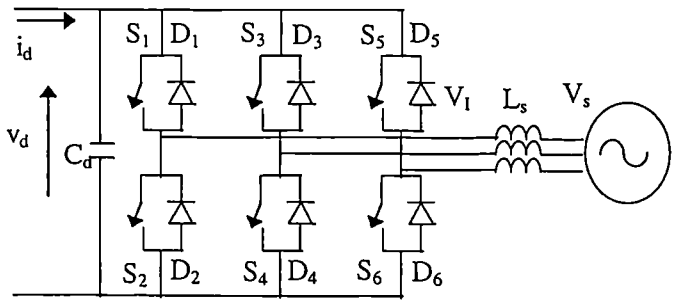

Figure 5.1 Basic circuit of six pulse voltage source inverter

Commutation

Each a.c. phase current is carried by the semiconductors in the corresponding inverter leg. The a.c. line current waveform depends on the inverter switching pattern and the nature of the load. The current change rate is limited by the inductor (L_s). The current commutation between the semiconductors could be natural or forced which depends on the operation conditions.

natural commutation

Taking the first leg (S_1 D_1 S_2 D_2) of figure 5.1 as an example, if the a.c. line current carried by S_1 reduces to zero and changes direction (transferring to D_1) before S_1 is turned off and S_2 is turned on, the current is naturally commutated (line commutation). The semiconductor conduction sequence is S_1 D_1 S_2 D_2. In this case, the current injected into the grid is leading the inverter a.c. terminal voltage (converter taking a current lagging its terminal voltage), therefore the inductive reactive power is taken by the inverter.

forced commutation

If S_1 is turned off before the phase current changes direction, the current will be forced to transfer to D_2 since the current in inductor (L_s) could only change continuously. Hence forced commutation takes place. The semiconductor current carrying sequence is S_1 D_2 S_2 D_1. In this case, the current injected into the grid is lagging the inverter a.c. terminal voltage and the reactive power is generated by the inverter.

free wheeling diode

The diodes inversely connected in parallel with self-commutated semiconductors provide the path for commutation current hence the reactive power circulation. Also they allow dc current and real power to flow in either direction, therefore this circuit could also work as a rectifier.

switching semiconductor

Though SCRs with commutation networks were used in early VSI inverters, using commutation networks with SCRs results in a bulky converter and limits the inverter to low switching frequency. The reverse blocking capability of SCR is not utilised because of the need for inverse parallel connected diodes. The later-developed self-commutated semiconductors, GTO, BJT, MOSFET and IGBT, are now more commonly used. In particular, IGBTs are favoured in medium power (a few hundred kVA) power inverters.

5.2.2 Switching mode

The switching of six valves in a three phase VSI is not independent and the constraint is that the DC link should not be shorted. The switching patterns of the basic VSI inverter could be broadly divided into square-wave switching and high-frequency switching:

square-wave switching

In square-wave switching mode, the upper and lower valves of each inverter leg are switched on and off alternatively with an equal period of 180° while corresponding devices in the three legs are triggered one after another at 120° intervals to generate the six-step voltage waveform. Figure 5.2 shows the ideal inverter a.c. terminal phase-to-phase voltage waveforms of the square-wave switching. The a.c. output frequency is controlled by the inverter and the ratio of input d.c. voltage and fundamental component of a.c. output voltage is fixed.

With square-wave switching, natural commutation is possible if reactive power generation is not required. The switching frequency and power losses of the semiconductor are relatively low but harmonic contents are very high.

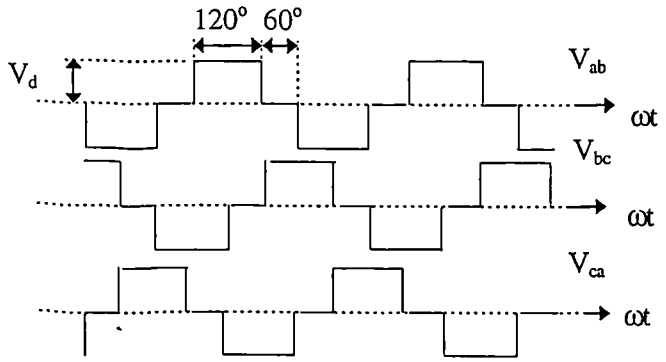

Figure 5.2 Voltage waveforms of square-wave switching

High-frequency switching (sinusoidal PWM, selective harmonic elimination)

The object of using the faster, self commutated devices is not only to enable the inverter to generate higher frequency a.c. output but primarily to enable the high-frequency switching techniques to be applied to the inverter to reduce the harmonic distortion. There are various ways to develop the switching patterns, for example, the switching

pattern can be derived by comparing a triangle waveform with a sinusoidal waveform (sinusoidal PWM) or following a set of pre-calculated switching patterns (selective harmonic elimination). The ratio of fundamental component of ac output to the d.c. voltage can also be controlled. A typical selective harmonic elimination voltage waveform is shown in figure 5.3. The function of higher frequency switching techniques is the redistribution of the harmonic spectrum in frequency domain by chopping the waveform in time domain. The more switching can be made within each cycle, the more low order harmonics could be eliminated. As consequence, the harmonics are shifted to higher frequency region where the voltage harmonics become less harmful in the inductive dominated system and can be easily filtered out with a much smaller size of filter so reducing the cost and operating loss [26].

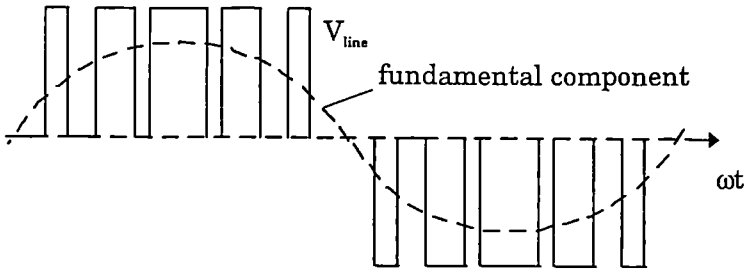

Figure 5.3 Voltage waveforms of a high frequency switching pattern

In order to implement the higher switching frequency techniques, the inverter should have the force commutation capability whether leading reactive power generation is needed or not. Self-commutated devices have made possible great progress in the high-frequency switching technique of converters. Owing to the absence of commutation circuits, the weight, cost and efficiency of the self-commutated inverters have improved and much higher switching frequencies can be achieved.

The drawback of higher frequency switching techniques is that the power loss of the inverter is increased rapidly with the frequency increasing. With high power inverters, especially GTO inverters, the losses in the snubber circuit are not negligible when the switching frequency is high. The switching frequency is quite often limited by the thermal limit. Another restriction for high frequency switching inverters is the minimum pulse width. Due to the finite turn-off time and recovery time of the devices, there is a limit to how fast the current can be transferred from one device to another in the same

phase. Exceeding this limit will result in a DC link short circuit. The minimum pulse width should be always set well beyond this limit.

Soft switching techniques

Soft switching techniques are being developed and used in inverters recently. With soft switching, the semiconductors can be switched at zero voltage and/or zero current condition to reduce the inverter losses [31, 32, 57]. One type of soft switching inverter, the resonant dc link VSI, is shown in figure 5.4, where the instantaneous zero input voltage to the inverter is obtained by using a high frequency resonant DC link. The DC voltage reaches zero periodically to provided the zero voltage switching opportunities for the main electronic switches. The high frequency switching harmonic minimisation technique could also be implemented in the soft switching converter to reduce both harmonic distortion and switching losses [25].

The disadvantages of resonant DC link inverters is that the power semiconductors have to withstand higher blocking voltage (twice DC input voltage without clamping circuit), also the high frequency oscillation circuit will introduce extra losses. More important, when considering a variable voltage and current dc link in the addressed application, the resonant dc link and its control could be very difficulty to implement. Therefore this circuit will not be investigated further.

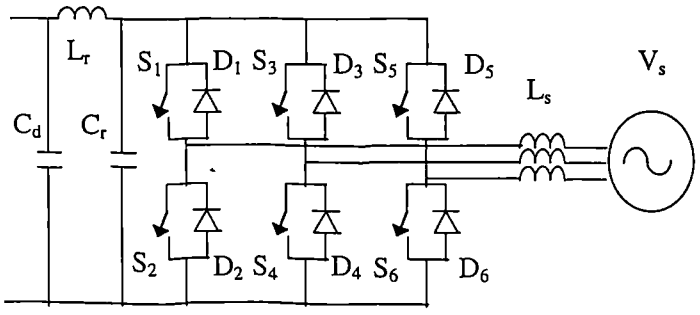

Figure 5.4 Resonant DC link voltage source inverter circuit

5.3 Grid Power Characteristics of VSI

In this section the power characteristics of the grid connected inverters are studied. In this study, it is assumed that the system is balanced therefore the single phase equivalent

circuit can be used for study of the three phase system. It is also assumed that the inverters are so constructed and switched that the harmonics can be ignored and only fundamental components are considered, therefore all the variables are sinusoidal.

Power into a power system

A power system network can be modelled by nodal method, for a power network with n nodes, the node voltages and injecting currents are related by:

$$\dot{I}_k = \sum_{i=1}^{n} Y_{ki}\dot{V}_i \qquad \text{for node } k=1,\ldots, n \qquad (5.1)$$

where

$$Y_{kk} = \sum_{i=0\neq k}^{n} y_{ki} \qquad \text{is self-admittance of node } k$$

$$Y_{ki} = -y_{ki} \qquad \text{is mutual admittance between node } k \text{ and } i$$

$\dot{I}_k$ is the current injected into the bus k and $\dot{V}_i(V_i\angle\theta_i)$ is the voltage of bus i, y_{ki} is the branch admittance between node k and i. θ_i is the voltage phase angle with respect to the reference bus.

The real and reactive power injected at bus k is then given in polar co-ordinate form by

$$P_k = \sum_{m\in k} V_k V_m (G_{km}\cos\theta_{km} + B_{km}\sin\theta_{km})$$

$$Q_k = \sum_{m\in k} V_k V_m (G_{km}\sin\theta_{km} - B_{km}\cos\theta_{km}) \qquad (5.2)$$

$$\theta_{km} = \theta_k - \theta_m$$

Equations (5.2) are called the power flow equations. For the power system steady state analysis, a wind farm may be considered as a PQ node or PV node, depending on the control strategies. Ideally the real power, P_k, produced by the wind farm should be the optimal power following the change of the wind speed and reactive power, Q_k, should meet the system reactive power management or voltage regulation requirement. It is clear, from equations (5.2), that the real and reactive power injected into the system are decided by the nodal voltages and their phase angles. Therefore, if the magnitude and

phase angle of the inverter output a.c. voltage are appropriately controlled, the desired real and reactive power may be delivered into the power network from the wind farm.

Ideally, a wind farm would be controlled by the power system control centre equipped with modern high speed computer which monitors major variables, performs the power network analysis and sets up the desired control variables (e.g. V_k and θ_k for a VSI interface wind farm). The schematic of such a control system is shown in figure 5.5. The control system would co-ordinate all power generation devices in the power system, such as conventional power plants, renewables and storage equipment. Which is necessary to operate the system optimally, especially, in a power system where the intermittent power makes up a high percentage of the system capacity.

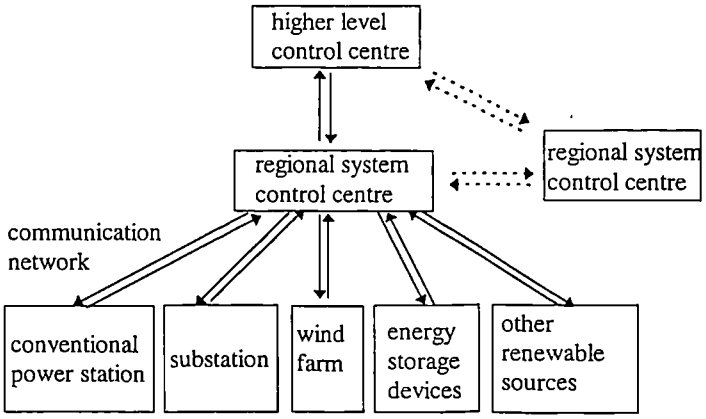

Figure 5.5 Schematic of power system control system

However, this thesis will mainly address the power converter, therefore, a simplified system is discussed in the following section.

Simplified system

Assuming that the system connected with the wind farm can be expressed as an infinite bus and an equivalent impedance, then the single phase equivalent circuit of the simplified two node system shown in figure 5.6 may be used for the power analysis. In figure 5.6 (a), the VSI is represented by a voltage source, $V_{I(1)}$, which is the inverter ac terminal voltage and i_{s1} is the current injected into the grid. The three phase VSI is usually connected to the grid through a power transformer whose impedance is included

in Z_s. Assuming R small, the circuit is simplified further to figure 5.6 (b) by ignoring resistance.

Figure 5.6 Simple circuits of grid connected VSI

With system voltage $V_S\angle 0$, inverter a.c. terminal voltage fundamental component $V_{I(1)}\angle\delta$, the equations (5.2) can be simplified to

output power from the inverter:

$$P_I = V_{I(1)}^2 \frac{R_s}{Z_S^2} + V_{I(1)}V_S\left(\frac{X_s}{Z_S^2}\sin\delta - \frac{R_s}{Z_S^2}\cos\delta\right)$$

$$Q_I = V_{I(1)}^2 \frac{X_s}{Z_S^2} - V_{I(1)}V_S\left(\frac{R_s}{Z_S^2}\sin\delta + \frac{X_s}{Z_S^2}\cos\delta\right) \qquad (5.3)$$

and power into the grid:

$$P_s = -V_s^2 \frac{R_s}{Z_s^2} + V_{I(1)}V_S\left(\frac{X_s}{Z_s^2}\sin\delta + \frac{R_s}{Z_s^2}\cos\delta\right)$$

$$Q_s = -V_s^2 \frac{X_s}{Z_s^2} - V_{I(1)}V_S\left(\frac{R_s}{Z_S^2}\sin\delta - \frac{X_s}{Z_S^2}\cos\delta\right) \qquad (5.4)$$

It is reasonable to assume the resistance between the inverter and equivalent bus of the ac system is negligible, in which case the power flow expressions of equations (5.3) and (5.4) are further simplified to

$$P_S = P_I = \frac{V_S V_{I(1)}}{X_S}\sin\delta$$

$$Q_S = \frac{V_S V_{I(1)}}{X_S}\cos\delta - \frac{V_S^2}{X_S}$$

$$Q_I = -\frac{V_s V_{I(1)}}{X_s}\cos\delta + \frac{V_{I(1)}^2}{X_s} \qquad (5.5)$$

The difference between Q_I and Q_S is the reactive power consumed by the inductance L_s, the reactive power loss:

$$\Delta Q_s = Q_I - Q_s$$
$$= \frac{V_{I(1)}^2}{X_s} - \frac{2V_s V_{I(1)}}{X_s}\cos\delta + \frac{V_s^2}{X_s} \qquad (5.6)$$

phasor diagram

The simplified system can also be expressed by the phasor diagram shown in figure 5.7. where $X_s = 2\pi f L_s$ and f is the system frequency, $V_{I(1)}$ and I_{s1} are the fundamental frequency inverter AC voltage and current, $I_{s1(p)}$ and $I_{s1(q)}$ are respectively the real and reactive component of I_{s1}.

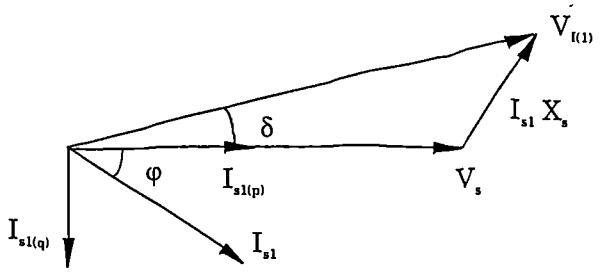

Figure 5.7 VSI phasor diagram (fundamental component)

If the converter output voltage is made to lead system voltage by an angle $\delta<180^0$, $I_{s1(p)}$ is in phase with the grid voltage, then real power flows from inverter to grid and the converter is operating in the inverter mode. If the converter voltage is made to lag the grid voltage by an angle, $I_{s1(p)}$ is out of phase with the grid voltage, hence the power flows from the grid to the d.c. side of the converter, the converter is in the rectifier operation mode.

If $I_{s1(q)}$, is lagging the grid voltage, the converter is in the reactive power generation mode. If $I_{s1(q)}$ is leading the grid voltage, the converter is in the reactive power consumption mode.

It is clear that the converter is able to generate or absorb real power and reactive power by regulating the power angle and voltage magnitude, i.e. to operate in all four quadrants of the P_s-Q_s plane shown in figure 5.8.

Figure 5.9 shows the characteristics of the real power against the power angle and figure 5.10 shows the characteristics of reactive power against the power angle. The conditions are follows:

V_s=1.0 pu, X_s=0.2 pu, $V_{I(1)}$=0.8, 0.9, 1.0, 1.1, 1.2 pu.

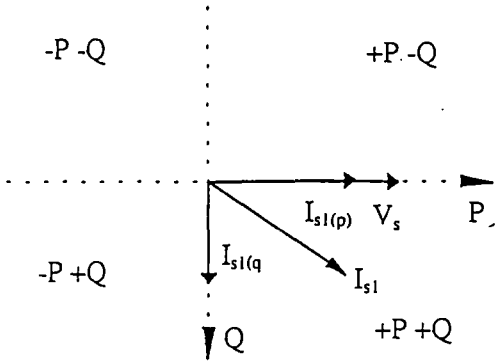

Figure 5.8 P-Q plane

The inverter output voltage magnitudes $V_{I(1)}$ are the parameters in these figures, the high magnitude curves correspond the high $V_{I(1)}$ values. The real power and reactive power operating chart (P_s-Q_s diagram) derived from the equations of (5.5) is shown in figure 5.11 with power angle, δ (as labels in Fig. 5.11), and voltage, $V_{I(1)}$, as parameters. Circles of increasing radius represent characteristics for increasing $V_{I(1)}$ magnitude.

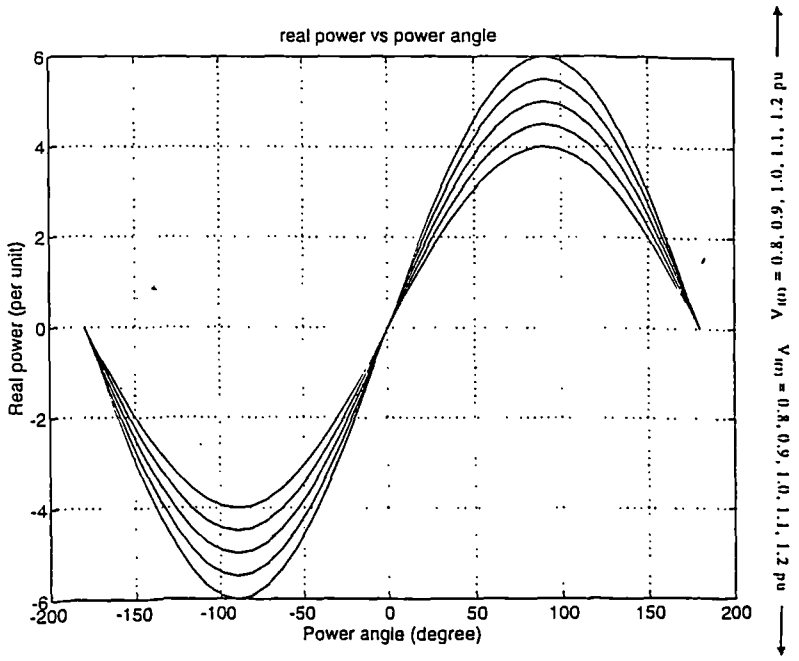

Figure 5.9 VSI real power against the power angle and magnitude

The effects of the grid voltage V_s and coupling inductance L_s are not presented in the characteristics, however, it is obvious that both P_s and Q_s are proportional to the reciprocal of L_s, P_s is proportional to V_s and Q_s is proportional to the difference of V_s and $V_{I(1)}$; Based on the P_s-Q_s characteristic, various control strategies could be derived.

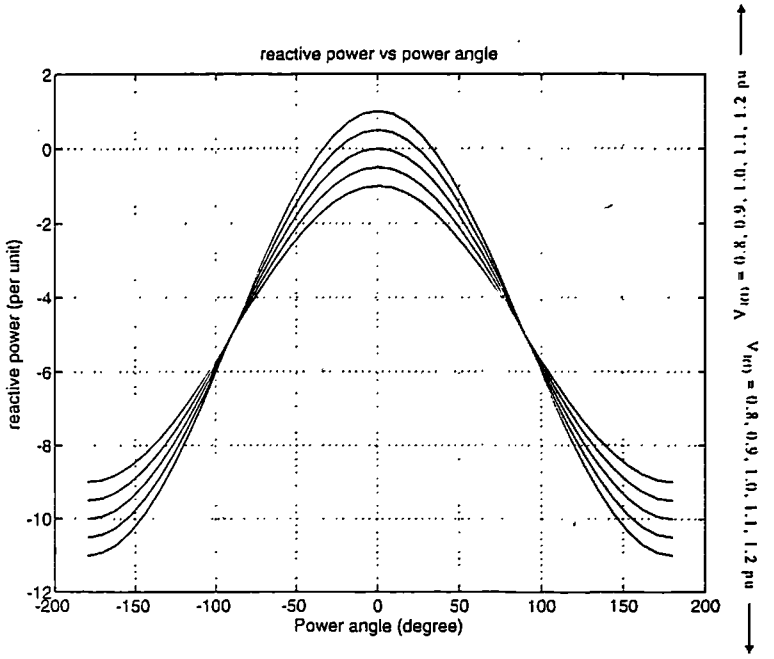

Figure 5.10 VSI reactive power against the power angle and magnitude (grid terminal)

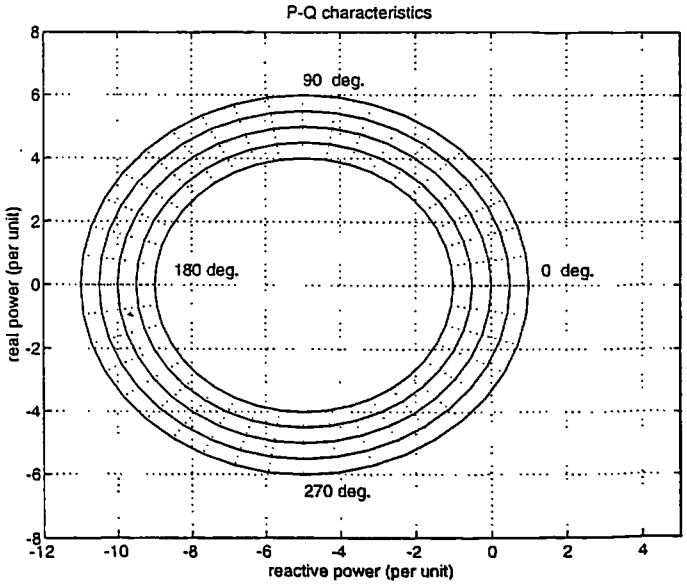

constant inverter ac voltage ———

constant inverter power angle .....

Figure 5.11VSI characteristics of real and reactive power (grid terminal)

Observing these characteristics, It can be noticed, in a simple system,

- $V_{I(1)}$ needs to be increased with increasing P_s to keep the unit power factor operation,
- Q_s is reduced with increasing P_s in a constant $V_{I(1)}$ operation,
- The system should normally be operated within small power angle range and a $V_{I(1)}$ around V_s to achieve a high power factor.

Comparison with synchronous generator

From figures of 5.9 and 5.10, it can be seen that the real power and reactive power characteristics of a grid connected VSI are similar to those of a grid connected synchronous generator. However, the power control is performed in different way. In a synchronous generator, the real power and the power angle δ are dependent on the mechanical input power where control variable is input power rather than power angle which should be limited within the system steady stability range. The reactive power and machine voltage is determined by the excitation current, which is limited by the machine VA capacity.

In a VSI, the power angle is a direct control variable. The fundamental component of the inverter output voltage, $V_{I(1)}$, is adjustable in phase with respect to the grid voltage $V_s\angle 0$ by timing the semiconductor gate signal with respect to a reference waveform and the power angle is not limited by system steady stability requirement any more. There are also various methods to control the voltage $V_{I(1)}$ magnitude, such as controllable front-end rectifier, dc chopper or fundamental component controllable switching techniques. Therefore the output real and reactive power of VSI can be controlled by operating the power electronics converters. If the optimal operation characteristics of the wind turbine are matched, the maximum power could be captured and delivered into the grid.

The power transfer enhancement technique for the generator and rectifier system, discussed in chapter 4, enables the system to follow the optimal power curve (cubic relation between the power and generator speed) by regulating the load presented to the generator-rectifier. In the following sections, the loading regulation strategies for

realising the optimal real power transfer and the reactive power control are discussed on the basis of a general VSI without distinguishing the real circuit and its switching mode.

5.4 Optimal Power Transfer From Generator-Rectifier System

In order to capture the optimal power from the wind, the shaft speed should be proportional to the wind speed (to follow the optimal C_p curve) until the rated power is reached. Subsequently, the power will be limited either by blade pitch angle control or aerodynamic stalling, yaw limiting is also being used in some turbines. Then the turbine will operate at the rated power until cut off speed is reached.

In order to avoid damaging transient overspeed, for example, turbine designers often specify some departure from the simple ideal shaft/wind speed relationship especially for stall-regulated turbine. Means of controlling shaft speed rapidly in response to a signal derived externally or via electrical power are required. The use of the VSI to regulate loading is an effective and flexible method.

The wind turbine speed could be controlled by the reaction torque of the generator. Equilibrium is established when the operating point on the generator-rectifier characteristic matches the operating point on turbine power/speed curves, i.e. the power extracted from the wind. One group of such possible operating trajectories is shown in figure 5.12 (a) and (b) where the frequency is the parameter. It is clear that the d.c. link of the rectifier terminal should be controlled so that the d.c. terminal voltage V_d and current I_d track the curves shown in figure 5.12 (d) and (e). Thus the ideal speed-power relationship maps directly to an ideal dc voltage-current relationship.

In the steady state, assuming lossless d.c. link and lossless converters, the real power into the grid is equal to the power from the rectifier-generator system:

$$P_r = P_d = P_I = V_d \times I_d \qquad (5.7)$$

where P_r, P_d, and P_I are respectively rectifier input power, inverter input d.c. power and inverter output power. V_d and I_d are d.c. link voltage and current. In grid connected VSI case, the real power delivered to the grid by the inverter is

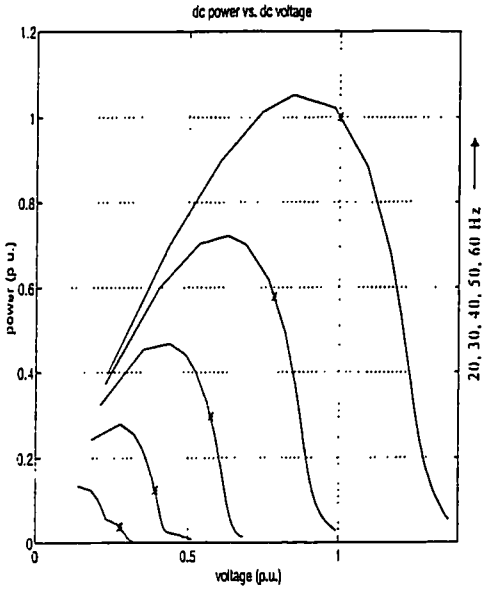
dc power vs. dc voltage
power (p.u.)
voltage (p.u.)
20, 30, 40, 50, 60 Hz

(a)

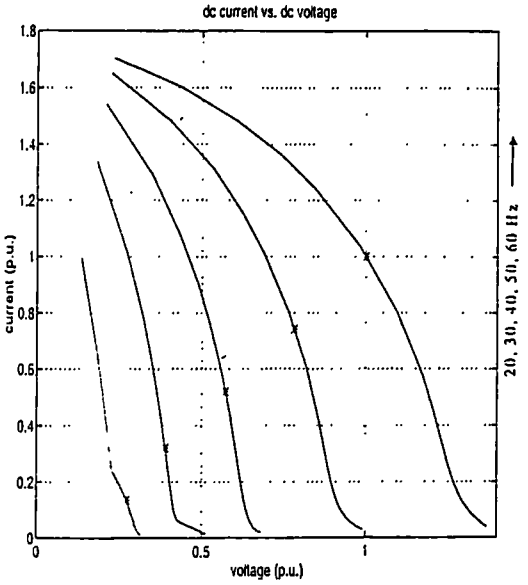
dc current vs. dc voltage
current (p.u.)
voltage (p.u.)
20, 30, 40, 50, 60 Hz

(b)

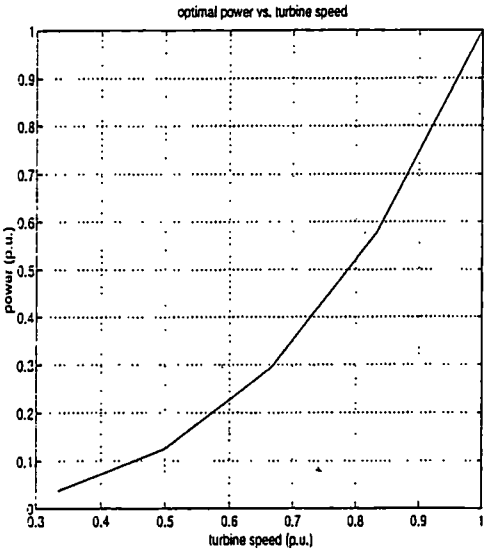
optimal power vs. turbine speed
power (p.u.)
turbine speed (p.u.)

(c)

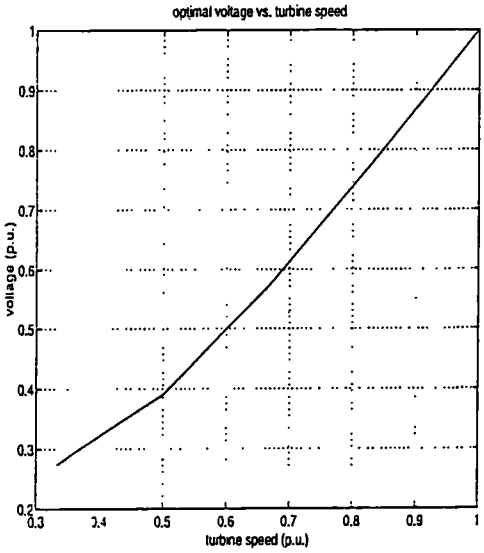
optimal voltage vs. turbine speed
voltage (p.u.)
turbine speed (p.u.)

(d)

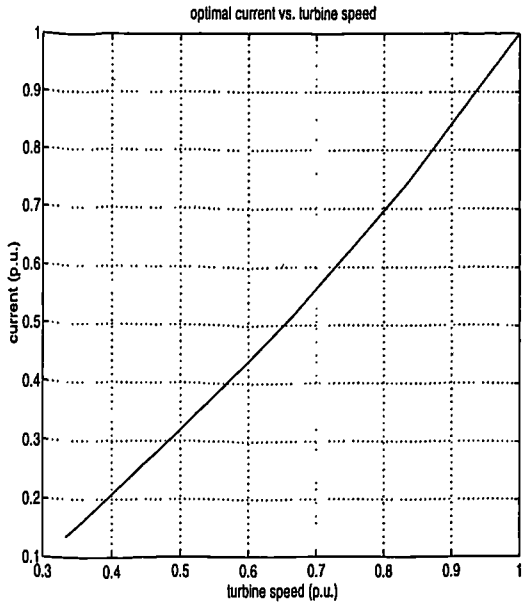

(e)

Figure 5.12 Optimal power capture generator-rectifier characteristics

(a) Optimal P_r curve on P-V characteristics

(b) Optimal P_r curve on P-V characteristics

(c) Optimal P_r curve vs. frequency

(d) Optimal V_d curve vs. frequency

(e) Optimal I_d curve vs. frequency

$$P_s = P_I = \frac{V_s V_{I(1)}}{X_s} \sin\delta$$

for a fixed switching pattern and transformer tap, the ratio of d.c. link voltage and inverter output a.c. voltage, K_{dv}, is fixed, that is $V_{I(1)} = K_{dv} V_d$. Thus

$$I_d = \frac{V_s K_{dv}}{X_s} \sin\delta \qquad (5.8)$$

indicating that the VSI may be represented by a current source for the real power transfer analysis. The PM generator rectifier equivalent circuit (chapter 3 and 4) may be combined with the VSI equivalent current source to form the circuit shown in figure 5.13 for steady state real power analysis. In figure 5.13, E_{eg} is the Thevenin equivalent voltage source. Without power transfer enhancement capacitor, E_{eg} is proportional to the shaft speed. The capacitor power enhancement technique increases E_{eg}, especially in the

high frequency range as shown in chapter 4. The current source can be controlled by regulating the power angle (δ) or varying the ratio of rectifier d.c. terminal voltage to inverter a.c. output voltage at transformer grid side (K_{dv}). It is also effected by grid voltage variation and by the coupling impedance which may exhibit saturation.

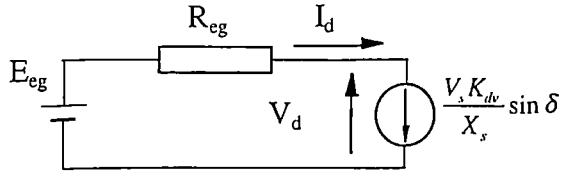

Figure 5.13 Equivalent circuit for dc power transfer analysis

For a certain grid voltage and transformer tap ratio, if a pair of (K_{dv} δ) are chosen to make $V_s K_{dv} \sin\delta / X_s$ follow the optimal I_d curve, the maximum power could be captured and transferred in to the grid. There will normally be more than one pair (K_{dv} δ) which are feasible to produce the optimal d.c. current. The choice of values for K_{dv} and δ will influence to reactive power generated or absorbed.

5.5 Optimal Power Capture Of Power Angle Controlled VSI

Since the diode rectifier has no control ability, the dc link power regulation is set at the inverter. If a simple dc link is used and the inverter dc/ac voltage ratio is fixed, the only control variable is the power angle. As discussed above, the VSI, being represented as a current source, can be controlled to follow the optimal current curve by varying the power angle. Obviously, the maximum current which could be injected into the grid is $V_s K_{dv} / X_s$, which occurs at δ=90°. Therefore, the value of $V_s K_{dv} / X_s$ should be larger than the maximum value of the optimal current.

With the optimal current tracking strategy, the inverter system and control are simple. For every value of the shaft speed, there exists a corresponding optimal power and optimal d.c. current. Such optimal speed/power or speed/dc current relationships can be stored in the memory of the controller and compared with the real operating points to decide the amount of required power angle adjustment. Specified departures from the

ideal can be performed by simply using a set of stored departure values. When the rated power is reached, the power control will co-operate with turbine control and cause the system to leave the $C_{p(max)}$ curve and follow a predetermined trajectory set by the wind turbine operating strategy. The block diagram of such a control system is shown in figure 5.14.

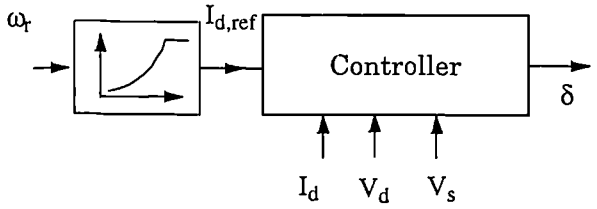

Figure 5.14: Controller block diagram of power angle control system

5.6 Reactive Power Control

5.6.1 Reactive power and inverter ac output voltage variation

The ideal wind energy conversion system should be able to operate at a desirable power factor when the optimal power curve is chased. However, if the power angle is the only control variable, the reactive power and hence power factor cannot be regulated when the rectifier d.c. terminal voltage and current follow the optimal trajectory. Figure 5.15 shows a reactive power curve when the system follows a cubic power-frequency curve to capture the maximum power and the a.c. output voltage magnitude is proportional to the d.c. link voltage shown in figure 5.12. The conditions of figure 5.15 are V_s =1.0 p.u. & X_s=0.2 p.u. inverter a.c. voltage reaches 1.0 p.u. at rated speed.

Observing the characteristics shown in figure 5.15, the reactive power of the inverter has to be varied widely to deliver the available real power into the system. Obviously, if a basic VSI with control of power angle alone is used, the maximum power can be captured from the wind and each d.c. voltage level corresponds to a unique real power output. However, the reactive power cannot be controlled freely without changing the real power operation point. The reactive power generation ability of the self-commutated grid connected inverter cannot be fully used. The uncontrolled variation in

reactive power could lead to unacceptable changes in supply voltage to other users of the system and would infringe statutory regulations applicable to private generators.

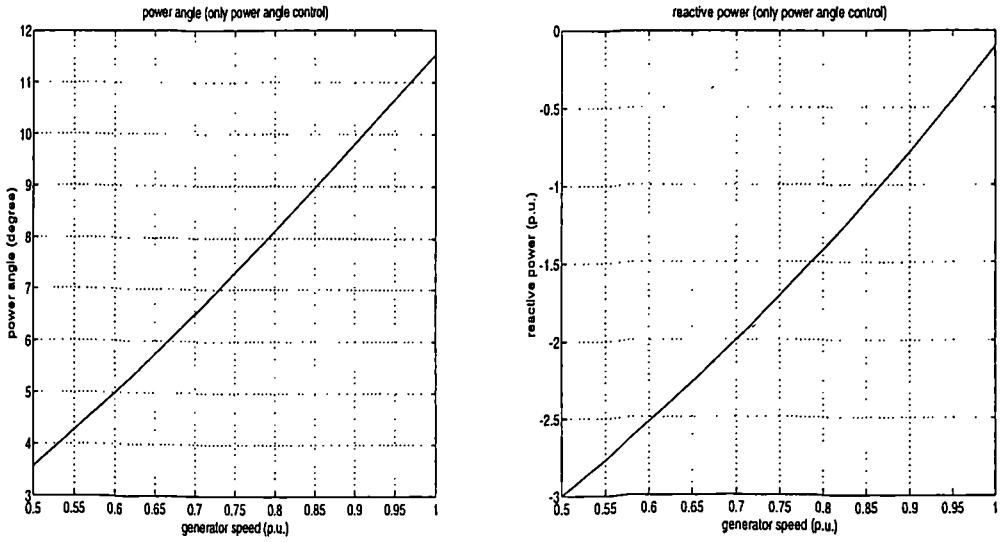

(a) power angle (b) inverter reactive power

Figure 5.15: Characteristics of only power angle controlled VSI

Reactive power and voltage variation is thus an important aspect of the power quality. Controlled reactive power generation is often needed to support the system voltage. As a result, reactive power compensation facilities may be required to control reactive power for keeping the system voltage level. Though the ratio setting of the grid transformer can improve the power factor, a fixed-tap transformer cannot reduce the range of voltage variation (in per unit terms) which may result in difficulties for the grid operation. Even in a strong system, the wind farm economic aspects could be effected by the charge made by the grid for the supplied reactive power.

Therefore it is necessary to use additional methods to control the magnitude of the inverter ac voltage and the reactive power while the optimal real power is captured.

5.6.2 Possible methods to smooth reactive power and voltage variation

Combination with Energy Storage Devices

In some cases, the DC link may be connected to energy storage devices. The power exchange between the DC link and these devices could be such controlled to keep a

smooth power into the grid and a DC link voltage at the desirable level. For instance, at high wind speed, the energy from wind could be directed to the energy storage device; at lower wind speed, the energy could be released from the energy storage device. In this way, the whole system could provide the smooth real and reactive power to the customer and power system. However, this would not automatically answer the requirements of a varying dc voltage at rectifier dc terminal. In addition, the required energy storage devices may not always be available or cost-effective with present techniques. Such an approach represents an entire new field of research and development.

Tap-Changing Transformer

A tap changing transformer could be used as converter transformer coupling the inverter and the grid. During operation, such a transformer could change the ratio, to regulate the voltage of the inverter output at the system coupling point and therefore the reactive power. However, the variation range of wind speed and dc link voltage is beyond the normal regulation range of a tap-changing transformer. This method could only partly meet the reactive power and voltage control requirement. There would be serious doubts concerning the operating life and the reliability of an electromechanical tap charger and the cost of a suitable solid-state unit.

Reactive Power Compensator

The ASVC (advance static var compensator) or another controllable reactive power compensation device could be used to supply or absorb the reactive power. However, such devices would make the whole system more expensive and the reactive power generating ability of a self commutated grid connected inverter would not be fully used. In this case, a line commutated inverter may be more cost-effective, this scheme will be addressed later in this thesis.

It is clear, the rectifier d.c. terminal needs one d.c. voltage profile for rectifier optimal power transfer; the inverter needs to generate an a.c voltage profile for optimal power

transfer and reactive power control; The two voltages profiles differ. Some approaches to answer this problem of matching are:

- dc/ac voltage ratio controllable inverter
- dc/dc converter in DC link
- ac/dc voltage ratio controllable rectifier

Inverter input/output voltage ratio control by varying switching pattern

For a given input dc voltage, the output voltage fundamental component of the inverter can be controlled by regulating the switching pattern, such as PWM switching. Different from the variable electrical machine drives, in this case, only the magnitude and angle of the voltage should be controlled and the output frequency is fixed at the grid frequency.

With the natural sine PWM wave switching controller constructed by electronics circuits, the control of output voltage fundamental component could be quite easily implemented by changing the magnitude of the reference sine wave. However, with micro processor implemented regular sampled sine PWM or harmonic elimination switching, the real time calculation of the switching angle may be necessary to generate magnitude controllable waveforms. The SPWM method will be investigated in detail in chapter 8.

DC/DC converter

A DC/DC converter could be placed between the rectifier and the inverter dividing the DC link into two levels. The rectifier side, provides conditions for optimal power capture; the inverter side, provides a controllable DC voltage to realise the optimal real power transfer and the reactive power regulation. The working principle is the same as the tap-changing transformer, but carried out in d.c. rather than a.c., also this scheme offers a flexible and wide range of voltage regulation. The DC/DC converter approaches will be detailed in Chapter 9.

Rectifier input/output voltage ratio control

Using SCR or other controllable semiconductor rectifier, instead of diode rectifier, can also provide a controllable dc link voltage. However, the large number of phases of the modular PM generator would require large number of semiconductors and their associated control and firing circuitry. This scheme is unlikely to be economic competitive, therefore not be investigated further.

However, for the consistency of power control discussion, by assuming a power angle and ac output voltage magnitude controllable VSI available, the following sections will address the power control strategies and system effects of such an inverter.

5.7 VSI Power Factor and Output AC Voltage Control

The discussion of power factor or reactive power control in this section is based on the simplified system in section 5.3. For a complex a.c. network, the network analysis method could be used.

5.7.1 VSI power factor (reactive power) control

Given the ideal real power and power displacement factor, P_{ideal} and $\cos\varphi_{ideal}$, the desired reactive power is

$$Q_{ideal} = P_{ideal} \times \tan\varphi_{ideal}$$

Based on equation (5.2),

$$P_{ideal} = \frac{V_s V_{I(1)}}{X_s}\sin\delta$$
$$Q_{ideal} = \frac{V_s V_{I(1)}}{X_s}\cos\delta - \frac{V_s^2}{X_s} \qquad (5.9)$$

then

$$V_{I(1)}\sin\delta = \frac{P_{ideal} X_s}{V_s}$$
$$V_{I(1)}\cos\delta = \frac{X_s}{V_s}(Q_{ideal} + \frac{V_s^2}{X_s})$$

Therefore the required power angle and a.c. output voltage magnitude are

$$\delta_{ideal} = \tan^{-1}\left(\frac{P_{ideal}}{(Q_{ideal} + V_s^2/X_s)}\right)$$
$$V_{I(1)ideal} = \frac{P_{ideal} X_s}{V_s \sin\delta_{ideal}} \qquad (5.10)$$

But $V_{I(1)ideal} = K_{dv,ideal} \times V_{d,r,ideal}$, $V_{d,r,ideal}$ is the ideal rectifier terminal d.c. voltage, $K_{dv,ideal}$ is the product of transformer tap ratio and the ratio of inverter a.c. line-line voltage to inverter d.c. terminal voltage and should be controllable to meet the requirement of $V_{I(1)ideal}$ and $V_{d,r,ideal}$. Therefore the control variables in such a system are δ and K_{dv}. The practical implementation of K_{dv} control is addressed later.

5.7.2 VSI power factor and AC output voltage control characteristics

Figure 5.16 illustrates the required power angle and ac voltage magnitude to deliver the optimal power at unity power factor. The simplified circuit of figure 5.6 is used to generate figure 5.16 using the same parameters as for figure 5.9.

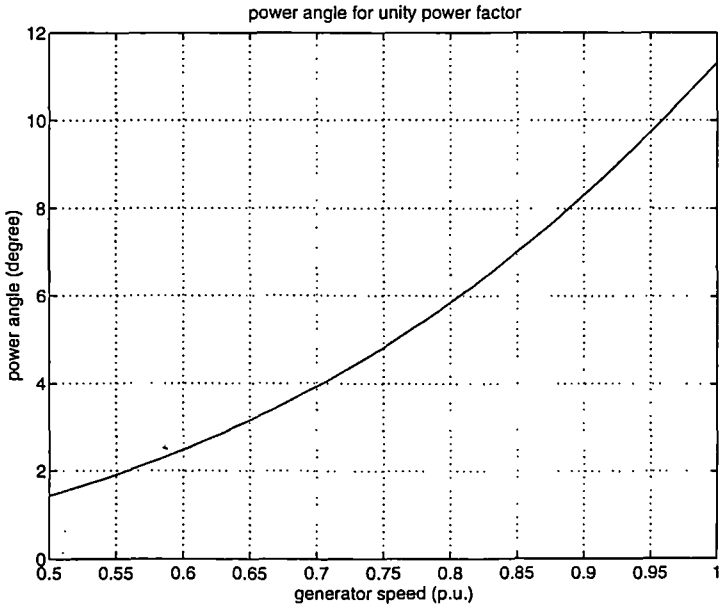

(a) power angle

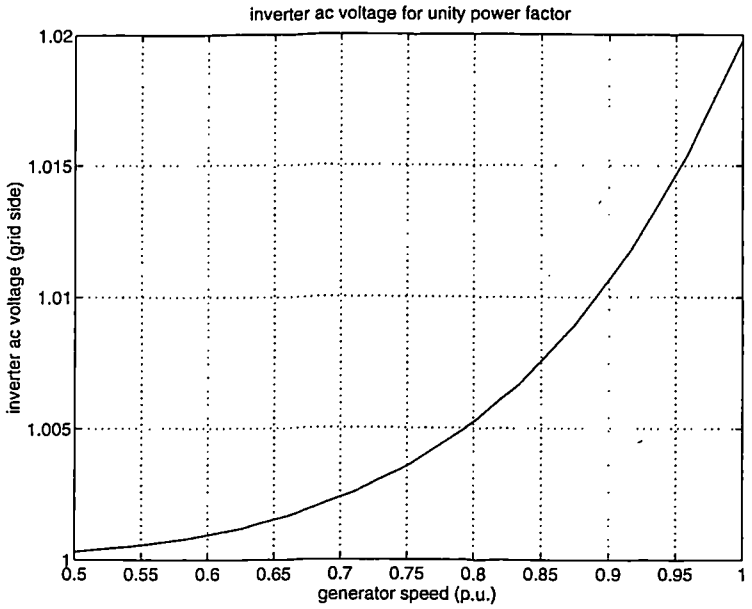

(b) inverter ac voltage

Figure 5.16 : Unity power factor operation characteristics

Figure 5.17 illustrates the power angle and the reactive power consumption if a.c. voltage magnitude fundamental component is controlled as constant (1.0 pu).

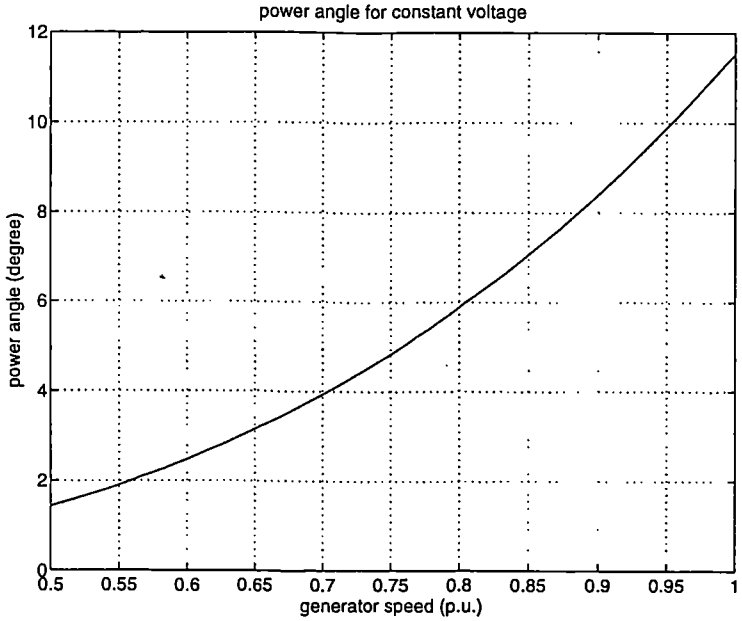

(a) power angle

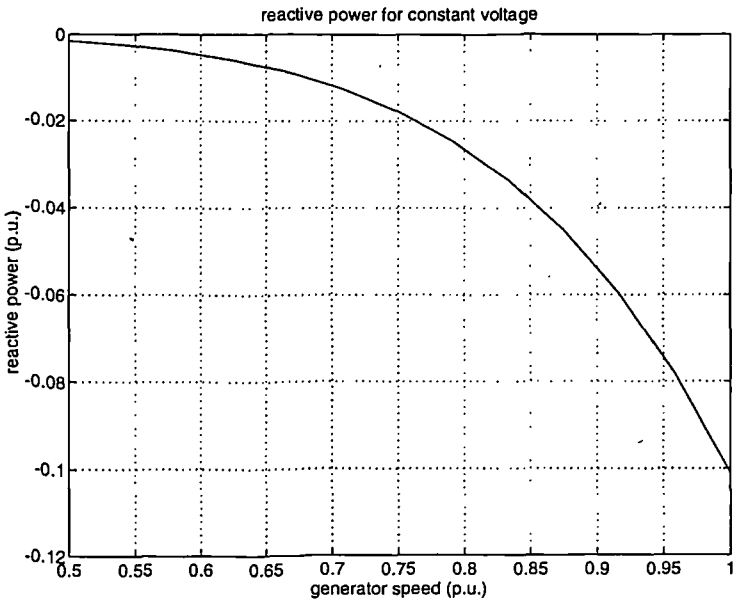

(b) reactive power

Figure 5.17 constant voltage control operation characteristics

5.8 VSI in a Test Network

In this section, the effects of a power angle and ac voltage controllable VSI interfaced wind farm on the power system is analysed. A 9 bus test system [88] is modified for this study. It is assumed that the multi-machine wind farm has a total capacity of 32% system peak demand and a equivalent VSI, (which, in practice, would be a number of VSIs associated with individual turbines), connects the wind farm to the grid (bus 2) through a 0.2 pu inductor as shown in figure 5.18. The loading and generation conditions are given in Table 5.1 and system parameters are given in Table 5.2.

Table 5.1 Loading and generations

	Parameters
P_2 +i Q_2	1.0 +i 0.35
P_5 +i Q_5	1.25+i 0. 5
P_6 +i Q_6	0.9+i 0.3
G_1 (slack bus)	V=1.04, θ_1=0
G_2 (PV bus)	P=0.85, V=1.025
G_3 (PV bus)	P=1.63, V=1.025

Table 5.2 Test system parameters

	Z	Y
1-2	0.0119 +i 0.1008,	+i 0.1045
2-3	0.0085 +i 0.0720	+i 0.0745
3-5	0.0320 +i 0.1610	+i 0.1530
4-5	0.0100 +i 0.0850	+i 0.0880
4-6	0.0170 +i 0.0920	+i 0.0790
1-6	0.0390 +i 0.1700	+i 0.1790
2-7	+i 0.2	0
1-8	+i 0.0586	0
3-9	+i 0.0625	0
4-10	+i 0.0576	0

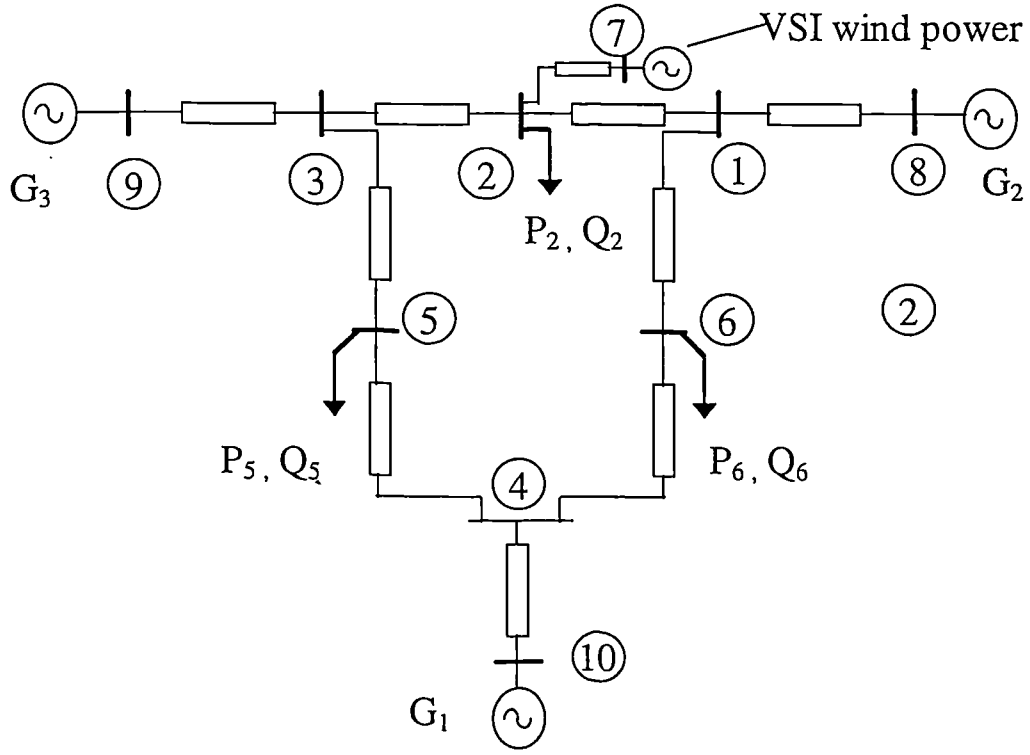

Figure 5.18 VSI wind power test system

A range of power flow analyses have been carried out with P-Q decouple power flow analysis method, yielding the following results:

Figure 5.19 shows: (a) the voltage angle difference between bus 7 and bus 2 (θ_{72}), (b) inverter reactive power, (c) bus 2 and bus 5 voltage; in each for variation of the real power generated by the wind farm from 5% to 100% with a controller regulating power angle only. It indicates that the inverter has to take relative large amounts of reactive power at low wind speed and the voltage fluctuates over a wide range at the connection bus (bus 2) and the voltage fluctuation is more than 2% at bus 5. This could cause problems to the system operation.

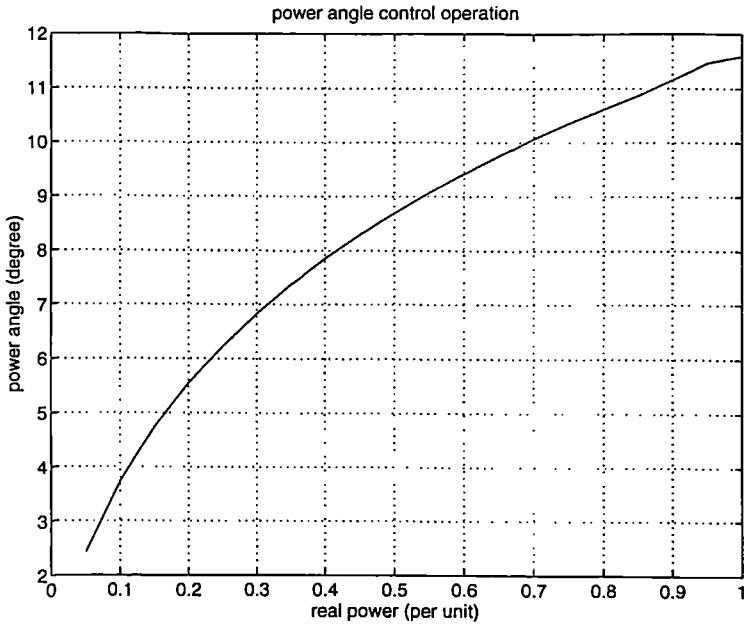

(a) voltage angle difference (θ_{72})

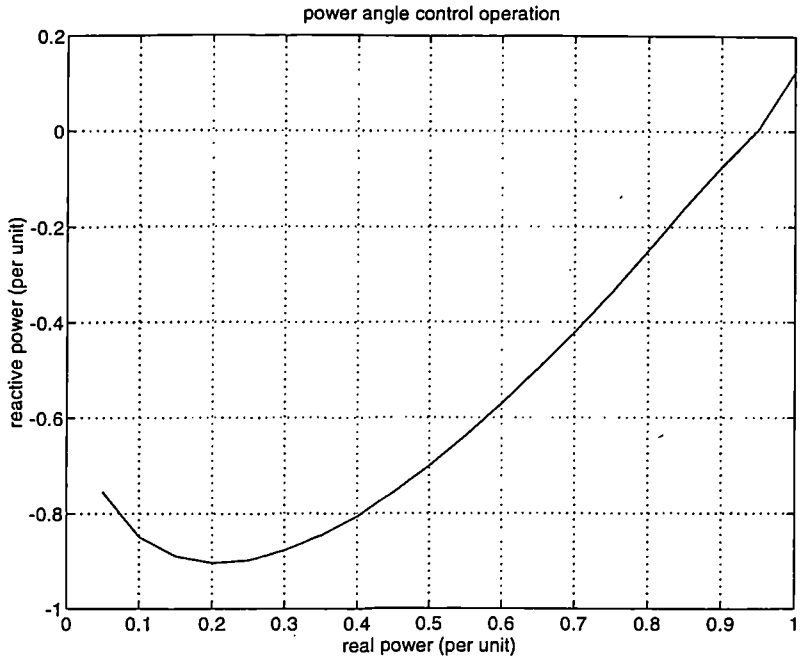

(b) VSI reactive power

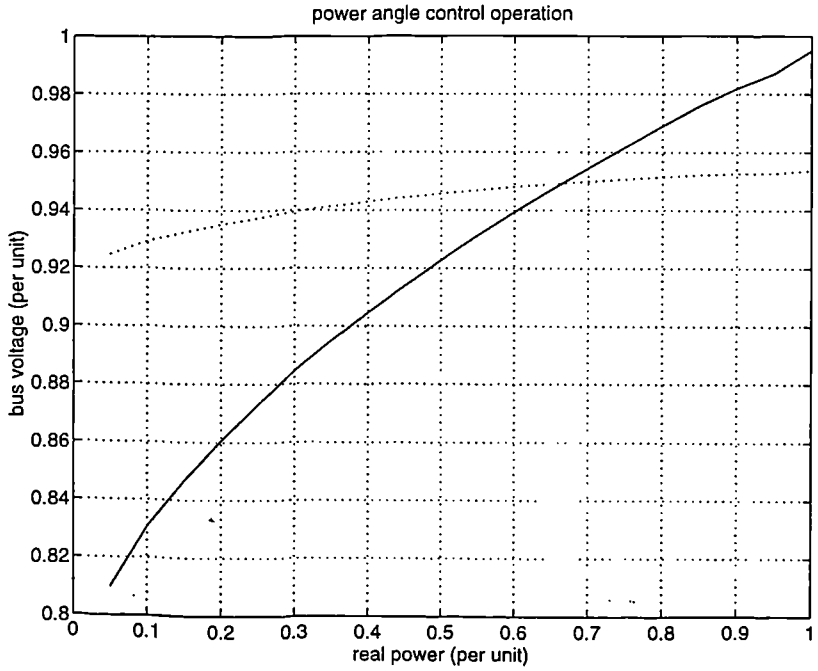

Bus 2 voltage ———
Bus 5 voltage .....
(c) bus voltages

Figure 5.19 VSI in only power angle control operation

Figure 5.20 shows (a) the variation of the inverter power angle, and (b) inverter ac voltage and bus 5 voltage but now with a unit power factor at the wind farm. In this case, the voltage fluctuation is limited to 2% at bus 5. The inverter ac terminal voltage and other bus voltages have less fluctuation than bus 5.

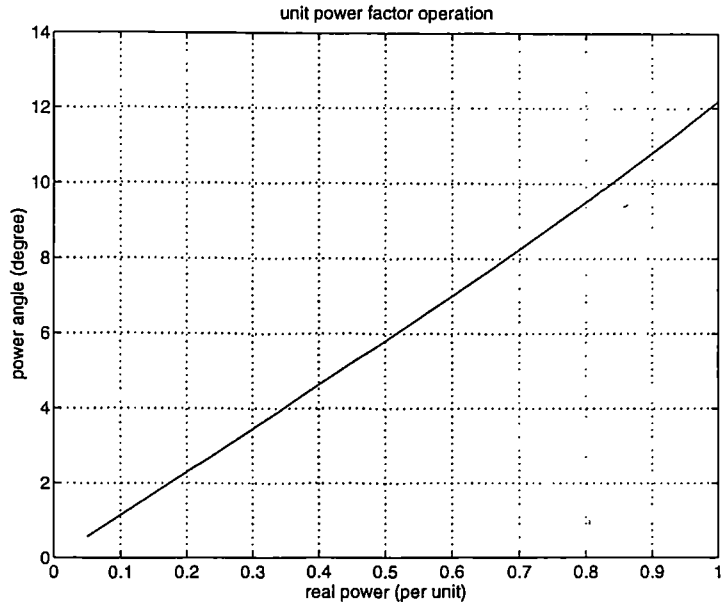

(a) voltage angle difference (θ_{72})

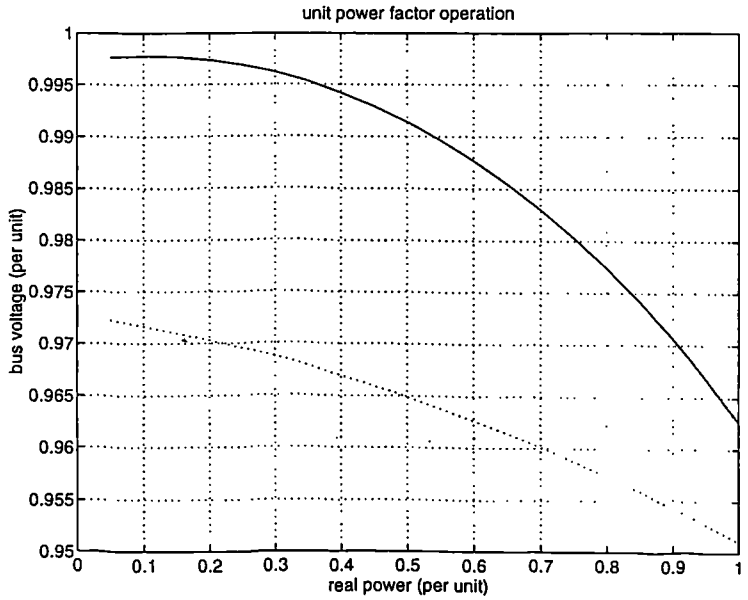

VSI ac voltage ———

Bus 5 voltage .....

(b) bus voltages

Figure 5.20 VSI in unit power factor operation

Figure 5.21 shows (a) the inverter power angle, (b) the reactive power generated by the VSI and (c) the voltage at bus 5 with the VSI controlled to maintain 1.0pu voltage at bus 7. Again, the voltage fluctuation at other points is acceptable.

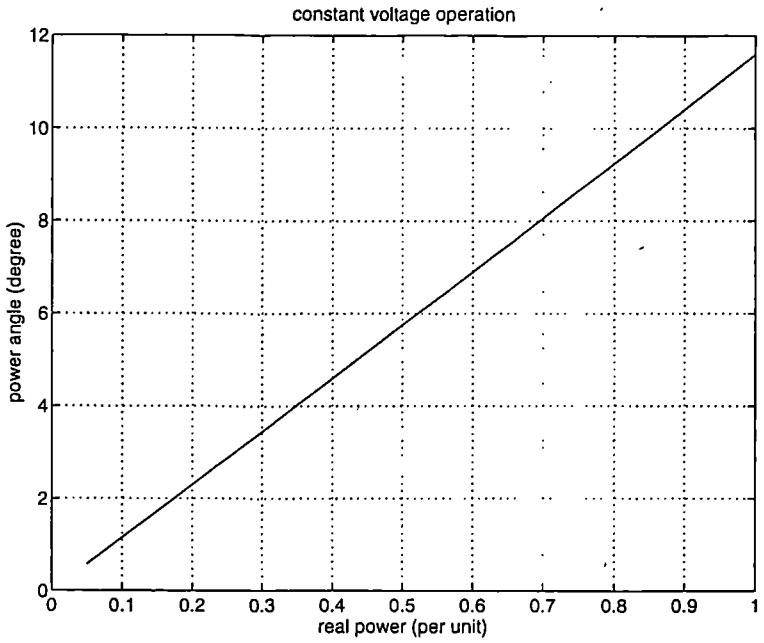

(a) voltage angle difference (θ_{72})

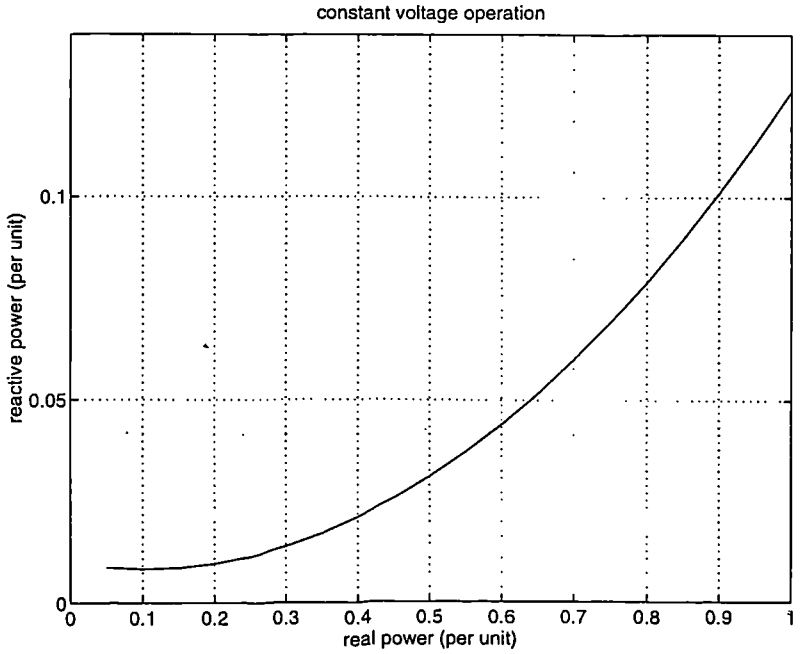

(b) VSI reactive power

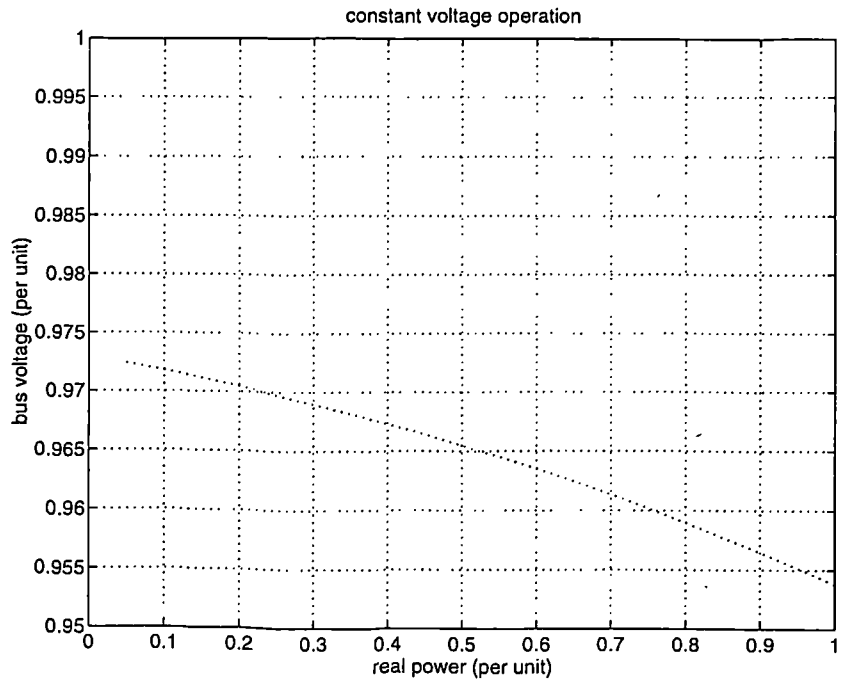

(c) bus voltage (bus 5)

Figure 5.21 VSI constant voltage operation

Comparing the power flow analysis results with the simple system results, it can be seen that the bus voltage profiles, inverter terminal voltage/reactive power are not only dependent on the control strategies but also upon the system configuration and loading/ generation condition. The wind farm VSI control should therefore take the system and operating conditions into account.

5.9 Conclusions

This chapter has discussed the Voltage Source Inverter (VSI) and its application as a grid interface inverter in a direct drive and variable speed wind energy conversion system with PM generator and diode rectifier.

The basic construction and operation of VSI are presented. The VSI grid power characteristics are studied. The operation of the grid connected VSI powered from a varying voltage DC link is analysed. The results shows that it is necessary to control

both power angle and voltage magnitude in order to transfer the optimal power and to have a good reactive power performance.

Potential methods to achieve both power angle and voltage magnitude control of the inverter are proposed and analysed for further studied.

The strategies of power angle and voltage magnitude control are proposed on the basis of the power angle and voltage magnitude controllable inverter. Simulation results are presented. The studies show that the main control variables are the power angle and the ratio of rectifier terminal d.c. voltage to inverter a.c. voltage. VSI could be controlled to transfer the optimal power from the generator-rectifier system and to satisfy the reactive power requirement on a.c. system side.

The operations of VSI in a test system are studied. The optimal control of the VSI interfaced wind farm could be performed by varying the controller's power angle and voltage settings with considering the individual system conditions.

Chapter 6.

Current Source Inverter for Grid Connection

This chapter discusses the application of current source inverter (CSI) for the grid interface inverter. Again, the harmonic is ignored. Attention is focused on the line commutated thyristor inverter (SCR-CSI). The control principle for maximum power transfer is addressed. The performances of the grid connected CSI are investigated in a simplified system and in a 9 bus test system.

6.1 Circuits and Switching Modes of Current Source Inverter (CSI)

6.1.1 Typical CSI circuits

Figure 6.1 shows the circuit configuration of a basic three phase CSI. As in the VSI, there are three legs, each containing two valves, however, the valves in a CSI carry current only in one direction. An inductor is placed in the DC link to maintain the DC current relatively constant. The changes in the inverter DC voltage can be balanced by $L_d di_d/dt$, but with only a small di_d/dt,, hence effectively maintaining a constant dc current for a given operating point. Due to the DC link inductance, CSIs are not sensitive to short circuit fault or switching errors in the circuit.

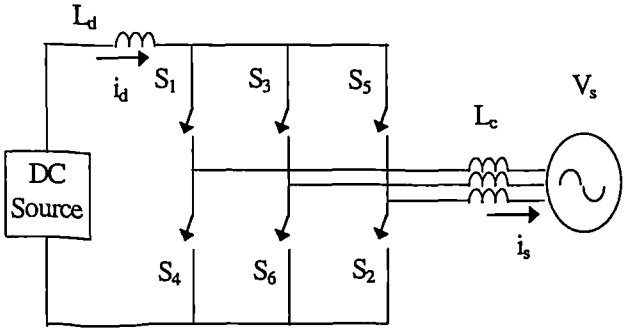

Figure 6.1 Basic structure of current source inverter

Switching elements

The semiconductors in a CSI have to withstand reverse voltage, therefore thyristors with blocking reverse voltage capability should be used, although, the asymmetrical voltage blocking self-commutated semiconductors (GTO, IGBT, etc.) could also be used with diodes connected in series for blocking reverse voltage.

Commutation

The DC current is commutated among the upper group (S_1, S_3, S_5) and the lower group (S_2, S_4, S_6) semiconductors. The semiconductor conduction sequence for square wave switching is indicated by the subscripts of the switch label in figure 6.1. The commutation could be either natural or forced depending on the relation between current and voltage at the converter a.c. terminals when commutation takes place. Several forms of CSI are briefly described below:

line or load voltage commutated CSI

The line voltage commutated CSIs, also called phase controlled converters, normally use SCRs. As the name implies, these converters are commutated by the ac voltages presented on the converter ac side, the transfer of current from one device to the next occurs naturally because of the presence of the ac voltages. Such phase-controlled converters represent a mature technology and have been widely used in HVDC transmission systems, voltage controllable rectifiers, variable frequency synchronous motor drives. Due to their reliability and economic advantages, they are very attractive and a further detailed analysis will be given later.

Autosequentially-commutated CSI (ASCSI)

For the leading reactive power generation, forced commutation is essential. One type of force-commutated CSI, the auto-sequential-commutated CSI, is shown in figure 6.2.

The capacitors and diodes in figure 6.2 are the commutation elements. The six capacitors provide reverse voltages for commutation. The six diodes maintain the correct charging direction of the commutation capacitors to ensure successful

commutation and isolate the capacitors from the ac voltage. The reverse commutation voltage is applied on the outgoing SCR by switching on the incoming SCR. The converter may produce voltage spikes at the a.c. terminal which demands derating of the devices.

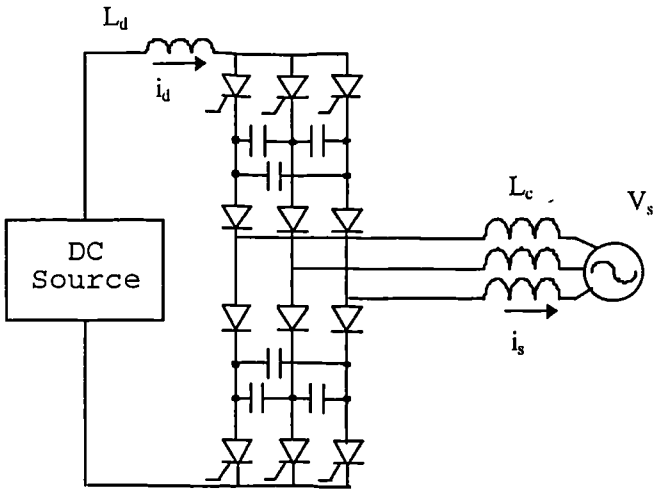

Figure 6.2 Autosequentially-commutated current source inverter

self-commutated CSI

If self-commutated devices such as GTOs or IGBTs with diodes connected in series are used to construct the converter valves of figure 6.1, the converter can be operated at any power factor. A typical self-commutated CSI structure is shown in figure 6.3. Capacitors may be connected at the output terminals of the inverter to absorb the overvoltages induced when the current is cut off so that the semiconductor can be switched without causing undue voltage overshoot, the capacitors also act as the low-pass filter.

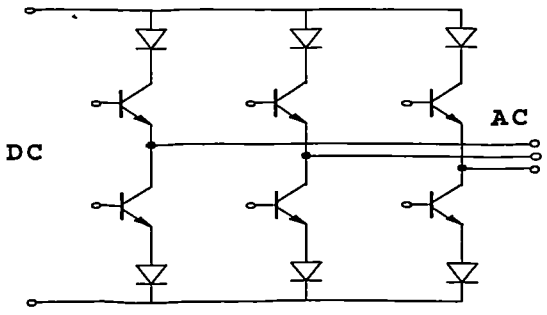

Figure 6.3 Self-commutated CSI

6.1.2 Switching modes

The basic constraint of the CSI is that a current path must always exist for the DC link current. Under this constraint, similar to VSI case, there are square wave switching and higher frequency switching techniques for the CSIs.

square wave switching

In square wave switching mode. Each of the six valves is on for a 120^0 period and the lower group of valves has a phase skew of 60^0 with respect to the upper group. The ideal ac line current waveforms are shown in figure 6.4. With constant input d.c. current, the output of a CSI is dual to a VSI, i.e. the square wave switching CSI has a line current waveform similar to the line voltage waveform of the square wave switching VSI. If leading reactive power generation is required, the inverter has to be force commutated. Otherwise, the inverter can be line commutated.

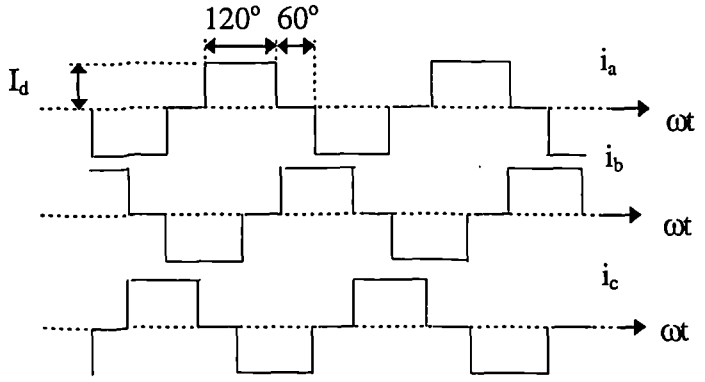

Figure 6.4 Square wave operation of current source inverter

PWM wave switching

The PWM switching technique could also be applied to self-commutated CSI to synthesise a PWM current wave at the output. However it is not possible to pulse-width modulate the central 60° of the current waveform with the basic circuit configuration, because a path must always exist for the current to flow from the DC side to the AC side. A typical output current of the three-phase PWM CSI is shown in figure 6.5.

soft switching CSI

Similar to the VSI case, soft switching techniques could also be applied to the CSI to minimise the switching power loss. One such circuit, the resonant DC link CSI, is

shown in figure 6.6. The output current of resonant DC link CSI is composed of a series of discrete resonant current pulses. The switching action occurs at the zero crossing instants of the link current. The fundamental frequency components of the resonant dc link CSI output current is synthesised by these pulses. The disadvantage of the circuit is the high peak current through the semiconductors.

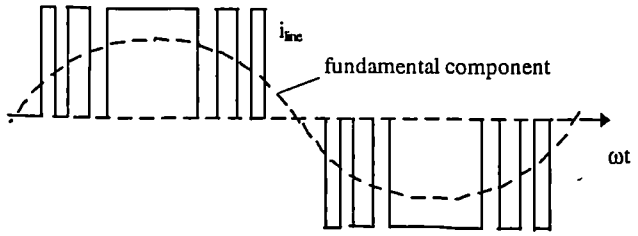

Figure 6.5 Current waveform of PWM CSI

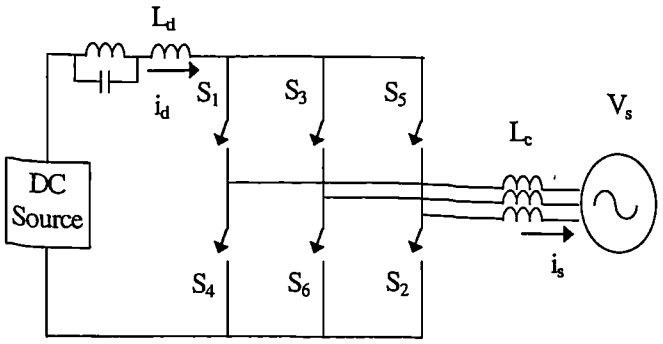

Figure 6.6 Resonant dc link CSI

6.2 Grid Connected Ideal CSI

This section describes a grid connected ideal CSI, which is self commutated. Commutation inductance is ignored and balanced operation is assumed, hence this inverter could operate at any power factor and the current commutation could be completed instantly.

Power characteristics

For a CSI without commutation inductance, the a.c. current may be changed instantly, the relation of the inverter a.c. terminal phase voltage (v_s) and the inverter output a.c. current (i_s) is shown in figure 6.7. α is the inverter ignition (delay) angle and is measured as shown in figure 6.7 (30° from the phase voltage zero crossing point).

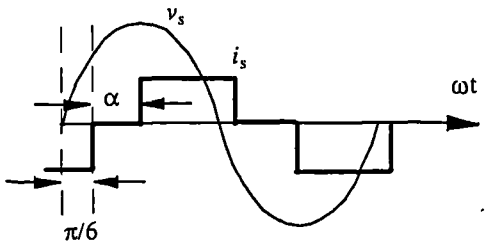

Figure 6.7 Waveforms of grid voltage and CSI current

Considering the fundamental frequency components only and choosing the ac grid line-neutral voltage, as the reference phasor $\dot{V}_S = V_S \angle 0$, then the voltage and current can be expressed by the phasor diagram shown in figure 6.8 where I_{s1} is the fundamental component of the inverter output ac current, $I_{s1(p)}$, and $I_{s1(q)}$ are respectively the real and reactive components of I_{s1}, ϕ_1 is the displacement angle (the angle between the voltage of the inverter ac terminal (v_s) and the inverter output a.c. current fundamental component). In the ideal CSI case, ϕ_1 is equal to the delay angle α, therefore the output power of the inverter has a power factor of cosα.

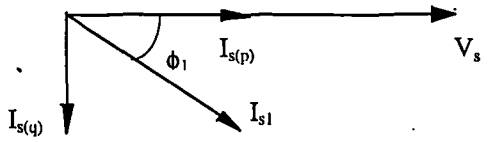

Figure 6.8 Phase diagram of grid connected CSI

The real and reactive power can be expressed as:

$$P_s = \sqrt{3} \times V_s I_{s1} \cos\phi_1$$

$$Q_s = \sqrt{3} \times V_s I_{s1} \sin\phi_1 \qquad (6.1)$$

In square wave switching mode, the fundamental ac current on the grid side is related to the dc current by

$$I_{s1} = a_t \frac{\sqrt{6}}{\pi} I_d$$

I_{s1} is the transformer grid side current, a_t is the transformer ratio.

In a current source converter, d.c. current will not change direction, the transition from inverter mode to rectifier mode is effected by controlling the ignition angle to reverse the d.c. voltage. The average d.c. voltage at the inverter d.c. terminal depends on the a.c. grid voltage and the ignition angle and can be expressed as

$$V_d = a_t \frac{3\sqrt{2}}{\pi} V_s \cos\alpha$$

The average dc link voltage of the CSI and therefore the power is decided by the ignition angle. The converter can generate or absorb both real power and reactive power if the ignition angle α can be shifted from 0 to 360 degrees (the self-commutated CSI case). Similar to the VSI cases, forced commutation is required for all the leading power factor operation modes while for lagging power factor operation, natural commutation takes place. For a certain d.c. current value I_d with a fixed switching pattern (fixed ratio of I_d to I_{s1}), the real or reactive power but not both could be controlled by timing the gate signals to regulate the ignition angle α. However, both the phase angle and current magnitude need to be controllable for providing controllable real and reactive power.

The real and reactive power characteristics of the grid connected CSI are shown in figure 6.9 where the d.c. current and delay angle are used as parameters. The circular dashed lines correspond to d.c. currents from 0.1 pu to 1.0 pu, the solid radial lines correspond to delay angles from 0° to 360° (as marked in the figure). The grid voltage is fixed at such a value which will produce 1.085 pu average dc voltage at 0° delay angle. Positive real power represents rectifier mode and positive reactive power corresponds to the reactive power taken by the converter.

Optimal real power control

Considering the optimal operation condition of the generator-rectifier system, a varying d.c. voltage is required at the rectifier d.c. terminal. The average dc voltage should be controlled to follow the optimal d.c. voltage curve, then the d.c. current and power would trace the optimal curves to realise maximum power capture.

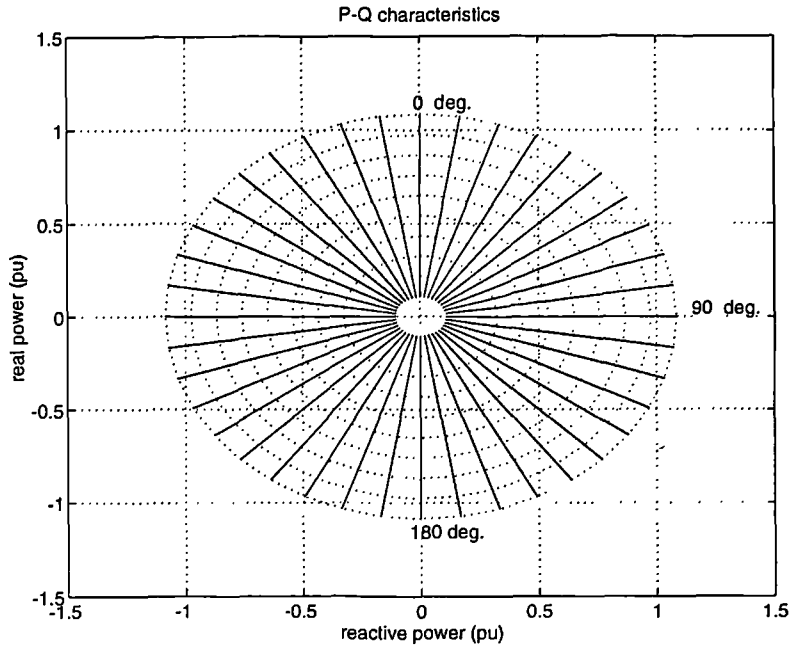

Figure 6.9 CSI real and reactive power characteristics (parameter: α and I_d)

Assuming a lossless inverter, the input d.c. power should be equal to the output a.c. power,

$$P_s = \sqrt{3} V_s I_{s1} \cos\phi_1 = P_d = V_d I_d$$

If the relation of a.c. current and d.c. current (including the transformer ratio and switching pattern factors) is expressed as $\sqrt{3}\, I_{s1} = K_{di}\, I_d$, the d.c. and a.c. voltages are related by

$$V_d = K_{di}\, V_s \cos\phi_1$$

Therefore the d.c. power transfer could be analysed with the circuit shown in figure 6.10. If the CSI is controllable in K_{di} and ϕ_1, the optimal real power could be delivered by the generator and rectifier system and transferred into the grid with a desired power factor.

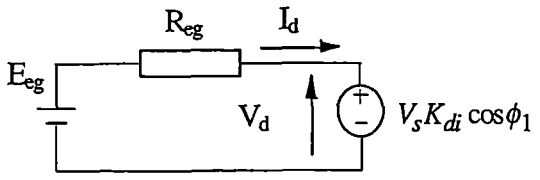

Figure 6.10 Equivalent circuit for dc power transfer analysis (ideal case)

6.3 Self Commutated CSI vs. VSI

Both self-commutated CSI and VSI can operate at any power factor. However, self-commutated CSIs require switching elements which can withstand negative voltages, but the available high power self commutation semiconductor devices cannot normally withstand negative voltage. Consequently, power diodes must be connected in series with each switching device. As a result, the overall cost of the converter and operating losses are increased.

VSIs usually offer more convenient control. For example, the voltage source inverter can be switched off very rapidly as a means of circuit protection without any difficulty arising from the stored energy. On the other hand, CSIs would generate large overvoltage, an additional shunt-connected capacitor may thus be required which will increase the cost.

Self-commutated devices ease the implementation of higher frequency switching techniques. Both self-commutated VSI and CSI could operate with high frequency switching techniques and result in reduced low order harmonics and increased high order harmonics. Basically a VSI is a voltage harmonic source while a CSI is a current harmonic source. Usually, a network, having a high impedance (the series tuned circuit) to harmonic current, and being able to support any waveform of voltage impressed upon it, is best supplied by a voltage source inverter, while the current source inverter is suitable for a parallel tuned network, which has a low impedance to harmonics, and the current harmonics will produce less voltage harmonic pollution. Therefore, from the harmonic point of view, a high frequency switching VSI is preferred over a high frequency switching CSI for the present application.

For these reasons, the self commutated CSI is not studied further in this thesis. However, the line commutated thyristor CSI, which has the advantages of low cost, reliability and higher power level components available, will be investigated in the following sections.

6.4 Phase Controlled Line-Commutated Thyristor CSI (SCR-CSI)

Circuit and operation

The basic circuit of a six pulse three phase SCR-CSI is shown in figure 6.11.

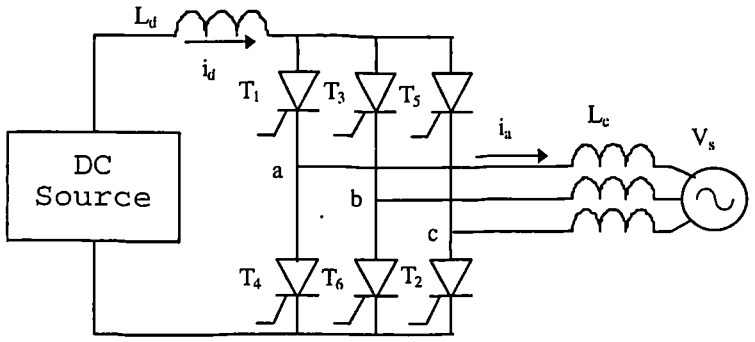

Figure 6.11 Basic structure of current source inverter

As discussed in the ideal CSI case, for a given a.c. line voltage, by phase control, controlling the instant at which the thyristor gate pulse is applied with respect to the a.c. voltage waveforms (delay angle α), the phase relation between the phase current and grid voltage, and therefore, the power output can be regulated and the power direction can also be reversed. Square wave switching is normal and is assumed.

Theoretically, for a delay angle in the range of 0° to 180°, the a.c. voltage has the correct polarity to commutate the current naturally. With a delay angle of 0° to 90°, the converter operates in a rectifier mode and for the range of 90° to 180° it operates in the inverter mode.

In practice, some inductance is present in the circuit, the current commutation is not completed instantaneously. It takes a finite time for the current to decay from I_d to 0 in the outgoing device and for the current to build up from 0 to I_d at the same rate in the incoming device (both in the upper group or in the lower group) The time period is called commutation or overlap period u (commutation or overlap angle). During the overlap period, the two phase voltages are shorted together through commutating inductance L_c (the inductance between the inverter and the reference point of the a.c. system) in each phase. The commutation interval, u, varies with the ignition angle α, L_c, d.c. current and a.c. voltage. The existence of an overlap angle extends the conduction

period of the outgoing semiconductor, reduces the average d.c. voltage and increases the displacement angle, so that inversion always begins at a α less than 90°.

In inverter operation, the extinction (recovery) angle, γ, is often used, γ is the period from the outgoing semiconductor stopping conduction to a positive voltage being applied on the device and it is related to α and u by

$$\gamma = 180^\circ - (\alpha + u) \qquad (6.2)$$

Figure 6.12 shows these angles. In inverter operation, a sufficient margin angle (γ_{min}), greater than the device turn off time, should be maintained to avoid commutation failure for reliable operation. Therefore the feasible operation range of a SCR-CSI is given by $(\alpha+u)<180^\circ - \gamma_{min}$.

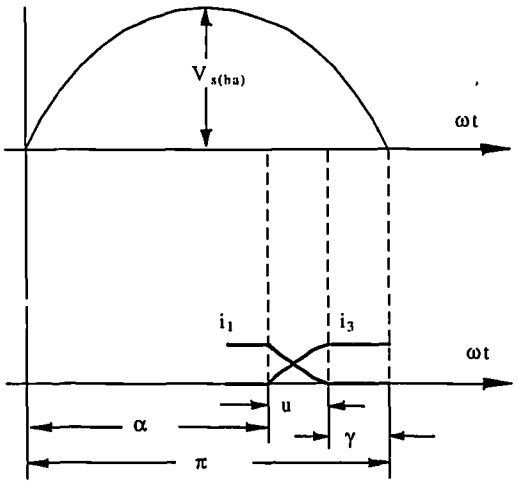

Figure 6.12 Relation of delay angle, overlap angle and extinction angle

Fundamental relations

Considering the effects of the overlap angle u, the basic equations of the inverter are as follows [58, 5]:

for u<60°

$$V_d = \frac{3\sqrt{2}}{\pi} V_s \cos\alpha - \frac{3\omega L_c}{\pi} I_d$$

$$\cos(\alpha+u)=\cos\alpha-\frac{2\omega L_c}{\sqrt{2}V_s}I_d$$

$$\tan\phi_1=\frac{2u+\sin 2\alpha-\sin 2(\alpha+u)}{\cos 2\alpha-\cos 2(\alpha+u)} \qquad (6.3.a)$$

The overlap angle u will increase with increasing I_d and reducing V_s when u exceeds 60° the following alternative formulae apply.

for u≥60°

$$V_d=\frac{3\sqrt{6}}{\pi}V_s\cos(\alpha-30^o)-\frac{9\omega L_c}{\pi}I_d$$

$$\cos(\alpha+u+30^o)=\cos(\alpha-30^o)-\frac{2\omega L_c}{\sqrt{6}V_s}I_d$$

$$\tan\phi_1=\frac{2u+\sin 2(\alpha-30^o)-\sin 2(\alpha+u+30^o)}{\cos 2(\alpha-30^o)-\cos 2(\alpha+u+30^o)} \qquad (6.3.b)$$

Only under abnormal modes, the converter will operate with an overlap angle larger than 60°. For example, after a fault near the converter, the nearly normal value of d.c. current needs to be commutated by a reduced a.c. voltage. Normally the converter operates with an overlap angle less than 60°. The d.c. current and the r.m.s. value of the a.c. current fundamental component are related by

$$I_{s1}=a_t k\frac{\sqrt{6}}{\pi}I_d \qquad (6.4)$$

For normal operation (u<60°), the coefficient *k* can be expressed as [58]

$$k=\frac{\sqrt{[\cos 2\alpha-\cos 2(\alpha+u)]^2+[2u+\sin 2\alpha-\sin 2(\alpha+u)]^2}}{4[\cos\alpha-\cos(\alpha+u)]}$$

Figure 6.13 gives a comparison of the delay angle, α (as marked in the figure) and the displacement angle (ϕ_1) with commutation angle taken into account. The following parameters are used

V_s=1.085 pu, commutation reactance X_L=0.05 pu and d.c. current 0.1, 0.2, ...,1.0 pu. It can be seen that a higher d.c. current will result in a larger difference between the delay angle and the displacement angle, the difference tends to be larger at high power factor (

α approaching 0° or 180°). The P-Q chart is shown in figure 6.14 where the dashed line shows the ideal converter characteristics for comparison, again, I_d (0.1, 0.2, ...,1.0 pu) and α (5°, 15°, ..., 155°) are used as parameters with V_s=1.085 pu and X_L=(ω L_c)=0.05 pu.

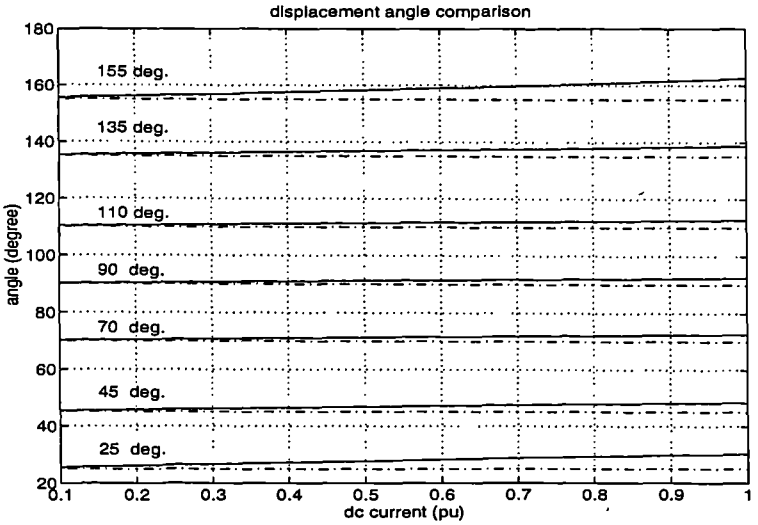

displacement angles ———
delay angles.....

Figure 6.13 Delay angle and displacement angle vs dc current

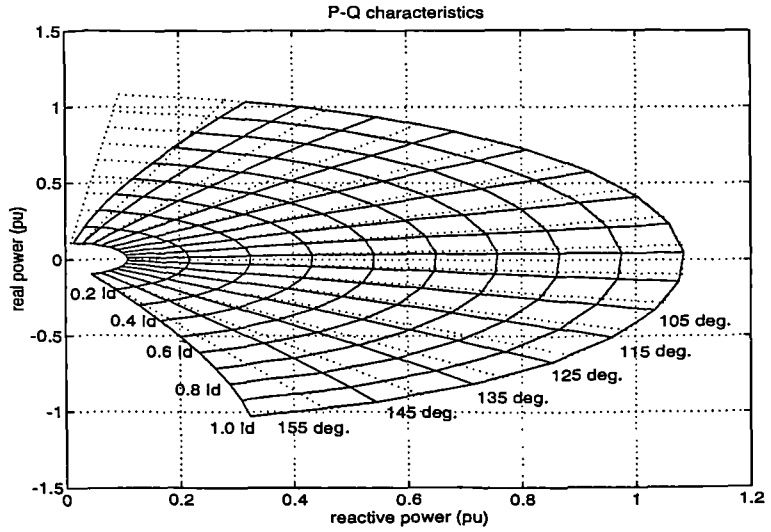

converter characteristics (overlap angle effect)———
ideal converter characteristics.....
dc current and delay angle are labelled

Figure 6.14 Thyristor CSI P-Q chart diagram (parameter: α and I_d)

6.5 Power Control of SCR-CSI

6.5.1 Power controller

For the maximum power capture, it is necessary to follow the optimal trajectories of rectifier terminal voltage and current in figure 5.12. In SCR-CSI case, the d.c. voltage may be expressed as (equation 6.3),

$$V_d = K'_{di} V_s \cos\alpha - X_L' I_d \qquad (6.5)$$

where $K'_{di} = a_t \frac{3\sqrt{2}}{\pi}$, $X'_L = \frac{3X_L}{\pi}$ for u $\leq 60°$

Therefore, the circuit shown in figure 6.15 may be used for the DC link power transfer analysis of SCR-CSI. Clearly, within the limits set by V_s and X'_L, any desired magnitude of real power can be achieved by phase angle control.

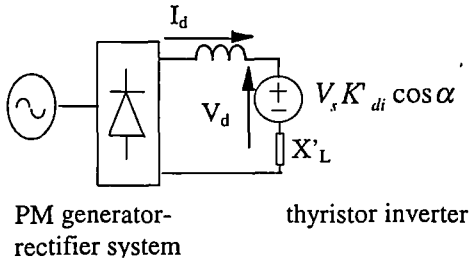

Figure 6.15 Equivalent circuit for dc power transfer analysis of SCR-CSI

Again, the wind turbine speed can be controlled by the generator reaction torque which, in turn, is determined by the ignition firing angle of the inverter. Firing angle is thus the principal control parameter for the generator speed in this system. Real power optimal equilibrium is established when the operating point on the characteristic matches the operating point on optimal turbine power/speed curves. For any given shaft speed, there exists a set of corresponding optimal power, DC link voltage and current. From equation (6.5) for a set of the given V_s, V_d and I_d, a corresponding delay angle can be decided. Such relationship could be stored in the memory of the controller and compared with actual operating points to decide the amount of firing angle adjustment required. A suitable controller block diagram is shown in figure 6.16. The inputs are machine speed (or frequency), DC link voltage, current and a.c. network voltage. The single output is the ignition angle (α).

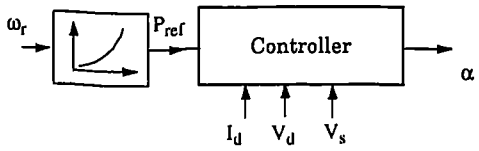

Figure 6.16 Schematic power controller

6.5.2 Phase angle controlled SCR CSI in a simplified system

A simplified system shown in figure 6.17 is used to study the performance of a phase angle controlled SCR CSI, where the line commutated SCR inverter is connected to an infinitive a.c. bus through a transformer. The commutation reactance is 5%. It is assumed that the wind speed varies from 0.33 pu to 1.0 pu. A smaller extinction angle could result in a better power factor, so that the extinction angle is set as 14° at the rated operation condition.

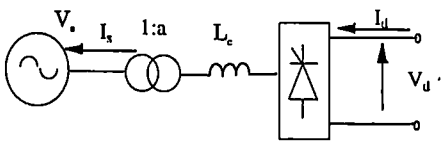

Figure 6.17 SCR-CSI in a simple system

The resulting real power, reactive power and the corresponding delay angle, extinction angle and overlap angle are shown in figure 6.18.

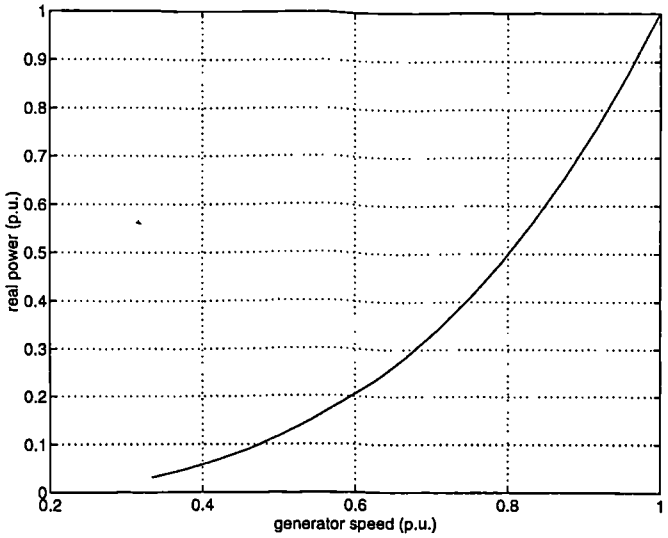

a) real power

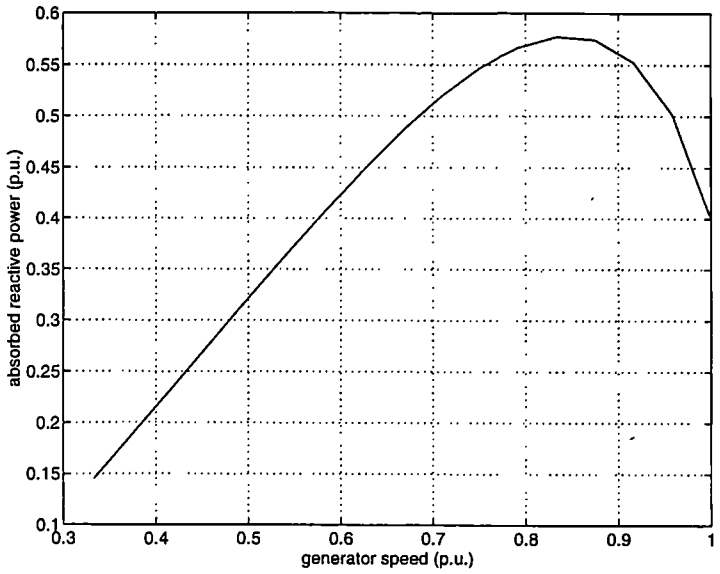

b) reactive power

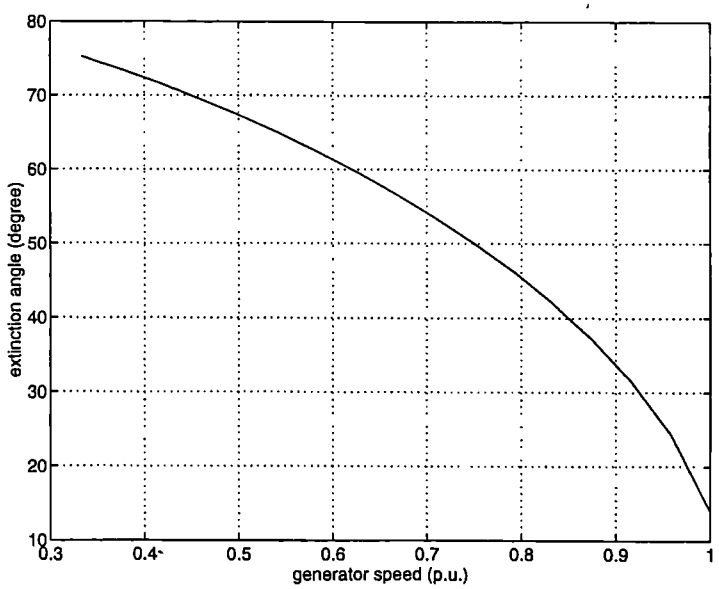

c) extinction angle

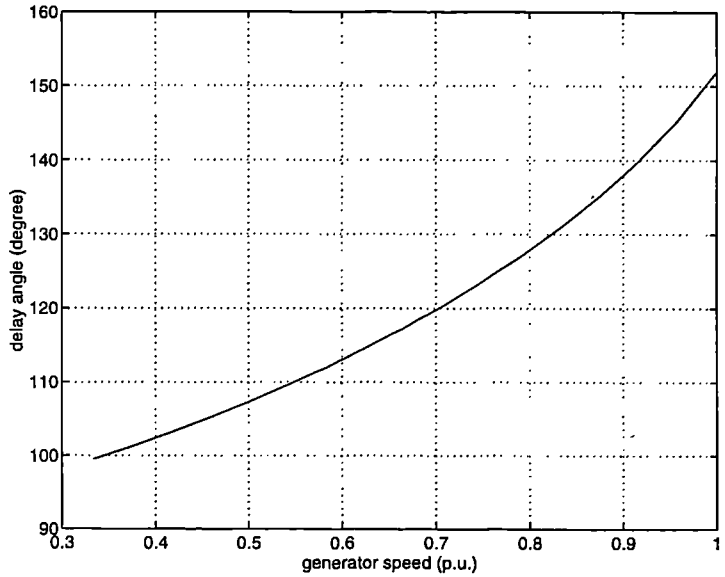

d) delay angle

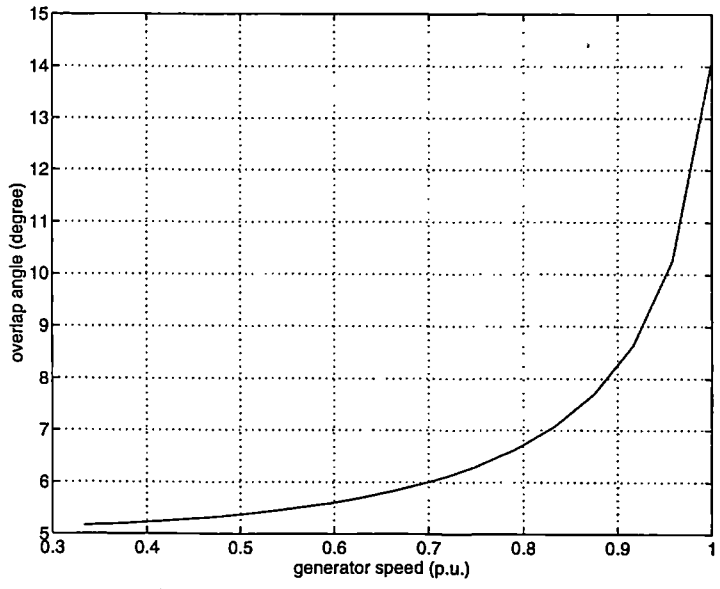

e) overlap angle

Figure 6.18 Operation characteristic of a phase angle control SCR-CSI in simple system

The operation curve is also plotted on the SCR converter P-Q characteristics in figure 6.19.

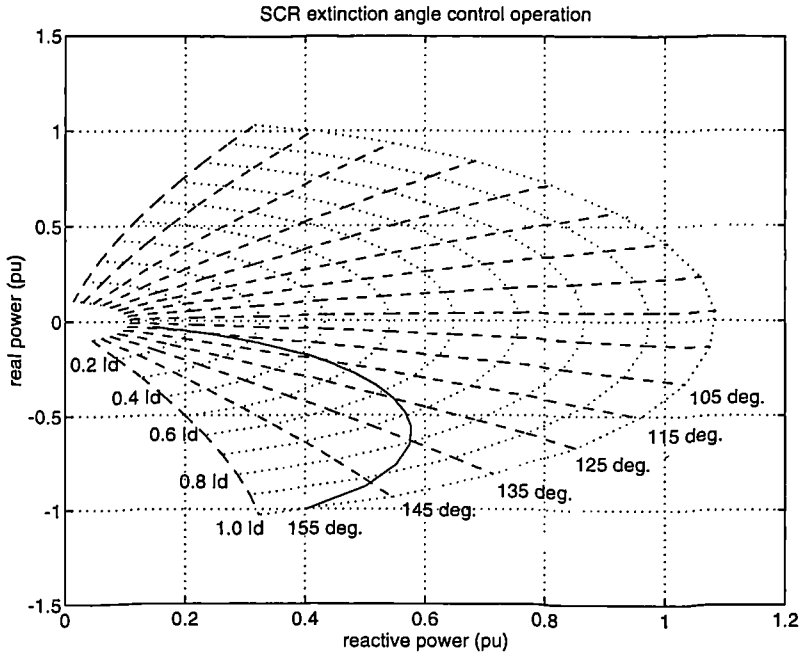

Figure 6.19 P-Q trajectory of a phase angle control SCR-CSI in simple system

The result indicates that the system could deliver optimal power into the grid by phase angle control. It also shows the system requires a large range variation of phase angle to transfer the desired power and needs a significant amount of reactive power to be supplied by the grid.

The reactive power is related to d.c. current, grid voltage and ignition angle. The reactive power transmission to the SCR inverter may reduce the voltage at the connecting point and cause problems for the operation of both the inverter and the system.

6.6 Line Commutated SCR-CSI in the Test System

In this section, the behaviour of the line commutated SCR-CSI in a test system is studied. The same system and operation conditions as that in section 5.8 are used, except that the SCR inverter interfaces the wind farm directly to the bus 2 as shown in figure 6.20.

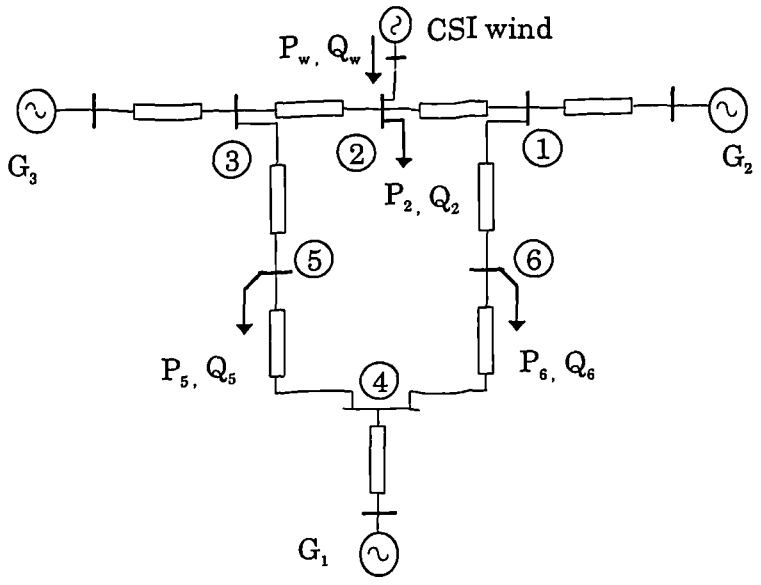

Figure 6.20 Thyristor CSI wind power test system

Power flow analysis with SCR inverter

The power flow equations in chapter 5 can still be used for the power system analysis, however, in the CSI case, the magnitude and power angle of the inverter a.c. terminal voltage fundamental component are not the direct controllable variables. The ideal P and Q could not be simply achieved by regulating these parameters. The direct control variable is the delay angle α.

The SCR inverter may be represented by its real and reactive power (P_w, Q_w) injected at the connected bus to perform the network power flow analysis. For optimal power operation, the generator-rectifier system should follow the optimal d.c. power, voltage and current ($P_{d,opt}$, $V_{d,opt}$, *and* $I_{d,opt}$) curves (section 5.4). However, it should be noted that the generated power, the d.c. voltage and power factor are related via the phase angle control setting and the a.c. bus voltage which are effected by the real and reactive power generated by the inverter. Therefore an iterative computation between the inverter equations and power flow equations is required to analyse the system. For example, at a certain operating point *k*, the following procedure may be followed:

- choose a $\gamma^{(k)}$, to satisfy equation (6.5) for a set of grid voltage $V_2^{(k)}$ (bus 2), optimal $V_{d,opt}^{(k)}$, and $I_{d,opt}^{(k)}$,
- calculate the overlap angle $u^{(k)}$ and displacement angle $\phi_1^{(k)}$,

- calculate the real and reactive power ($P_w^{(k)}$, $Q_w^{(k)}$),
- perform power flow analysis to solve for a group of new system voltage (including $V_2^{(k)}$),
- if $V_2^{(k)}$ is converged the solution is found otherwise choose a new $\gamma^{(k)}$ with the renewed $V_2^{(k)}$ and repeat the above procedure.

A flow chart of such computation is given in figure 6.21.

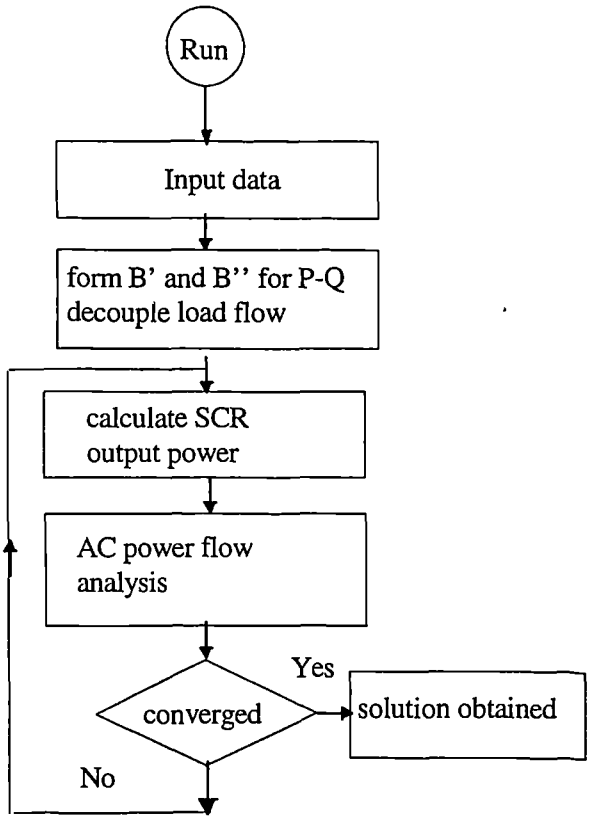

Figure 6.21 Flow chart for power analysis of ac system with SCR inverter

Calculation results

The computations of power flow analysis of the test ac system with SCR inverter are performed under the condition of the real power generated by the wind farm varying from 5% to 100%. Figure 6.22 shows the inverter extinction angle, the inverter reactive power, the voltages of the inverter connection bus (bus 2), bus 5 and bus 6.

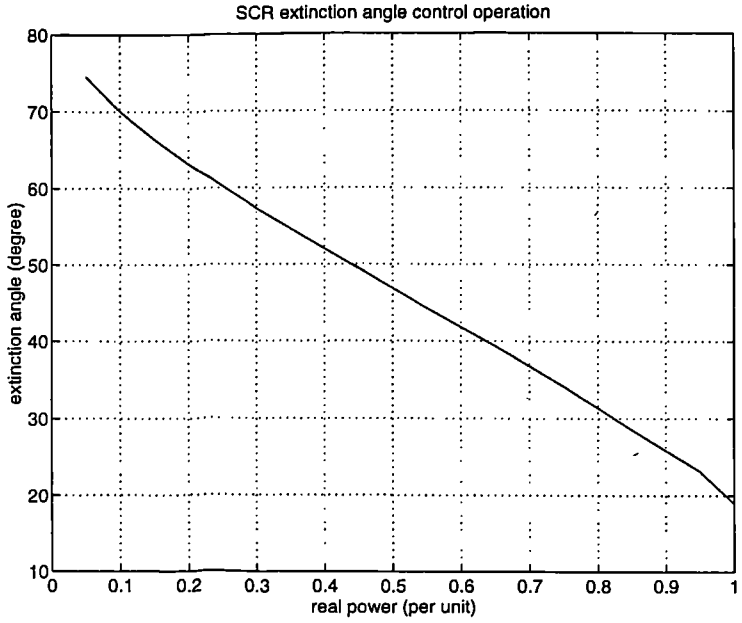

(a) inverter extinction angle(γ)

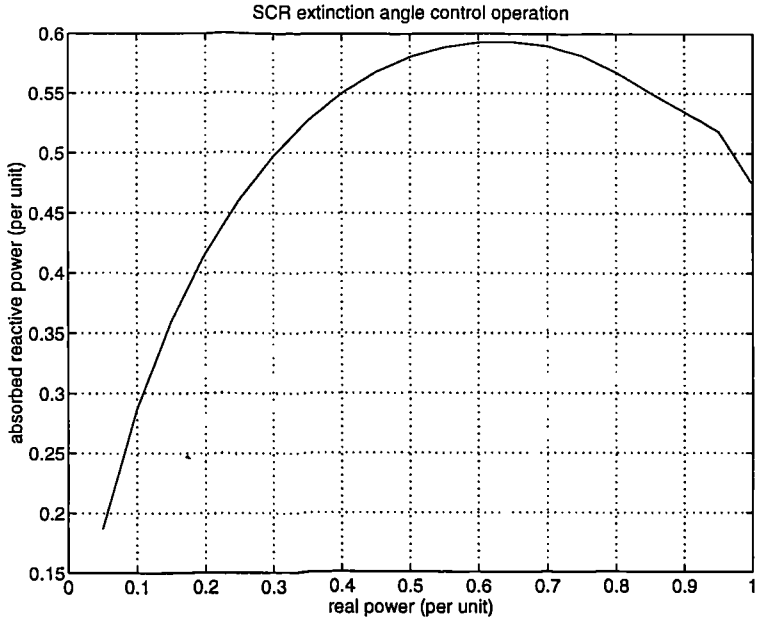

(b) CSI absorbed reactive power

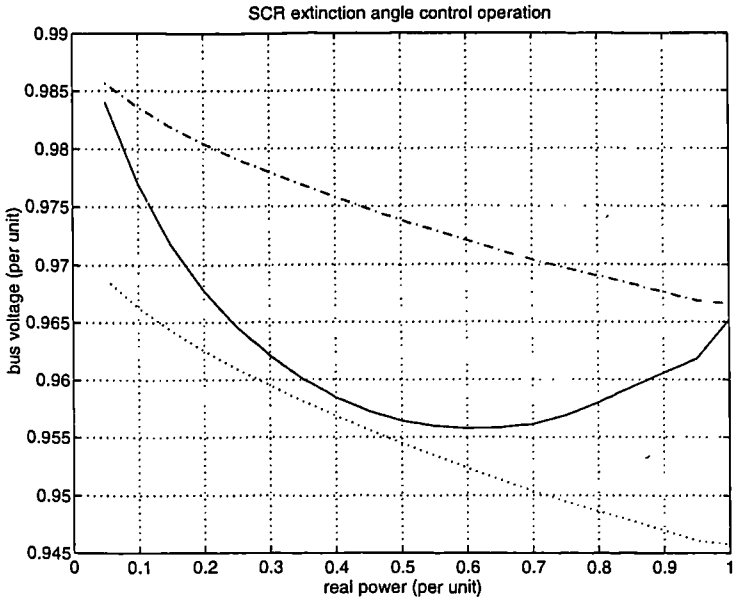

Bus 2 voltage ———
Bus 5 voltage .....
Bus 6 voltage .-.-.-.-.-.

(c) bus voltages

Figure 6.22 SCR-CSI with extinction angle control in a test system

It can be seen that the voltage fluctuation is quite significant in the considered system even with two generating buses, G_2 and G_3 operating as PV buses. The results show that the voltage fluctuates over a wide range (2.8%) at the inverter connection bus (bus 2) and the voltage fluctuation at bus 5 and bus 6 are 2.3% and 1.9% respectively. Considering the statutory limitation of 2% [88], the voltage fluctuation could cause problems to loads connected on these buses.

Obviously, the SCR-CSI needs a reactive power compensator to operate appropriately and economically since a charge is made for the reactive power supplied by the grid. Although the self commutated CSI with a controllable current ratio (the ratio of the d.c. current at rectifier terminal and the fundamental a.c. current into the a.c. network) could provide controllable real and as well as reactive power, it is less attractive than self commutated VSI (section 6.3). A tap changing transformer could reduce the range of the phase angle regulation and help the power factor control. However, in any case, for a CSI, harmonic filtering equipment is needed to attenuate the current harmonics,

therefore it is reasonable to consider adopting some form of compensation device to meet both the reactive power supply and harmonics minimisation requirements. Static PFC capacitor or an active SVC form of compensator may be considered singly or in combination. A detailed study of such systems is given in chapter 10.

6.7 Conclusions

Current Source Inverters (CSIs) and its application in the considered wind energy conversion system are discussed.

The typical circuits and operations of CSIs are presented. A comparison of self-commutated VSI and self-commutated CSI indicates the VSI is more attractive if self-commutated devices are used.

The line commutated SCR inverter and its optimal power transfer control are discussed in detail. The characteristics of SCR-CSI interfaced wind farm in the simplified system are studied. A computational analysis method of SCR-CSI interfaced wind farm in a network is presented and results are given for a test system.

The line-commutated SCR inverter has the advantage of economical, reliable and suitable for high power application, but the problems of reactive power and harmonics need to be solved. It is proposed to use an active compensator system in parallel with the inverter to control the power factor and to minimise the current harmonics.

Based on the studies of chapter 5 and chapter 6, the line commutated SCR CSI and self-commutated VSI are chosen as the candidates of the DC/AC frequency inverter for a comprehensive investigation.

Chapter

7.

Harmonic Considerations of Power Electronics Inverters

In this chapter, the harmonic characteristics of grid connected inverters are studied and harmonic minimisation techniques are discussed. Based on the studies of this chapter, chapter 5 and 6, technically feasible DC/AC conversion systems are proposed.

7.1 Introduction

Harmonic sources

In general, power system harmonics result from the non-linear impedance characteristic of the power equipment. Such equipment includes transformers which have non-linear magnetisation characteristics of the iron core, pulse burst heating, arc furnaces and domestic electronic equipment with rectifier such as television sets. However, with the advanced applications of power electronic devices which operate by on and off switching, the power electronics converters are now considered as the most serious harmonic pollution sources in power system. Clearly the harmonic performance is an important aspect of the power electronics interface of the renewable energy systems.

The orders and levels of the harmonic injected into the a.c. system are dependent on the converter configurations (pulse number, etc.), switching patterns (square wave, higher switching technique, etc.) and operating condition (dc link voltage, power angle, ignition angle). The inverter studies of chapter 5 and 6 indicate that the self-commutated VSI and line commutated SCR-CSI are the leading candidates for the grid interface inverter in the considered application. In this chapter, the harmonic characteristics of these two types inverters are addressed and harmonic reduction techniques are introduced.

Converters generate harmonic voltages and currents on the a.c. side and ripple on the d.c. sides. Due to the reactive component in the DC link, a CSI presents mainly current harmonics on the a.c. side and voltage ripple on the d.c. side while a VSI generates current ripple on the d.c. side and voltage harmonics on the a.c. side. DC ripple can be absorbed by the reactive components in the DC link so as not to cause problems to the operation of the generator and rectifier system. However, the harmonics on a.c. side could distort the a.c. system. These a.c. side harmonics are the main consideration of this study. From the point of view of the a.c system, a CSI is a current harmonic source while a VSI is a voltage harmonic source.

Harmonics can be classified as characteristic and noncharacteristic harmonics. The characteristic harmonics generated by a converter of pulse number p, which is the number of nonsimultaneous commutations per cycle of the fundamental a.c. component, are principally of order n=pq on the d.c. side and n=pq±1 on the a.c. side, q being any integer. In practice, some other order harmonics also exist often due to the unbalance of the circuit and/or of the switching control. This chapter is mainly focused on the characteristic harmonics.

Harmonic effects

Harmonic content is a very important aspect of power quality. The main problems associated with harmonic distortion are:

- Additional losses and heating, higher level noise in rotating machines;
- Overloading/overheating of power electric equipment and power factor correction capacitors;
- instability of converter controllers;
- Interference with telephone and telecommunication networks;
- Mal-operation of electric meters, measuring instruments and protective relays.

Power quality expression

The distortion relating to a particular nth harmonic content in an a.c. waveform may be expressed by the ratio of the r.m.s. amplitudes of the nth harmonic component to the fundamental component as:

n^{th} voltage harmonic factor $$VHF_{(n)} = \frac{V_{(n)}}{V_{(1)}} \times 100\%$$

n^{th} current harmonic factor $$CHF_{(n)} = \frac{I_{(n)}}{I_{(1)}} \times 100\% \qquad (7.1)$$

where $V_{(1)}$ and $I_{(1)}$ are fundamental components of the voltage and current and $V_{(n)}$ and $I_{(n)}$ are the nth order harmonic components of the voltage and current. In the voltage and current waveform, the distortion component, the summation of the r.m.s. value of the harmonic components, can be defined as:

$$V_{dis} = \left[V^2 - V_{(1)}^2\right]^{1/2} = \left[\sum_{n=2}^{\infty} V_{(n)}^2\right]^{1/2}$$

$$I_{dis} = \left[I^2 - I_{(1)}^2\right]^{1/2} = \left[\sum_{n=2}^{\infty} I_{(n)}^2\right]^{1/2} \qquad (7.2)$$

where V and I are rms value of voltage or current waveform. To quantify the distortion in the voltage and current waveforms, the total harmonic distortion, the ratio of the distortion component to the r.m.s. value of fundamental component, is often used. The total voltage harmonic distortion (*TVHD*) and the total current harmonic distortion (*TCHD*) are:

$$TVHD = \frac{V_{dis}}{V_{(1)}} \times 100\%$$

$$TCHD = \frac{I_{dis}}{I_{(1)}} \times 100\% \qquad (7.3)$$

The harmonic standards varies between the various system voltage levels and between counties. Normally, it is required that the TCHD of the current injected into the system is below 5%.

The power factor of power injected into an a.c. system can be defined as:

$$PF = \frac{V_s I_{(1)} \cos\phi_1}{V_s I} = \frac{I_{(1)}}{I}\cos\phi_1 = \frac{I_{(1)}}{I} DPF \qquad (7.4)$$

V_s is the ac system voltage with the ideal sinusoidal voltage waveform. The displacement power factor is defined as $DPF=cos\ \phi_1$. ϕ_1 is the phase angle between V_s and $I_{(1)}$.

It is noted that a higher distortion in the line current will result in a smaller value of the current ratio $I_{(1)}/ I$ and hence a poorer power factor and utilisation of equipment. The power factor will always be less than unity when harmonic components exist, even in the case that the current is in phase with the voltage, as in the diode rectifier case.

System and methods for the studies

In this chapter, it is assumed that the a.c. system is balanced and the considered inverter is the only harmonic source in the a.c. system. Although the harmonic distortion in a complex system could be analysed by harmonic power flow methods, the simplified system of an inverter connected to an infinite balanced three phase a.c. bus, is sufficient to evaluate the harmonic performance and the harmonic reduction methods of the inverters. It is also assumed that the inverter is in the balance operation, the semiconductors have ideal switching characteristics.

The harmonic analysis can be performed in both the frequency domain and the time domain. Although the time domain analysis gives the waveforms and hence could include the transient harmonics therefore a better understanding of all parts of the system, the frequency domain analysis is relatively simple and is sufficient to check compliance with standards. In this chapter, frequency domain harmonic analysis methods are used. In the later chapters, the harmonic performance from the time domain analysis and experiments will be presented along with the investigated inverters.

7.2 Harmonics of Grid Connected VSI

Harmonic analysis model

The system comprising VSI and ac grid may be represented by the simple single phase equivalent circuit shown in figure 7.1(a). Where the ac grid is represented by a sinusoidal voltage source, the inductance L_s, which is the inductance between ac system and VSI, normally represents the coupling inductor, transformer and ac system equivalent impedance and the resistance is usually ignored. The circuit models for the frequency domain study are given in figure 7.1(b) and (c), it is assumed that the inductance is free of losses and L_s is independent of frequency. Therefore,

$$X_{(n)} = \omega_{(n)} L_s = n\omega_{(1)} L_s = nX_s \tag{7.5}$$

where $\omega_{(1)} = 2\pi f$, f is ac system frequency.

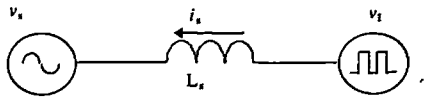

(a) single phase equivalent circuit

(b) fundamental component (c) nth harmonic component

Figure 7.1 Single phase circuits of grid connected VSI

The voltage waveform at the inverter terminal could be synthesised on the basis of the inverter switching patterns and then the voltage harmonics, $V_{I(1)}$, $V_{I(2)}$, $V_{I(3)}$, ... $V_{I(n)}$, etc. can be obtained by Fourier analysis of the inverter ac terminal voltage waveform. The current harmonics, $I_{I(1)}$, $I_{I(2)}$, $I_{I(3)}$, ... $I_{I(n)}$, etc., can be calculated in frequency domain by applying the voltage harmonics to the circuits shown in figure 7.1.

AC Voltage waveforms and harmonics of VSI

Assuming the semiconductors have ideal switching characteristics then the output voltage waveform of the voltage source inverter is determined entirely by the pattern in which the semiconductors are turned on and off and, in the case of multi-pulse systems introduced later in this chapter, the way by which they are combined in the transformer.

The general waveforms of voltage and current are independent of the type of valves employed.

The ac voltage waveforms generated by the VSI are normally in the form of the quarter-symmetry step waveforms, such as the example shown in figure 7.2. By choosing the starting point of the Fourier integration, the waveform could be an odd function and the harmonics have rms values:

$$V_{(n)} = \frac{4}{\pi\sqrt{2}}\left[\int_0^{\alpha_1} V_{d1}\sin n\alpha d\alpha + \int_{\alpha_1}^{\alpha_2} V_{d2}\sin n\alpha d\alpha + \ldots + \int_{\alpha_{m-1}}^{\pi/2} V_{dm}\sin n\alpha d\alpha\right] \tag{7.6}$$

where V_{d1}, V_{d2} ... V_{dm} are the voltage values of the waveform as shown in Figure 7.2.

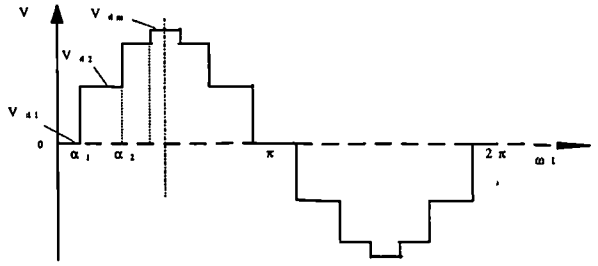

Figure 7.2 A general ac voltage waveform of VSI

Current harmonics injected into the grid

For the simplified system in figure 7.1, the inverter voltage, grid voltage and the impedance between the VSI and ac network, determine the current waveform. Referring to the circuits shown in figure 7.1(b) and (c), the fundamental current $I_{s(1)}$ and n^{th} harmonic current $I_{s(n)}$ can be calculated by

$$I_{s(1)} = \left|\frac{V_{I(1)}\angle\delta - V_s}{X_s}\right| = \frac{1}{|X_s|}\sqrt{(V_{I(1)}\cos\delta - V_s)^2 + (V_{I(1)}\sin\delta)^2} \tag{7.7}$$

and

$$I_{s(n)} = \left|\frac{V_{I(n)}}{nX_s}\right| \tag{7.8}$$

where

V_s AC system voltage

$V_{I(1)}$ fundamental frequency component of inverter output voltage

$V_{I(n)}$ n^{th} harmonic frequency component of inverter output voltage

δ power angle between $V_{I(1)}$ and V_s.

Power quality

VHF and TVHD can now be calculated using equations 7.1 and 7.3.

Current harmonic factor:

$$CHF_{(n)} = \frac{V_{I(n)}}{n\sqrt{(V_{I(1)}\cos\delta - V_s)^2 + (V_{I(1)}\sin\delta)^2}} \times 100\% \tag{7.9}$$

total current harmonic distortion:

$$TCHD = \frac{\left[\sum_{n=2}^{\infty}\left(\frac{V_{I(n)}}{n}\right)^2\right]^{1/2}}{\sqrt{(V_{I(1)}\cos\delta - V_s)^2 + (V_{I(1)}\sin\delta)^2}} \times 100\% \tag{7.10}$$

Displacement power factor and power factor:

$$DPF = \cos\phi_1 = \frac{\sin\delta}{\sqrt{(\cos\delta - V_s/V_{I(1)})^2 + (\sin\delta)^2}} \tag{7.11}$$

$$PF = \frac{\cos\phi_1}{\sqrt{(I_{dis}/I_{s(1)})^2 + 1}} \tag{7.12}$$

In summary, the frequency domain harmonics analysis of VSI can be carried out by following steps:

1. synthesise the inverter terminal voltage waveform,
2. calculate voltage harmonics by integrating the Fourier coefficient expression of the inverter terminal voltage waveform,
3. apply the voltage harmonics as voltage sources to the frequency domain equivalent circuits to calculate the current harmonics,
4. calculate the harmonic factor for individual harmonics, the total harmonic distortion and power factor.

7.3 Harmonic and Power Quality of Six-Pulse, Square-Wave VSI

In this section, the harmonic performance of the six-pulse, square-wave VSI is analysed with the above described procedure.

7.3.1 Voltage and current harmonic spectra

The ac phase voltage waveforms (inverter ac terminal to neutral point of the three phase system) of a six-pulse, square-wave inverter are shown in figure 7.3.

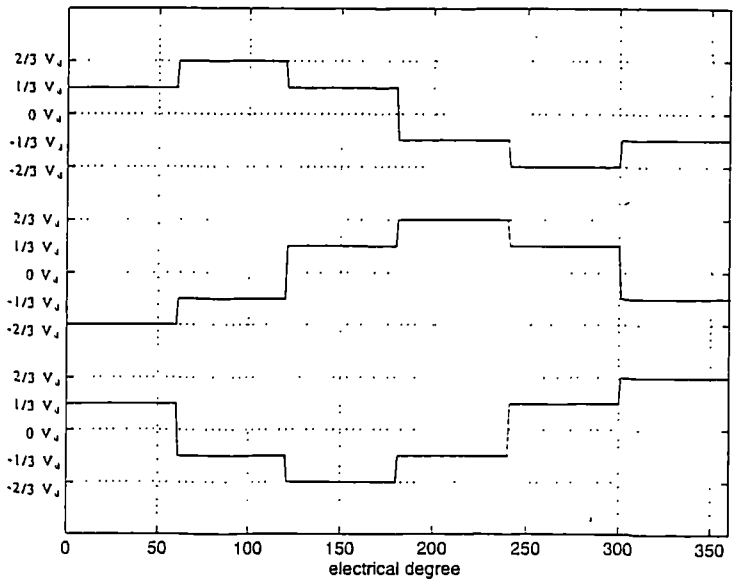

Figure 7.3 Voltage waveforms of a six pulse VSI

The rms values of the inverter terminal voltage waveforms can be calculated by using equation (7.6), then

$$V_{(n)} = \frac{4}{\pi\sqrt{2}}\left[\int_0^{\frac{\pi}{3}} \frac{V_d}{3}\sin n\alpha d\alpha + \int_{\frac{\pi}{3}}^{\frac{\pi}{2}} \frac{2V_d}{3}\sin n\alpha d\alpha\right] = \frac{4}{\pi\sqrt{2}}\frac{V_d}{3}\cdot\frac{1}{n}[1+\frac{1}{2}\cos\frac{n\pi}{3}] \qquad (7.13)$$

Only the fundamental component and odd order harmonics are presented in the phase to neutral voltage, they are related to the dc link voltage by:

$$V_{(1)} = 0.45V_d \quad \text{and} \quad V_{(n)} = \frac{1}{n}V_{(1)} \qquad (7.14)$$

Even harmonics should be absent as should all multiple order harmonics of 3. The typical voltage and current harmonic spectra (n=6q±1) are presented in figure 7.4 and 7.5. The following parameters are used, δ=10°, X_L= 0.2 pu, $V_{I(1)}$= 1.2 pu and V_s= 1.0 pu.

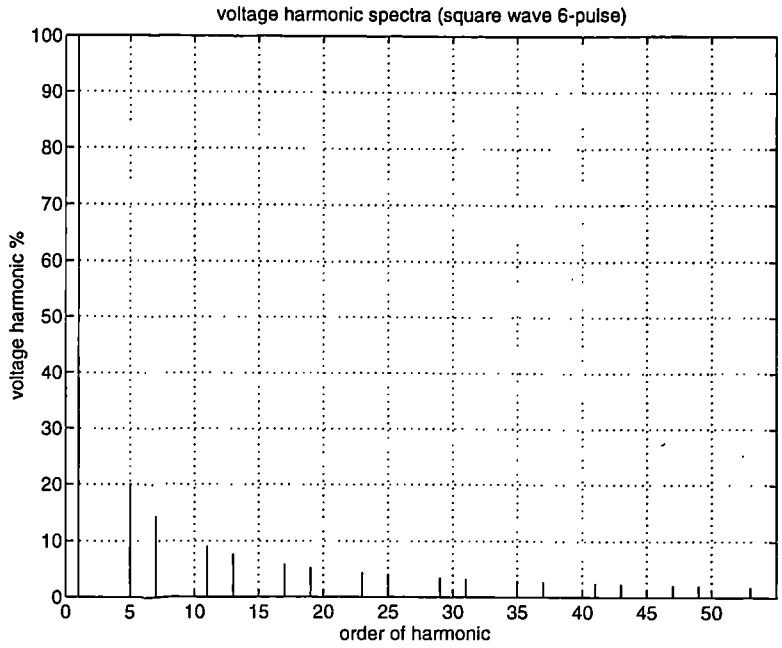

Figure 7.4 Voltage harmonic spectra of a six pulse square wave VSI

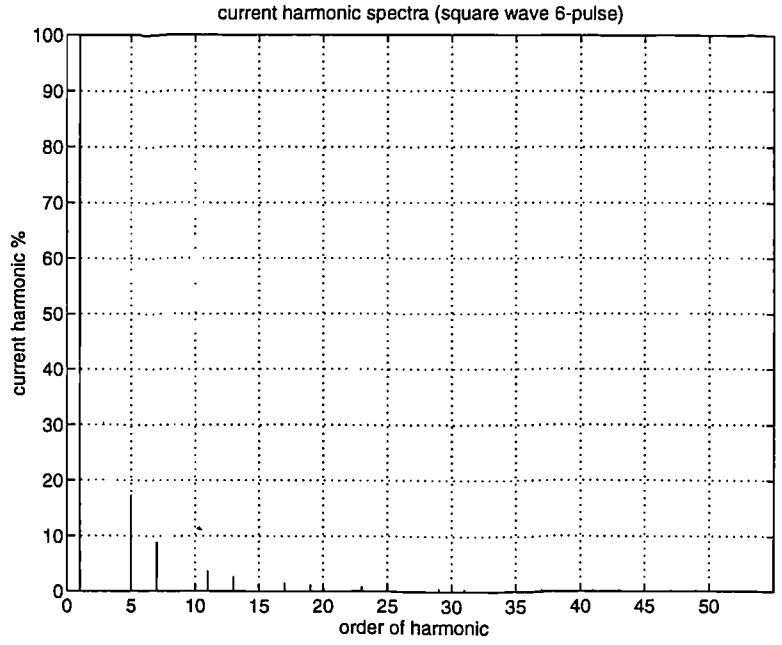

Figure 7.5 Current harmonic spectra of a six pulse square wave VSI

7.3.2 Harmonic distortion

For the six pulse, square wave grid connected VSI, the power quality expressions may be simplified to:

$$VHF_{(n)} = \frac{V_{(1)}/n}{V_{(1)}} 100\% = \frac{1}{n} 100\%$$

$$CHF_{(n)} = \frac{I_{s(n)}}{I_{s(1)}} 100\% = \frac{1}{n^2 \sqrt{(\cos\delta - V_s/V_{I(1)})^2 + (\sin\delta)^2}} 100\%$$

$$TVHD = \frac{V_{dis}}{V_{I(1)}} \times 100 = \left[\sum_{n=2}^{\infty} (1/n)^2 \right]^{1/2} \times 100\%$$

$$TCHD = \frac{\left[\sum_{n=2}^{\infty} (1/n^2)^2 \right]^{1/2}}{\sqrt{(\cos\delta - V_s/V_{I(1)})^2 + (\sin\delta)^2}} \times 100\%$$

From the power quality equations, it can be seen that the main factors affecting power quality are the power angle and the ratio of grid voltage to inverter ac voltage fundamental component. The quality of power generated by VSI is analysed as follows.

VHF and TVHD are the voltage ratios of the output voltage components of the inverter. For the fixed switching pattern and circuit configuration, these ratios are fixed and are independent of the dc link voltage, though the absolute value of voltage components are proportional to the dc link voltage. For instance, in square wave six-pulse inverter case, the ratio of fundamental component to the nth harmonic is n. VHF and TVHD are directly decided by the switching pattern and are not effected by the dc link voltage, power angle or system voltage.

CHF and TCHD are the ratios of the harmonic currents. The absolute values of the harmonic currents, are directly proportional to the dc voltage, while the grid voltage (V_s), and the power angle (δ), affect only the fundamental component. For a certain dc voltage, the higher order current harmonics are fixed, therefore a higher value of the fundamental current gives lower CHF and TCHD. Referring to the VSI phasor diagram, $I_{s(1)}$ reaches its maximum when δ approaches 180° and its minimum at 0° Therefore the CHF and TCHD are maximum at 0° and minimum at 180°. It can be seen that for a certain value of $I_{s(1)}$, a power angle approaching 0° (reactive power generation) gives the

worst harmonic performance, the best harmonic performance is at a power angle of 180° (reactive power absorption).

Both CHF and TCHD are expressed in terms of the relative values of the fundamental and harmonic components at a particular operating point, the absolute values of the harmonics must also meet the statutory standard.

DPF (Displacement Power Factor) represents the basic relation of the real power and reactive power and is not related to the harmonic distortion directly. For a fixed power angle other than zero in the studied region, DPF increases with increasing $V_{I(1)}/V_s$ ratio up to a maximum (unity DPF at purely real power operation), and then reduces again. The inverter is in reactive power absorption mode before the maximum point and the reactive power generation mode afterwards.

PF, the power factor, reflects the relation between the delivered real power and the required system capacity (carrying the real power, reactive power and harmonics). PF has similar characteristics to DPF except that the power factor is reduced by the harmonic contents in the high harmonic distortion zone.

Based on these equations, the harmonic distortions have been calculated for different power angle and $V_{I(1)}/V_s$ ratios. The TCHD, DPF and PF are presented for $V_{I(1)}/V_s$ varying from 0.5 to 1.5 in figure 7.6, figure 7.7 and figure 7.8 where power angle is used as the variable parameter. In figure 7.6, TCHD curves are given for power angles of 0°, 5°, 10°, 15°, 20°, 25° and 30° in downward sequence. The DPF and PF curves in figure 7.7 and 7.8 are for the same power angle but in upward sequence. For $V_{I(1)}/V_s$=1.0 and a small power angle, $I_{s(1)}$ is small and the TCHD is great. Also at a $V_{I(1)}/V_s$, $I_{s(1)}$ increases with δ and TCHD reduces. The TCHD peaks close to $V_{I(1)}/V_s$=1.0 and the peak is superimposed on a generally rising trend.

Though X_s does not appear explicitly in the equations of the harmonic expressions, it is an important factor affecting the absolute values of the harmonics. Larger X_s implies

larger difference between $V_{I(1)}$ and V_s required to transfer a certain amount of power (a certain value of ac fundamental current) into the grid at a given power angle. Therefore larger X_s means the lower harmonic distortion.

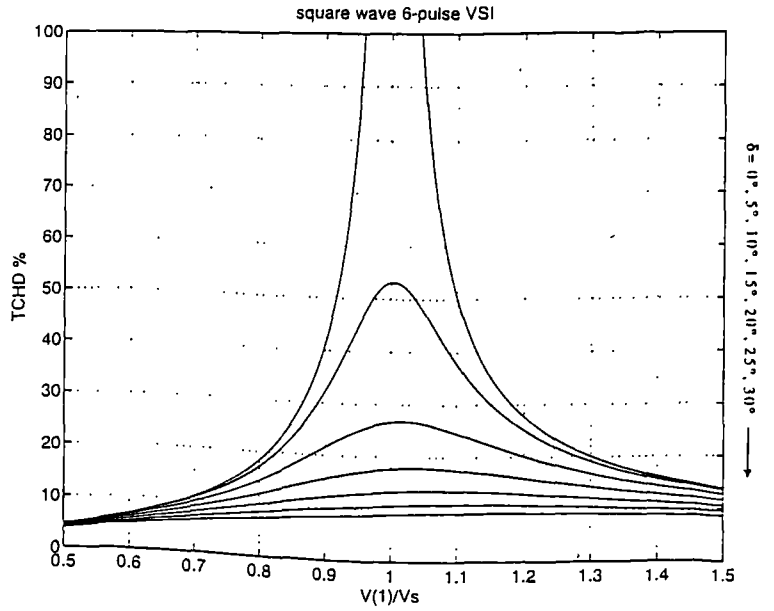

Figure 7.6 TCHD vs. $V_{I(1)}/V_s$ of 6-pulse square wave VSI

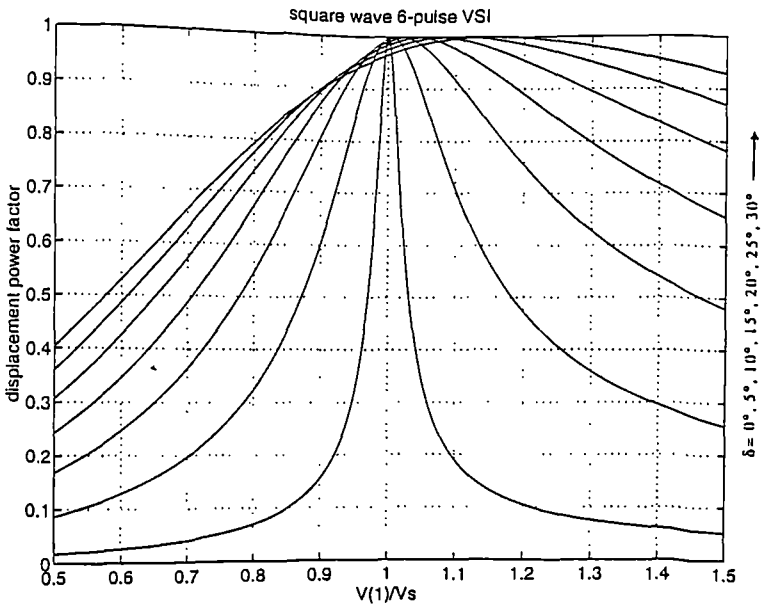

Figure 7.7 DPF vs. $V_{I(1)}/V_s$ of 6-pulse square wave VSI

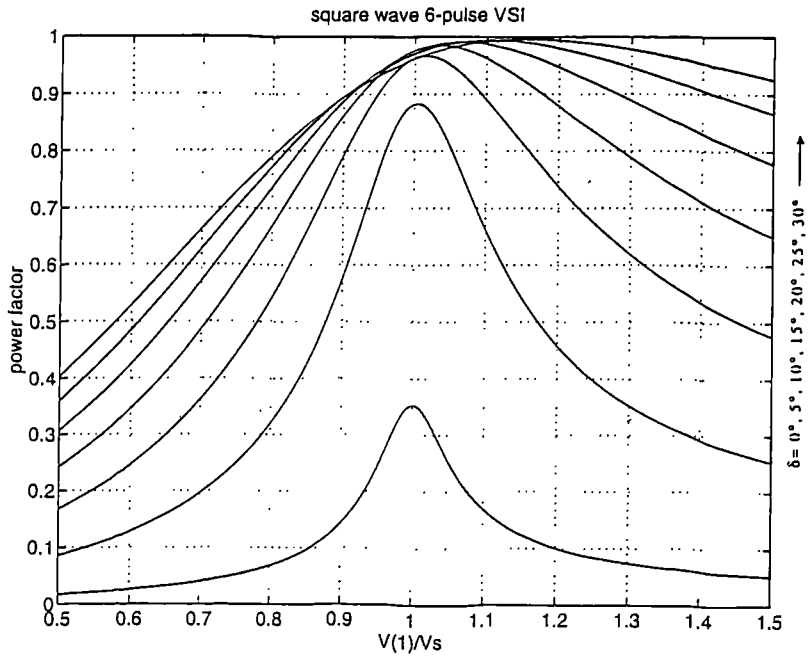

Figure 7.8 PF vs. $V_{I(1)}/V_s$ of 6-pulse square wave VSI

7.3.3 Harmonics performance of six pulse VSI in simple system

The harmonic performances of six-pulse VSI are calculated for the same simplified system and the same operation condition of chapter 5 (figure 5.15, 5.16, 5.17). The total voltage harmonic distortion (TVHD) and the total current harmonic distortion (TCHD) are given by the dashed lines and solid lines respectively in figure 7.9, figure 7.10 and 7.11 which correspond to the cases: power angle control; unity power factor control and constant ac terminal voltage control respectively. In order to evaluate the harmonic distortion appropriately, the TVHD and TCHD are presented as the percentages of the rated inverter ac voltage and current rather than the immediate voltage and current at the operating point.

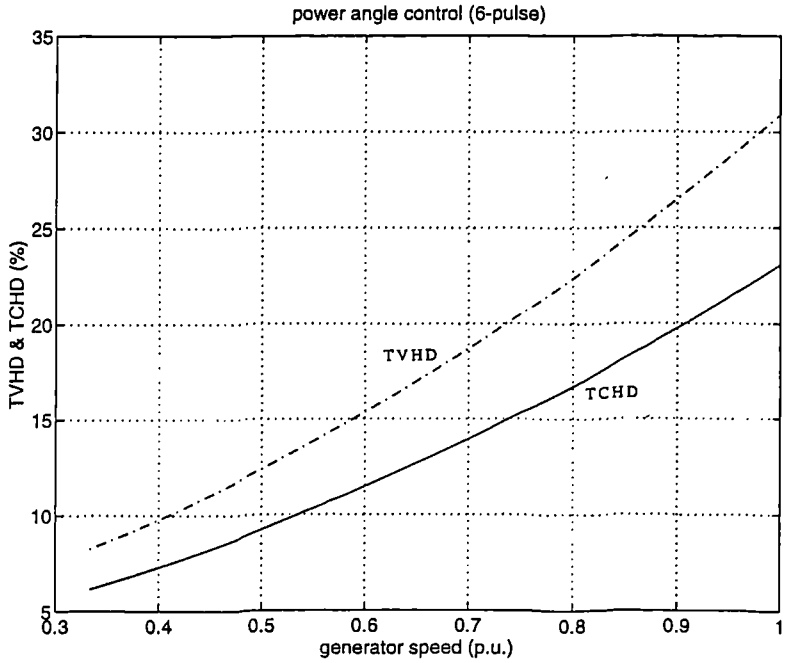

Figure 7.9 TVHD and TCHD for power angle controlled 6 pulse VSI in simple system

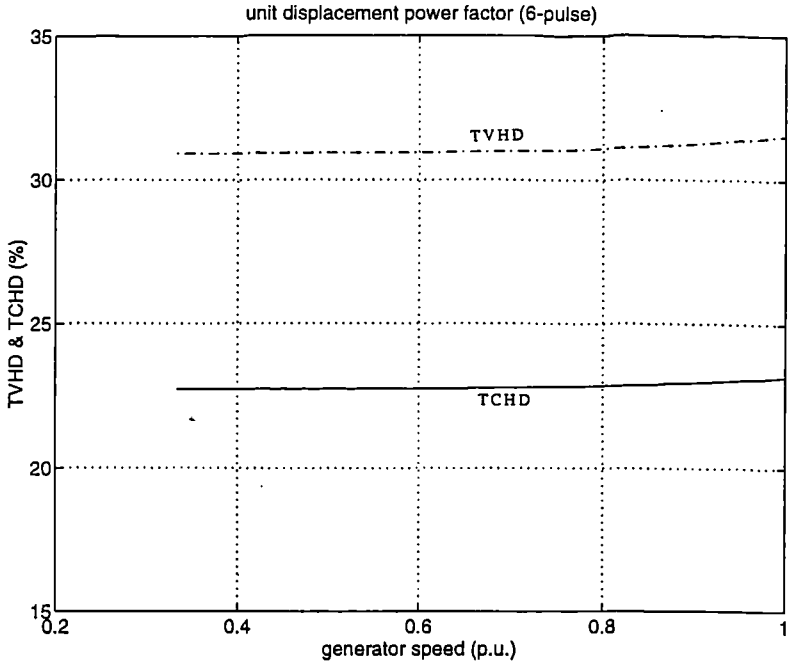

Figure 7.10 TVHD and TCHD for unity DPF controlled 6 pulse VSI in simple system

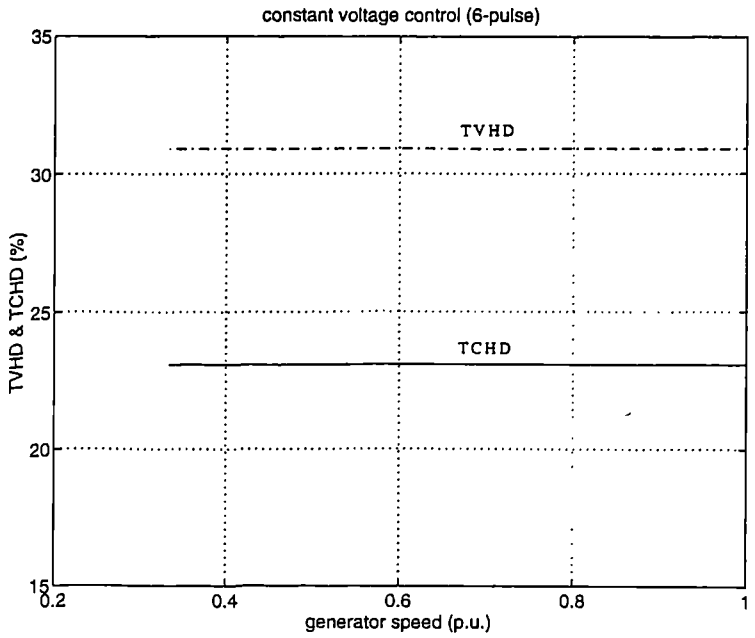

Figure 7.11 TVHD and TCHD for constant ac voltage controlled 6 pulse VSI in simple system

From these results, it can be seen that the TCHD of a six pulse square wave VSI is high, consequently the current waveform has a poor form factor and a poor ratio of fundamental to peak, which means that the device rating is poorly utilised. Harmonic currents could be reduced by appropriate choice of inverter voltage magnitude $V_{(1)}$ and power angle δ, however, these parameters also influence reactive power flow and the requirements for low harmonic current conflict with those for operation near unity power factor. The scope for harmonic reduction by this approach is restricted and so it is preferable to select $V_{(1)}$ and δ according to the needs for reactive power flow and to deal with harmonic currents by other means which will be discussed in later chapters.

7.4 Harmonics of Grid Connected SCR-CSI

The CSI, as a dual of the VSI, is a harmonic source of current. Ignoring overlap angle, the six pulse square wave switching SCR-CSI generates current harmonics with the same pattern as the voltage harmonics in a VSI. The discussion (section 7.2) applies.

However the current commutation can effect the current waveform and in turn the harmonic content. Overlap smoothes the edges of the current waveform and makes a better approximation to sine waves. For the characteristic harmonics with an overlap angle not exceeding 60°, the harmonic magnitudes could be expressed as [58].

$$I_{s(n)} = \frac{F}{nD} I_{s(1)} \qquad (7.15)$$

where

$$F = \left[\left(\frac{\sin[(n-1)\frac{u}{2}]}{n-1} \right)^2 + \left(\frac{\sin[(n+1)\frac{u}{2}]}{n+1} \right)^2 - 2 \left(\frac{\sin[(n-1)\frac{u}{2}]}{n-1} \right) \left(\frac{\sin[(n+1)\frac{u}{2}]}{n+1} \right) \cos(2\alpha + u) \right]^{1/2}$$

$$D = \cos\alpha - \cos(\alpha + u)$$

n is the order of the harmonic, $I_{s(1)}$ is the fundamental current and $I_{s(n)}$ is the n^{th} harmonic current.

Based on the above formulas, the current harmonic factors are calculated and presented against the overlap angle in figure 7.12 for extinction angle 0°, 20°, 40°, and 60°. The sequence of these curves are the harmonics of order 5, 7, 11, 13, 17, 19, 23 and 25 proceeding downward.

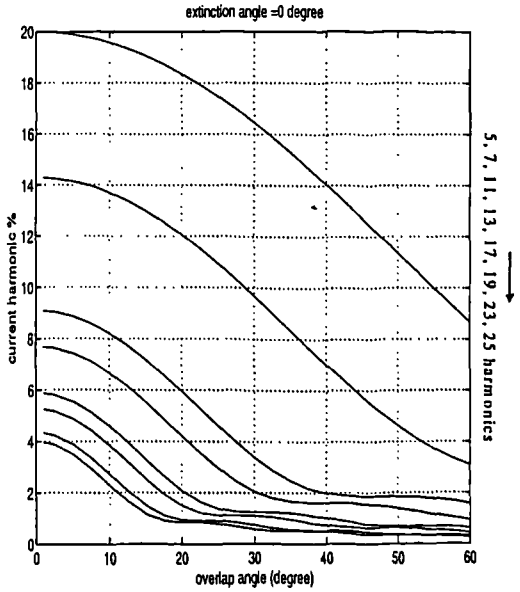

(a) 0° extinction angle

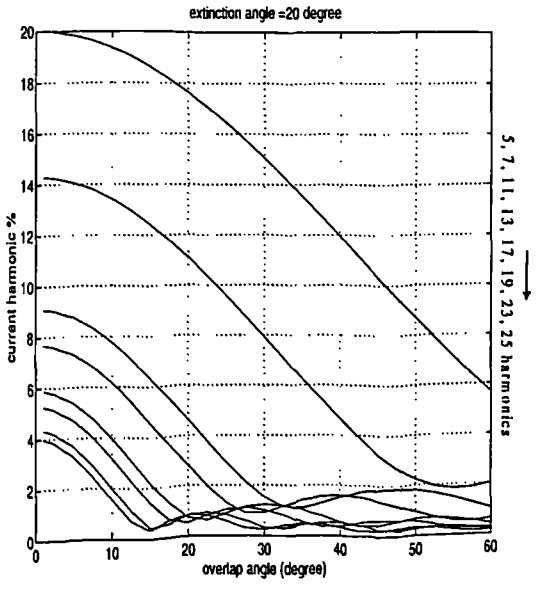

(b) 20° extinction angle

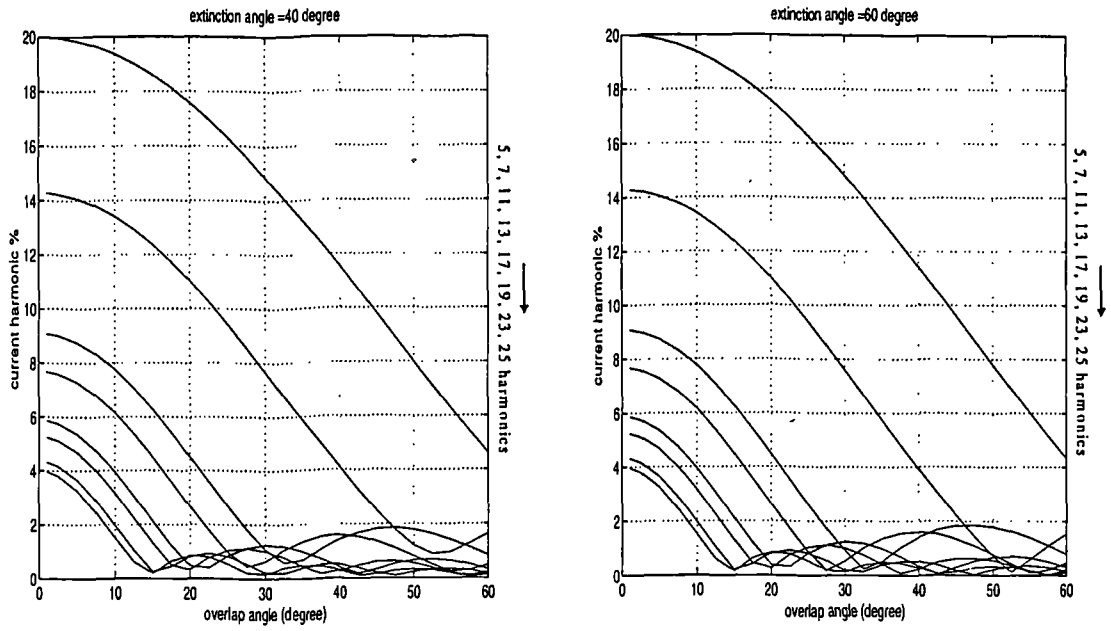

(c) 40° extinction angle (d) 60° extinction angle

Figure 7.12 Current harmonics of line commutated SCR CSI

The total current harmonic distortion is shown in figure 7.13 where the sequence of curves are extinction angle 0°, 20°, 40°, and 60° proceeding downward.

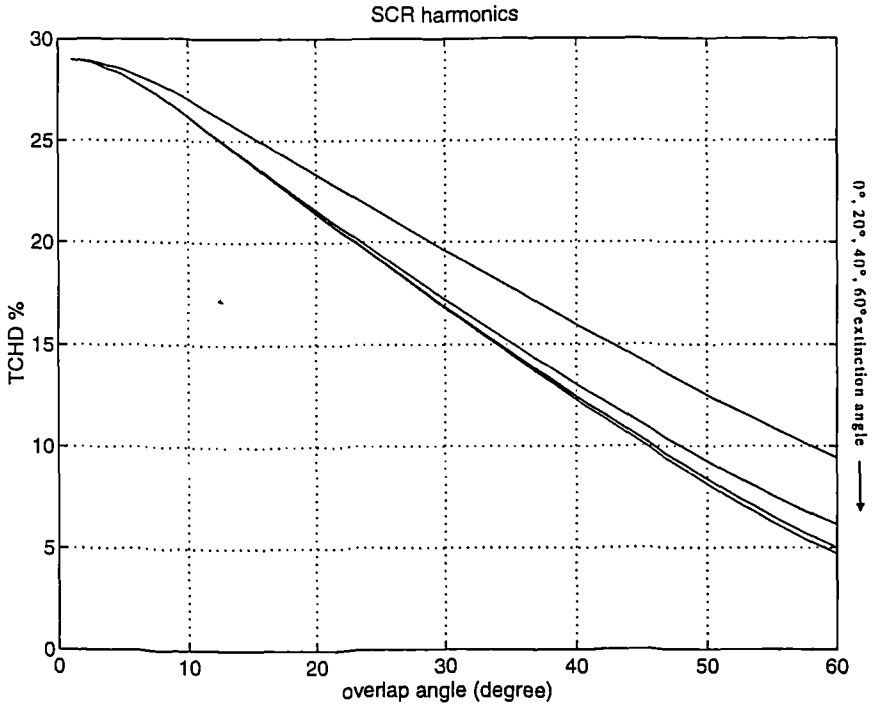

Figure 7.13 TCHD of line commutated 6 pulse SCR CSI

It can be seen clearly that a high overlap angle can significantly reduce the harmonic distortion and the reduction is more pronounced at a higher extinction angle.

7.5 Harmonics of Line Commutated Six Pulse SCR CSI in Simple AC System

The six-pulse SCR-CSI harmonic performance is calculated with the same simplified system and operation condition of section 6.5.2. The TCHD is given in figure 7.14 as a percentage of the rated fundamental current.

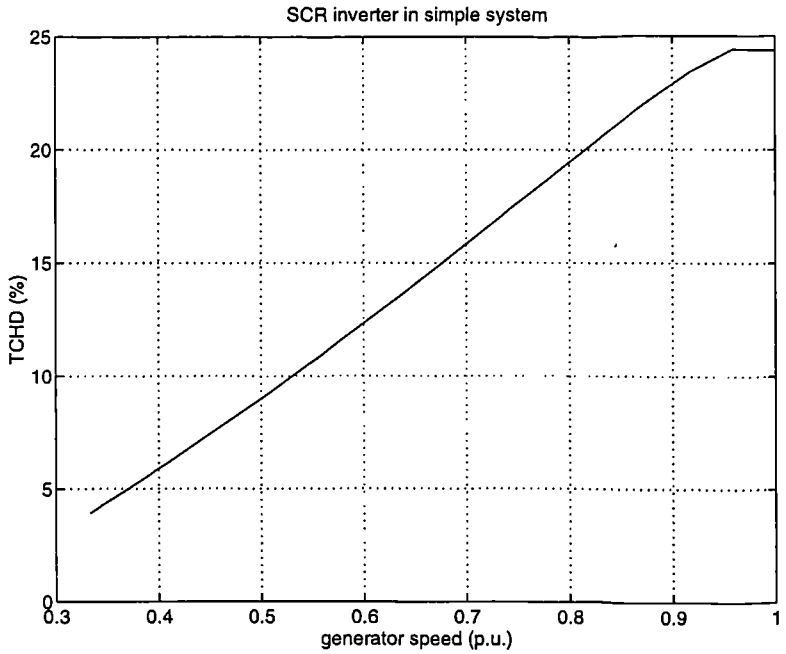

Figure 7.14 TCHD of the extinction angle controlled 6 pulse SCR CSI in simple system

It can be seen from figure 7.14, that the TCHD is similar to that of a VSI with just power angle control case, which represents serious harmonic pollution.

7.6 Harmonic Reduction Techniques

From the above analysis, it can be seen that neither VSI nor CSI can achieve satisfactory harmonic performance with their square wave switching and a basic six pulse configuration. Several techniques could be used to reduce harmonic pollution, such as conventional filters, high frequency switching techniques, multiple pulse converter

configuration and active compensation. In this section, these techniques are described and evaluated.

7.6.1 Passive harmonic filter

The use of filters is a common way to attenuate the penetration of harmonics into the grid from a harmonic source such as a power electronic converter. Passive filters have fixed impedance-frequency characteristics and provide a high admittance shunt path to certain harmonics. Passive filters are most conveniently used with current stiff converters to sink the harmonic current. They can also be used with VSI and are operated in conjunction with higher frequency techniques [26]. Only a brief summary of the technique is given here for completeness.

Passive filters consist mainly of passive reactive components (inductor and capacitor). Tuned and damped filters are used, . Their main features are:

tuned filter

- Maximum attenuation a single harmonic frequency,
- Relatively low loss which is mainly associated with the resistance of the inductor coils,
- Likely to become detuned due to the effects of temperature and frequency variations.

damped filter

- Attenuation over a spectrum of harmonics,
- Less sensitive to detuning effects than single tuned filter,
- Additional losses in the damping resistor.

In the case of CSI type static converters, such as those used in HVDC transmission systems, the converter behaves as a current harmonic source, then the harmonic currents are normally prevented from entering the rest of the system by the harmonic filter connected in parallel as sketched in figure 7.15. Tuned filters are often used for the lower order harmonic components and a damped high-pass filter is provided for the higher order harmonics. These filters are designed mainly to carry the higher order harmonics but they can also provide some reactive power to the system.

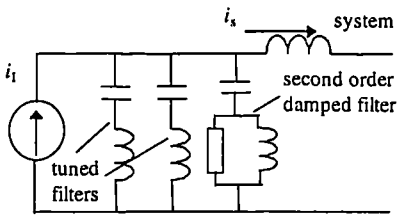

Figure 7.15 Shunt filters for current harmonic source

In the VSI case, the voltage harmonics are presented at the ac terminal of the inverter, thus the usual shunt filter arrangement cannot be used directly. However they may be connected to a tertiary winding of the transformer which used to connect the converter to the system.

The frequency drift of the system often requires that the filters be automatically adjusted or have a low Q-factor to be effective which may not be practical or economical for passive filters. It is also desirable to reduced the required filter size by using other harmonics reduction techniques.

7.6.2 Multiple pulse inverter system

Harmonic pollution can also be reduced by multiple pulse converter operation. This technique may be used in either VSI or CSI for either AC/DC or DC/AC conversion. For AC/DC conversion, the technique can be implemented by supplying the rectifiers with a multi-phase ac source, as the rectifier system discussed in chapter 3 or by using a phase shifted multi-winding transformer.

In a multi-pulse inverter (DC/AC conversion) case, the system consists of several six-pulse inverters, with outputs separated in phase by regular intervals. The outputs are combined in a phase shifting transformer which synthesises a single multi step ac waveform at its secondary winding. The remaining characteristic harmonics at grid side are the order of $n=pq\pm1$ where p is the total pulse number of the converter and q is any positive integer, the other characteristic harmonics are cancelled.

The phase shifts among the six pulse converters are 60°/k where k is the number of the six pulse converters (k=p/6). A pulse number of 12 can be easily obtained with simple connections of two six pulse inverter groups with Y/Y/Δ transformer. A 24 or higher pulse inverter system requires a phase shifting transformer where the phase shift can be implemented by either ring connection or zigzag connection. The voltage phasor diagram for a phase shift of φ degree by Y- zigzag connection is shown in figure 7.16.

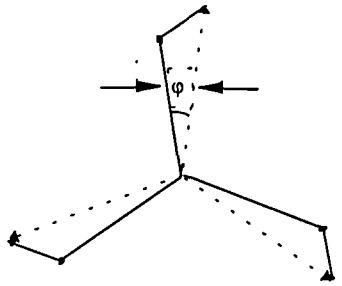

Figure 7.16 voltage vector diagram of Y- zigzag connection

The harmonic performances of the multiple pulse inverter systems have been calculated with the assumption that all the semiconductors and their control circuits operate ideally, and the converter transformer has the ideal characteristics (perfect harmonic cancellation). Figure 7.17 and 7.18 shows the voltage and current harmonic spectra of 12 and 24 pulse VSIs. The parameters used are the same as for figure 7.4 and 7.5.

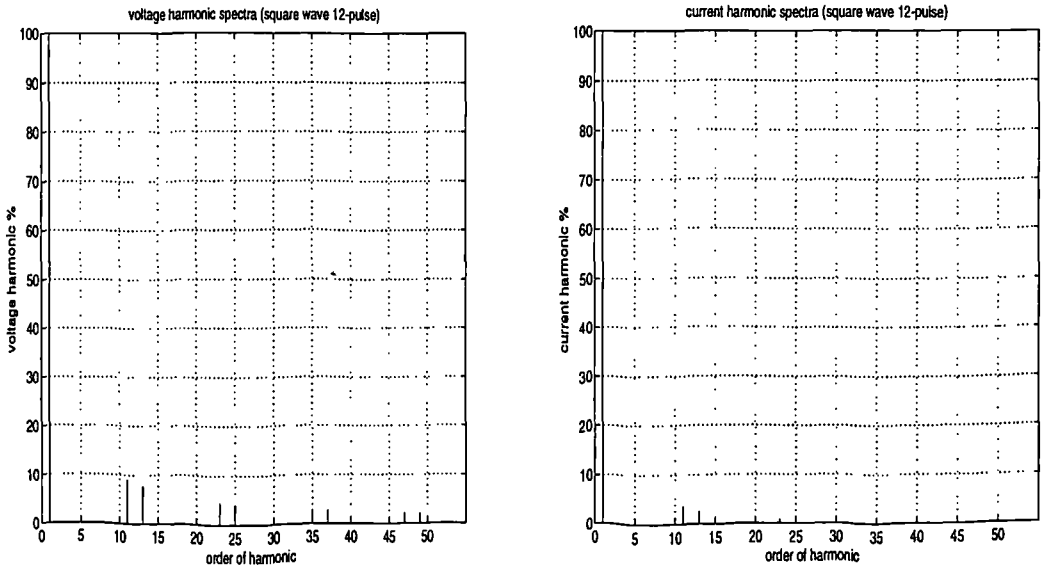

(a) (b)

Figure 7.17 Harmonic spectra of 12 pulse VSI (a) voltage (b) current

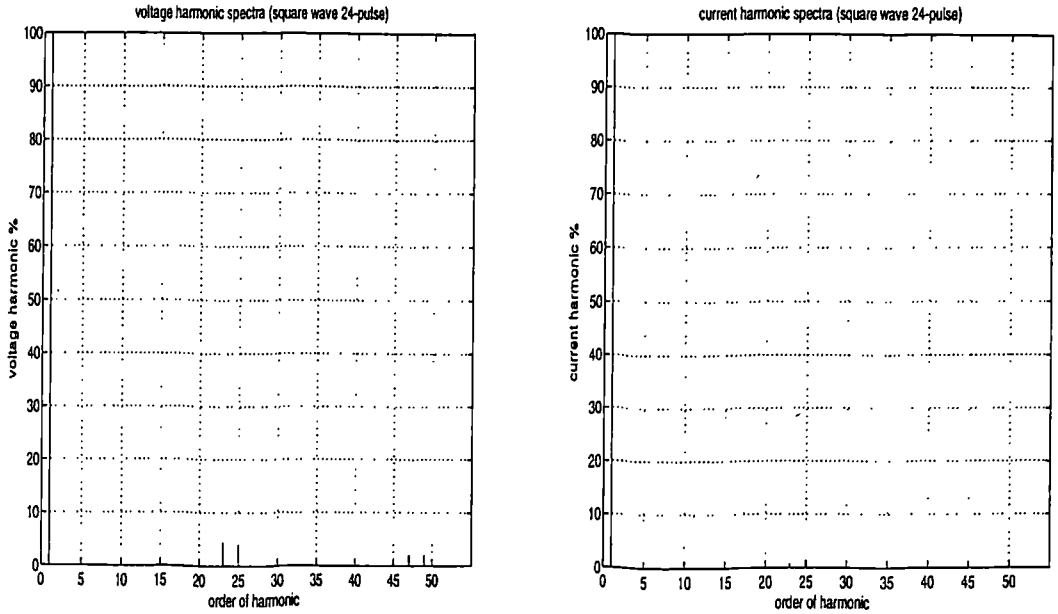

(a) (b)

Figure 7.18 Harmonic spectra of 24 pulse VSI (a) voltage (b) current

Figure 7.19 and 7.20 shows TVHD (dashed line) and TCHD (solid line) of 12 pulse and 24 pulse VSI in the same simple system and operating conditions as for figure 7.9, 7.10 and 7.11.

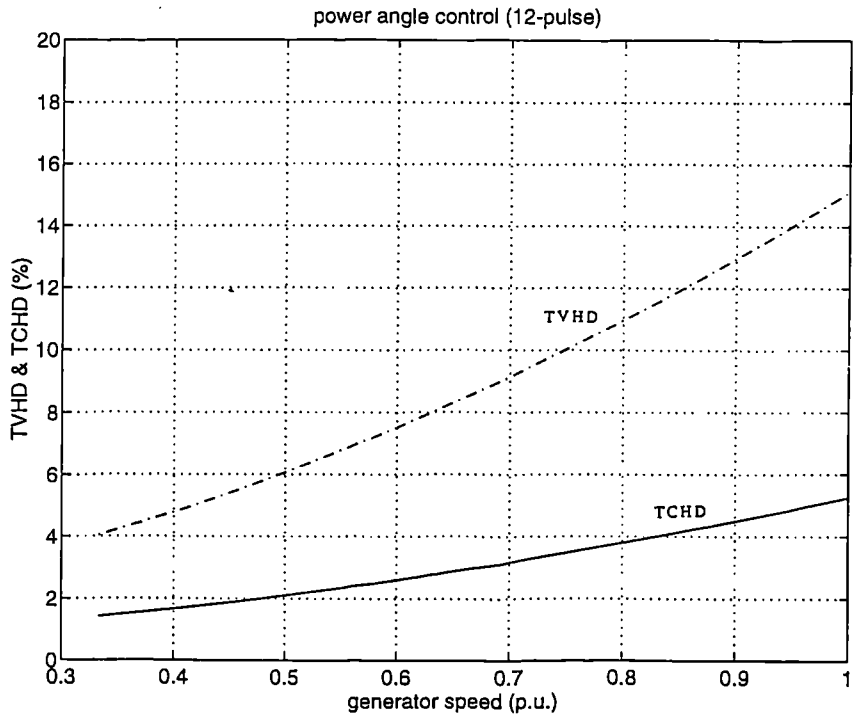

(a) power angle control

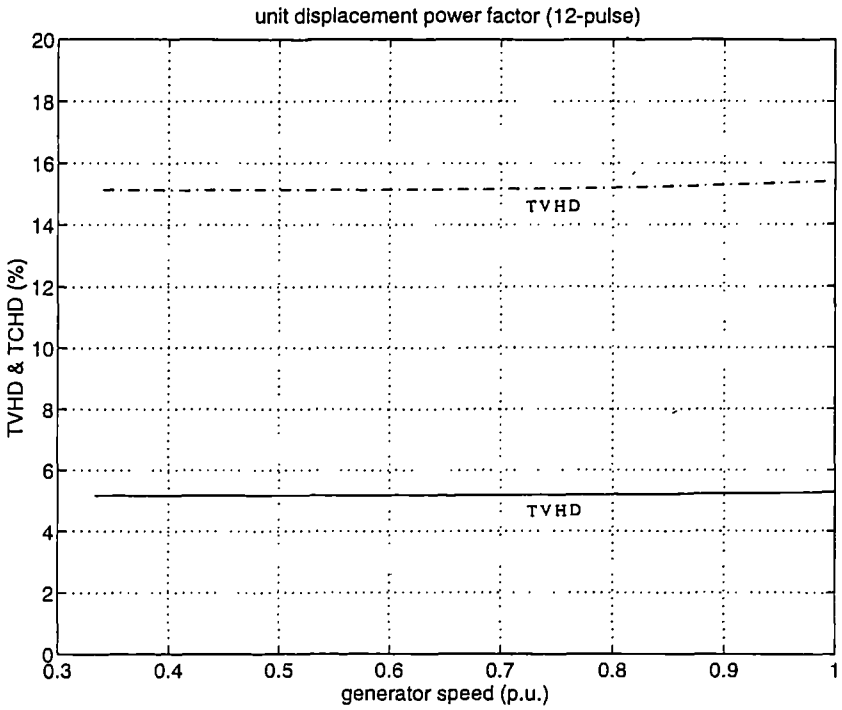

(b) unity power factor control

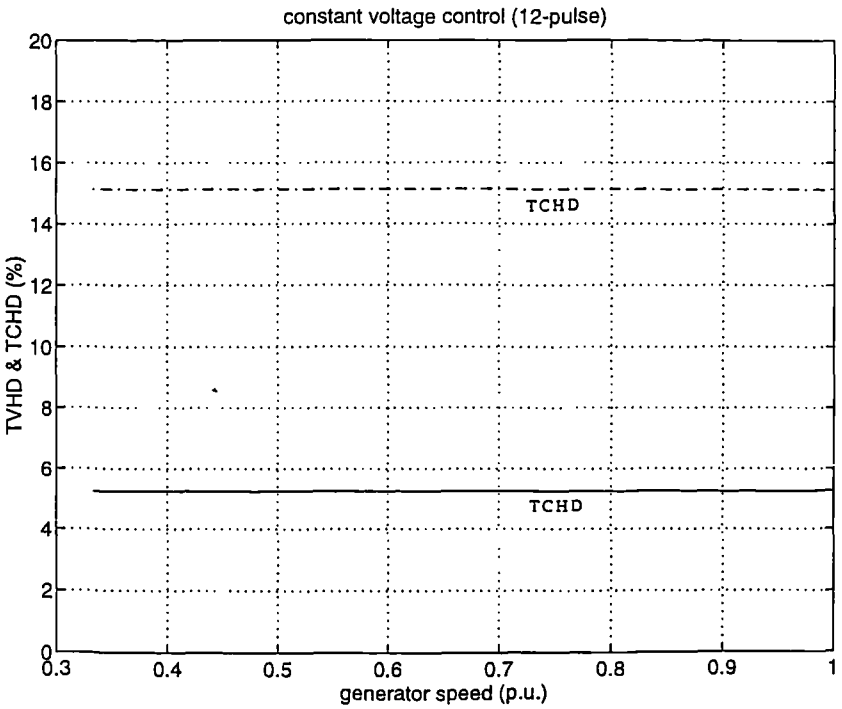

(c) constant ac voltage control

Figure 7.19 TVHD and TCHD of 12 pulse VSI in simple system

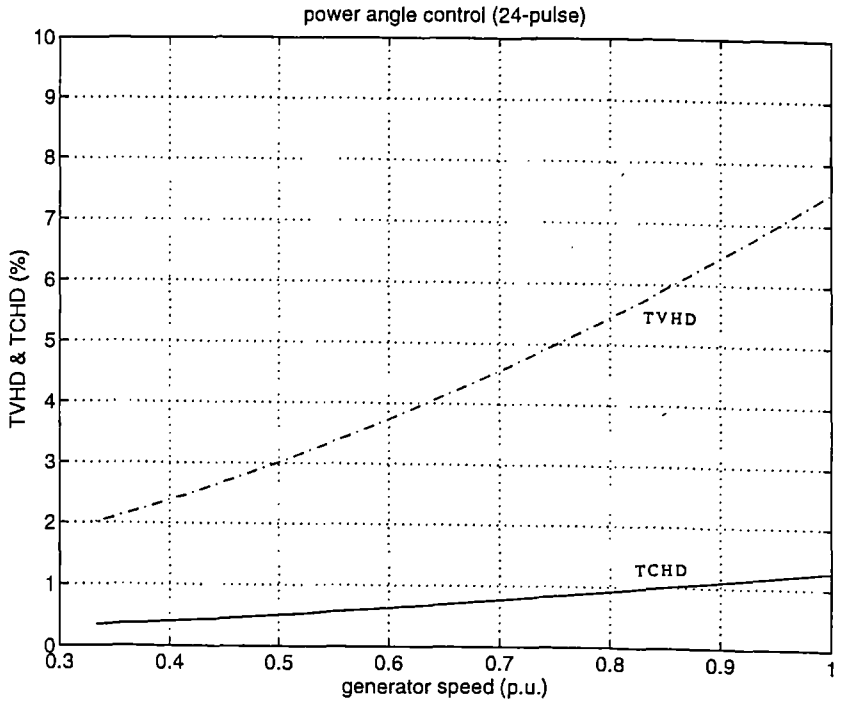

(a) power angle control

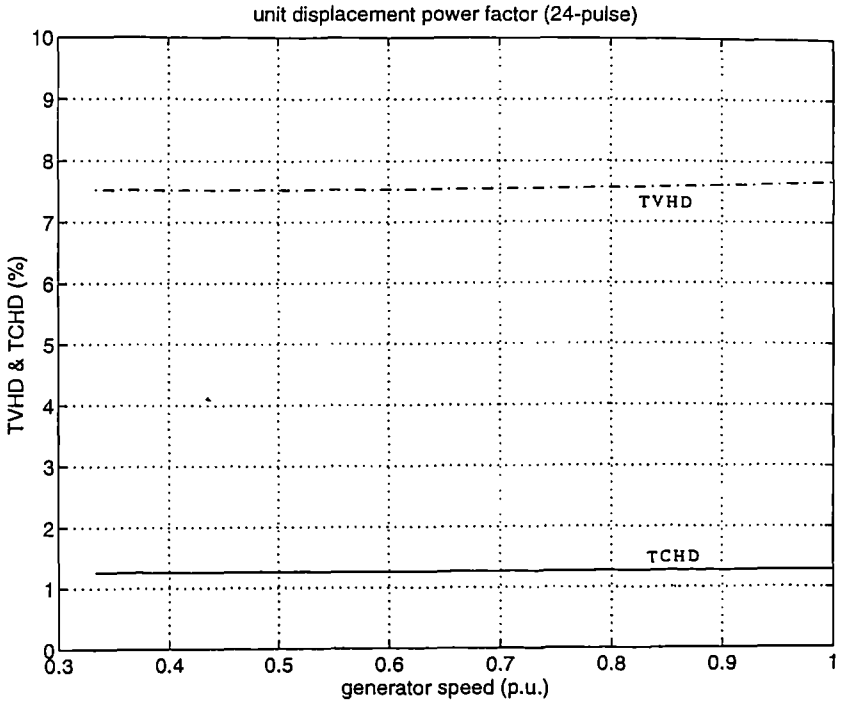

(b) unity power factor control

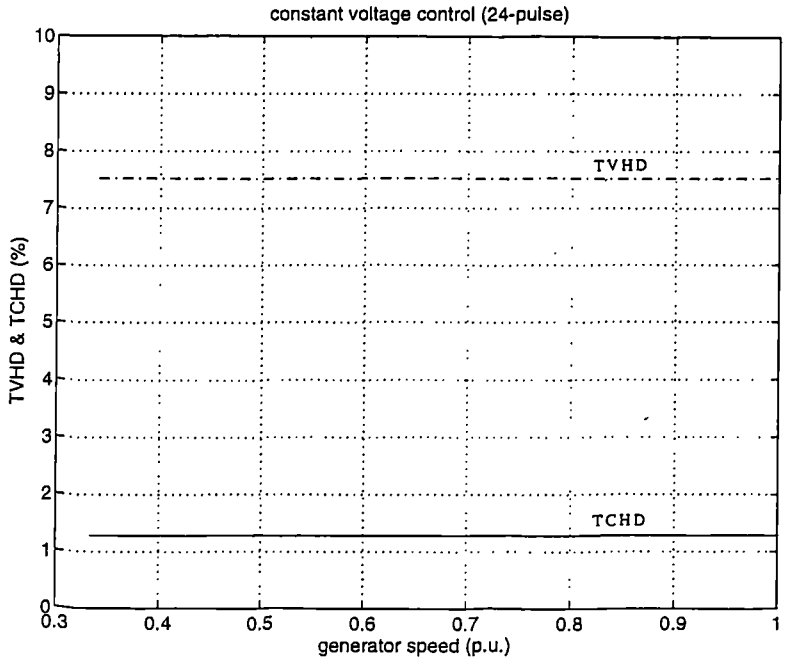

(c) constant ac voltage control .

Figure 7.20 TVHD and TCHD of 24 pulse VSI in simple system

Figure 7.21 shows TCHD of 12 pulse SCR-CSI with the same curve sequence as figure 7.13, figure 7.22 shows the TCHD characteristics of extinction angle controlled SCR-CSI in the same simple system and the same operating conditions as for figure 7.14.

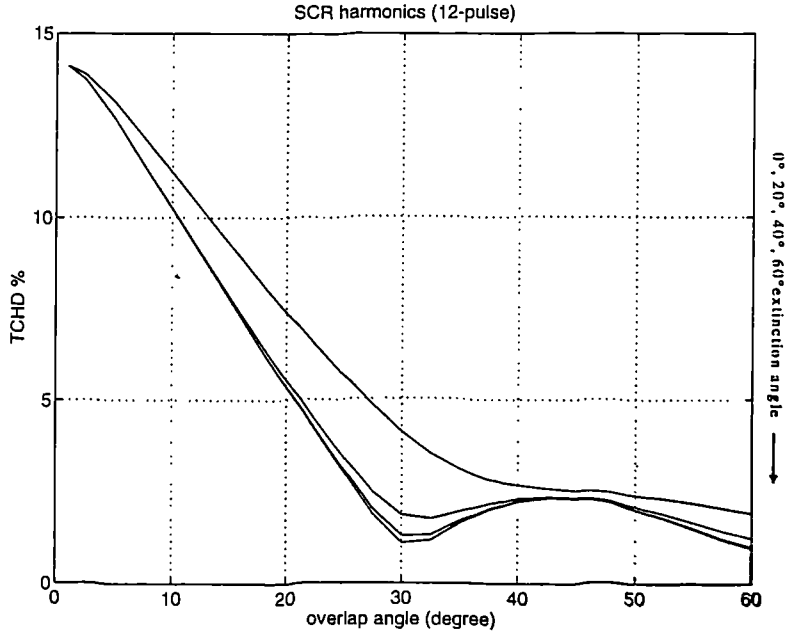

Figure 7.21 TCHD of line commutated 12 pulse SCR CSI

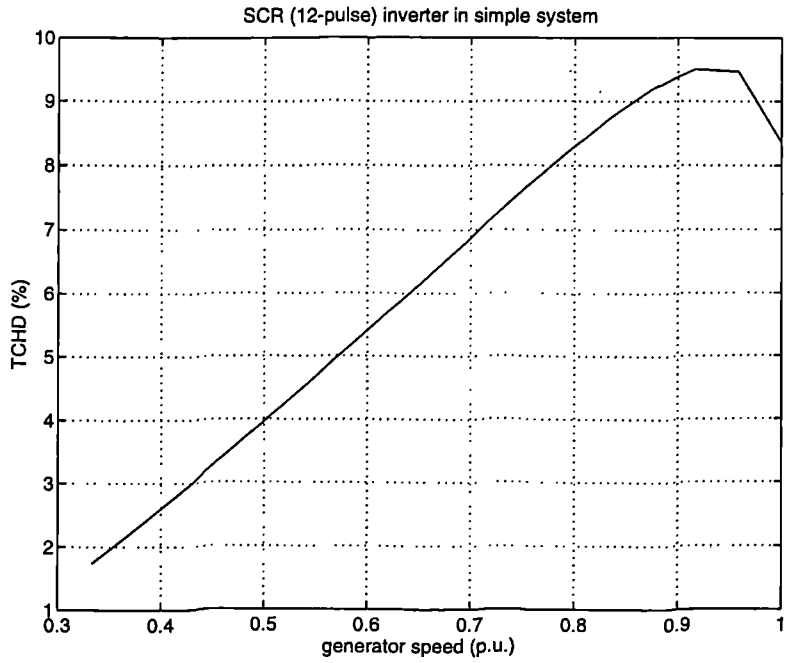

Figure 7.22 TCHD of line commutated 12 pulse SCR CSI in simple system

The reduction of the TCHD near rated speed is the effect of increased overlap angle. The results indicate that this means of reducing harmonics is very effective. Although, this technique is not ideal for applications such as motor drives where an output transformer is normally not necessary, a converter transformer is needed anyway to connect the wind energy conversion system to the grid, the transformer and its relatively complicated connection should not significantly increase the system cost, especially in the 12 pulse case. With increasing power level, the multi-phase circuit techniques could be more cost-effective than the high frequency techniques, whose switching losses may too high to be practical [66]. Therefore, the technique is a valid option for harmonic reduction. It will be used as one of harmonic minimisation methods for the inverter implementation investigations in later chapters.

7.6.3 High frequency switching techniques

With the advance of high switching frequency semiconductors, the high frequency switching techniques have been widely used in power electronics converters, such as machine drives, to reduced the generated low order harmonics. The function of higher

frequency switching techniques, such as sinusoidal pulse width modulation (SPWM) and selective harmonic elimination (SHE), is harmonic redistribution. SPWM can reduce low order harmonics and SHE can eliminate a chosen set of low order harmonics. The consequence is increased higher order harmonics and usually the increased of TVHD in a VSI case or TCHD in a CSI. However, in the inductive dominated power system, the voltage harmonic redistribution of the VSI to higher frequencies could lead to a reduction in current harmonics and the high order harmonics can be easily attenuated with a relatively smaller size of filter. Usually, the higher the switching frequency, the better the harmonic performance. Another aspect of the high frequency switching technique is the control of the fundamental component. The magnitude of the fundamental ac component can be controlled by varying the switching patterns. This feature allows a single one stage basic six pulse inverter circuit to generate an ac output with controlled fundamental component magnitude whilst giving satisfactory harmonic performance.

However, the current harmonics generated by CSI circuit would be injected into the system unless a parallel path is provided. The higher frequency switching technique could be used in CSI, but the redistribution of harmonics would not reduce total current harmonic distortion. High frequency switching CSIs are not suitable, therefore, for connecting to a series impedance type circuit. The high frequency switching will be addressed in detail with only self commutated VSI in the following chapters.

7.6.4 Active compensators

Active compensators are power electronic converters which can be controlled to fabricate a desired waveform at the connection point. They can be connected to the ac system in parallel or in series. Normally, parallel connection is used to correct a current waveform and series connection is used to correct a voltage waveform. The waveform can be corrected to be desired shape, therefore an active compensator could follow any frequency drift and not only suppress the harmonic distortion but also provide the

reactive power compensation. Thus it is sometimes also called a static var and harmonic compensator, and due to its flexibility, it has recently received wide attention.

Either a VSI or CSI as discussed earlier can be used as the basis of an active compensator. In a VSI type compensator, the switching is carried out into a capacitor connected at the dc side which acts as a voltage source to absorb and generate the required current changes on the ac side. In the CSI case, a inductor at the dc side maintains a current with negligible ripple to absorb and generate the voltage changes on the ac side. The physical size of the reactive components can be reduced by increasing the switching frequency. The power loss of the capacitor in VSI is negligible compared with that of the inductor used in a CSI type circuit.

Usually, the active compensator is implemented with self-commutated semiconductors and on-line computation is needed to determine the switching of the semiconductors. It is the natural choice of compensator for use alongside the line commutated SCR-CSI selected earlier. Therefore this combination is chosen for further study and presented in chapter 10. The dual of this system, using a six step VSI for the main inverter with a compensator, has already been rejected, since the self-commutated VSI with high frequency switching has the potential to generate reactive power and to reduce current harmonic distortion by itself.

7.6.5 Summary

The studies of harmonic reduction techniques indicate:

Multi-pulse circuit can reduce harmonic distortion effectively and can be used for both VSI and CSI, the cost increase of the converter transformer may not be significant in 12-pulse case.

A high switching frequency, self-commutated VSI could generate an ac waveform with controllable fundamental component and satisfactory harmonic content. This would be more efficient than a high switching frequency self-commutated CSI.

The VSI-based active compensator is an effective method to provide reactive power compensation and harmonic reduction. It is suitable for use with a line commutated SCR-CSI which is both reliable and economical.

7.7 Conclusion

In this chapter, the general harmonic performance of the basic CSI and VSI has been studied. The harmonic performance when operating to give optimal real power capture are presented based on the control strategies proposed in chapters 5 and 6.

The six-pulse square wave converters (VSI and CSI) cannot be directly used for the grid interface due to poor harmonic performance. The harmonic problem has to be solved with harmonic reduction techniques. Main harmonic reduction methods are discussed. Their suitability is analysed.

There are several ways to construct a DC/AC converter to transfer the optimal real power captured from the wind power generator and to generate the desired reactive power with satisfactory harmonic performance. However, the studies of the chapter 5, 6, and 7 favour the following systems which are worth further detailed investigations:

- higher frequency switching technique for the magnitude of voltage fundamental component and harmonic control in self-commutated VSI
- higher frequency switching or multi-pulse techniques for harmonic control in dc voltage controllable self-commutated DC/DC converter-VSI
- Active compensator for reactive power and harmonic compensation in line commutated SCR CSI system.

The above systems will be addressed in detail in later chapters.

Chapter

8.

Sine Pulse Width Modulation Voltage Source Inverter (SPWM-VSI)

8.1 Introduction

Studies of previous chapters have recommend that three types of DC/AC power converters are more attractive than the other possibilities and therefore should be given more detailed investigations. This chapter will study one of these candidates: high frequency switching self-commutated VSI.

There are several high frequency switching schemes available for pulse width modulation of the inverter output voltage to create the desired ac waveforms. These schemes can be classified as open-loop feedforward and closed-loop feedback schemes. The closed-loop PWM scheme usually regulates the ac current, the semiconductors are switched so as to generate a desired ac current waveform. Closed-loop schemes can give better transient performance and can incorporate advanced control feature, such as hysteresis, ramp comparison and predictive controllers. On the other hand, the inverter output voltage is the controlled variable in open-loop PWM schemes, where the inverter generates a magnitude-controllable ac voltage fundamental component. The operation mode of the VSI type grid interface discussed in chapter 5 requires the inverter to generate a phase angle and magnitude controllable fundamental component voltage to track the system optimal operation trajectory, so as to transfer optimal power with a good power factor. Therefore, the open-loop sinewave PWM (SPWM) is the subject of this chapter.

Carrier-based modulation and programmed switching are the main techniques employed in the open-loop PWM class. There are various carrier-based PWM and programmed

PWM schemes [50], out of these PWM schemes, the most commonly used scheme, the natural sinusoidal PWM, is chosen for study in this chapter.

8.2 Analysis of Sinusoidal Pulse Width Modulation VSI Interface

8.2.1 SPWM-VSI and A Numerical Analysis Method

In the sine wave PWM switching technique, a sinusoidal reference signal (V_{ref}) is compared with a triangular waveform (V_{tri}), the semiconductor switching is determined by crossing points of the reference signal and the triangular waveform. The frequency of the triangular waveform establishes the inverter switching frequency (f_{sw}). The frequency of the reference signal determines the inverter output frequency, that is ac grid frequency (f_s) in this application. The magnitude of the fundamental component can be controlled by regulating the modulation ratio (M_a) which is the ratio of V_{ref} peak value to V_{tri}.

$$M_a = \frac{\hat{V}_{ref}}{\hat{V}_{tri}} \tag{8.1}$$

The waveforms of a three phase sinusoidal PWM are shown in figure 8.1 where f_{sw} =750Hz and M_a =0.8 are chosen for a clear illustration.

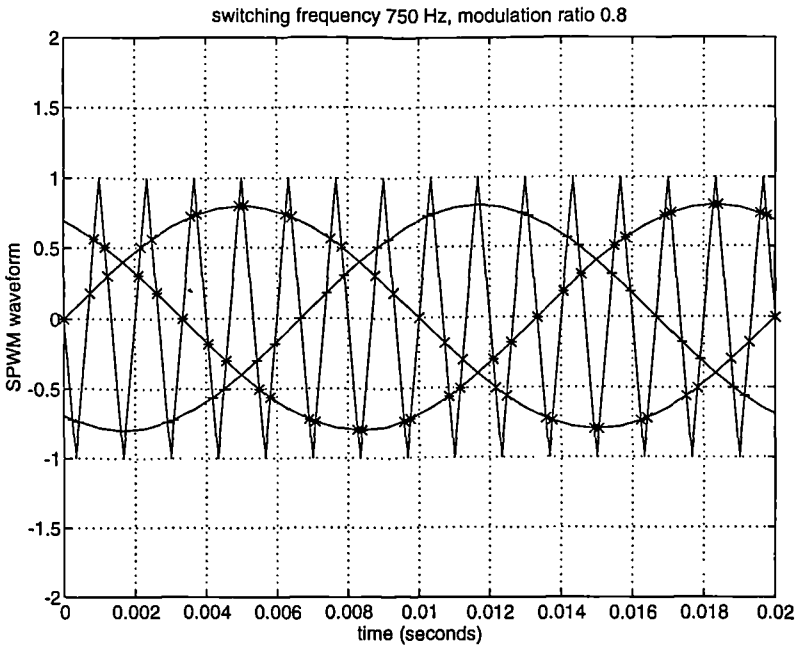

(a)

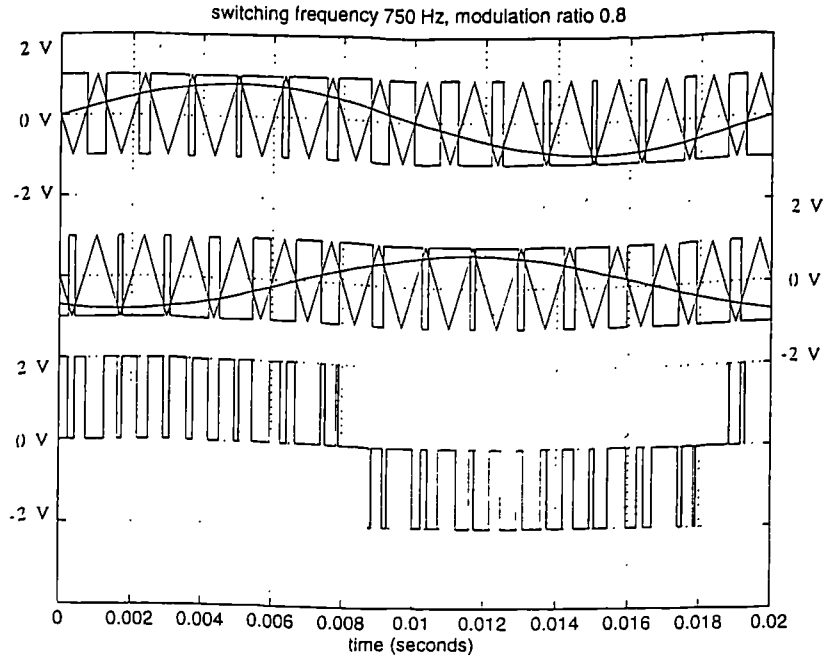

(b)

Figure 8.1 Sinusoidal PWM waveforms

(a) reference and triangular waveforms

(b) switching signals and line to line voltage waveform

It is usual to use synchronous PWM, where f_{sw}/f_s is a constant integer. This avoids undesirable subharmonics present with asynchronous PWM. In variable speed ac motor drives, the synchronous PWM is achieved by using a variable f_{sw}, though asynchronous PWM may be acceptable with a high value of f_{sw}/f_s [64]. However, in the studied application, the output frequency f_s is fixed at grid frequency and the switching frequency of synchronous PWM can be fixed to suit harmonic elimination and switching power loss requirements, Thus simplifying the implementation. Also, f_{sw}/f_s, should be an odd integer and a multiple of 3 to eliminate even harmonics and to take advantage of the absence of triple harmonics in a balanced three phase system.

A program has been developed based on the harmonic analysis approach reported in chapter 7 in MATLAB to perform the analyses of SPWM-VSI. The flowchart is shown in figure 8.2.

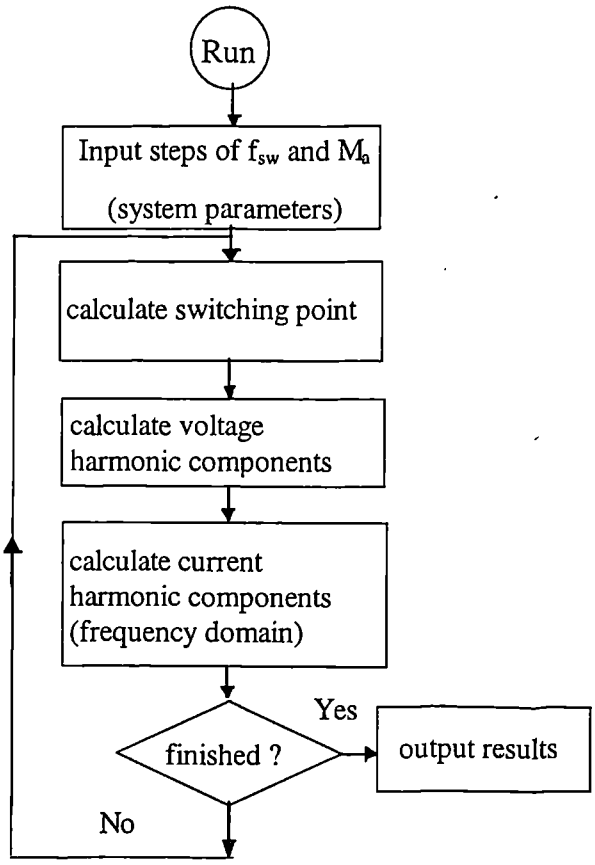

Figure 8.2 A flow chart of SPWM-VSI performance analysis.

The analysis program has been used to investigate the performance of SPWM VSI. The ratio of output voltage fundamental component to DC voltage ($V_{I(1)}/V_d$) is calculated and plotted against the modulation ratio in figure 8.3.

It can been seen that the output voltage fundamental component ($V_{I(1)}$) has a linear relation with dc link voltage (V_d) within the region of $M_a \leq 1.0$, the so called linear modulation region. In this region, the rms value of the fundamental ac voltage (line to line) is related to the dc voltage by [64]:

$$V_{I(1)} = \frac{\sqrt{3}}{2\sqrt{2}} M_a V_d \qquad (8.2)$$

Calculated results show that the switching frequency f_{sw} has no significant effect except for impractically low values of f_{sw}. Moreover, the order of the generated harmonics are not effected by modulation ratio variation in linear region, though, their magnitudes do

vary. This can be clearly seen by comparing the spectra shown in figure 8.4 (a) and 8.4 (b).

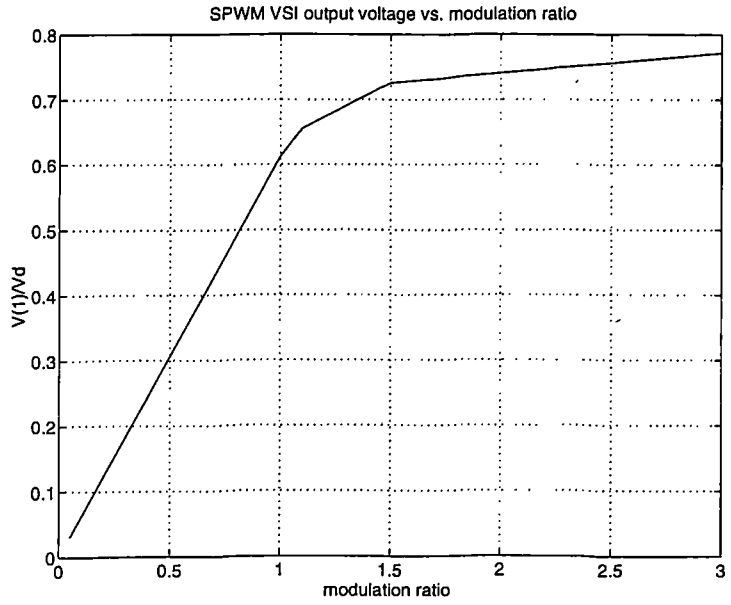

Figure 8.3 $V_{I(1)}/V_d$ against M_a of three phase SPWM VSI

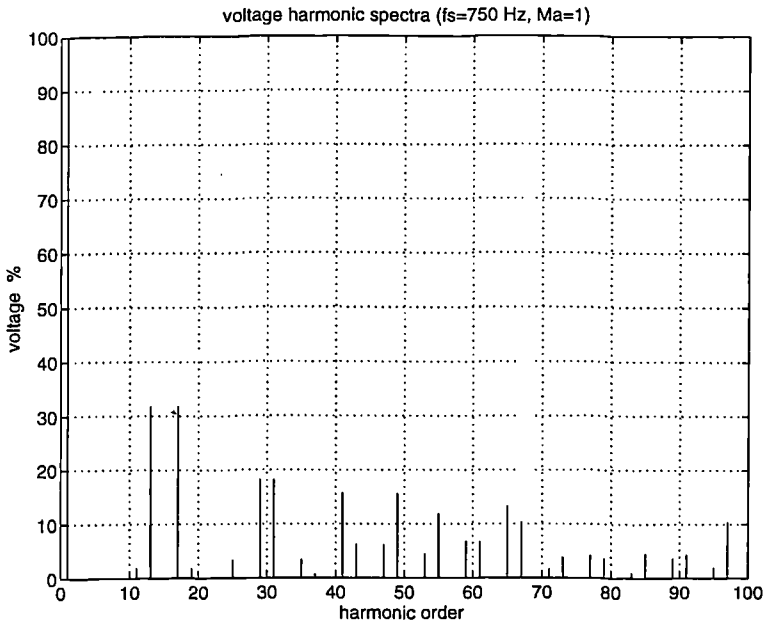

(a) M_a=1.0

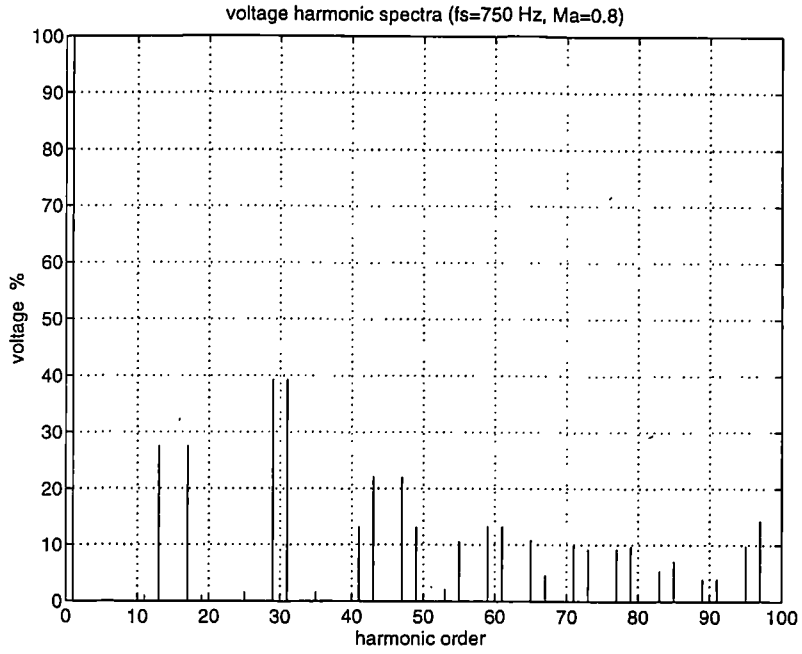

(b) M_a=0.8

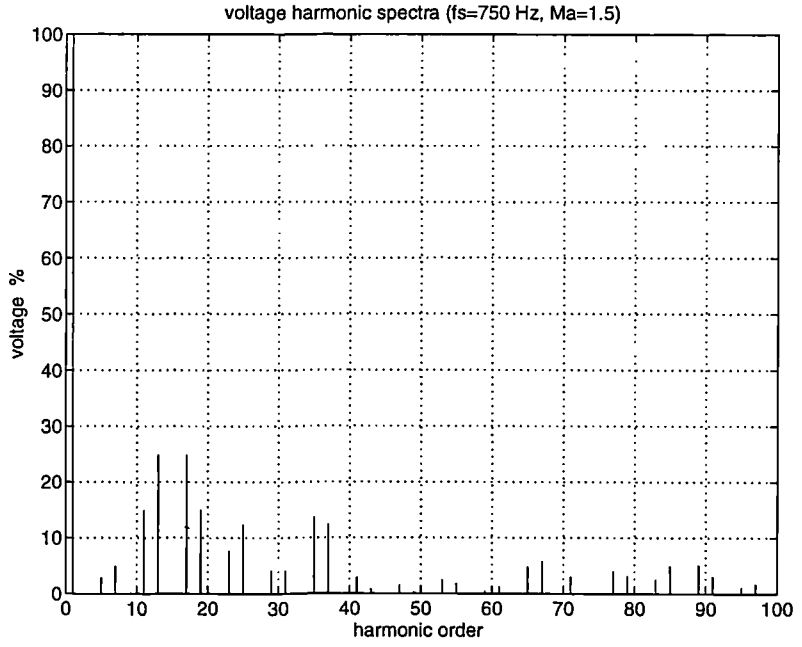

(c) M_a=1.5

Figure 8.4 SPWM voltage harmonic spectra (f_{sw}=750Hz)

Outside linear operation region, the fundamental output voltage and the dc link voltage are no longer simply related. It is also noted that additional low order harmonics appear

as shown in figure 8.4 (c). With M_a further increasing, the output voltage waveform begin to resemble a square wave six pulse inverter and a similar harmonic pattern can be expected.

8.2.2 Switch utilisation of SPWM VSI

Switch utilisation is an important aspect of inverter design for commercial reasons. This is characterised by the Switch Utilisation Ratio (SUR) which is the ratio of inverter output capacity to total device VI rating. The peak voltage and current stresses ($V_{d,peak}$ and $I_{s,peak}$) applied to the semiconductors, i.e. the maximum dc link voltage and maximum ac current, determine the basic inverter rating, that is $6\times V_{d,peak}\times I_{s,peak}$ for a 6-pulse inverter. The inverter output capacity can be expressed by the rms value of voltage fundamental frequency component $V_{I(1)}$ (line to line) and ac current fundamental frequency component $I_{s(1)}$. Therefore the switch utilisation ratio of a six pulse inverter can be expressed as:

$$SUR = \frac{\sqrt{3}V_{I(1)}I_{s(1)}}{6V_{d,peak}I_{s,peak}} \qquad (8.3)$$

It is noted that the maximum output fundamental voltage component in the linear region is about $0.612V_d$, which is less than achieved with square wave switching ($0.78V_d$). Ignoring dc voltage ripple and assuming harmonic free rated ac current operation ($I_{s.peak} = \sqrt{2}I_{s(1)}$), then for constant dc link voltage ($V_d=V_{d,peak}$) operation as in ac motor drives, the switch utilisation ratio can be found by substituting (8.2) into (8.3), yielding SUR=1/8 M_a. Then the maximum is 0.125 at M_a=1.0.

8.2.3 SPWM VSI wind energy interface in a simple system

8.2.3.1 Modulation ratio control of SPWM VSI

Sinewave Pulse Width Modulation (SPWM) is commonly used in VSI for ac motor drives and uninterruptible power supplies, where the input is usually a constant dc voltage derived from the ac system through a rectifier and the output has a fundamental component whose magnitude and frequency can both be controlled. In the investigated

wind energy grid interface application, however, the inverter output frequency is fixed at grid frequency, the inverter should operate under a varying input dc link voltage and produce an ac voltage fundamental component controllable in both phase angle and magnitude to transfer the optimal real power with independently adjustable reactive power generation or absorption.

Considering the simple system given in chapter 5 (section 5.3), the optimal operation of the generator and rectifier system requires the dc link voltage to be varied from about 0.4 to 1.0 times the rated dc link voltage for wind speed varying from 0.5 to 1.0 times of the rated wind speed (figure 5.12 (d)). However, the ac voltage fundamental component required for unity displacement power factor (DPF) operation (figure 5.16 (b)), varies over a much smaller range. The modulation ratio has to be varied to accommodate the dc voltage variation. For acceptable harmonic performance, the linear modulation region ($M_a \leq 1.0$) is preferred. To achieve the highest possible switch utilisation ratio, the maximum modulation ratio ($M_a = 1.0$) is used for the lowest dc link voltage, thereafter M_a decreases with increasing dc voltage. The value of M_a required for unity displacement power factor (DPF) operation in the simple system is plotted in figure 8.5. It is noted that a low M_a (about 0.41) has to be used for the rated wind speed.

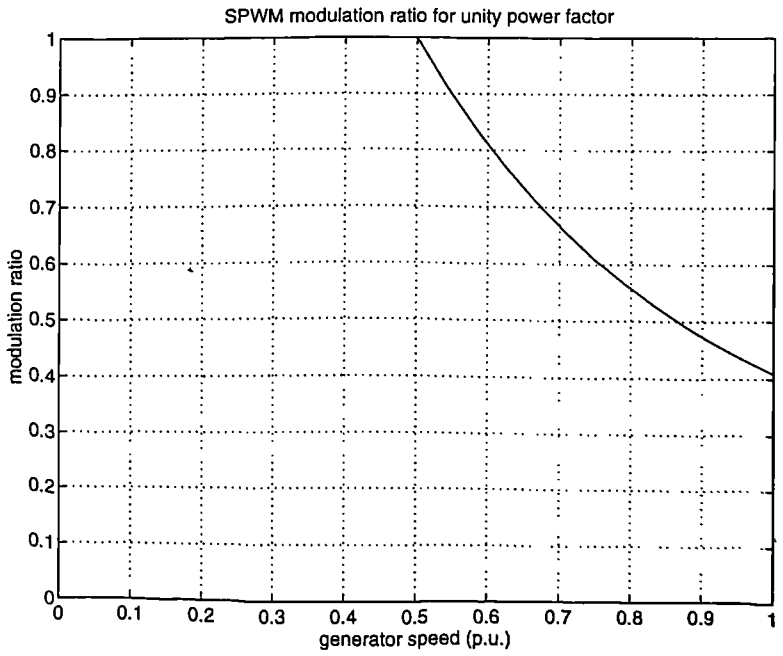

Figure 8.5 M_a curve of SPWM VSI in simple ac system (unity DPF)

8.2.3.2 Switch utilisation ratio of SPWM VSI interface

Assuming an ideal ripple free dc link voltage and an ac current with negligible harmonics, the following relations are held.

$$I_{s.peak} = \sqrt{2} I_{s(1),rate} \text{ and } V_{d.peak} = V_{d,rate}$$

Where $I_{s(1),rate}$ and $V_{d,rate}$ are rated ac current (rms) and dc voltage respectively. If the inverter operates within the linear modulation region, the switch utilisation ratio is given by

$$SUR = \frac{\sqrt{3} V_{I(1)} I_{s(1)}}{6 V_{d,peak} I_{s,peak}} = \frac{\sqrt{3} V_{I(1)} I_{s(1)}}{6 V_{d,peak} \sqrt{2} I_{s(1),rated}}$$
$$= \frac{\sqrt{3}}{6\sqrt{2}} \frac{\sqrt{3}}{2\sqrt{2}} \frac{M_a V_d}{V_{d,peak}} \frac{I_{s(1)}}{I_{s(1),rated}} = \frac{1}{8} \frac{M_a V_d}{V_{d,peak}} \frac{I_{s(1)}}{I_{s(1),rated}} \quad (8.4)$$

For unity DPF operation, $I_{s(1)}$ follows the same trajectory as real power in terms of per unit values (figure 5.12). The M_a characteristic shown in figure 8.5 and the dc voltage characteristic shown in figure 5.12 yield the switch utilisation ratio characteristic plotted in figure 8.6.

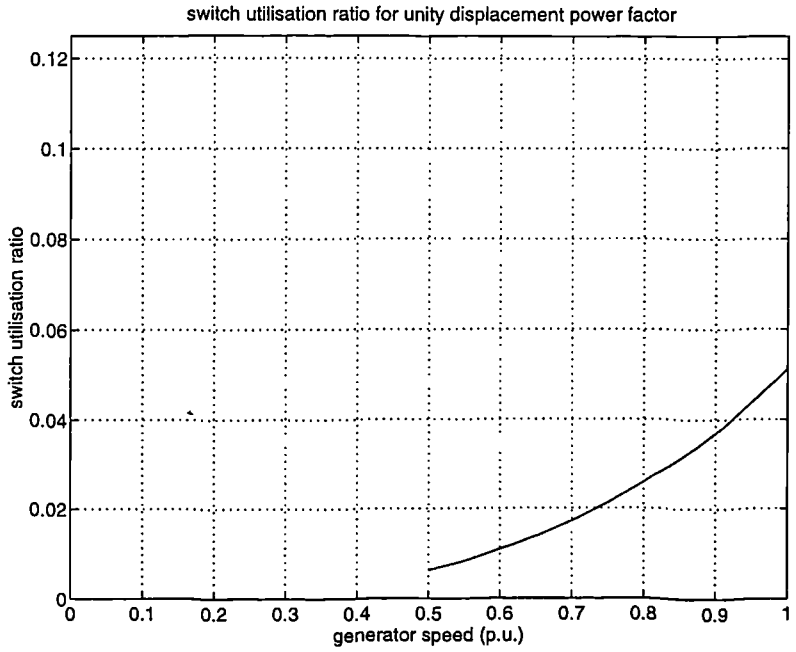

Figure 8.6 SUR of SPWM VSI in simple system (unity DPF operation)

From figure 8.6, it can be seen that SPWM VSI has a very poor SUR in this application. Because the inverter has to be operated at a low M_a at the rated condition.

8.2.3.3 Switching frequency and harmonic distortion of SPWM VSI

Total current harmonic distortions of SPWM-VSI in the simple ac system discussed in chapter 5 are calculated for various modulation ratios and switching frequencies, the results are plotted in figure 8.7 against switching frequency. The sequence of curves are for the modulation ratios of 0.4, 0.6, 0.8 and 1.0 proceeding downward.

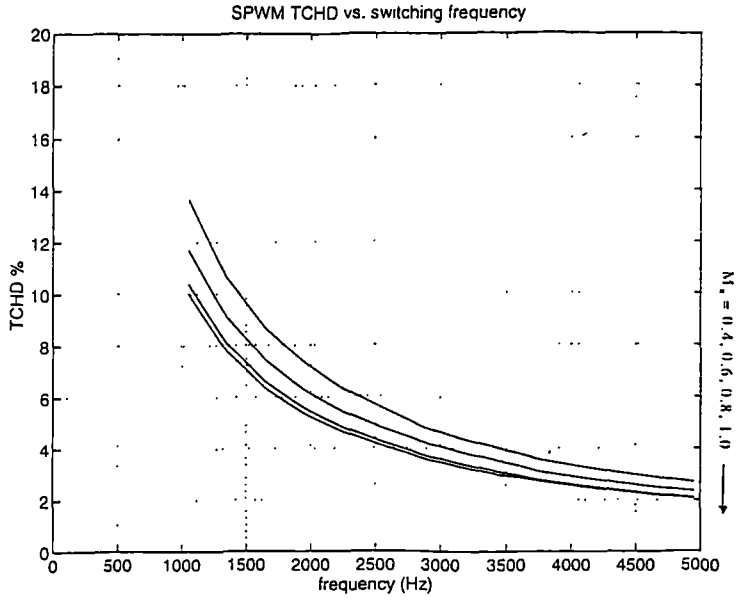

Figure 8.7 TCHD characteristics of SPWM (δ=10°, X_s=0.2)

It can be seen that higher switching frequencies yield better harmonic performance. For the studied case, the total harmonic distortion is improved significantly with switching frequency increasing up to about 2.5kHz. On the other hand, the semiconductor switching power loss is expected to increase in proportion to switching frequency typically reaching the same level as that of conduction loss at about 6kHz [23]. Moreover, a switching frequency between 6kHz-20kHz produces sensitive audible noise. Taking these considerations into account, a switching frequency of 3.15kHz (corresponding to 63×grid frequency) is chosen for fuller evaluation.

The simple system has been analysed under following conditions: P_{rated}=150kW, $V_{d,rated}$=600V, grid voltage V_s=440V 50Hz (147.9V at inverter side of transformer), The inverter operates at f_{sw}=3.15kHz, the coupling inductor X_s =0.2 pu with the rated power and grid voltage being taken as per unit system base values. It is assumed that the

system follows the optimal curves of figure 5.12, and that the modulation ratio and power angle follow the curves in figure 8.5 and 5.16(a). Then, for example, at half rated wind speed: $V_{d,0.5}$=241V, $\delta_{0.5}$=1.4°, $M_{a,0.5}$ =1.0 and at rated wind speed: δ_{rated} =11.3° $M_{a,rated}$ =0.41. The harmonic spectra for wind speeds of 0.5 pu and 1.0 pu are shown in figure 8.8 and 8.9. A selection of other results of inverter can be found in Table 8.1 (section 8.3.2).

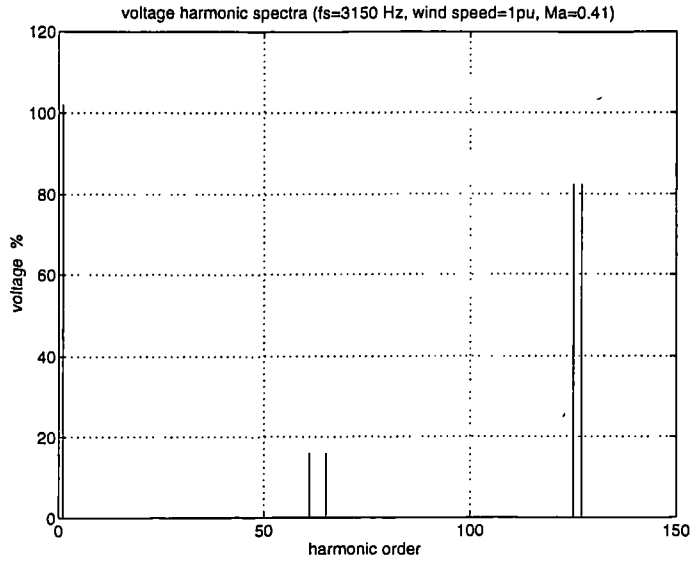

(a) voltage harmonic spectra

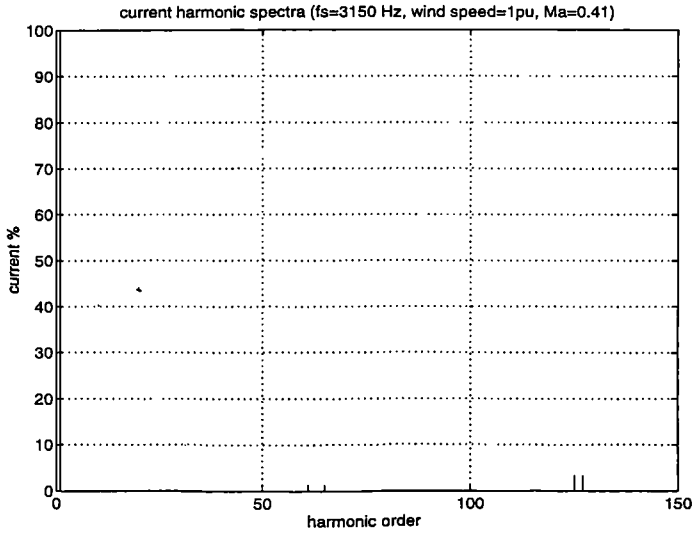

(b) current harmonic spectra

Figure 8.8 Harmonic spectra of SPWM-VSI in simple system (numerical frequency domain analysis, M_a=0.41, V_d=600V and δ=11.3°)

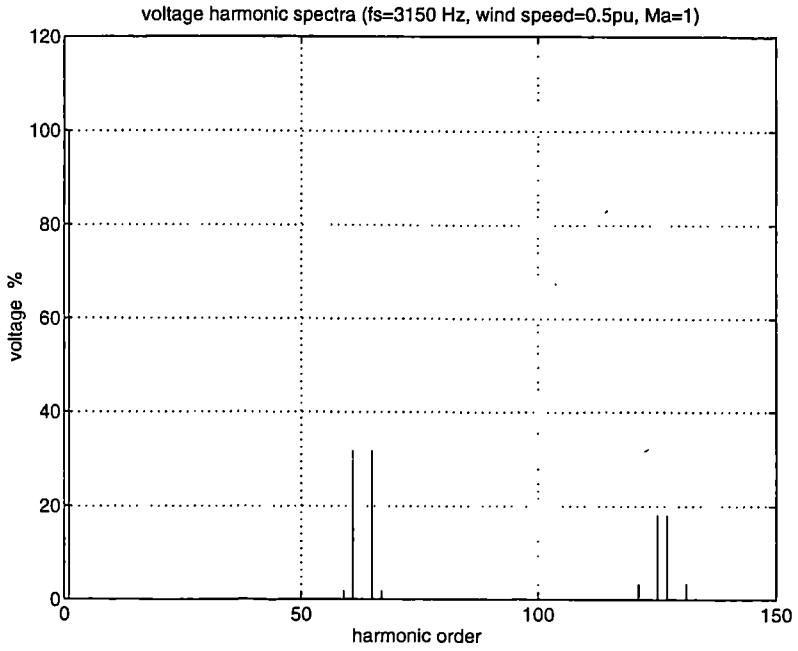

(a) voltage harmonic spectra

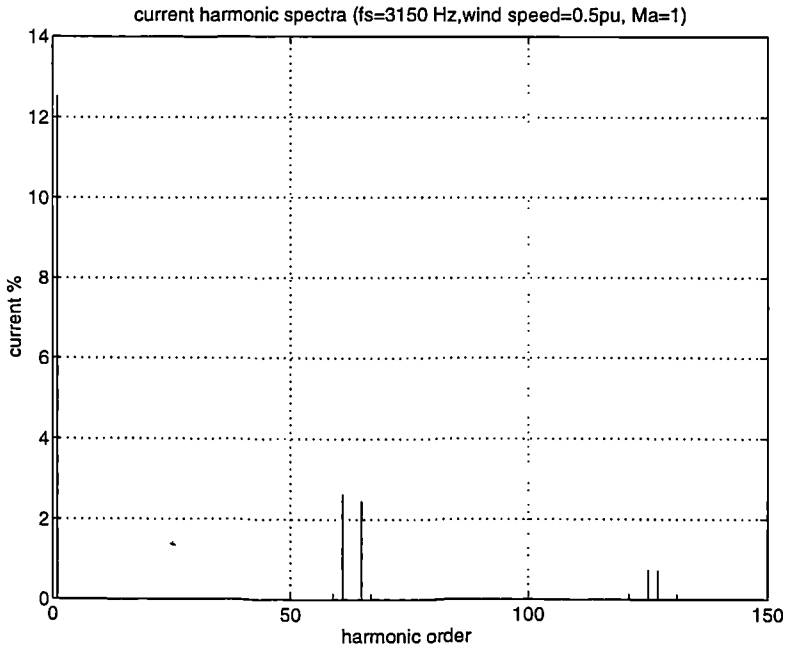

(b) current harmonic spectra

Figure 8.9 Harmonic spectra of SPWM-VSI in simple system (numerical frequency domain analysis, M_a=1.0, V_d=241V and δ=1.4°)

8.3 Time Domain Simulation Study of SPWM VSI Interface

Transient simulation of complex circuits and systems can now be achieved using computer analysis packages, such as PSPICE, SABER and EMPT etc., which find the solution of the non-linear system equations through a discrete time domain method from a description of the circuit components and their connections. The computer time domain solution can provide a means of assessing the accuracy of frequency domain analysis. It can also provide more detailed information for a practical system design. This section reports the simulation study of SPWM VSI interface using PSPICE. PSPICE simulator is a tool for computer simulation of analogue and digital circuits. It offers several forms of analyses, however, in this study, mainly transient analysis is used.

8.3.1 Simulation model

The simulation system model could be constructed using component models, including IGBTs, diodes and transformers, which can be described in detail by parameters or modelled by more basic components. The control and driving circuitry can also be simulated in great detail to the logic gate and amplifier level. However, such a simulation can be very time consuming. Appropriate modelling of a system always depends on the aspects of interest. In this chapter, we are concerned with such aspects as component utilisation, harmonic performance, and steady state power transfer, therefore, a simplified simulation model is sufficient.

The simulation system consists mainly of four parts as shown in figure 8.10. They are:

1) generator-rectifier-DC link,
2) voltage source inverter,
3) SPWM signal generator,
4) ac grid system.

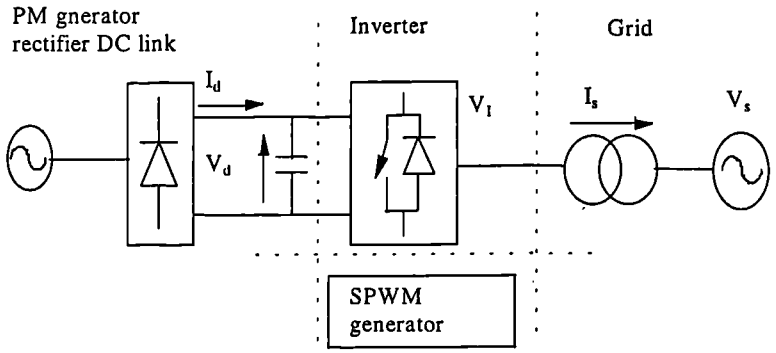

Figure 8.10 Sketched simulation system (SPWM VSI)

Generator-rectifier-dc link system: The simulation models of multiple generator and rectifier system used in chapter 3 and 4 can be used for this study. However, the generator-rectifier system produces a smooth dc link voltage and current with a large number of phases, therefore a dc voltage source, which takes the voltage at optimal V_d-wind speed curve, is used for steady state performance analysis.

AC grid system: The ac grid is simulated by a three phase sinusoidal voltage source connected to the inverter ac output terminal through the coupling inductor. In order to accelerate computation, the inverter transformer is omitted and all parameters are referred to the ac grid side.

SPWM signal generator: The switching generator includes a three phase sine wave generator, a triangular waveform generator and a comparator which generates gate driving signals as shown in figure 8.11.

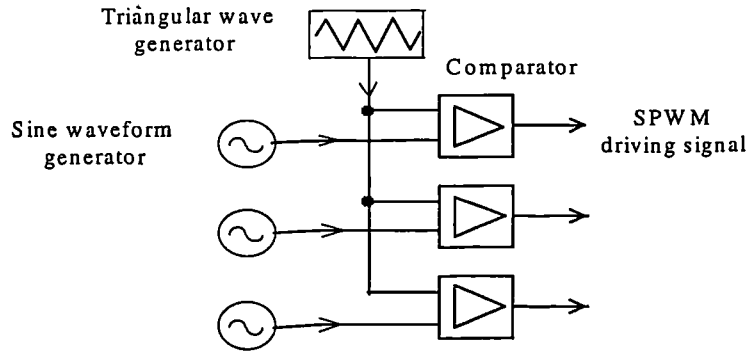

Figure 8.11 SPWM generator simulation model

Inverter system: The voltage source inverter is the principal section of the simulation model. For power circuit performance analysis, the six valves can be simulated by switches with very small on-state resistance and very large off-state resistance rather than detailed semiconductor modelling. However, the computational time and convergence performance can be improved by means of the Switching Functions concept [76], therefore in this simulation study the inverter simulation model is based on switching function concept. The inverter model shown in figure 8.12 includes dependent current sources (G_1, G_2 and G_3) and dependent voltage sources (E_1, E_2 and $E_{3)}$ which are controlled by signals produced from the SPWM generator and circuit voltage and current with the expression:

G_i: value={ $i_i \times V_{g,i}$ } and E_i: value={ $V_d \times V_{g,i}$ }; i=1,2,3.

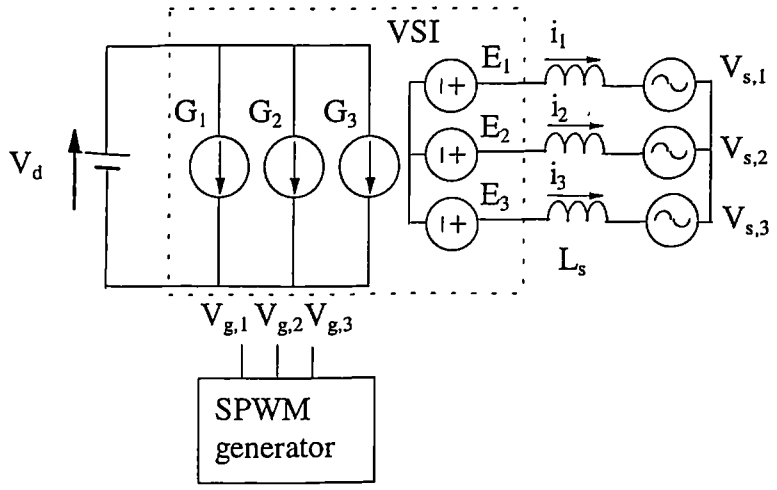

Figure 8.12 SPWM-VSI grid interface simulation model

8.3.2 Simulation Results

The simple power system described in chapter 5 with the SPWM described in the above section has been simulated, some of the results are presented in this section.

The generated SPWM signals for modulation ratio 1.0 and 0.41 are shown in figure 8.13. The waveforms shown in figure 8.14 are proceeding downward in the following sequence:

1. Inverter ac output voltage (line to line)
2. ac grid voltage (line to line)

3. ac grid voltage (phase)
4. ac current

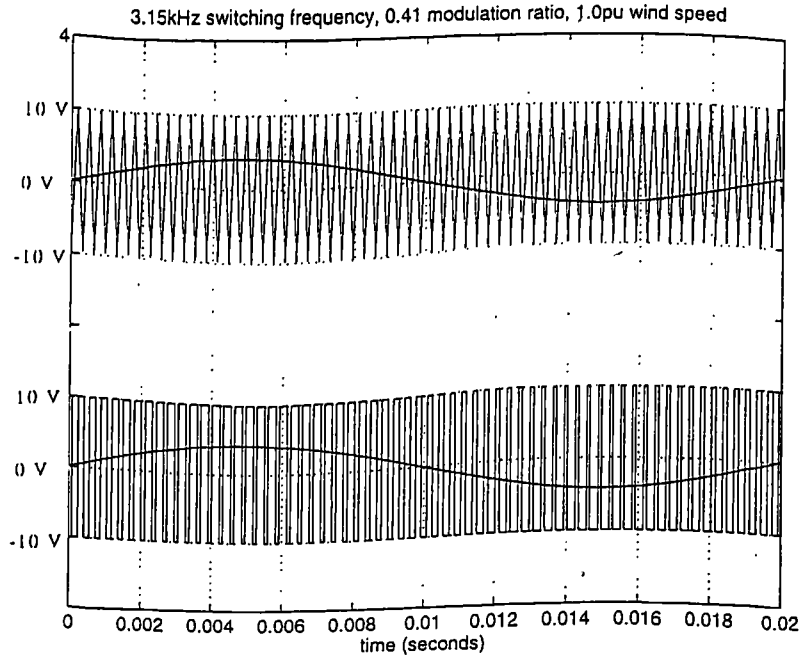

(a) switching frequency 3.15kHz and modulation ratio 0.41

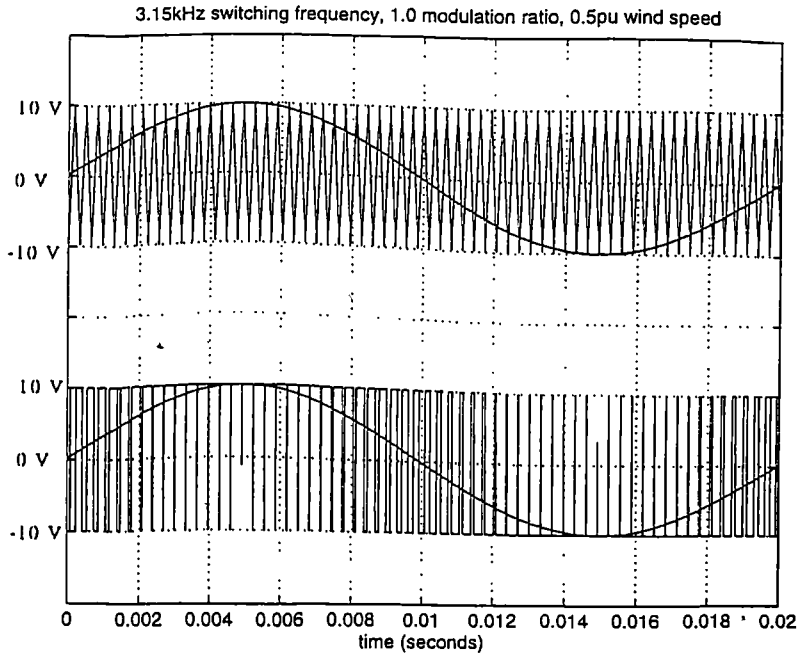

(b) switching frequency 3.15kHz and modulation ratio 1.0

Figure 8.13 SPWM driving signals

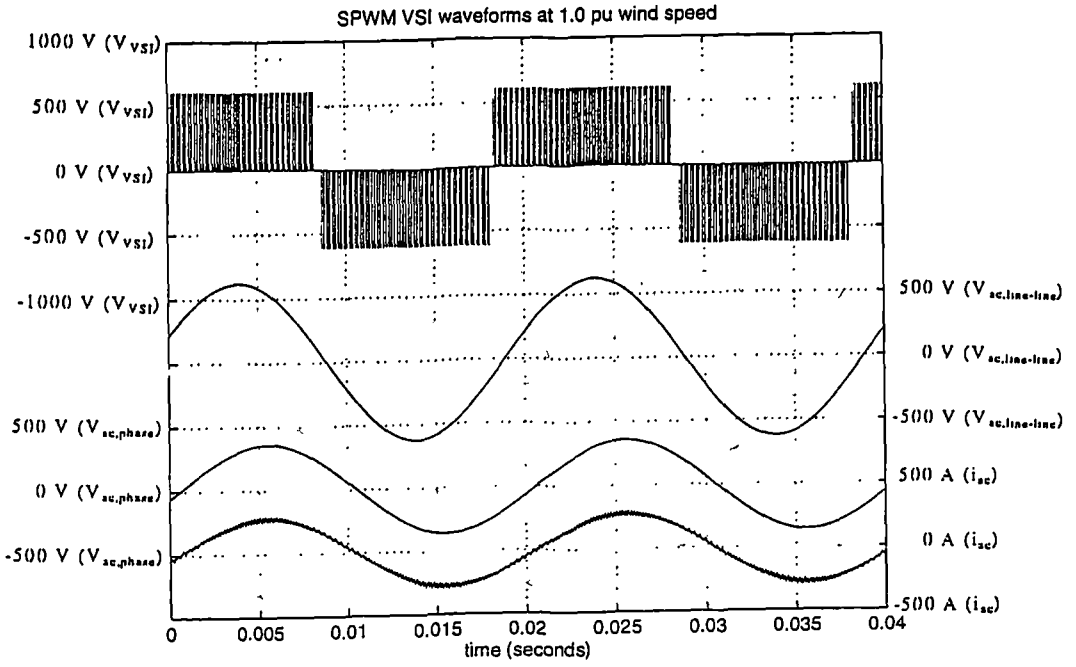

(a)

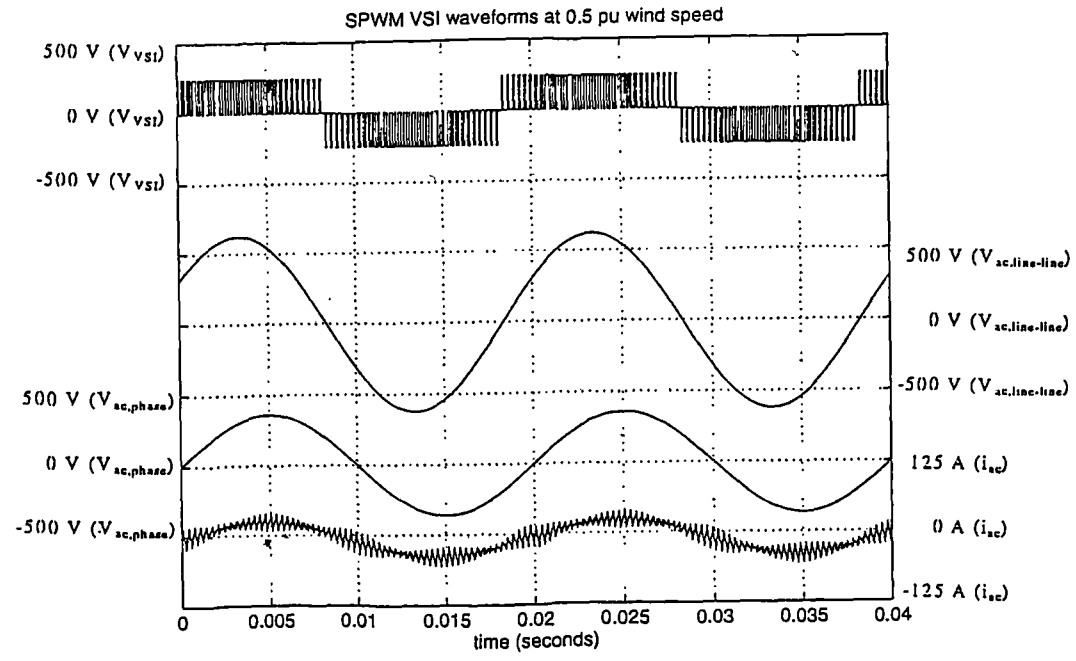

(b)

Figure 8.14 Waveforms of SPWM-VSI in simple system (simulation)

(V_s=440V and X_s =0.2 pu with V_s and rated current as based values)

(a) M_a=0.41, V_d=600V and δ=11.3° at 1.0 pu wind speed

(b) M_a=1.0, V_d=241V and δ=1.4° at 0.5 pu wind speed

The current waveform in figure 8.14 (b) has been multiplied by a factor of 4 for clarity.

From these waveforms, it can be seen that the phase voltage and current are in phase (unity DPF operation) and the current waveform has a rich harmonic content (about 33% of fundamental current component in figure 8.14 (b)), due to the small power angle and nearly unity ratio $V_{I(1)}/V_s$ as discussed in chapter 7. The TCHD is rather similar in the two cases 3.78% and 5% (based on the rated ac current). It is the difference in fundamental current which causes the dramatic change in waveform.

The harmonic spectra of the inverter ac terminal voltage (line to line) and inverter ac current are shown in figure 8.15 and 8.16.

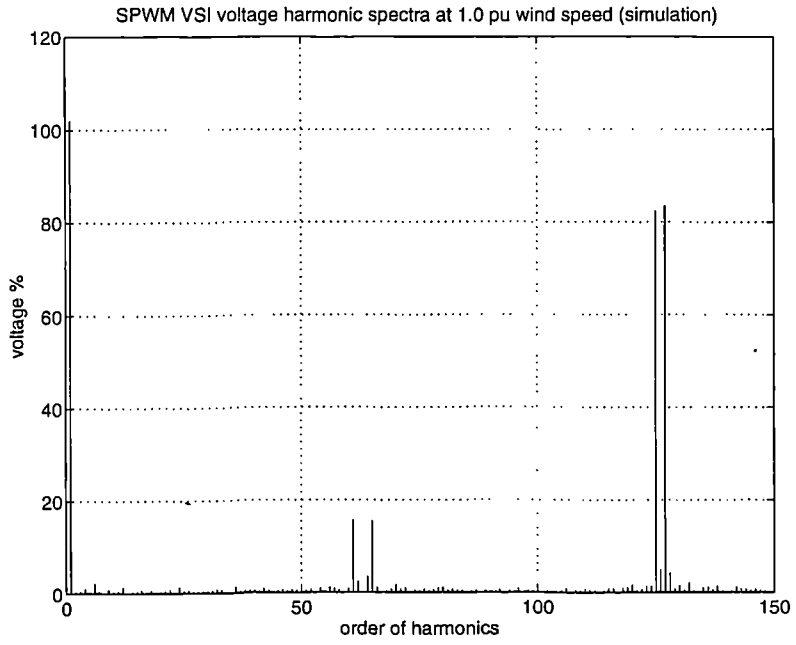

(a) voltage harmonic spectra

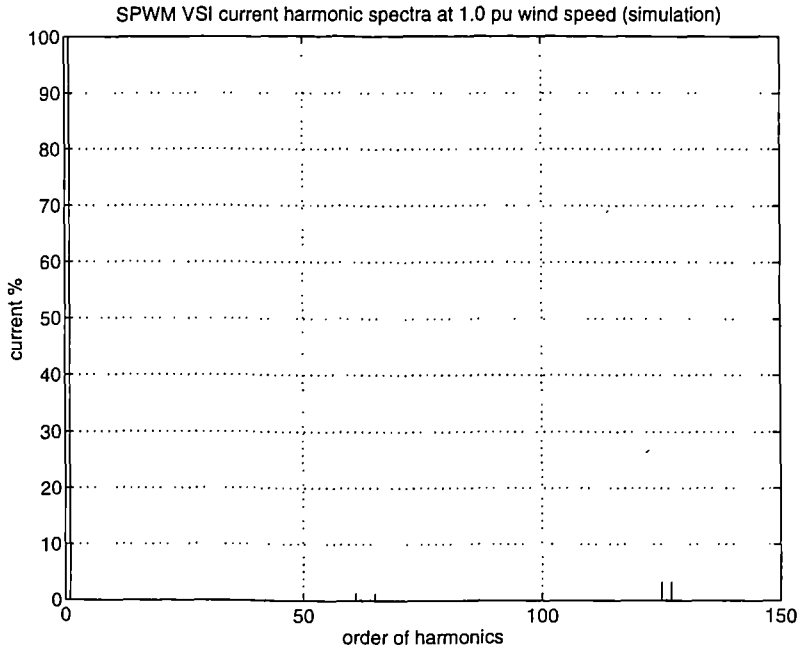

(b) current harmonic spectra

Figure 8.15 Harmonic spectra of SPWM-VSI in simple system (simulation, M_a=0.41, V_d=600V and δ=11.3°)

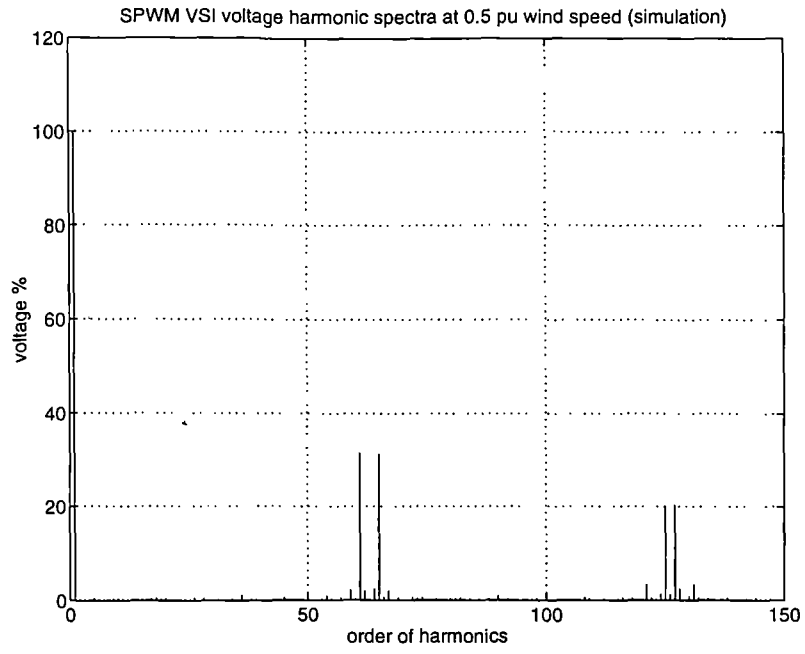

(a) voltage harmonic spectra

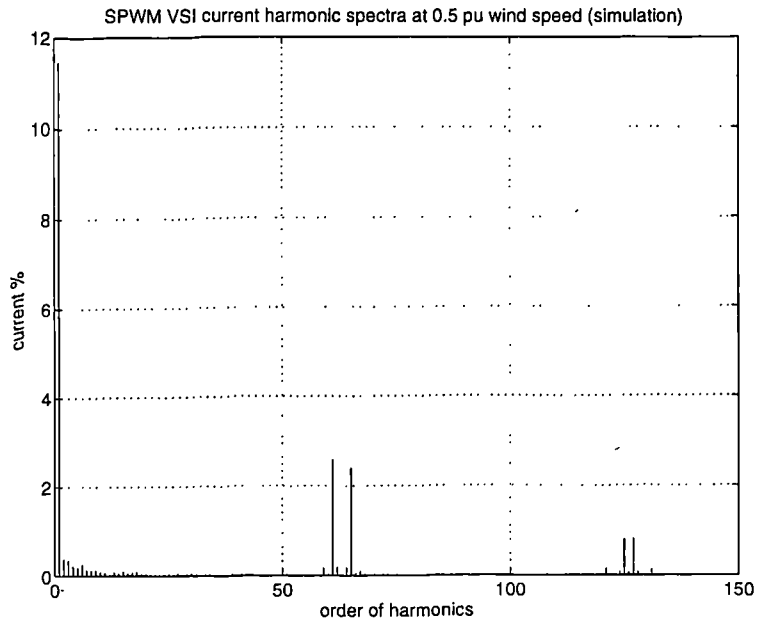

(b) current harmonic spectra

Figure 8.16 Harmonic spectra of SPWM-VSI in simple system (simulation, M_a=1.0, V_d=241V and δ=1.4°)

The harmonic spectra are presented as the percentage of grid voltage and rated ac current fundamental component. It can be seen the harmonics in figure 8.15 and 8.16 have very similar pattern with that in figure 8.8 and 8.9. Simulated average dc current I_d are respectively 73.04 and 247.3 for 0.5 pu and 1.0 pu wind speed. Some other results are given in Table 8.1 along with the numerical analysis results obtained using frequency domain analysis method in section 8.2.

Table 8.1 Comparison of numerical analysis and simulation results

	numerical analysis		simulation	
wind speed	0.5 pu	1.0 pu	0.5 pu	1.0 pu
grid current $I_{s(1)}$ (A rms)	24.6	196.8	22.4	195.2
power transferred (kW)	18.7	150	17.0 (17.6)$^+$	148.8 (148.4)$^+$
TVHD* (%)	52.0	118.5	53.2	119.7
TCHD** (%)	3.73	4.95	3.78	5.0

*, ** based on grid voltage and rated current respectively.

$^+$ calculated at dc side.

It can be seen the harmonic spectra from PSPICE simulation are in good agreement with analytical results.

8.4 Experimental Study of SPWM VSI Interface

A laboratory model of the SPWM-VSI interface system has been designed and built for experimental studies. This section reports the experimental work.

8.4.1 Experimental Model

The experimental model mainly consists of power circuit, driving circuit and control circuit are illustrated in figure 8.17.

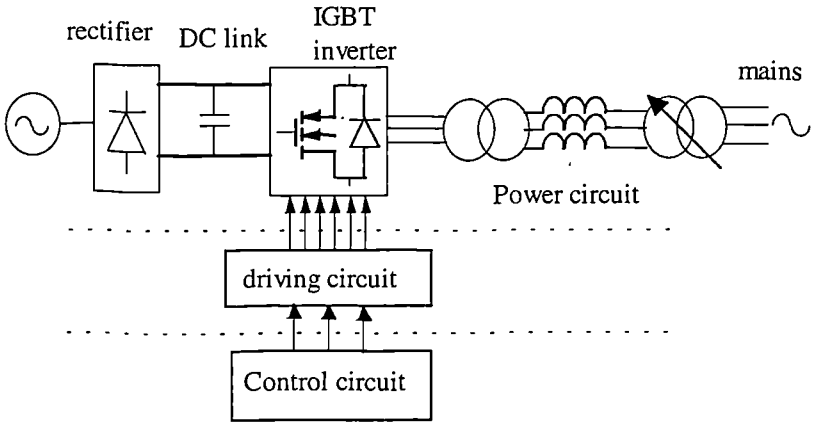

Figure 8.17 Block diagram of experimental system

Power Circuit

The power circuit consists of rectifier, dc link, VSI, transformer, inductors (20mH per phase). The connections are shown in figure 8.17. An IGBT module (SKM22GD121D, V_{ces}=1200V and I_c=22A) was used providing six IGBTs in three phase bridge connection.

Driving Circuit

IGBTs are voltage controlled devices which can be driven directly by COMS buffer ICs, this feature simplifies the driving circuit design. The designed driving circuit for the experimental model is shown in figure 8.18.

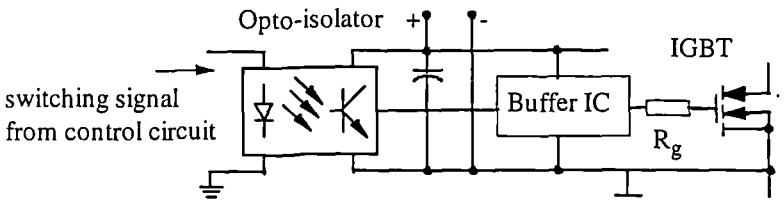

Figure 8.18 IGBT driving circuit (experimental model)

Control System

The basic requirements of the control system are

- synchronising to and tracking grid frequency
- setting optimal power angle and modulation ratio
- generating SPWM switching signal

The above requirements could be implemented in practice with analogue or digital hardware circuitry, or by a microcontroller or microprocessor. However, a PC computer was used instead for convenience of system calibration and control strategy development. However, the control algorithm developed in the PC could be easily transferred to a microprocessor or controller.

The block diagram of control system is shown in figure 8.19.

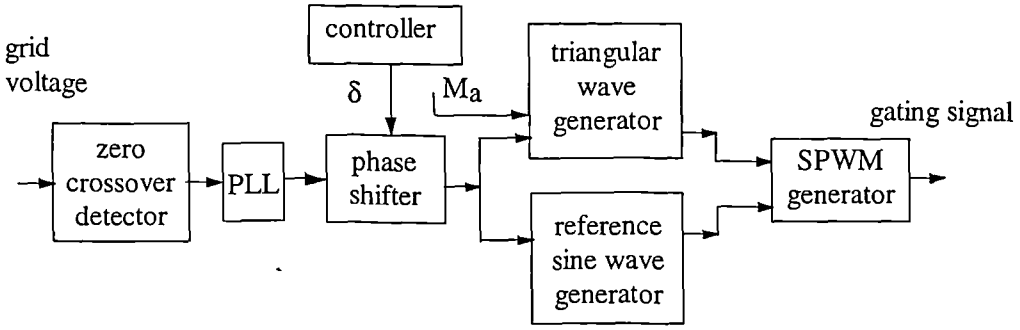

Figure 8.19 Block diagram of SPWM-VSI control system (experimental model)

Zero crossover detector: The function of synchronisation with the grid and frequency tracking has been implemented by a zero crossing circuit and a phase lock loop (PLL) as shown in figure 8.20. This circuit also generates a clock signal for the phase shifter.

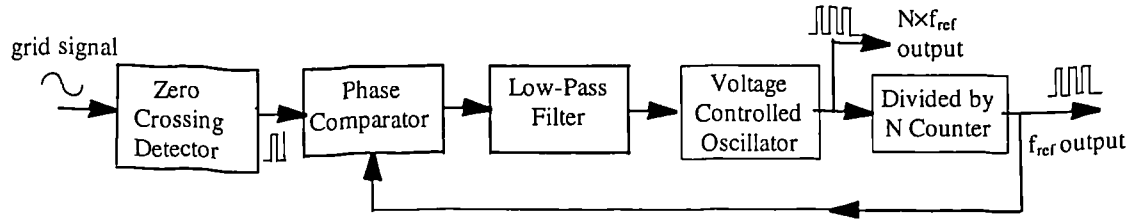

Figure 8.20 Block diagram of synchronisation (experimental model)

Phase shifter: The function of the phase shifter is to generate a phase shifted reference waveform with a controllable phase angle with respect to synchronous signal. The phase shifter is implemented by a counter circuit, the controller (computer) can set the counter with a value which represents the pulse number of clocking signal between the synchronous signal and phase shifted reference signal. The block diagram is shown in figure 8.21.

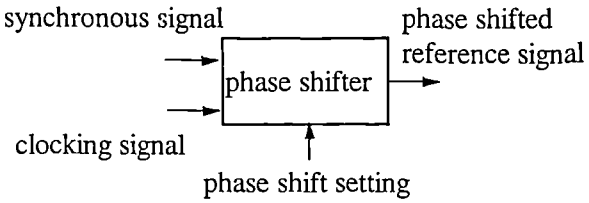

Figure 8.21 Principle and block diagram of phase shifter (experimental model)

Sine wave generator: a switching pattern generator produces three phase reference square waves whose higher order harmonics are filter out by filters to obtain the three phase sine waves.

Triangular waveform generator: consists of an integrator and a switching frequency square wave generator. The triangular waveform is generated by integrating the square wave which is synchronised with the three phase sine reference waveform at a frequency of 3.15kHz.

SPWM generator: The comparators produce gating signals by comparing the sine and triangular waves. The magnitude of either wave could be varied to effect the modulation

ratio regulation. In the designed circuit, the magnitude of the triangular wave is determined by the modulation ratio setting from the computer.

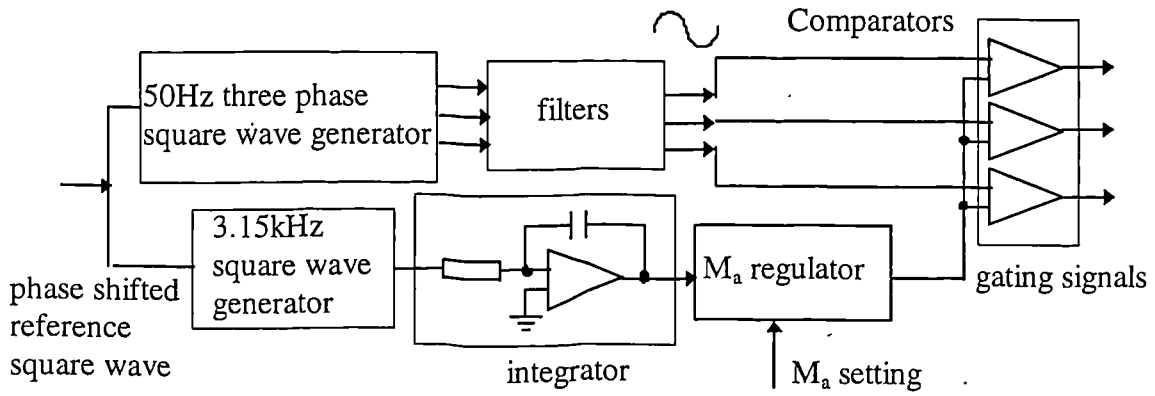

Figure 8.22 Block diagram of SPWM signal generation (experimental model)

Controller: The output of the controller comprises power angle and modulation ratio settings. The requirement of reactive power or power factor can be set by computer. The controller is implemented in software. The input and output signals communicate with sensors and circuits through a Super ADDA-8 card. (Parallel port A for power angle control, DA1 for modulation control, ADs for input signals).

A block diagram is shown in figure 8.23. The inputs could be machine speed, dc link voltage, current, and ac network voltage. The optimal speed/power relationship could be stored in the controller memory and compared with the actual operating points to decide the required adjustment of power angle and modulation ratio. The controller then sends commands to the phase shifter and modulation ratio regulator.

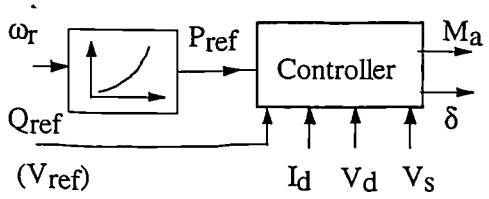

Figure 8.23 A block diagram of controller

8.4.2 Experimental Results

The generated 3.15kHz SPWM signals for modulation ratio 1.0 and 0.41 are shown in figure 8.24 and 8.25.

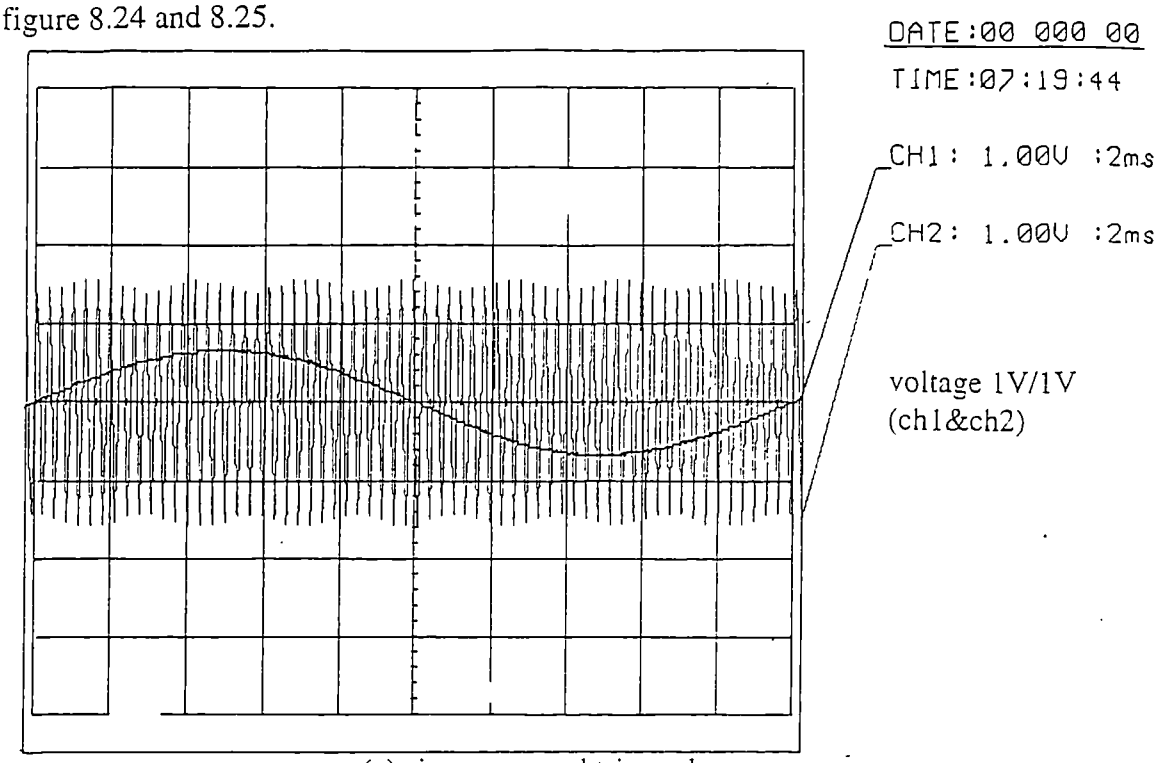

(a) sine wave and triangular wave

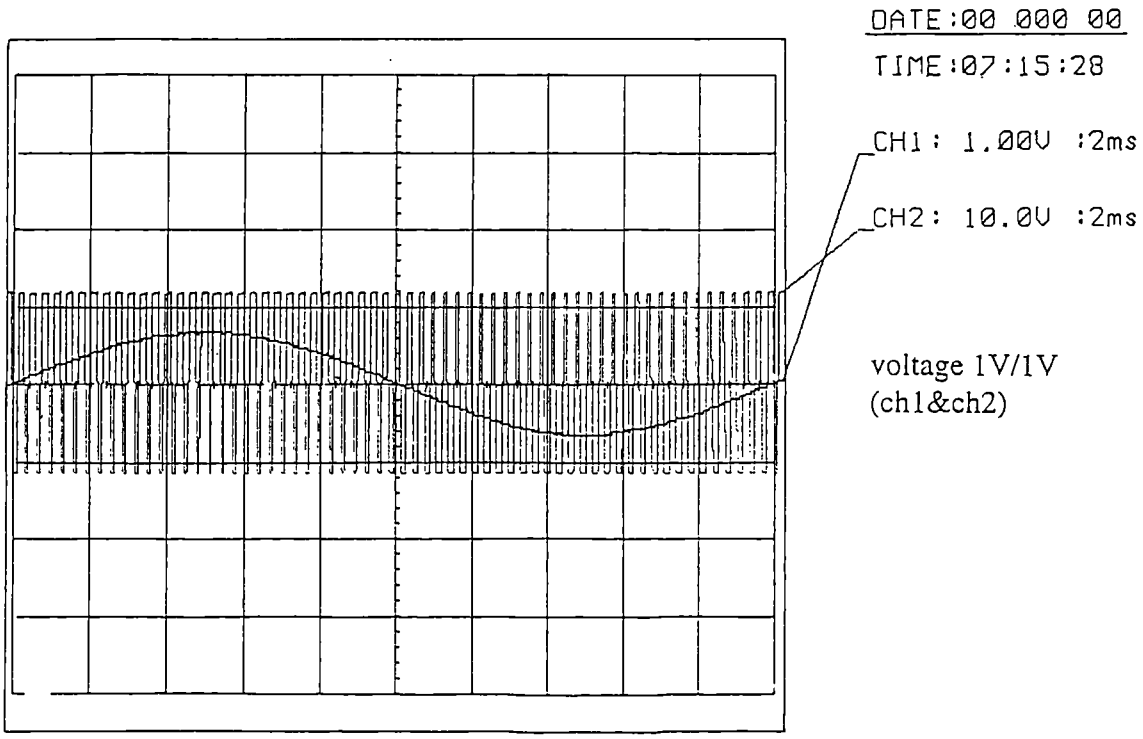

(b) sine wave and SPWM driving signals

Figure 8.24 SPWM signals at modulation ratio 0.41

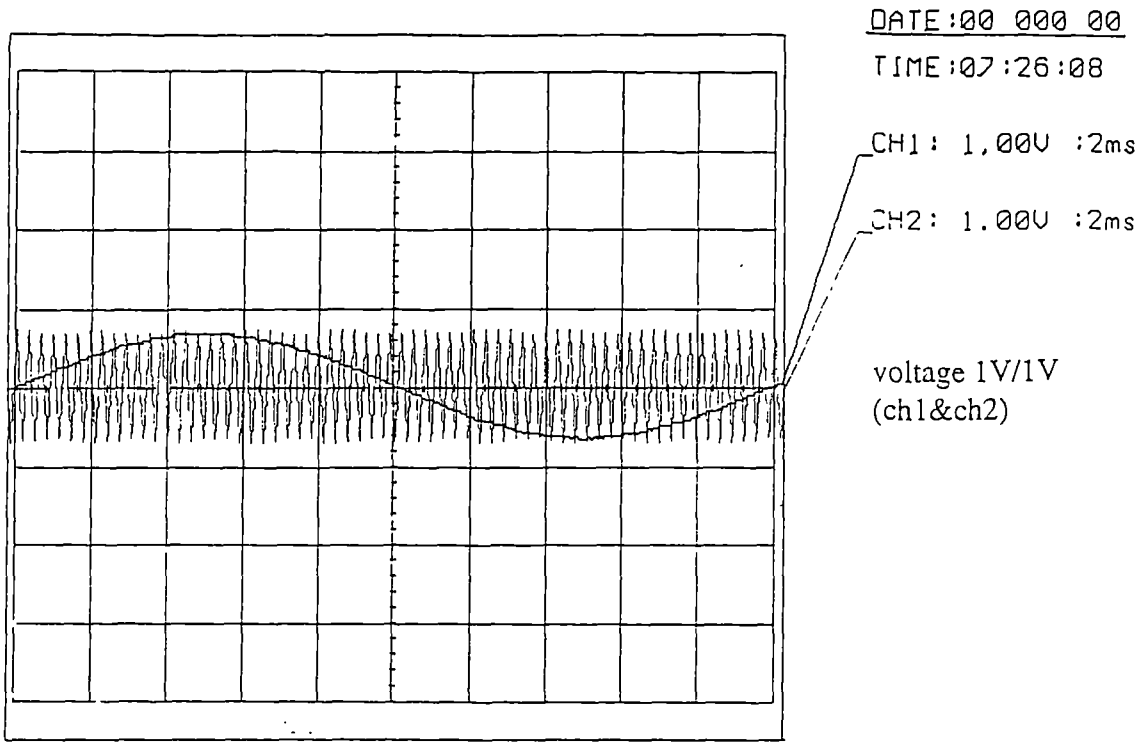

(a) sine wave and triangular wave

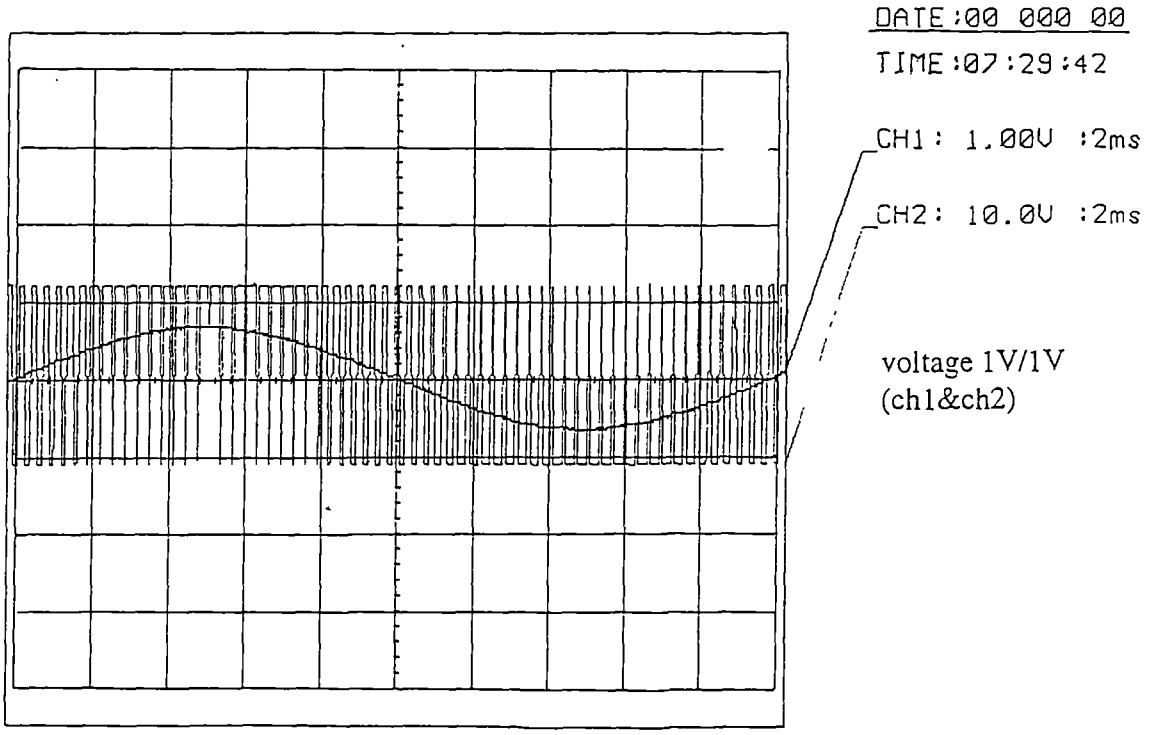

(b) sine wave and SPWM driving signals

Figure 8.25 SPWM signals at modulation ratio 1.0

The waveforms of grid voltages (line and phase to neutral), inverter ac voltage and ac current are shown in figure 8.26 and 8.27.

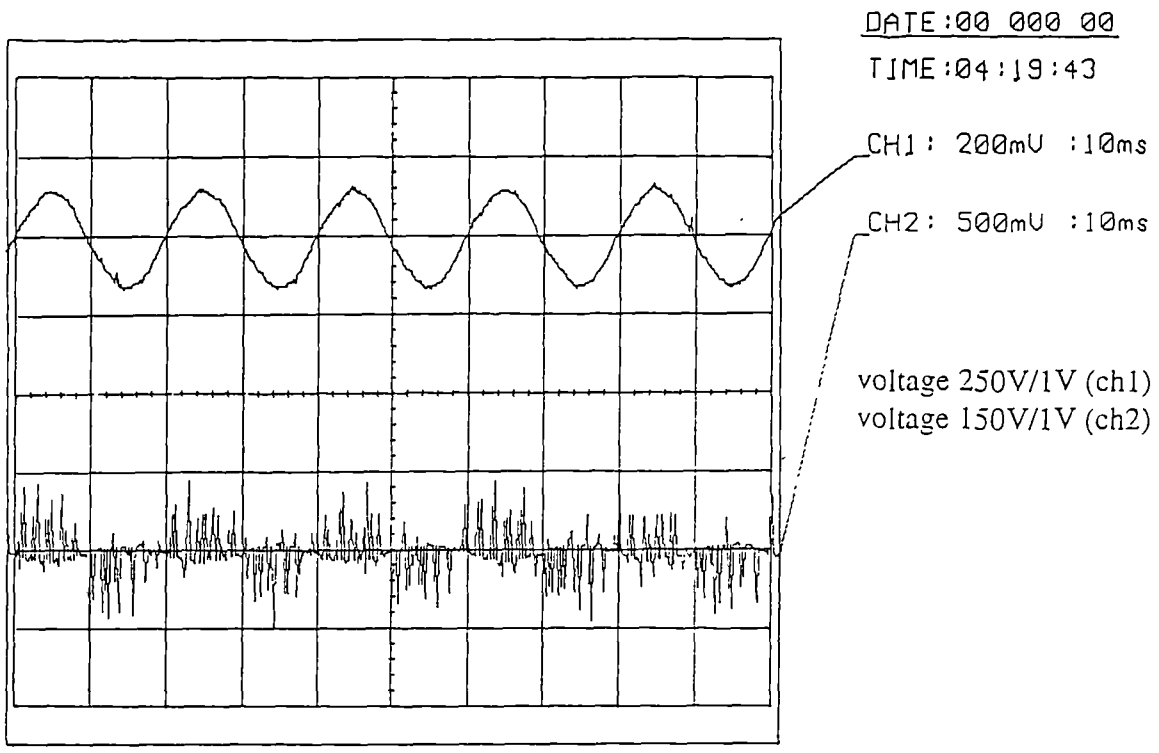

(a) grid voltage and inverter output voltage (line to line)

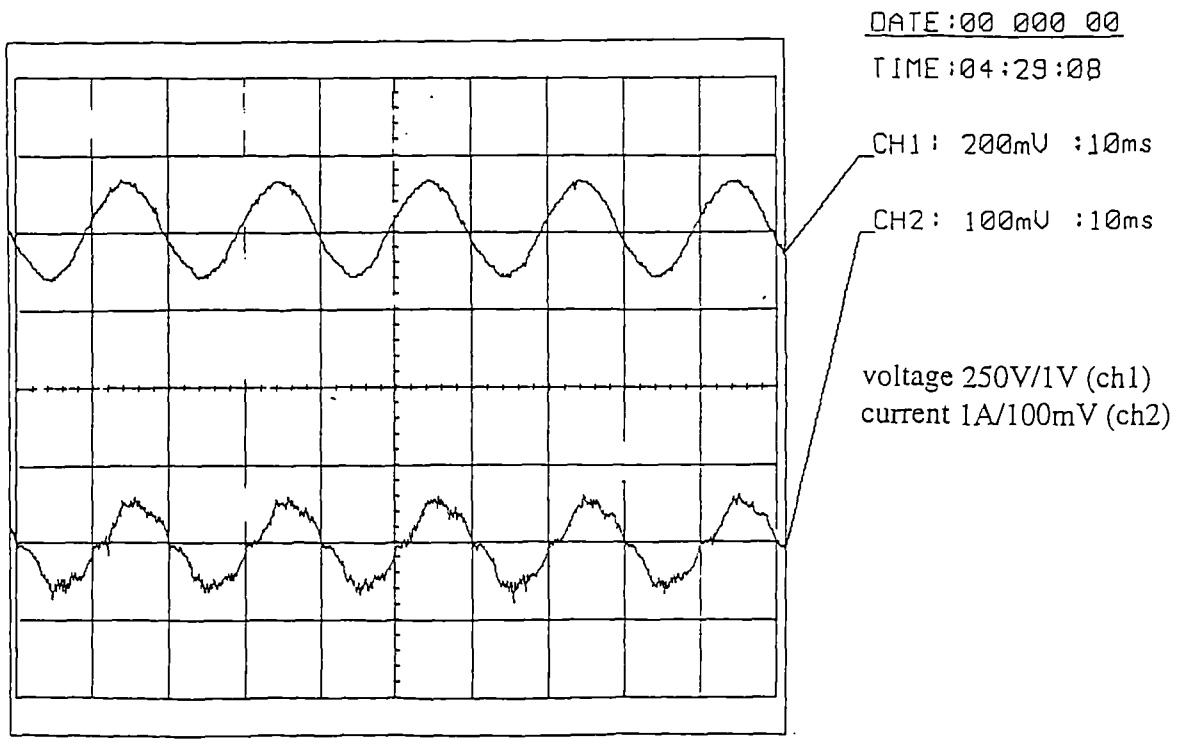

(b) grid voltage (line to line) and inverter output current

Figure 8.26 Waveforms of SPWM-VSI (experimental M_a=0.41 and δ=11.3°)

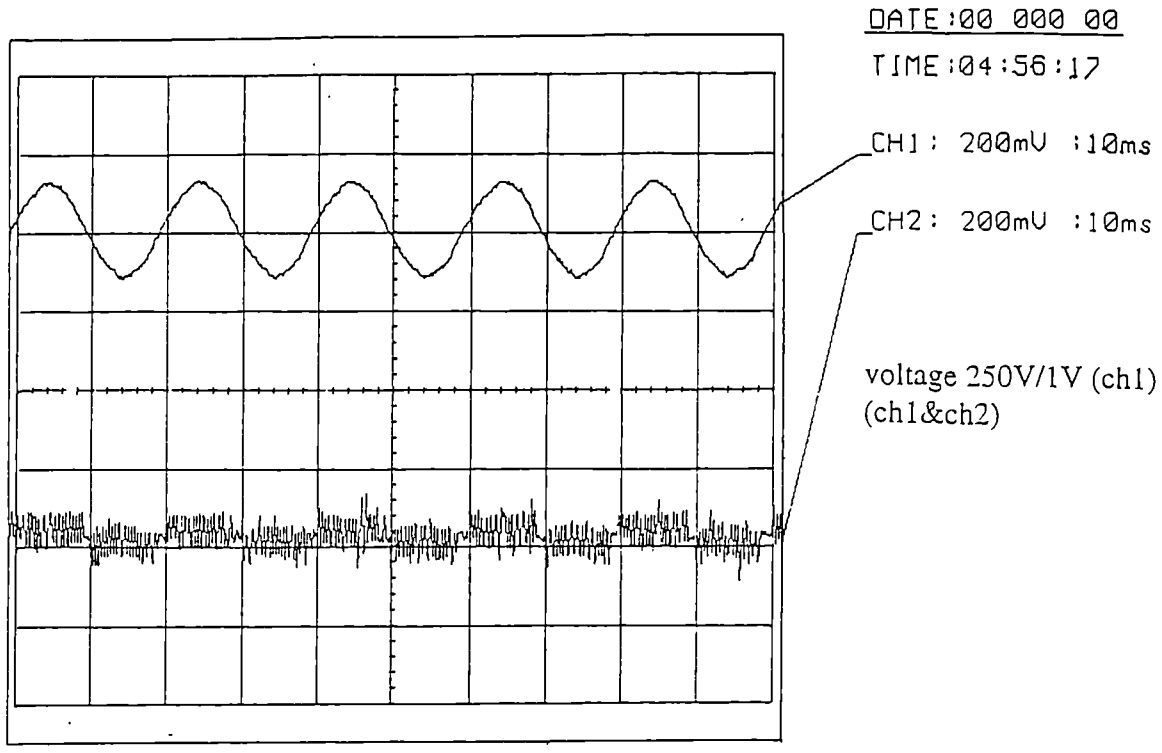

(a) grid voltage and inverter output voltage (line to line)

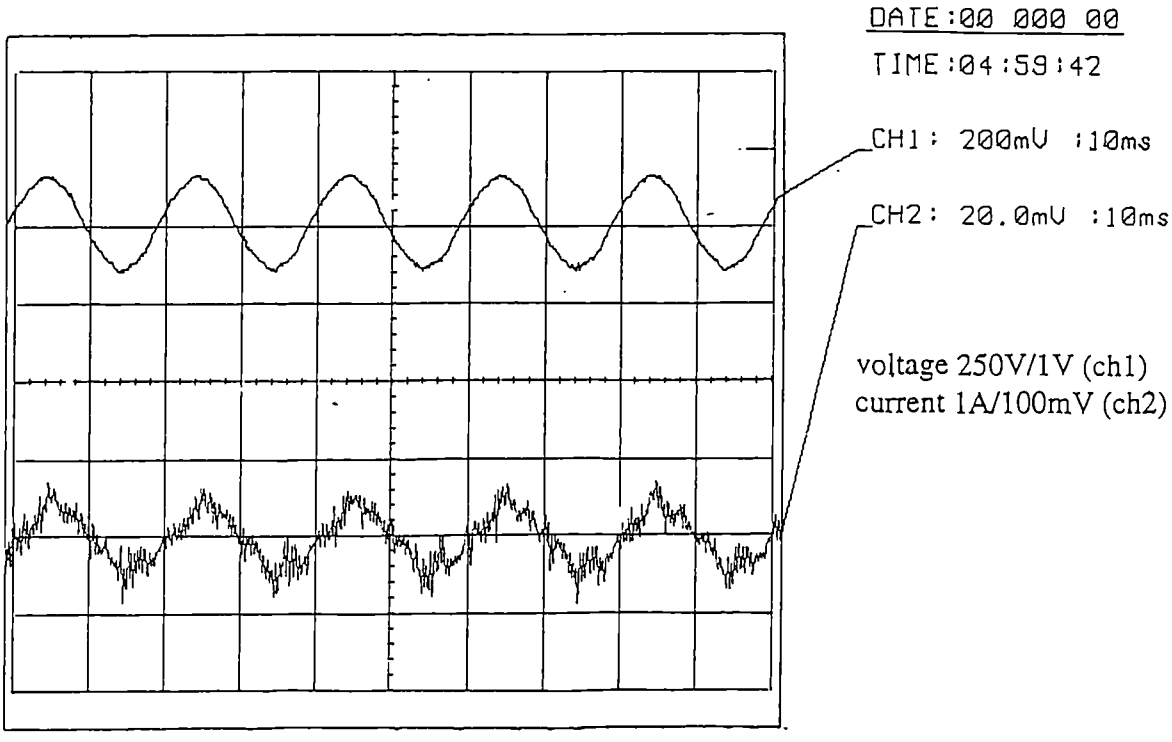

(b) grid voltage (line to line) and inverter output current

Figure 8.27 Waveforms of SPWM-VSI (experimental M_a=1.0 and δ=1.4°)

A data acquisition system collects the waveforms whose harmonics are then derived by Fourier analysis. The ac current harmonic spectra are shown in figure 8.28 and 8.29.

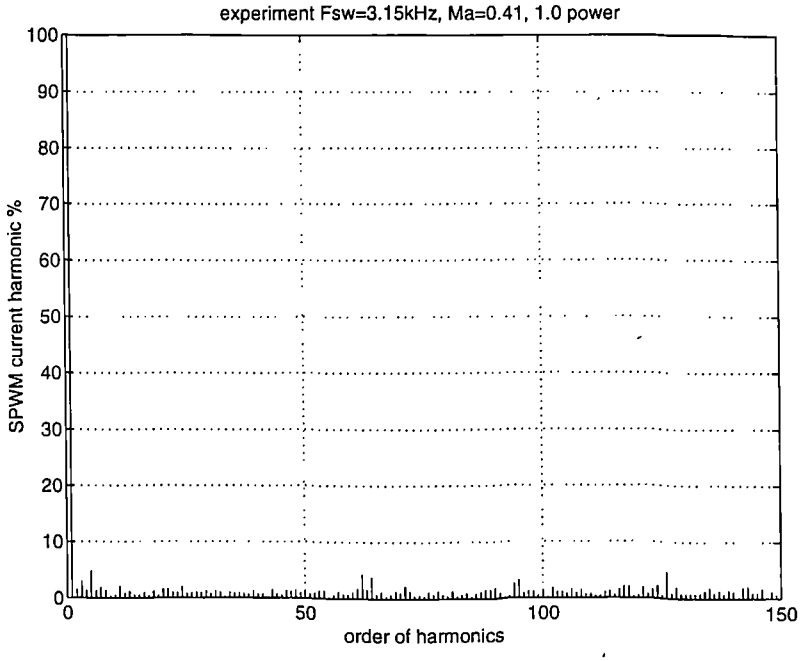

Figure 8.28 Current harmonic spectra (SPWM-VSI experimental M_a=0.41 and δ=11.3°)

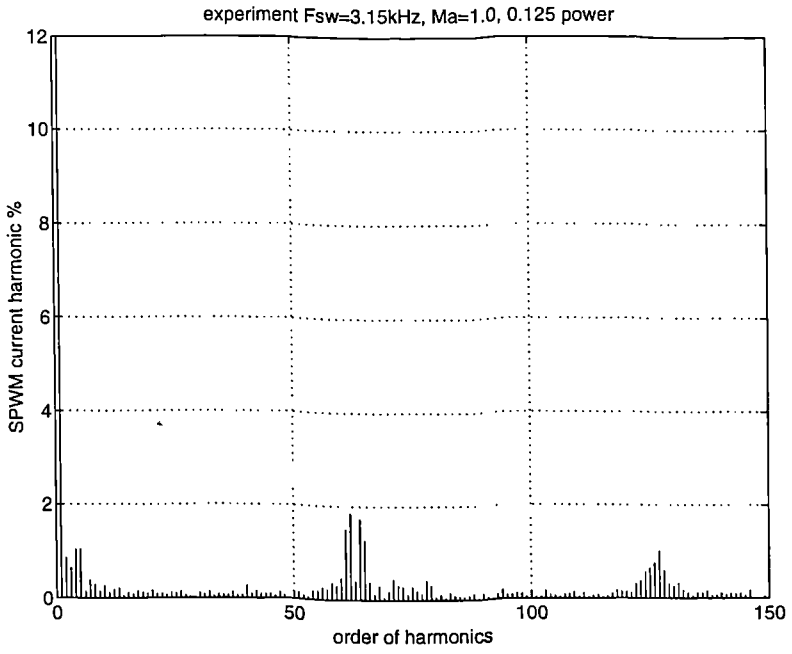

Figure 8.29 Current harmonic spectra (SPWM-VSI experimental M_a=1.0 and δ=1.4°)

The harmonic spectra are presented as the percentage of ac current fundamental at condition of M_a=0.41 and δ=11.3°. It can be seen the harmonics in figure 8.28 and 8.29 have similar pattern with that from simulation and numerical frequency domain analysis.

8.5 SPWM-VSI Wind Power In Isolated Systems

If no grid voltage is presented at inverter ac side, for example, in an isolated system, the SPWM-VSI type interface can still transfer power into the system, but the power angle is no longer useable as a control variable. The power factor will depend on the nature of the load. The transferred power is determined by the loading and inverter ac terminal voltage which is the only control and can be effected by regulating the SPWM modulation ratio. Figure 8.30 and 8.31 show the simulation and experimental waveforms of such a system.

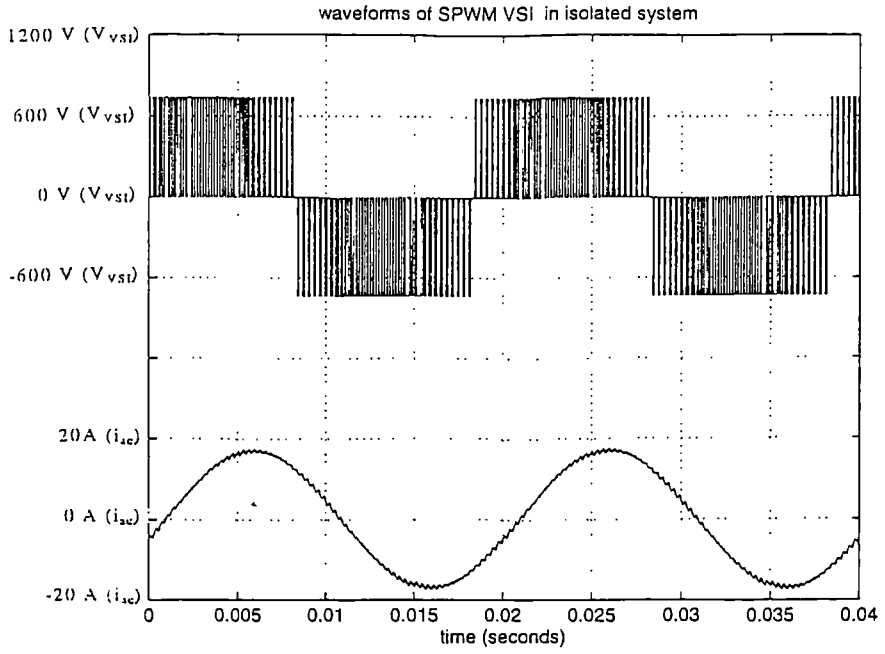

Figure 8.30 SPWM-VSI waveform in isolated system (simulation DPF=0.85)

(ch1: inverter ac voltage ch2: current)

(R_{load} =20Ω, L_{load} =20mH)

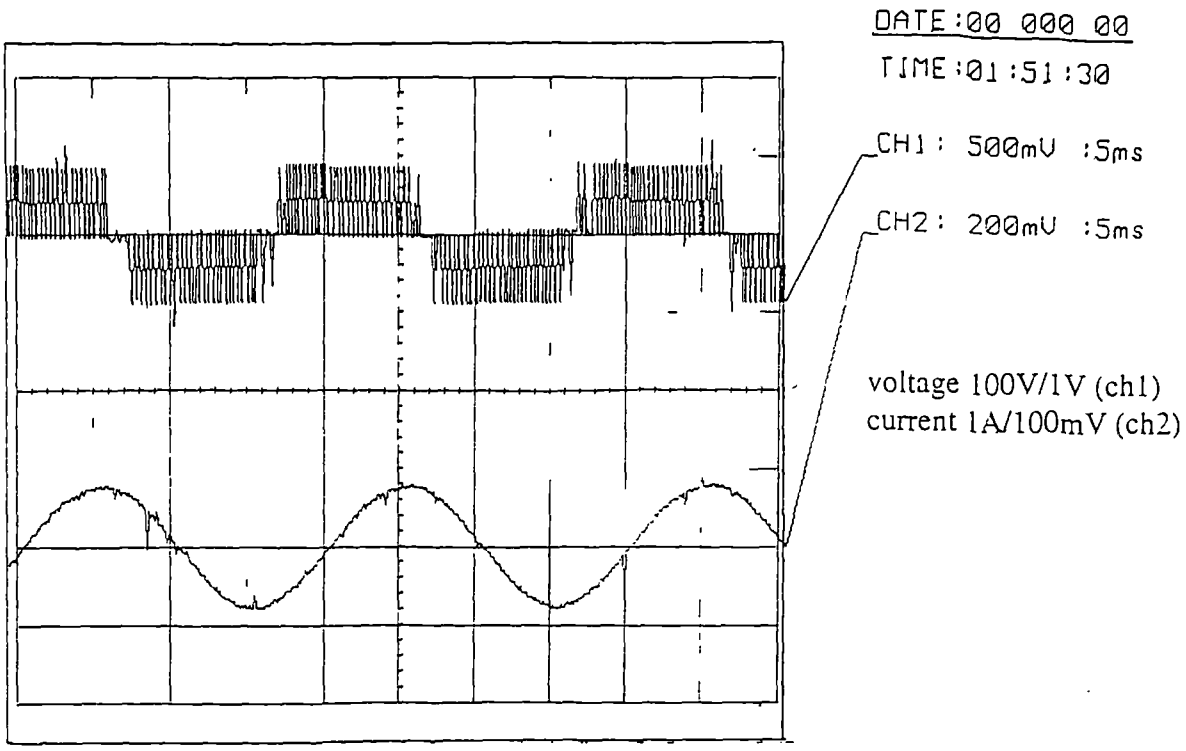

Figure 8.31 SPWM-VSI waveform in isolated system (experimental DPF=0.85)
(ch1: inverter ac voltage ch2: current)

8.6 Discussions

As a typical representative of high frequency switching VSIs, the SPWM VSI has been investigated in detail with respect to the implementation of power angle and fundamental voltage component control, switching utilisation factor and harmonic performance. SPWM VSI has the advantage of simple power and control circuitry and therefore easy implementation. There are also other higher switching frequency PWM schemes, some offering a slightly higher output voltage than SPWM at the same dc link voltage, such as harmonic injection techniques. Some could achieve satisfactory harmonic performance with a lower switching frequency and therefore a reduced switching power loss, such as programmed selective harmonic elimination. However, if the VSI is directly connected to a widely varying dc link, these schemes all suffer the disadvantage of low switch utilisation ratio since the inverter has to accommodate a

wide varying dc link voltage. That means the rated power has to be transferred at a correspondingly higher current level with accompanying higher conduction power losses.

8.7 Conclusions

In this chapter, the SPWM VSI type DC/AC power electronics interface has been discussed in detail.

The numerical method for SPWM VSI analysis has been developed and used for system performance investigation. In addition to analysis, simulation and experimental models have been implemented and the predicted performances has been demonstrated, similar results have been obtained in each case.

It is shown that SPWM VSI can be implemented in a basic six device inverter to realise the ac voltage and phase angle control required for optimal power transfer with controllable power factor and satisfactory harmonic performance. The simple structure is an attractive aspect of this type of interface, but, the low semiconductor utilisation is a serious drawback.

The studies of this chapter indicate that PWM VSI is technically feasible but not of high efficiency and therefore is overall not an attractive choice for the addressed application.

Chapter

9. DC Voltage Controllable Voltage Source Inverter (DC/DC Converter-VSI)

9.1 Introduction

Studies described earlier have shown that the high frequency switching VSI connected directly to a dc link with widely varying voltage and current results in low switch utilisation ratio (SUR), and consequently, high cost and losses. The VSI could operate more efficiently with a nearly constant dc voltage, which could be realised by placing a DC/DC converter between the rectifier and inverter to form a DC/DC converter - VSI system.

In many industrial applications, DC/DC converters are used to convert a dc voltage from one level to another, such as traction motor control in electric automobiles, trolley cars, marine hoists, forklift trucks and main haulers. A high frequency DC/DC converter can be considered as the dc equivalent to an ac transformer with a variable turns ratio which can be continuously controlled via the switch duty ratio. There are isolated and nonisolated DC/DC converters. In the dc power supplies, DC/DC converters are often used with an electrical isolation transformer, however, in dc motor drives, the isolation transformers are almost always omitted. In the addressed application, nonisolated converters can be used. The dc converter can be implemented with a single controllable semiconductor plus a diode and reactive components, this type of converter can only transfer energy in one direction. Although a bridge converter is capable of a bi-directional power flow, more controllable semiconductors are needed. Only uni-directional DC/DC converters are considered since bidiectional power flow is not required.

9.2 High Frequency Switching DC-DC Converter

High frequency switching DC/DC converters are power electronic circuits where the semiconductor devices switch at a rate that is fast compared with the variation of the input and output waveform. The relation between the average input and output voltages is controlled by the semiconductor on and off duration (t_{on} and t_{off}) or the switch duty ratio (D), where $D=t_{on}/T_{sw}$ and $T_{sw}=1/f_{sw}$. f_{sw} is the switching frequency.

9.2.1 DC/DC converter circuit

A switching mode DC/DC converter can be constructed with a controllable semiconductor (GTO, MOSFET, IGBT or BJT etc.), a diode and reactive components (capacitor and inductor). The connections of these components determine both the input/output voltage ratio range and the level of current and voltage stress imposed on the components. DC/DC converters may be divided into two categories [55]: direct and indirect, depending on whether a dc path exists between the input and output. In a direct converter, there is a direct path between input and output at one position of the switch, while in indirect converter there is no such path exists for a switch position.

9.2.1.1 Direct DC/DC converter

The two commonly used DC/DC converter circuits, step down (buck) and step up (boost) are shown in figure 9.1, are of the direct type. In these circuits, the direction of power flow is from V_d to V_o.

(a) step down (buck) converter (b) step up (boost) converter

Figure 9.1 Direct DC/DC converters

Buck converters

In the buck converter shown in figure 9.1 (a), when the switch is turned on, the input current flows through the inductor and into the load. When the switch is turned-off, the current in the inductor, takes the path through the diode and is sent into the load while the voltage is maintained by the filter capacitor.

The converter can operate either in continuous or discontinuous modes, defined by whether the inductor current is continuous or discontinuous. If the mean inductor current is less than a critical value, I_{LB}, where

$$I_{LB} = DT_{sw}/(2L)\times(V_d - V_o) = V_d DT_{sw}/(2L)\times(1-D)$$

the converter enters the discontinuous mode [64]. The output voltage cannot be higher than the input voltage in either mode. In the continuous conduction mode, the input and output average voltage and current are related by:

$$\frac{V_o}{V_d} = D \qquad \frac{I_o}{I_d} = \frac{1}{D} \tag{9.1}$$

The ripple component of the inductor current, Δi_L, is determined by the voltage difference $V_d - V_o$, switching frequency f_{sw} and inductance L as:

$$\Delta i_L = \frac{V_d(1-D)}{Lf_{sw}} \tag{9.2}$$

Boost converters

Figure 9.1 (b) shows a boost converter, when the switch is turned-on, the diode is reverse biased, the current flows through the inductor and energy is stored in it. When the switch is turned-off, the voltage across the inductor and the input voltage are in series and together provide energy to charge the output capacitor to obtain a voltage higher than the input voltage.

Again, the inductor current can be either continuous or discontinuous. If the inductor current is less than a boundary current I_{LB} [64].($I_{LB} = V_o DT_{sw}/(2L)\times(1-D)$), the inductor

current becomes discontinuous. In the continuous conduction mode, the input and output average voltage and current are related by:

$$\frac{V_o}{V_d} = \frac{1}{1-D}$$
$$\frac{I_o}{I_d} = 1-D \qquad (9.3)$$

and the ripple current in the inductor is:

$$\Delta i_L = \frac{V_d D}{L f_{sw}} \qquad (9.4)$$

High harmonic components are present in a direct DC/DC converter. For a buck converter, in which the input current is discontinuous, a smoothing input filter may be required. While in a boost converter, the input current is continuous, however, the high voltage ripple is present at the input terminal.

The ac components of the converter currents must circulate through capacitors to prevent their appearing at the converter terminals. This requires that the high frequency impedance of the capacitor to be much smaller than the sum of the high frequency impedance of the external networks in parallel with the capacitor. Similarly, the switching voltage ripple has to be dropped in the inductor so as not to appear at the converter terminals. It is preferred that the high frequency impedance of the inductor is larger than the combination of the high frequency impedance of the external networks. The ideal external system conditions for a direct DC/DC converter are a high impedance at higher current ripple terminal and a low ac impedance at the higher voltage ripple terminal.

Thus for a buck converter it is preferable to have a high impedance network at the input terminal and a low impedance network at the input terminal is desirable for boost converters. The external system may not have such ideal characteristics, but the situation can be improved by using additional parallel capacitance or series inductance as appropriate.

9.2.1.2 Indirect DC/DC converter

The up/down (buck/boost) converter and the Cuk converter are shown in figure 9.2. Each provides a negative polarity output voltage with respect to the common terminal of the input. In these converters, the output voltage can be either higher or lower than the input voltage.

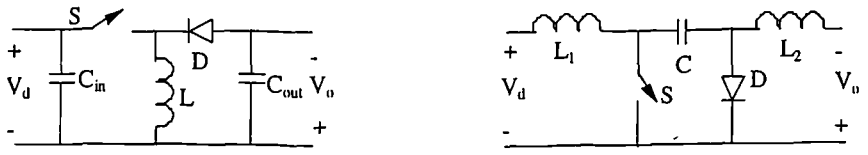

(a) buck and boost converter (b) Cuk converter

Figure 9.2 Indirect DC/DC converter

In a buck/boost converter, when the switch is on, the inductor is charged and the diode is reverse biased. When the switch is off, the energy stored in the inductor is transferred to the output through the diode. In the continuous conduction mode, the input and output average voltage and current are related by:

$$\frac{V_o}{V_d} = \frac{D}{1-D}$$
$$\frac{I_o}{I_d} = \frac{1-D}{D} \qquad (9.5)$$

In a Cuk converter, which named after its inventor, the capacitor acts as the primary means of storing and transferring energy from the input to the output. When the switch is off, the inductor currents i_{L1} and i_{L2} flow through the diode. C is charged through the diode by energy from the input and L_1. Energy stored in L_2 feeds the output. When the switch is on, V_c reverse biases the diode. The inductor currents i_{L1} and i_{L2} flow through the switch. C discharges through the switch, transferring energy to the output and L_2. The input feeds energy to L_1. In the continuous conduction mode, the terminal average voltage and current have the same relation as that of buck/boost converter. (Equation 9.5).

The semiconductors in the indirect converters suffer higher stresses (peak voltage and peak current) than that in the direct converters, which results in poor switch utilisation

ratio. Therefore, the direct type converter would be normally used unless either a negative output voltage or both up and down conversion ratios from the same converter is needed.

9.2.2 Control of the switching DC/DC converter

To keep the output voltage at a desired level, closed-loop feedback control is normally used. The output voltage is compared with a reference voltage and the error signal is used to drive the switch so that the output voltage can follow the predetermined reference voltage closely. Two types of control methods are commonly used.

constant frequency operation. the switching frequency is kept constant and the on/off periods are varied. This type of control is also know as Pulse-width modulation (PWM) control because the width of the pulse is varied.

variable frequency operation. in this scheme, the switching frequency is varied. The on time and/or off time are varied too. It is so called frequency modulation. The frequency has to be varied over a wide range to obtain the full output voltage range. This type of control would often generate harmonics at unpredictable frequencies and the filter design would be difficult.

The ripple from DC/DC converter switching depends inversely on the switching frequency. A high frequency can reduce the load ripple current and minimise the size of reactive components in the circuit. However a high frequency could result in high power losses, therefore the switching frequency is a compromise.

9.3 DC/DC Converter-VSI for Wind Energy Interface

As discussed previously, in order to meet the optimal operation requirements of both generator-rectifier and inverter-grid, it is preferred that the rectifier terminal dc voltage and inverter ac voltage follow quite different operational curves. This has been implemented by using a SPWM VSI in the last chapter, but the low switch utilisation ratio of SPWM VSI is discouraging from the economy view point.

In a DC/DC converter-VSI system, the DC/DC converter divides the dc link into two levels. At rectifier side, it provides optimal power transfer conditions for the generator and rectifier; At the inverter side, it provides a controllable DC voltage at the inverter DC terminal to realise the optimal real power transfer and the reactive power regulation. The working principle is similar to a tap-changing transformer, but this scheme is more flexible and gives a wider range of voltage regulation.

Either a step down or a step up DC/DC converter can meet the voltage regulation requirements. The DC/DC converter can keep the inverter dc terminal voltage at a nearly constant level so as to improve the SUR of the grid inverter. For a given generator-rectifier system, the step down converter requires that the grid inverter operates at a lower dc voltage and a higher current, while a step up converter allows the grid inverter to operate at a higher dc voltage with a lower ac current. The optimal choice can be made by taking into account of the design and operation of both generator-rectifier and grid inverter. In this chapter, a boost DC/DC converter is discussed.

9.3.1 Ratio control of DC/DC converter

A DC/AC power conversion system consisting of DC/DC converter and VSI is sketched in figure 9.3.

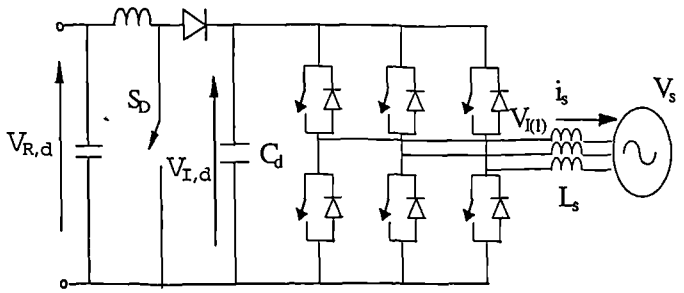

Figure 9.3 Schematic DC/DC converter-VSI

Assuming VSI operating with a fixed switching pattern, i.e. the ratio of VSI ac fundamental voltage to its dc voltage is constant, The ideal voltage ratio N_k of the

DC/DC converter can be calculated by the required inverter ac voltage ,$V_{d,Iideal}$ (figure 5.16), and the optimal rectifier dc terminal voltage, $V_{d,Rideal}$ (figure 5.12), as:

$$N_k = \frac{V_{d,I\,ideal}}{V_{d,Rideal}}$$

If the system is such designed that N_k is set at 1 at the rated condition. A typical N_k curve may take the form shown in figure 9.4. Consequently, the resultant boost converter switch ratio D under continuous operation mode is shown in figure 9.5.

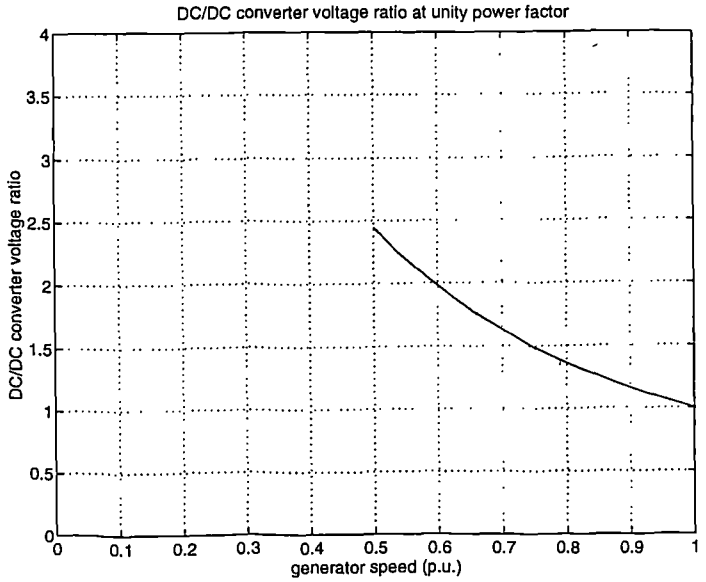

Figure 9.4 Step up DC/DC converter voltage ratio N_k

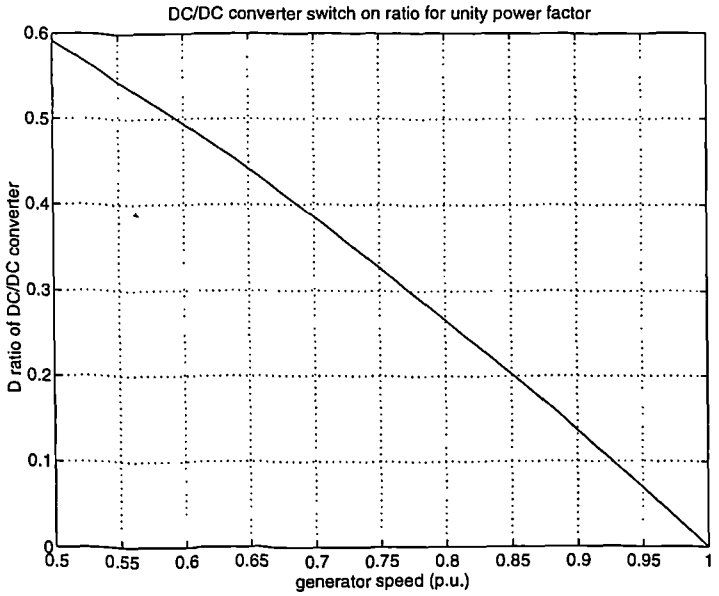

Figure 9.5 Step up DC/DC converter on time ratio D

To improve the performance characteristics such as regulation, transient response, etc., a feedback control loop could used to regulate the DC/DC converter for inverter dc terminal voltage control. The block diagram of a suitable controller is shown in figure 9.6. The generator speed is measured and the ideal inverter dc voltage is calculated from the speed and the power angle. The on/off ratio is controlled to produce the required inverter DC terminal voltage.

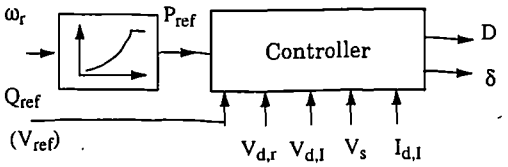

Figure 9.6 A block diagram of DC/DC converter-VSI control system

9.3.2 Switch utilisation ratio of DC/DC converter-VSI interface

The switch utilisation ratio of the VSI can be calculated for the operation strategy discussed above. The SUR curve of a 6-pulse square wave switching VSI is shown in figure 9.7. For harmonic elimination switching of the VSI, increasing the number of harmonics eliminated, causes the inverter ac fundamental voltage to be slightly reduced along with the SUR.

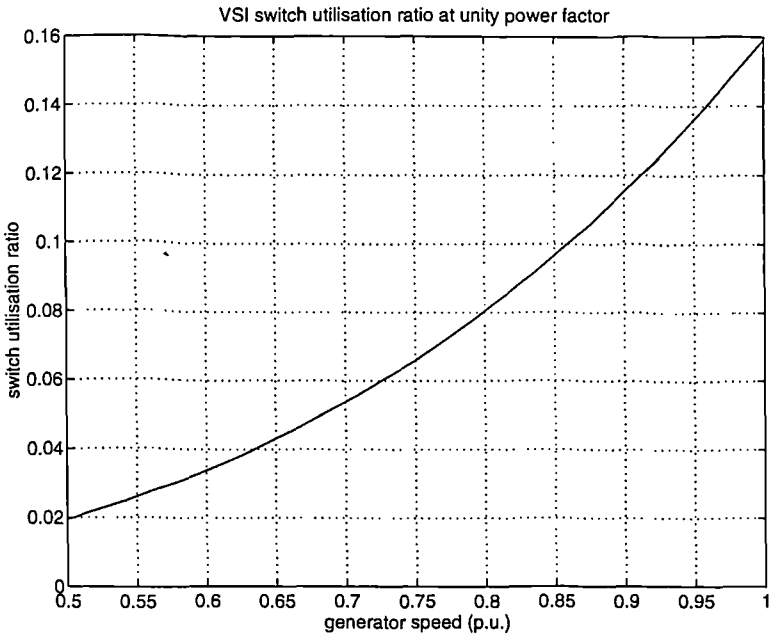

Figure 9.7 VSI switch utilisation ratio in DC/DC converter-VSI

The switch utilisation ratio of a step up DC/DC converter is at its highest for zero D and reduces with increasing conduction time [64] as sketched in figure 9.8.

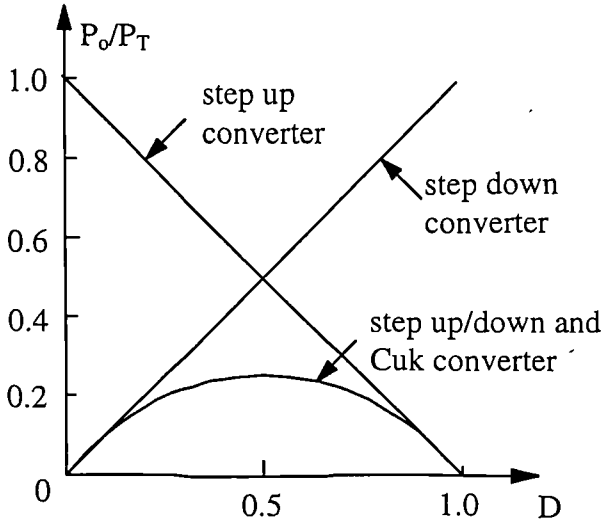

Figure 9.8 DC/DC converter switch utilisation ratio

9.4 Harmonic Minimisation of DC/DC Converter-VSI

9.4.1 Harmonic of DC/DC converter

The harmonics generated by the switching of the DC/DC converter should be prevented from interfering with the operation of the rectifier and the grid inverter. A dc capacitor could be placed at the rectifier terminal to keep a smooth dc link voltage for the rectifier. The dc capacitor at the inverter dc terminal should be able to absorb the current ripple from both the DC/DC converter and the inverter within the permitted voltage ripple limit.

9.4.2 Selective harmonic elimination switching

The DC/DC converter frees the VSI from the voltage regulation duty, therefore the more efficient harmonic minimisation method can be easily implemented for a VSI. The selective harmonic elimination (SHE) scheme has better harmonic performance than SPWM switching or can achieve equal harmonic performance at a lower switching frequency.

The switching angles for harmonic elimination switching strategies have been calculated by using the Newton-Raphson iteration method. Following the procedure described in section 7.2, the line to line voltage waveform can be synthesised and the harmonic spectra can be calculated. The results of eliminating 5th, 7th, 11th and 13th harmonics in a six pulse VSI are shown in figure 9.9 and figure 9.10. The TCHD characteristics against power angle and $V_{I(1)}/V_s$ ratio are presented in figure 9.11. The same conditions as that of figure 7.6 are used.

It can be seen that the selected harmonics are eliminated while the higher order harmonics are increased, but the total current harmonic distortion has been improved comparing with square wave switching.

The harmonic performance could further be improved if more harmonics are eliminated, however, this will result in more switching power losses.

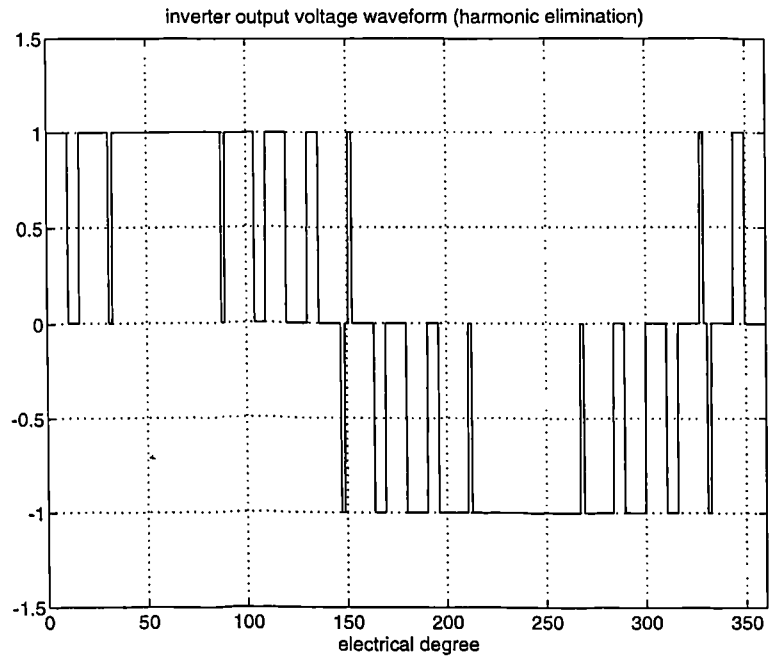

Figure 9.9 Voltage waveform of selective harmonic elimination
(5th, 7th,11th and 13th harmonics elimination)

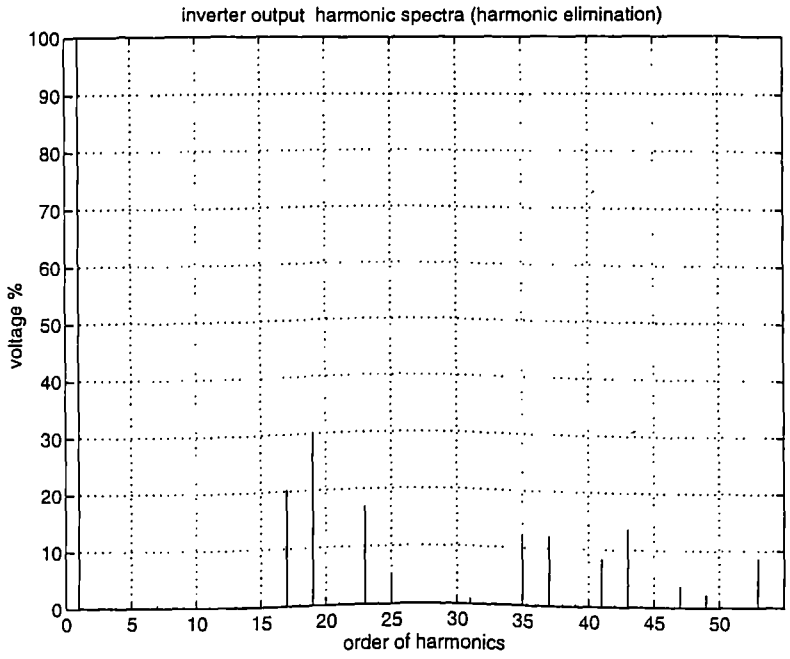

Figure 9.10 Voltage harmonic spectra of selective harmonic elimination (5th, 7th,11th and 13th harmonics elimination)

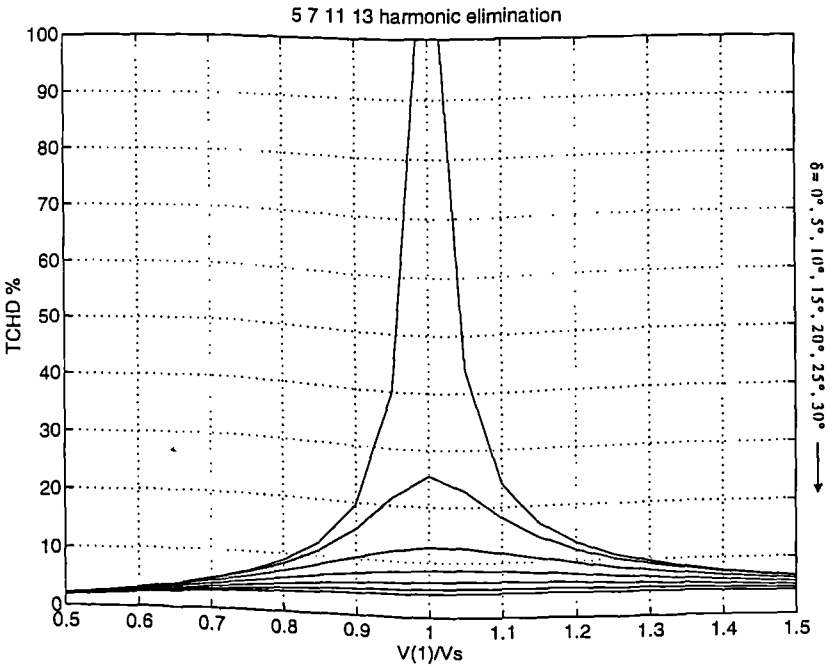

Figure 9.11 TCHD vs. power angle and $V_{I(1)}/V_s$ ratio (5th, 7th,11th and 13th harmonics elimination)

9.4.3 Harmonic elimination in multi-pulse inverter system

The multi-pulse inverter system is an effective way to minimise harmonics. The harmonics of 12-pulse and 24-pulse VSI have been presented in chapter 7. The total current harmonic distortions are shown in figure 9.12 and 9.13, which should be compared with figure 9.11.

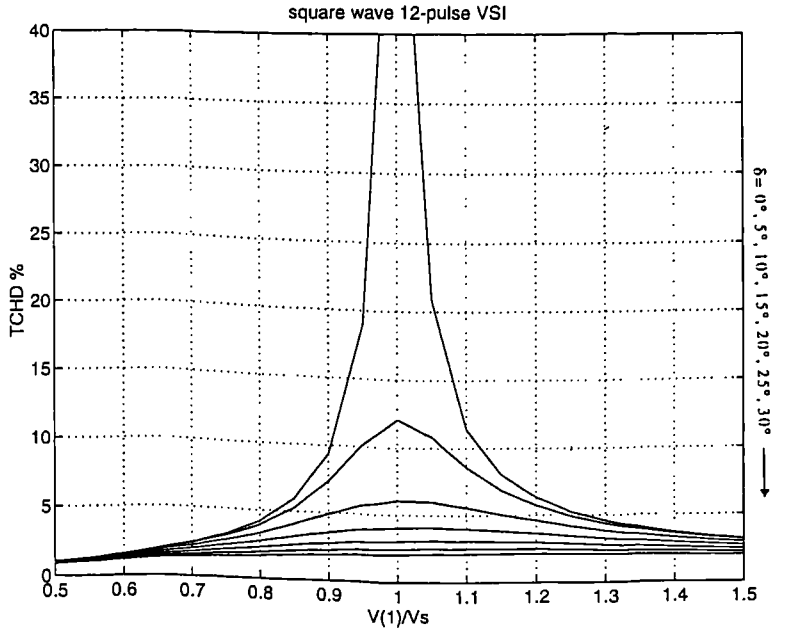

Figure 9.12 TCHD vs. power angle and $V_{I(1)}/V_s$ ratio (12-pulse inverter system)

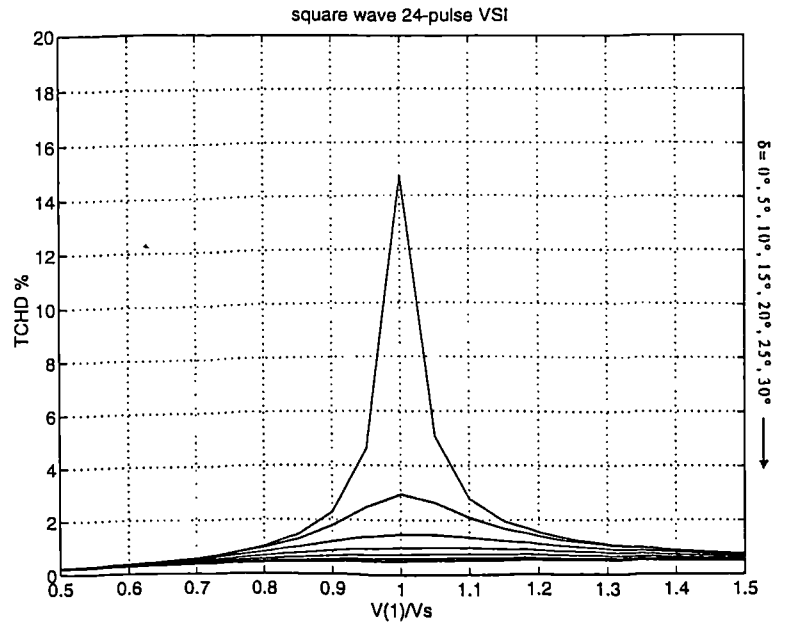

Figure 9.13 TCHD vs. power angle and $V_{I(1)}/V_s$ ratio (24-pulse inverter system)

In a n-pulse inverter system, only n×k±1 harmonics exist, their magnitudes are the same as for a six pulse system. However, in high frequency switching inverter, the harmonic magnitudes of the remaining harmonics are increased.

9.4.4 Selective Harmonic Elimination (SHE) switching in multiple inverter system

Combinations of multi-pulse connection and selective harmonic elimination switching techniques have also been investigated. The switching angles are calculated for eliminating 11th, 13th, 23rd and 25th harmonics in a 12-pulse system and for eliminating 23rd and 25th harmonics in a 24-pulse system. It is found that the combinations do not give the satisfactory harmonic performance and produce high TCHD. The reason is that harmonic elimination accentuates the harmonics of higher frequency, which the multi pulse arrangement is incapable of cancelling.

The voltage waveform of one combination (eliminating 11th &13th harmonics in a 12-pulse inverter system) is shown in figure 9.14. The corresponding voltage harmonic spectra and the total current harmonic distortion characteristics are presented in figure 9.15 and 9.16.

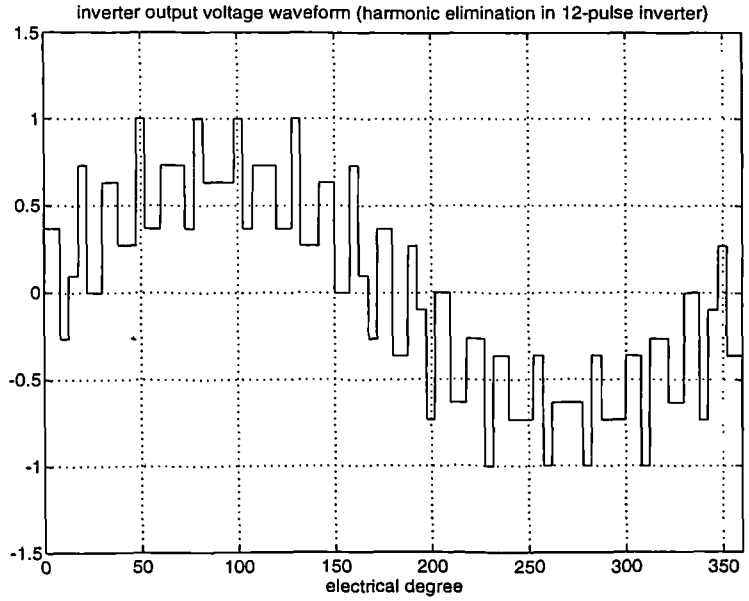

Figure 9.14 Voltage waveform (line-line) of SHE 12-pulse inverter system (eliminating 11th &13th harmonics)

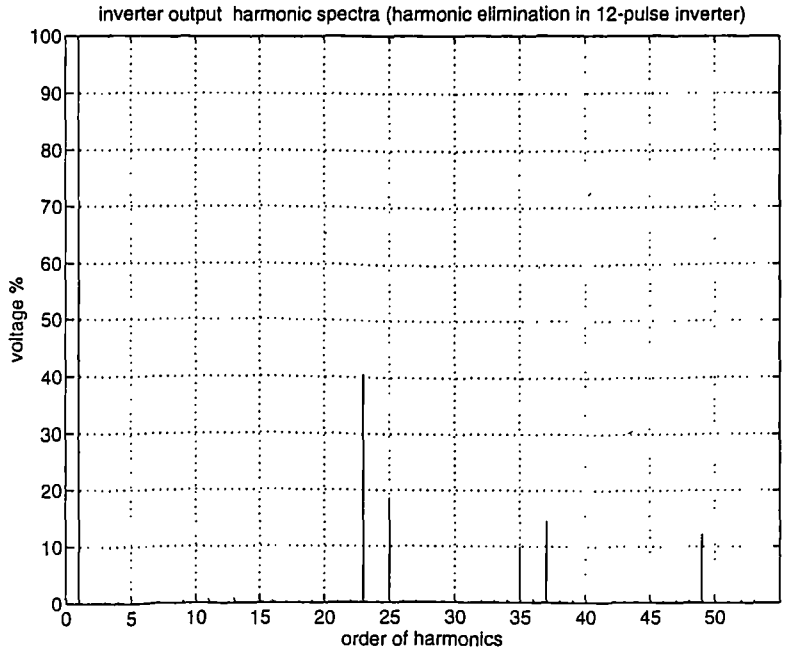

Figure 9.15 Voltage harmonic spectra of SHE 12-pulse inverter system (eliminating 11th &13th harmonics)

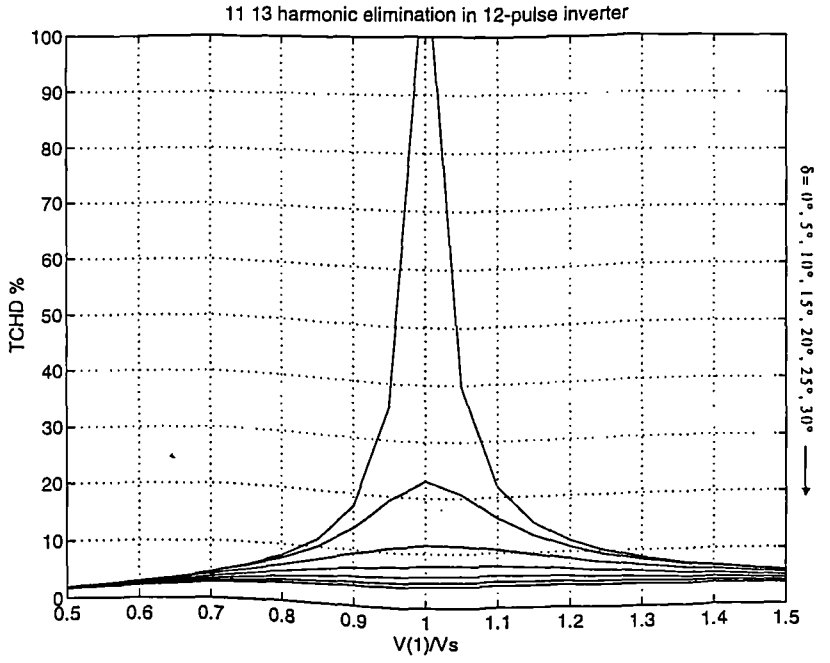

Figure 9.16 TCHD vs. power angle and $V_{I(1)}/V_s$ ratio in SHE 12-pulse inverter system (eliminating 11th &13th harmonics)

9.4.5 Comparison of harmonic reduction methods

A harmonic performance comparison of high frequency switching techniques and multiple pulse inverter systems is made in this section.

The worst harmonic performance condition, (zero power factor), was taken for the comparison. The conditions are: 0^{o} power angle, 1.2 pu inverter ac output voltage fundamental component and 1.0 pu the grid voltage. The considered cases are detailed in Table 9.1. The analysed results are given in Table 9.2 where the harmonic distortion was calculated by counting up to the 101st harmonic.

Table 9.1 Inverter harmonic reduction options

Identifier	Particulars
SS6	Square wave switching six pulse inverter system
SS12	Square wave switching twelve pulse inverter system
SS24	Square wave switching twenty-four pulse inverter system
SHE1	Selective harmonic elimination strategy to eliminate 5th, 7th, 11th, and 13th harmonics.
SHE2	Selective harmonic elimination strategy to eliminate 5th, 7th, 11th, 13th, 17th and 19th harmonics.
SHE3	Selective harmonic elimination strategy to eliminate 5th, 7th, 11th, 13th, 17th, 19th, 23rd and 25th harmonics.
SS12SHE4	Selective harmonic elimination strategy to eliminate 11th, and 13th harmonics in twelve pulse inverter system
SS12SHE5	Selective harmonic elimination strategy to eliminate 11th, 13th, 23rd and 25th harmonics in twelve pulse inverter system
SS24SHE6	Selective harmonic elimination strategy to eliminate 23rd and 25th harmonics in twenty-four pulse inverter system

The multiple-pulse inverter system can significantly reduce the total current harmonic distortion with the penalty of increased equipment investment cost. On the other hand, high frequency switching techniques could reduce the harmonic distortion in a certain

range without requiring more power equipment than six pulse inverter but the power losses tend to increase rapidly as higher harmonics are eliminated by using more device transitions per cycle.

Table 9.2 Comparison of harmonic reduction strategies

Identifier	TVHD %	TCHD % Xs=0.1 pu	TCHD % Xs=0.2 pu	Number of transitions /device/cycle	DC link voltage / inverter output voltage (line-line)
SS6	30.5540	51.0172	28.8276	2	1.2826
SS12	14.9485	11.6082	6.3318	2	1.2826
SS24	7.4343	2.8326	1.5451	2	1.2826
SHE1	51.1433	24.4681	13.3462	18	1.3952
SHE2	51.2213	18.8583	10.2864	26	1.4032
SHE3	50.6887	15.2903	8.3401	34	1.4070
SS12SHE4	54.0684	22.1368	12.0746	10	2.5818
SS12SHE5	46.1085	10.1078	5.5134	18	2.3530
SS24SHE6	16.4295	3.1006	1.6912	10	1.7153

9.5 Time Domain Simulation Study of DC/DC Converter-VSI Interface

9.5.1 Simulation model

The main elements of the simulation system are shown in figure 9.17.

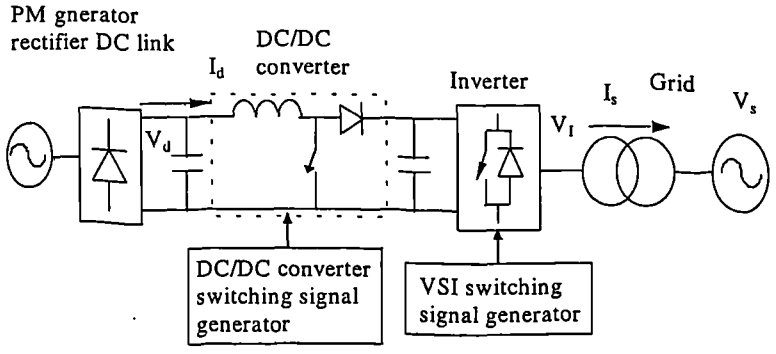

Figure 9.17 Simulation system (DC/DC converter-VSI)

DC/DC converter: The DC/DC converter consists of reactive components, diode and a semiconductor, the simulation model is shown in figure 9.17. The switching semiconductor is simulated by the switch function in PSPICE and the control signal for the DC/DC converter is generated by a controllable pulse type voltage source.

SHE PWM signal generator: The SHE switching signal generator generates the selective harmonic elimination switching signal according the switching angles calculated by using the Newton-Raphson method programmed in FORTRAN.

Multi-pulse VSI switching signal generator: The multi-pulse VSI switching signal generator is based on a controllable pulse type voltage source and can produce the switching signals to be used for switching the VSI to synthesise a multi-pulse voltage waveform therefore the multi-winding transformer is omitted.

The simulation models of the generator-rectifier-dc link system, AC grid system and inverter system are as described in chapter 8.

9.5.2 Simulation results

The simulation results of a typical operation condition (P=0.5 pu, δ=5.7°, D=0.28, $V_{d,R}$=0.71 pu) are presented in this section.

The simulated DC/DC converter waveforms are shown in figure 9.18. The waveforms proceed downward in the following sequence:

1. rectifier dc terminal voltage
2. inverter dc terminal voltage
3. inductor current
4. DC/DC converter switching signal

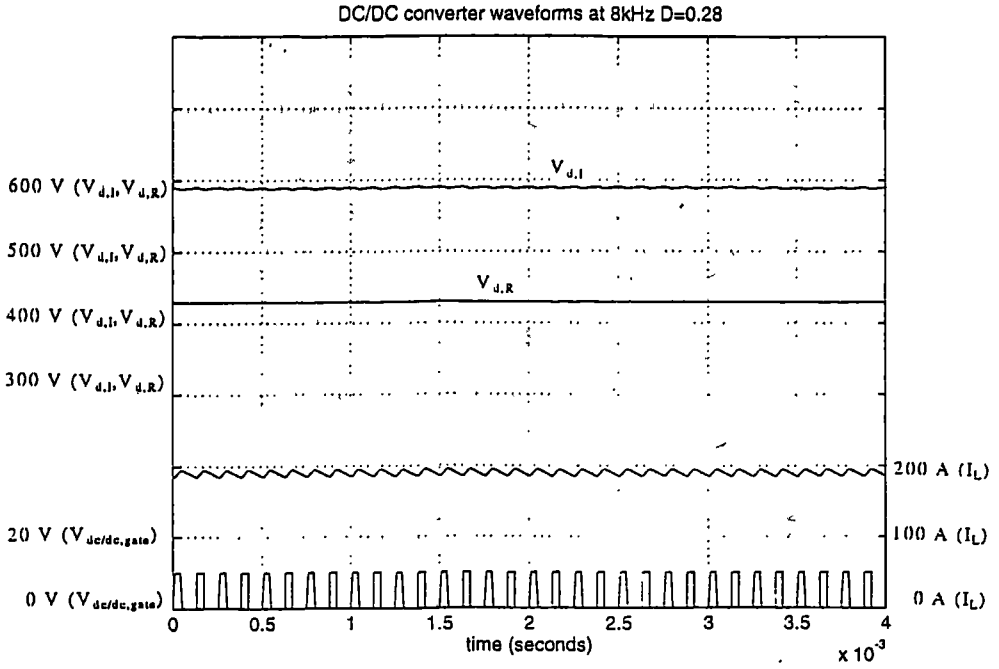

Figure 9.18 DC/DC converter waveforms (simulation)

The waveforms of the VSI and the grid are shown in figure 9.19 and 9.20. The waveforms proceed downward in the following sequence: 1 inverter ac terminal line to line voltage, 2 ac grid line to line voltage, 3 ac grid phase to neutral voltage, 4 ac current.

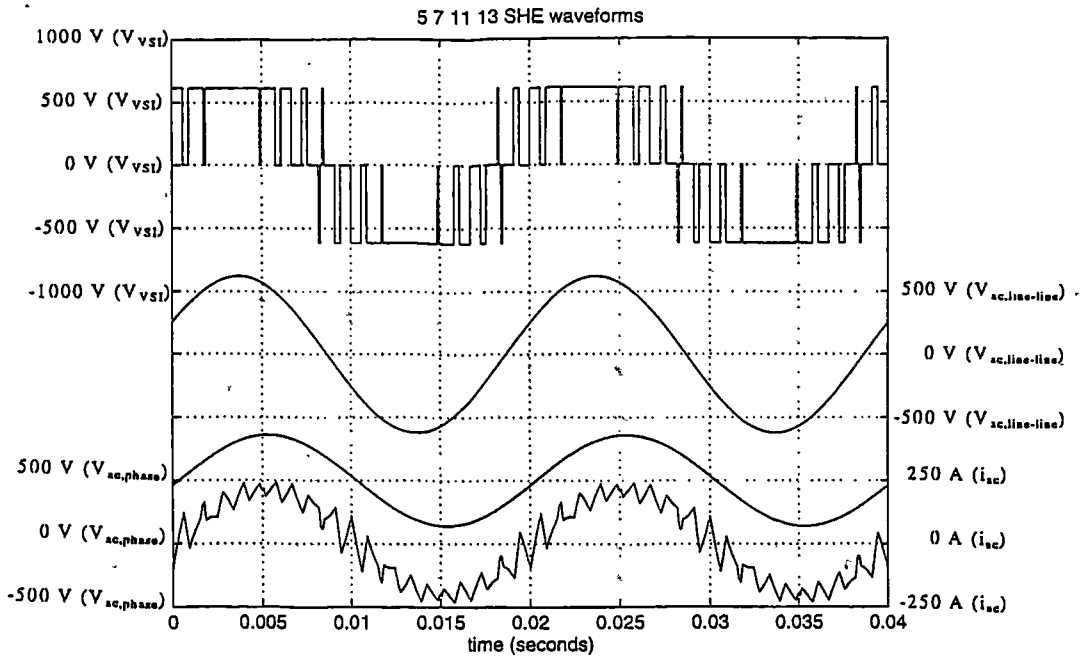

(a) 5,7,11,13 harmonic elimination

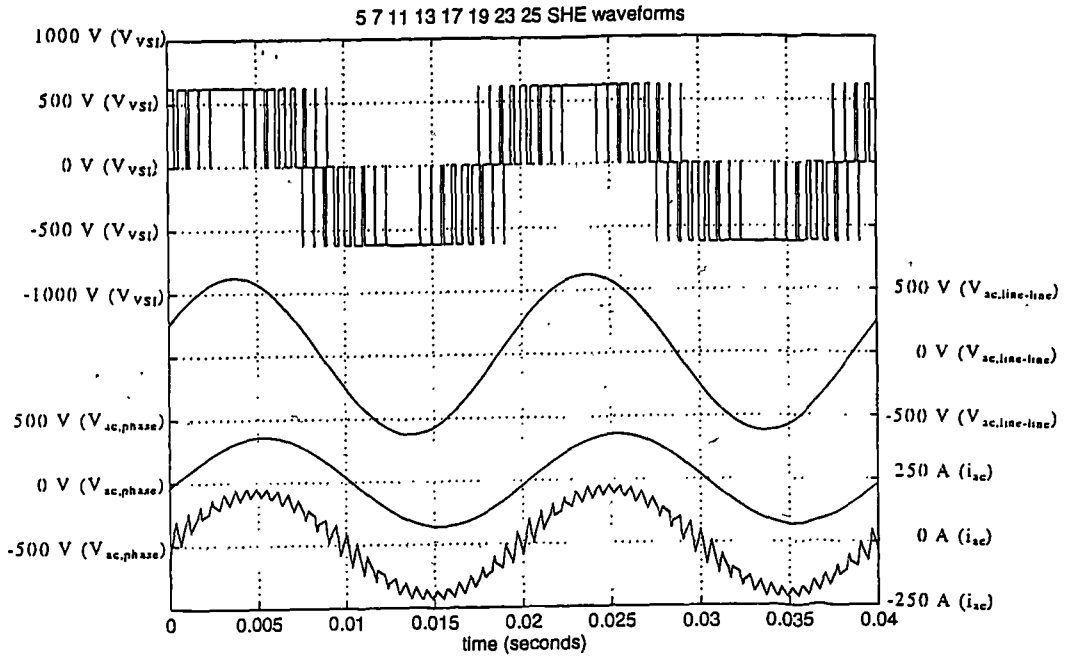

(b) 5,7,11,13,17,19,23,25 harmonic elimination

Figure 9.19 Waveforms of SHE-PWM VSI (simulation, D=0.28, δ=5.7°)

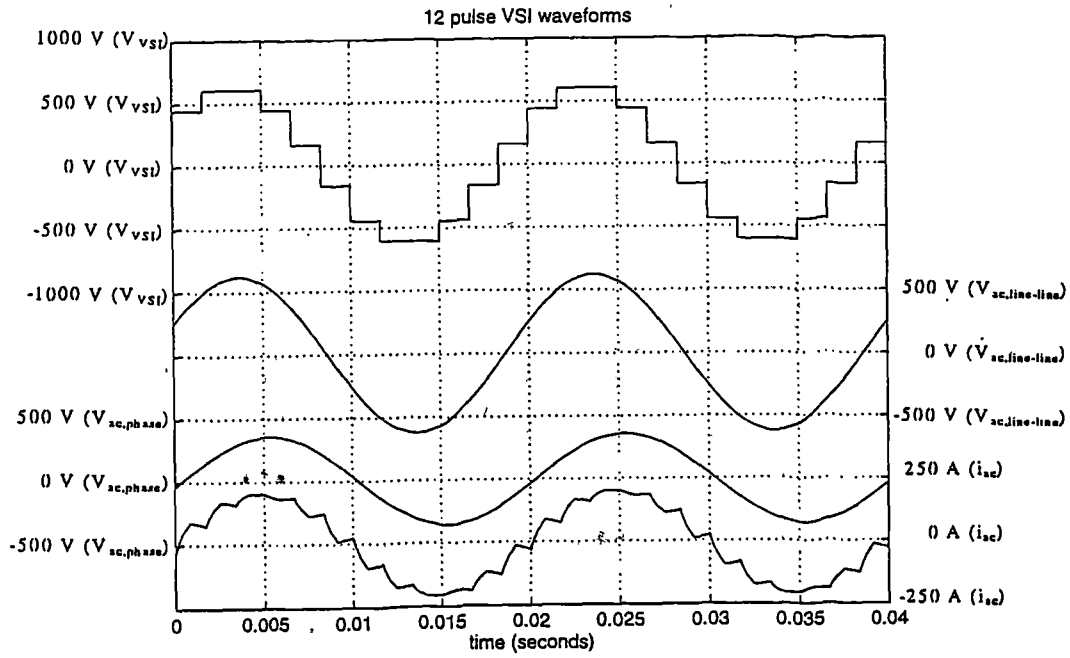

(a) 12 pulse inverter

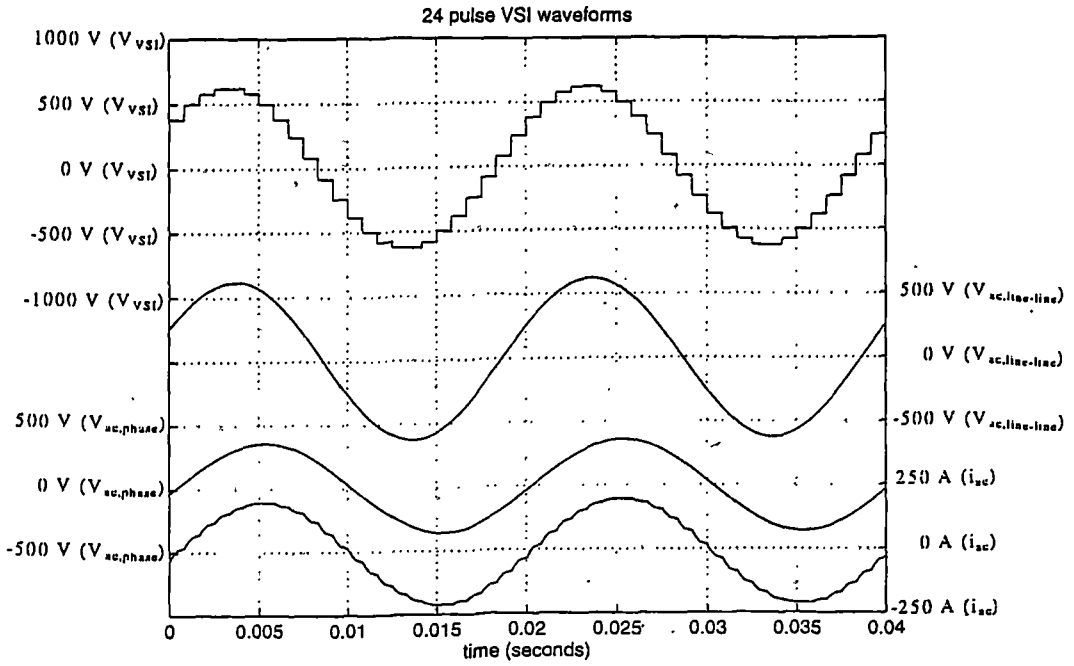

(b) 24 pulse inverter

Figure 9.20 Waveforms of multi pulse VSI (simulation, D=0.28, δ=5.7°)

The ac voltage harmonic spectra of the inverter are shown in figure 9.21 and figure 9.22. The harmonic spectra are presented as a percentage of grid voltage.

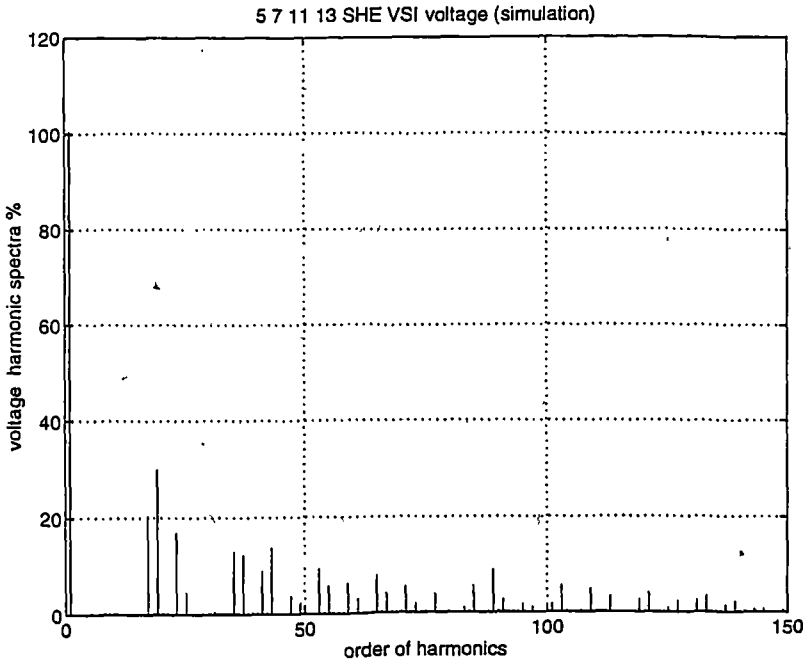

(a) 5,7,11,13 harmonic elimination

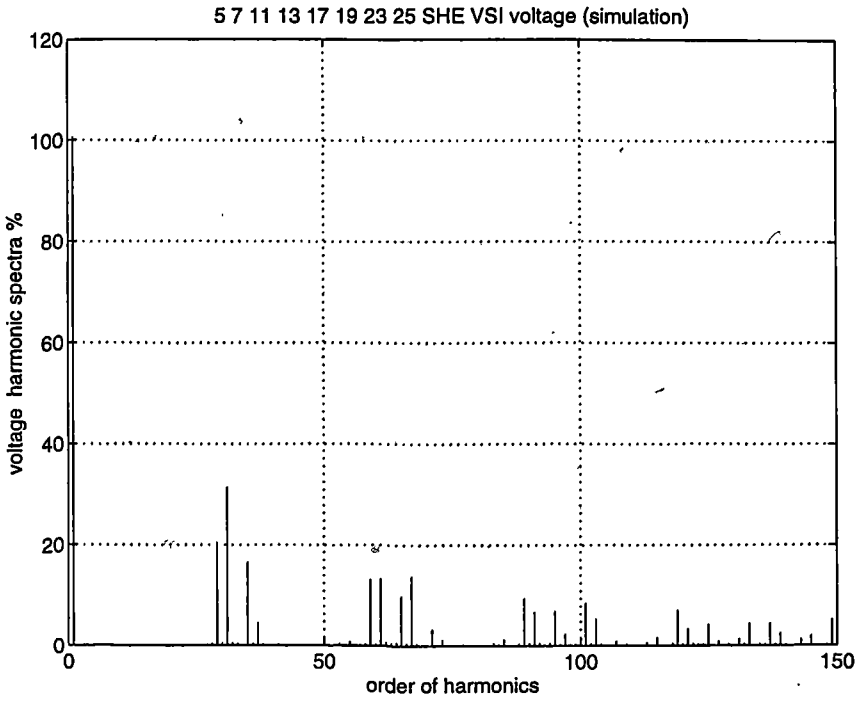

(b) 5,7,11,13,17,19,23,25 harmonic elimination

Figure 9.21 Voltage harmonic spectra of SHE-PWM VSI (simulation, D=0.28, δ=5.7°)

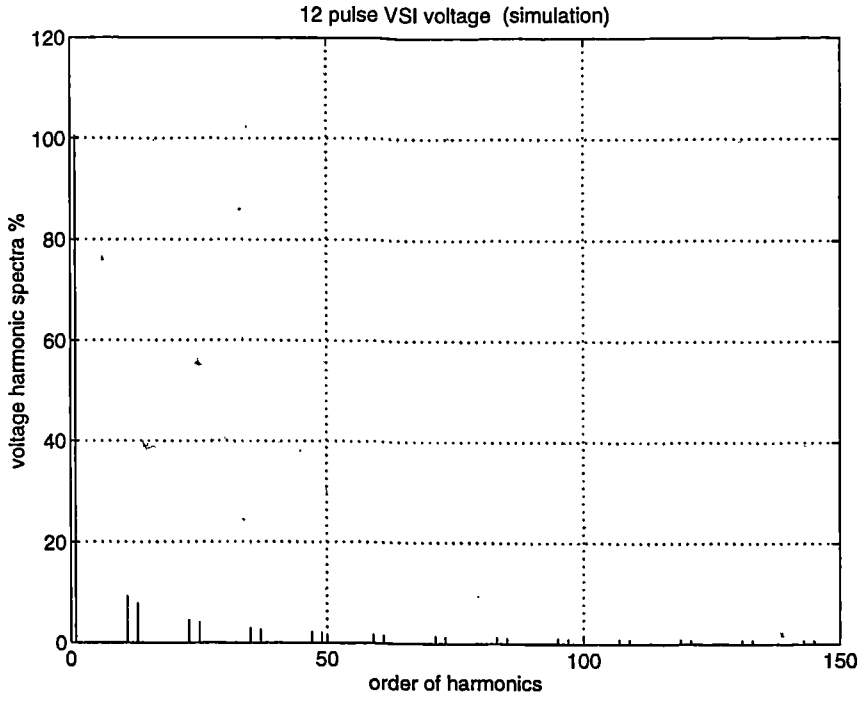

(a) 12 pulse inverter

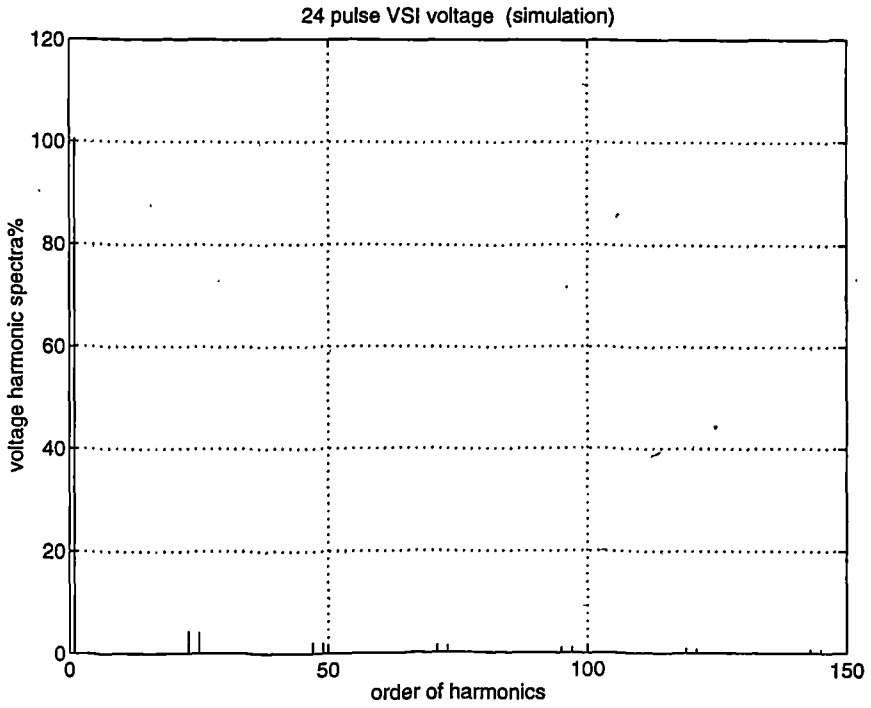

(b) 24 pulse inverter

Figure 9.22 Voltage harmonic spectra of multi pulse VSI (simulation, D=0.28, δ=5.7°)

9.6 Experimental Studies of DC/DC Converter-VSI System

9.6.1 Experimental model

A laboratory model DC/DC converter-VSI system has been designed and built for experimental investigation.

IGBT (IXSH40N60 600V/75A) is used as the controllable semiconductor of the DC/DC converter, the block diagram of the control circuit for the DC/DC converter is shown in figure 9.23. The switching frequency is 8 kHz.

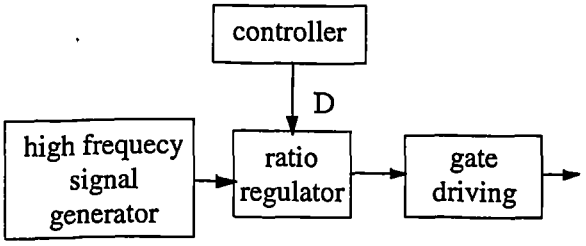

Figure 9.23 Block diagram of control circuit of DC/DC converter

The inverter system includes four 6 pulse IGBT VSIs. A multi-winding transformer provides four windings on the inverter side allowing the circuit configuration to be arranged for different case studies. i.e. 6-pulse, 12-pulse and 24-pulse.

Figure 9.24 shows the arrangement of the 12-pulse inverter where two six-pulse inverters are parallel connected to the DC link, the outputs of the two inverters are separated in phase by 30 electrical degree (360°/12) and are connected to Δ and Y inverter side windings of the grid coupling transformer.

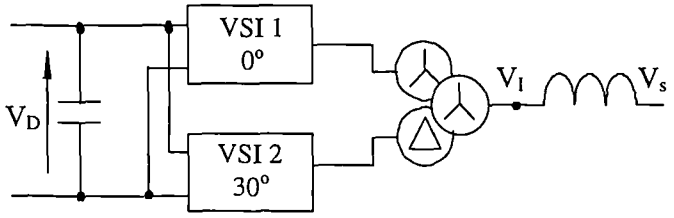

Figure 9.24 Schematic 12-pulse inverter system

The arrangement of the 24-pulse inverter is shown in figure 9.25, The four 6-pulse inverters can be parallel connected to the DC link, their outputs are phase-shifted by intervals of $360^0/24$ that is 0^0, 15^0, 30^0 and 45^0 respectively and connected to the transformer which in turn advance these voltages by 0^0, 15^0, 30^0 and 45^0 respectively to synthesise a 24-step voltage waveform.

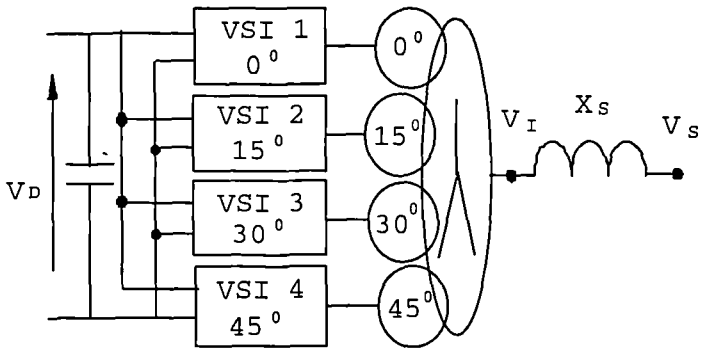

Figure 9.25 Schematic 24-pulse inverter system

The switching signal pattern generator is implemented with EPROM and can be used to generate the required switching signal (multi-pulse or selective harmonic elimination).

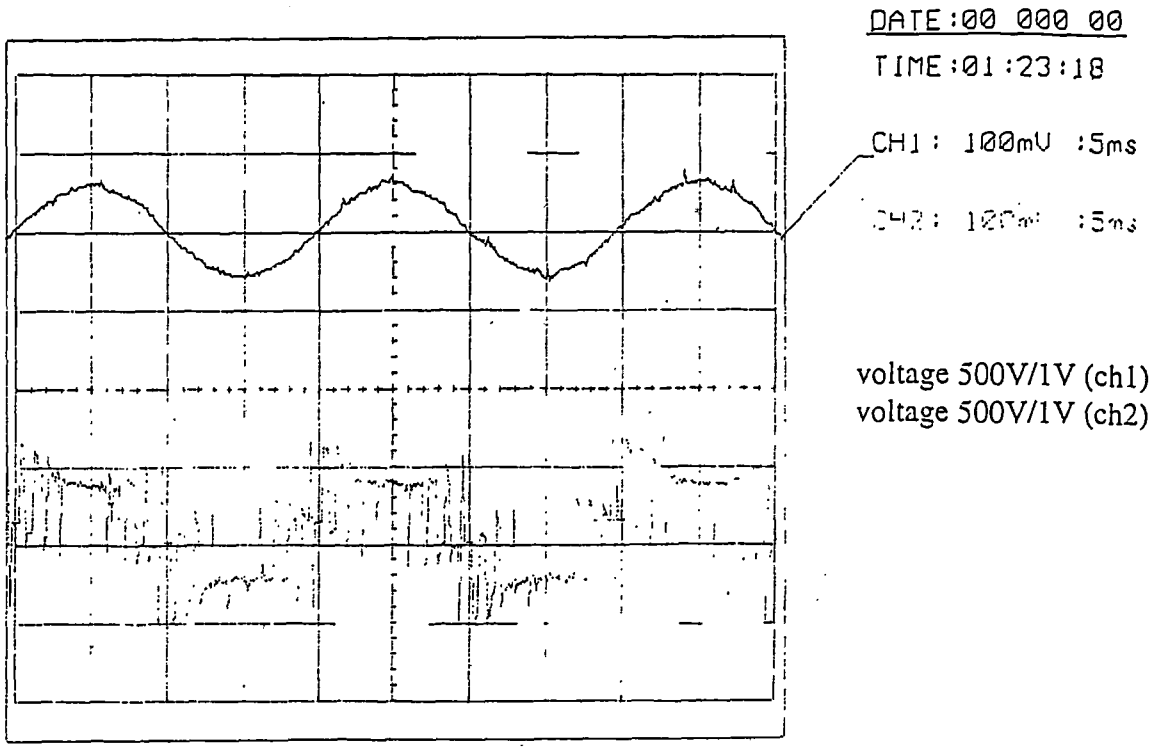

(a) grid voltage and inverter output voltage (line to line)

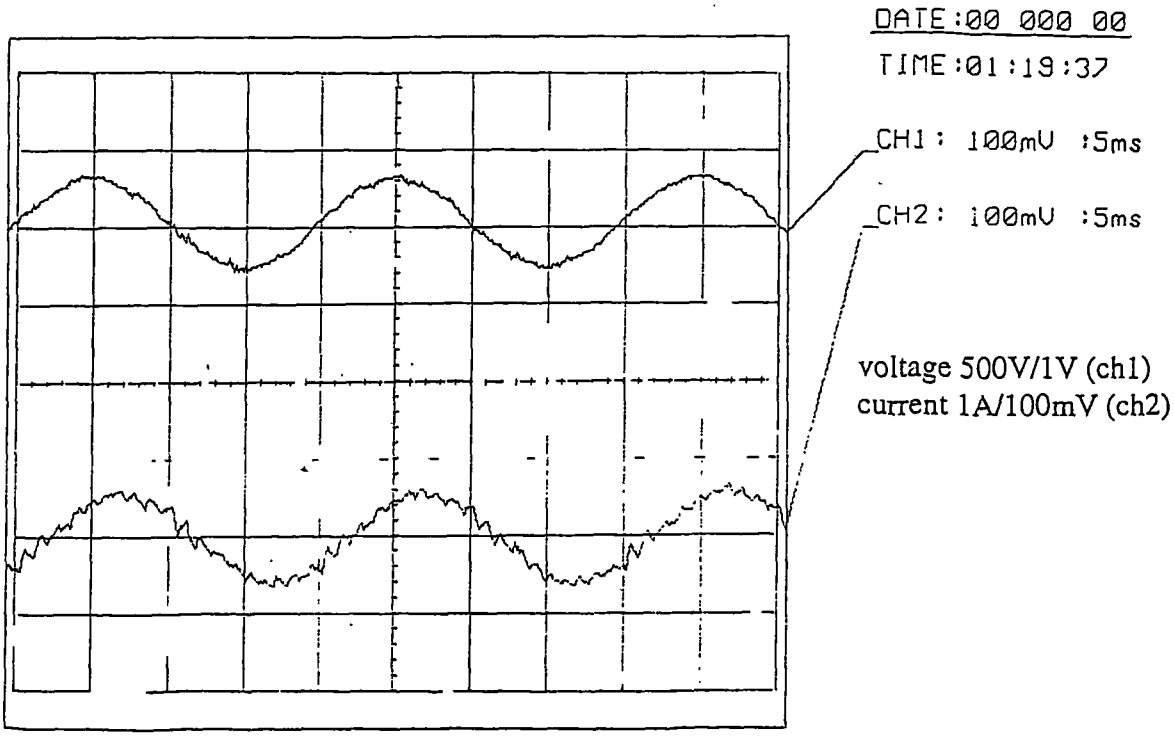

(b) grid voltage (line to line) and inverter output current

Figure 9.27 System waveforms of SHE PWM-VSI (experimental, 5,7,11,13. harmonic elimination, δ=5.7°)

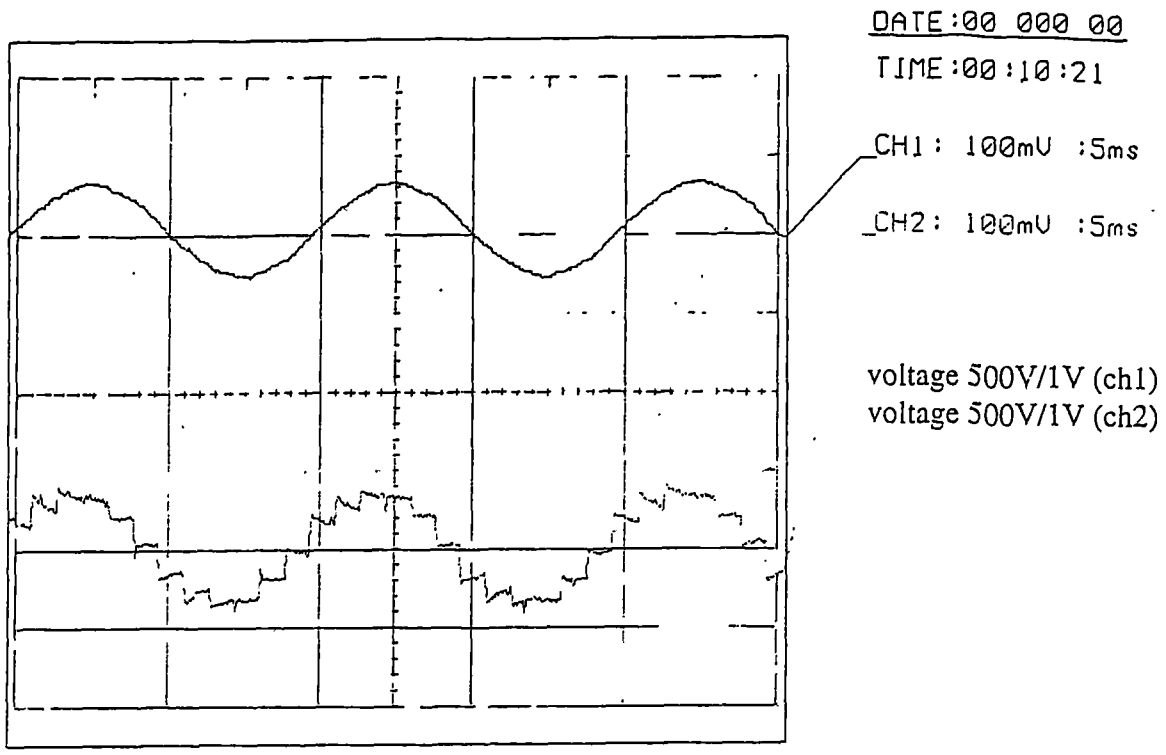

(a) grid voltage and inverter output voltage (line to line)

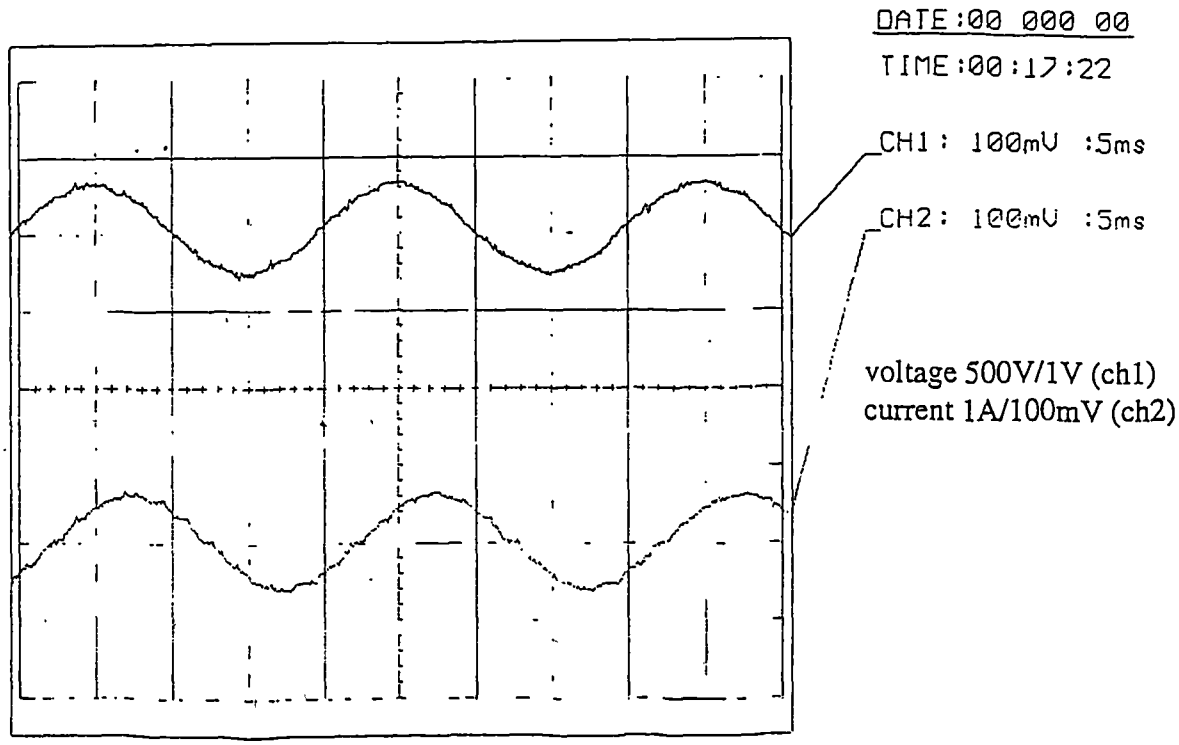

(b) grid voltage (line to line) and inverter output current

Figure 9.28 System waveforms of 12-pulse VSI (experimental, δ=5.7°)

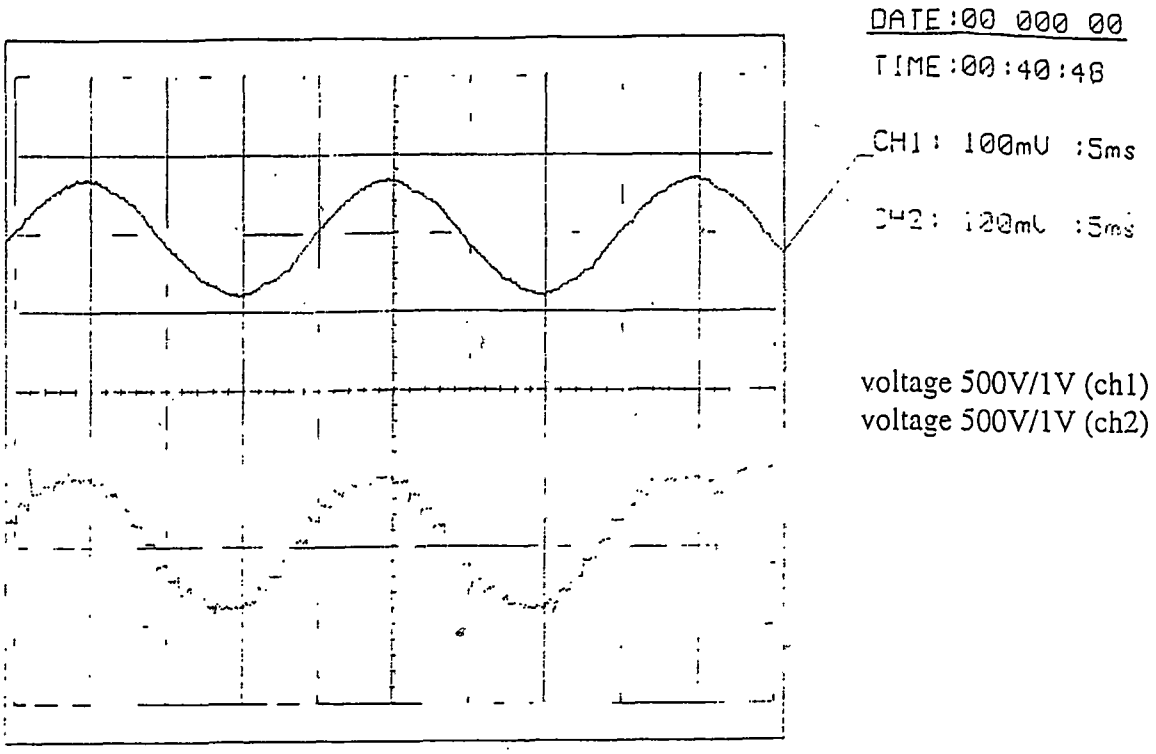

(a) grid voltage and inverter output voltage (line to line)

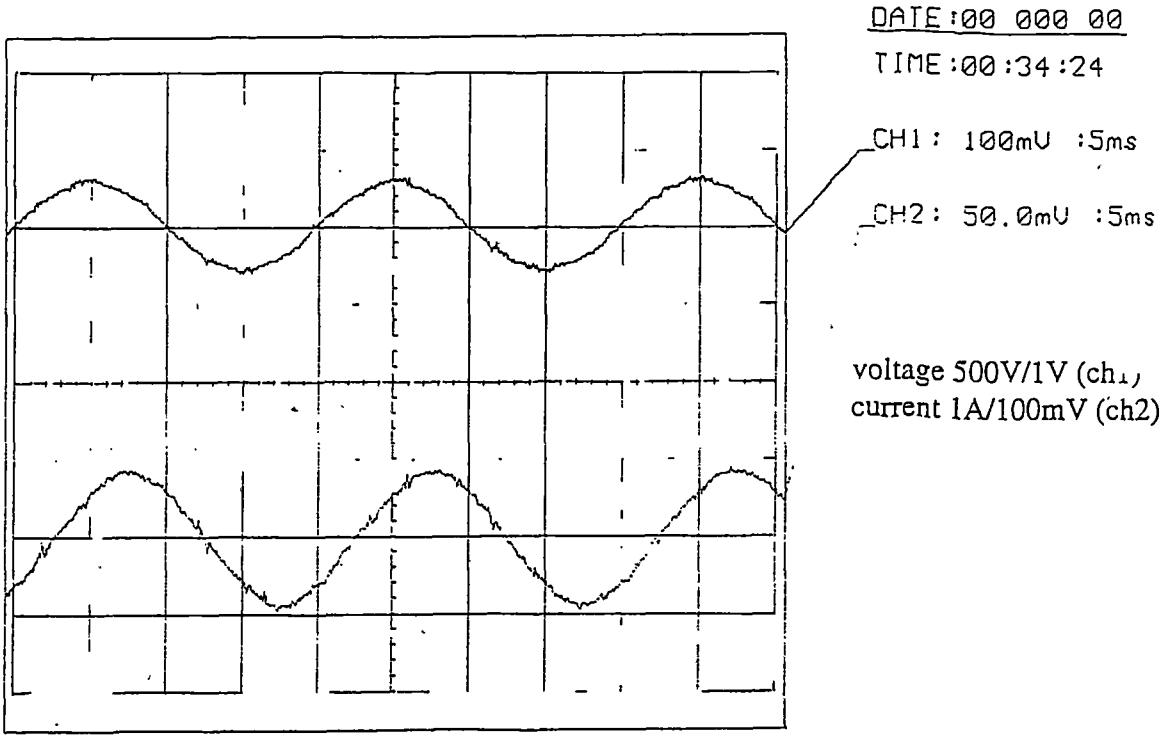

(b) grid voltage (line to line) and inverter output current

Figure 9.29 System waveforms of 24-pulse VSI (experimental, δ=5.7°)

The harmonic spectra of the inverter ac voltage are shown in figure 9.30. The harmonic spectra are presented as a percentage of grid voltage.

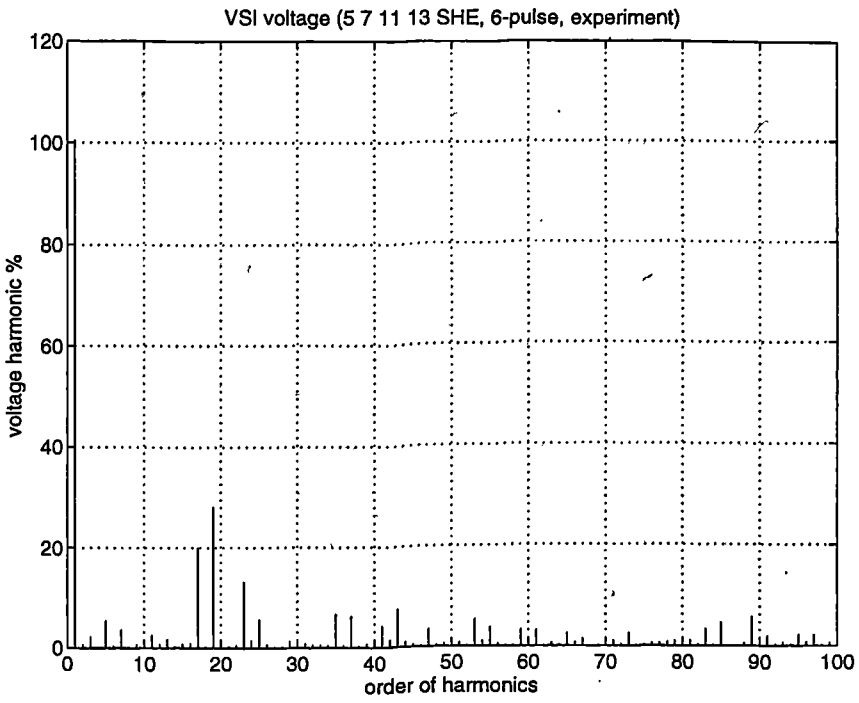

(a) 5,7,11,13 harmonic elimination

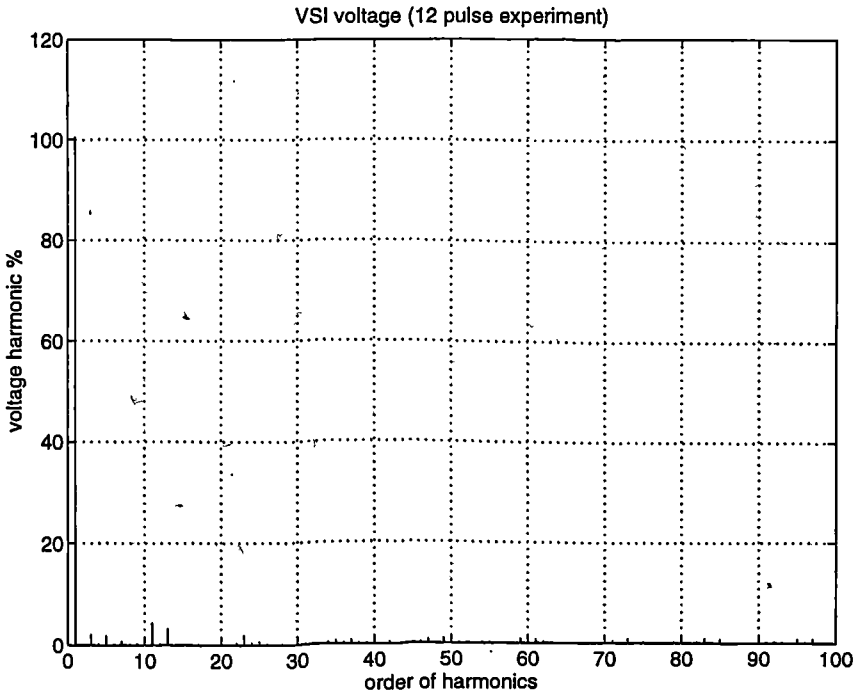

(b) 12 pulse inverter

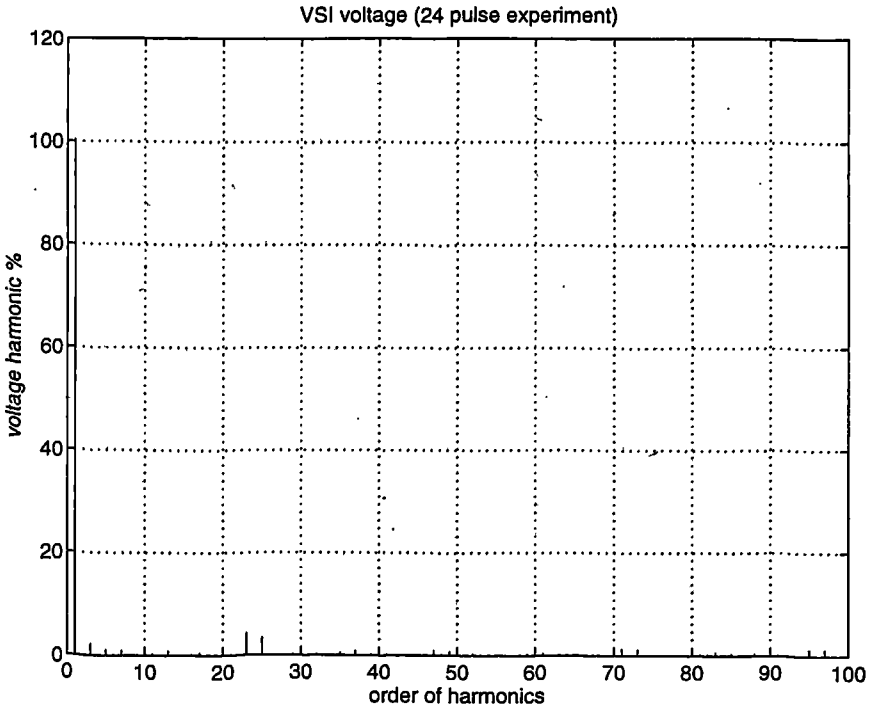

(c) 24 pulse inverter

Figure 9.30 VSI voltage harmonic spectra (experimental and δ=5.7°)

From these figures, it can be clearly seen that the harmonic distortion is significantly reduced in a 24-pulse inverter system and harmonic filters may not be needed. It can also be seen that the harmonic spectra are in good agreement with the results from analysis and PSPICE simulation.

9.7 Discussion

The multiple pulse inverter connection is more effective in reducing harmonic distortion than high frequency switching techniques. The disadvantage is that more facilities may be required. However, the equipment cost increase may not be significant in a wind farm, if multiple inverters are needed for several wind generators, and the investment may not be significantly higher than for high frequency techniques. In the 24-pulse case, the external filter may not required since the TCHD could be lower than the normal requirement (5%).

9.8 Conclusion

In this chapter, the DC/DC converter-VSI power conversion system has been discussed. This system enables both power angle and magnitude of inverter ac voltage fundamental component to be controlled for optimal power transfer and reactive power regulation. This system can work well in both strong and weak ac systems.

The magnitude of the inverter ac voltage fundamental component is controlled by high frequency switching dc/dc converter which gives a higher VSI switch utilisation factor than SPWM method. The system and the control strategies have been discussed.

Freeing the VSI from voltage control duty, allows more efficient harmonic minimisation methods to be used. The typical harmonic minimisation techniques, selective harmonic elimination and multi-pulse inverter techniques are discussed.

Simulation and laboratory experimental models have been developed. The simulation and experimental results are in good agreement, showing that the proposed system has the expected performance.

Chapter

10. Active Compensated Line Commutated SCR CSI

10.1 Introduction

For the last 30 years, line commutated SCR converters have been used in high voltage direct current (HVDC) transmission. The SCRs have higher power capacity than the newly developed semiconductor devices. The SCR converters are a mature technology and are proved to be reliable and economical, though their reactive power and harmonic current requires a compensation system to meet grid connection requirements. Therefore such converters may be a strong candidate for the addressed application if the reactive power and harmonic problem can be treated properly.

Due to the variable nature of the wind and the often electrically weak location for wind farms, it is expected that reactive power and harmonic current will vary over a greater range than in a typical HVDC system. Consequently a more flexible compensation system may be required. In this chapter, a VSI based active compensator and line commutated SCR-CSI system is examined. The reactive power control and harmonic minimisation are addressed under optimal power capture operation of a variable speed wind energy conversion system.

10.2 System Design

10.2.1 System configuration

The main elements of the SCR-CSI with VSI-based active compensation system with current reference direction studied in this chapter are presented in figure 10.1. The main

inverter is a line commutated SCR-CSI. Its function is to transfer the real power from the PM generator-rectifier system to the grid. The three-phase SCR bridge is switched in a six-step sequence and the ignition angle can be adjusted with respect to the grid voltage to vary the dc link voltage and so regulate the power transfer. The optimal real power transfer can be realised by ignition angle control as discussed in chapter 6. The function of the VSI based active compensator is to eliminate harmonic pollution and to provide reactive power compensation.

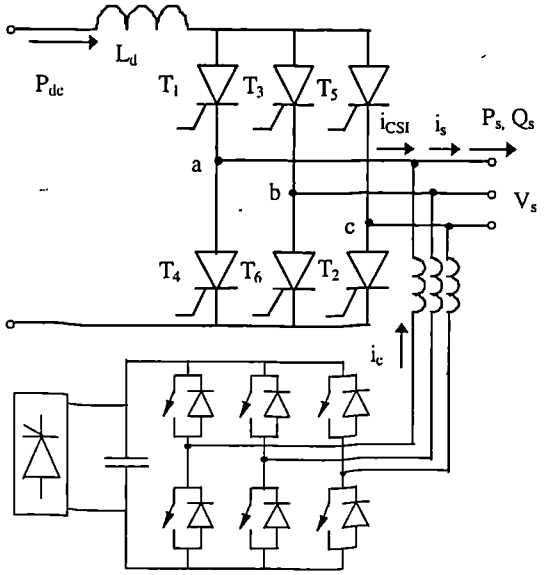

Figure 10.1 Schematic of SCR-CSI and VSI based active compensation system

10.2.2 VSI based active compensators

Power electronic converters can be controlled to fabricate a desired waveform at the connection point to function as active compensators. Normally, the converter is connected in parallel to the harmonic source to correct a current waveform.

In order to compensate the distorted current (i_{CSI}) generated by the line commutated SCR inverter, the parallel-connected active compensator is required to generate a compensation current (i_c) which can be added to the SCR inverter ac current to produce a sinusoidal waveform (i_s) at a desired power factor.

$i_{c.ref}$, the desired compensation current should be equal to the difference between the ideal system current $i_{s.ref}$ and the inverter ac current i_{CSI}. The relation is shown in figure 10.2.

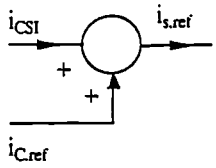

Figure 10.2. Reference current relation

Taking $i_{s,ref}$ as an ideal sinusoidal waveform and i_{CSI} as a typical six pulse waveform, the required active compensator current, $i_{s,ref}$ takes the form shown in figure 10.3. The sequence of waveforms are i_{CSI}, $i_{s,ref}$ and $i_{c,ref}$ proceeding downward.

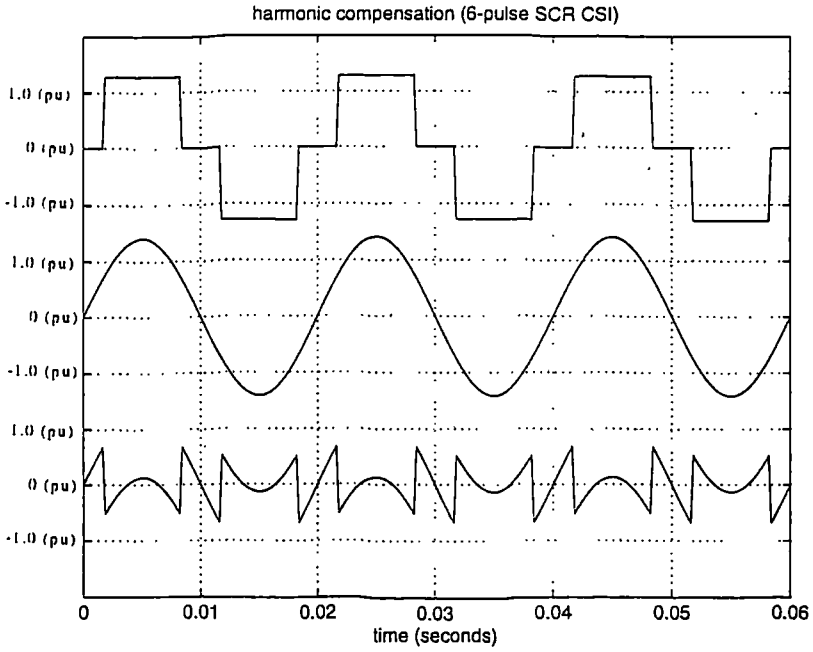

Figure 10.3 Active compensated 6-pulse SCR CSI waveform (harmonic compensation)

In order to generate the desired compensation current, the VSI compensator should be operated in closed-loop current control mode which offers good dynamic performance. Suitable current controllers for the VSI can be divided into three basic types [14]: Hysteresis, ramp comparison and predictive controllers whose block diagrams are shown in figure 10.4, where the desired current and actual current are compared and the error between these two is used to control the compensator.

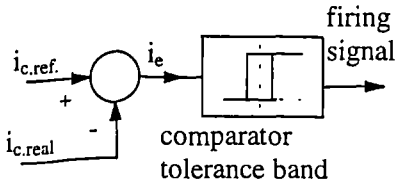

(a) Hysteresis controller

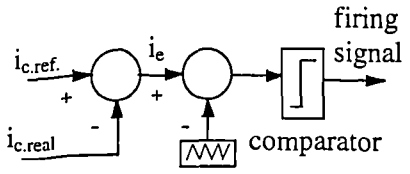

(b) Ramp comparison controller

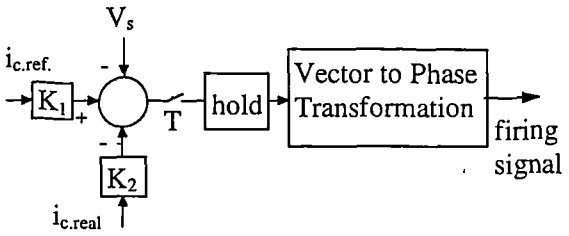

(c) Predictive controller

Figure 10.4 VSI current controllers

Hysteresis controllers utilise some type of hysteresis in the comparison of the real currents to the current references. The control for one inverter leg is shown in figure 10.4 (a). When the line current becomes greater (less) than the current reference by the hysteresis band, the inverter leg is switched to the negative (positive) dc direction to drive the current back into the hand. The hysteresis band specifies the maximum current ripple, the inverter switching frequency varies over a fundamental inverter period.

The ramp comparison controller compares the current error to a triangle waveform to generate the inverter firing signals as shown in figure 10.4 (b). The switching signal is generated in a similar way to SPWM but the current error is used to replace the sinusoidal reference waveform. With this type of control, the inverter is switched at the frequency of the triangle wave and its output current contains well defined harmonics.

The block diagram of a predictive controller is shown in figure 10.4 (c). This controller calculates the inverter voltage vector required to force the current to follow the current reference once every sample period. The switching frequency of the controller is well defined, however more system information and more complex calculations are required. The calculation may delay the system response.

Due to the complexity of the predictive controller and the switching frequency variation of hysteresis controller, the ramp comparison controller was chosen for simulation and experimental study.

In order to drive the output current to follow a specified waveform, an appropriate VSI input dc voltage is required, which may be provided by a controllable rectifier fed from the ac power supply. There is no real power flow associated with the compensation of harmonic currents or with the generation of reactive power into the grid. The controllable rectifier would only be rated to make up losses in the VSI.

10.2.3 Compensation schemes

The active compensation system can operate in different modes by choosing the system reference current waveform or using other compensation facilities, e.g. static capacitors, together with the active compensator.

Harmonic elimination: the system reference current ($i_{s.ref}$) is chosen as a sinusoidal waveform in phase with the fundamental component of thyristor inverter ac current. The waveforms of this scheme have been shown in figure 10.3. The compensator is required to provide only the harmonic components, therefore a small VSI rating is sufficient.

Harmonic elimination and reactive power compensation: In this scheme, the system reference current is a phase shifted sinusoidal waveform with respect to the fundamental component of the SCR inverter ac current as shown in figure 10.5. Consequently, this scheme requires a higher compensator rating which depends on not only the magnitude

of the SCR inverter current but also the correcting angle which is defined as the phase angle between the ideal system reference current, $i_{s.ref}$, and the SCR inverter ac current fundamental component $i_{CSI(1)}$.

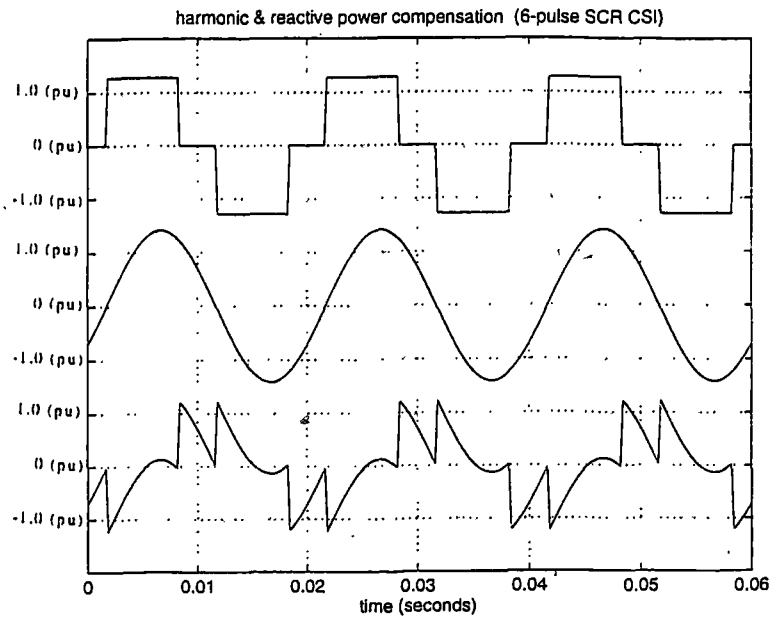

waveform sequence(downward): 1 i_{CSI}; 2 $i_{s.ref}$; 3 $i_{c.ref}$

Figure 10.5 Active compensated 6-pulse SCR CSI waveform (Harmonic and reactive power compensation)

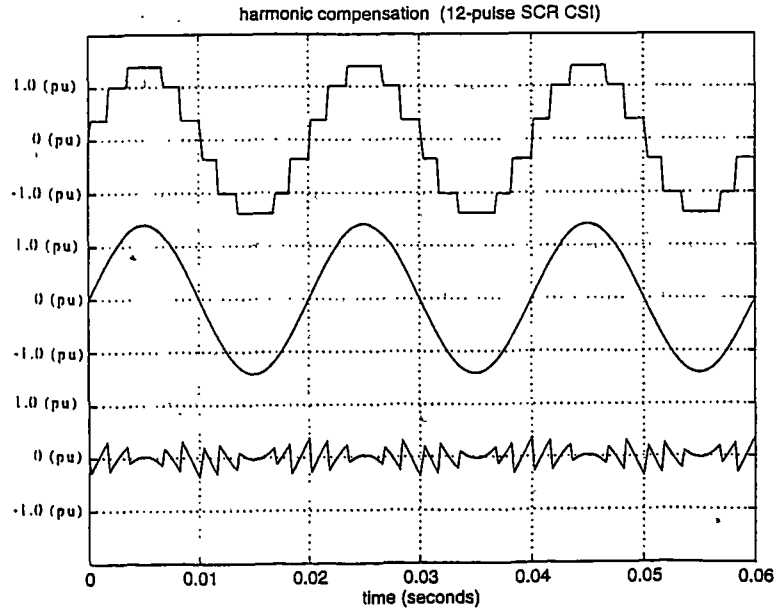

(a) Harmonic compensation

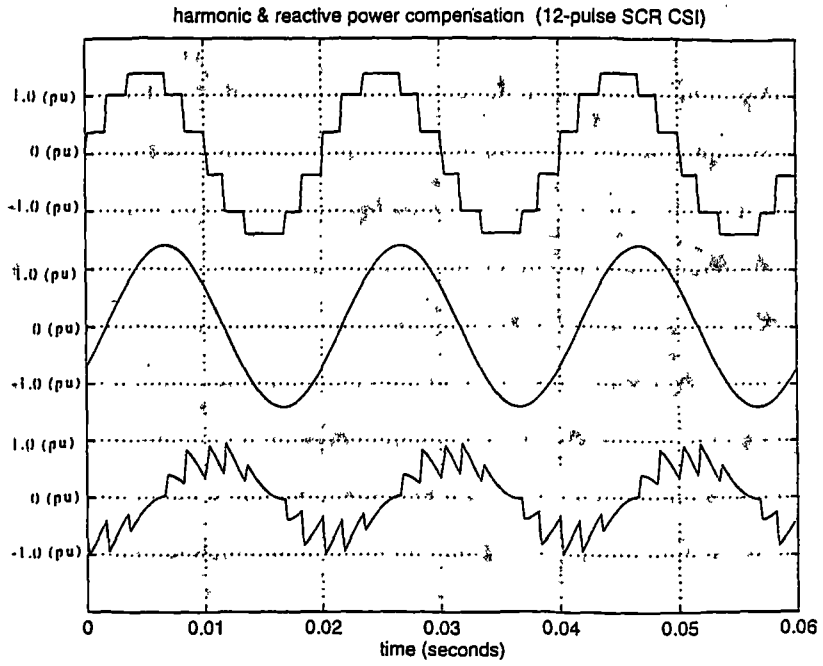

(b) Harmonic and reactive power compensation (correcting angle 30°)

waveform sequence(downward): 1 i_{CSI}; 2 $i_{s.ref}$; 3 $i_{c.ref}$

Figure 10.6 Active compensated 12-pulse SCR CSI waveform

Combination with other harmonic and reactive power compensation techniques: These techniques can significantly reduce the required rating of the active compensator, resulting in a more economical system. The waveforms for 12-pulse SCR inverters are shown in figure 10.6 and for the ac capacitors combinations (correcting angle 30° to unity power factor) in figure 10.7.

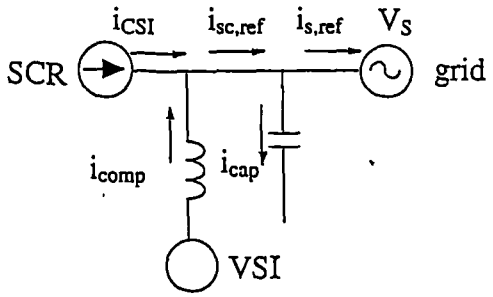

(a) current reference direction

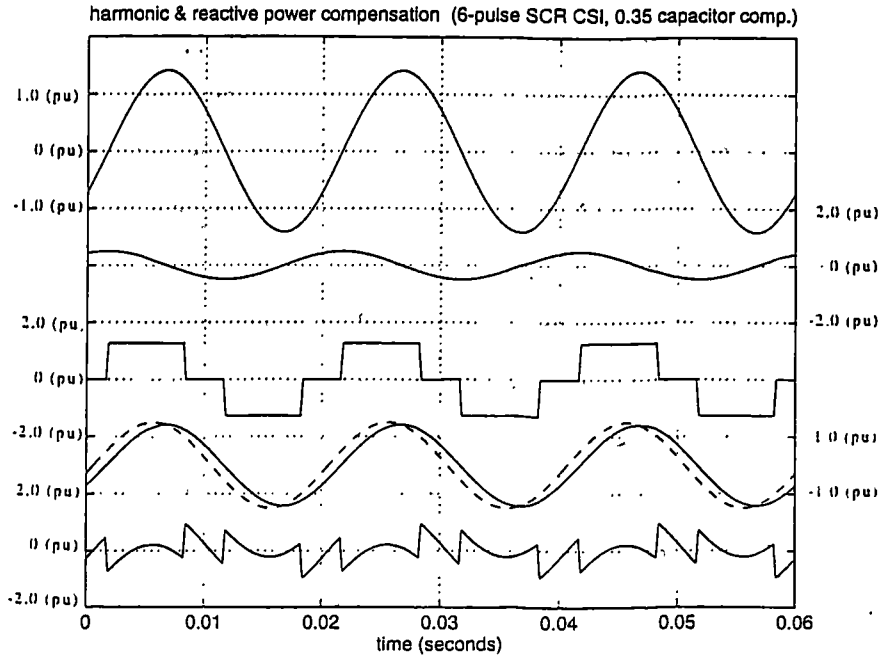

(b) 6-pulse SCR CSI

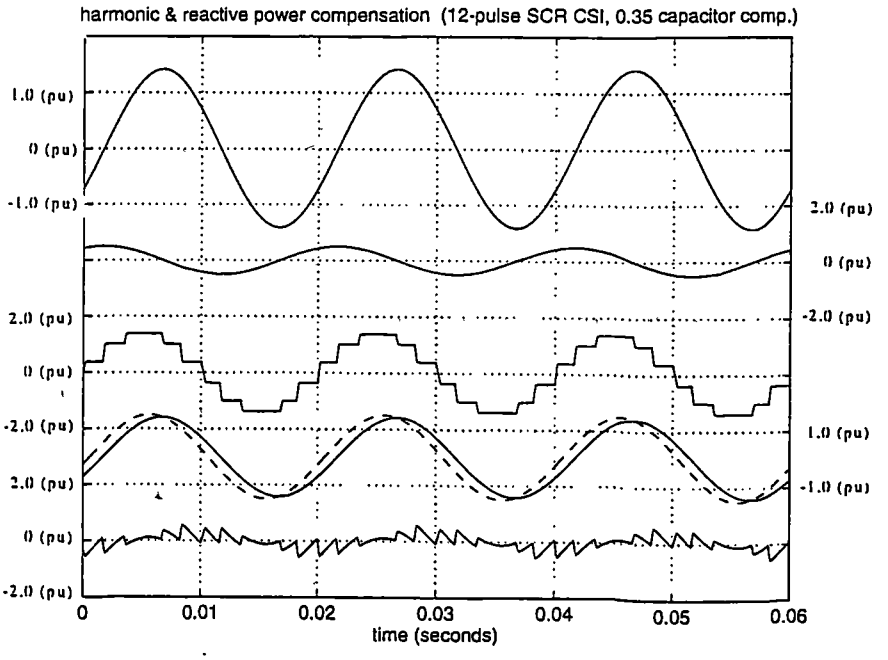

(c) 12-pulse SCR CSI

waveform sequence (downward): 1 V_S; 2 i_{cap}; 3 i_{CSI}; 4.- - - - $i_{sc,ref}$; ---- $i_{s.ref}$, 5 $i_{c.ref}$

Figure 10.7 Capacitor combination active compensated SCR CSI waveform

10.2.4 Compensator current rating

The required RMS current rating of the VSI compensator may be calculated by integrating the ideal active compensator waveform shown in the relevant figure. The calculated results for 6 pulse and 12 pulse SCR inverters with a correcting angle range for 0° to 90° are presented in figure 10.8. 1.0 pu current is the grid sine-wave current RMS value and it is assumed that the fundamental inverter ac current is kept at 1.0 pu. It shows that with a 12-pulse main inverter, the harmonic distortion is significantly reduced which in turn reduces the harmonic correction burden of the compensator. As expected, the required compensator current is increased with increasing correcting angle. A higher rated compensator is needed for higher reactive power generating capacity.

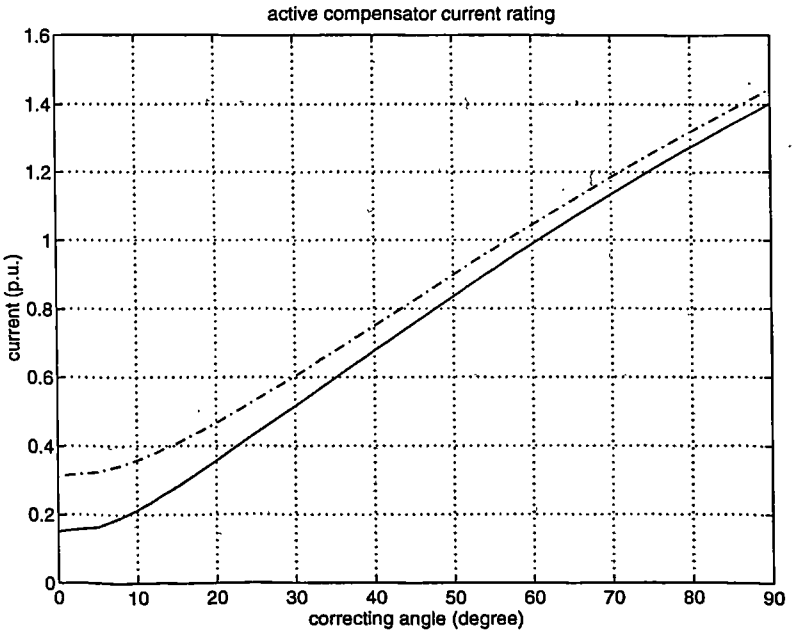

6-pulse .-

12-pulse ----------

Figure 10.8: Active compensator rating vs. correcting angle

10.3 Use As A Wind Energy Interface in A Simple Power System

The simple SCR-CSI system studied in chapter 6 is used for the performance analysis of the active compensated SCR-CSI conversion system.

The characteristics of the phase angle controlled SCR-CSI in a simple system has been discussed in chapter 6 where a group of operation curves is given in figure 6.18. The extinction angle shown in figure 6.18 (c) is the phase angle between SCR inverter ac current fundamental component and ac grid voltage, i.e., the approximate correcting angle required to operate the system at unity displacement power factor. Based on the characteristics in figure 6.18 and the parameters for those characteristics, the SCR inverter fundamental current (rms) curve can be calculated using equation (6.4) and is shown in figure 10.9. An active compensator can be designed to follow the variation of ac current and extinction angle to compensate the harmonic and reactive power.

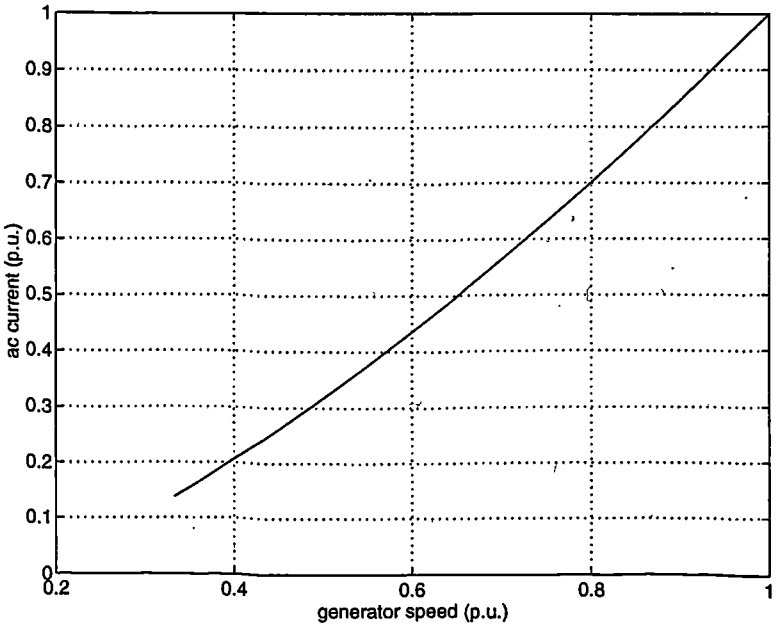

Figure 10.9: SCR inverter ac current

The ratings of active compensator for use with SCR-CSI systems are studied with reference to the operation curves shown in figure 6.18 (c) and figure 10.9 for alternative compensation schemes.

i) Pure harmonic compensation only

The pure harmonic compensation scheme corresponds to 0 degree correcting angle. It can be seen from figure 10.8 that the required current rating is 0.31 p.u. if a 6-pulse inverter is used or 0.15 for a 12-pulse inverter.

ii) Harmonic compensation and unity displacement power factor operation

In this scheme, the compensator is used to bring the overall displacement power factor to unity. Figure 10.10 shows the compensator current as a function of generator speed. As expected, the rating of the active compensator is much higher than that of the pure harmonic compensation scheme.

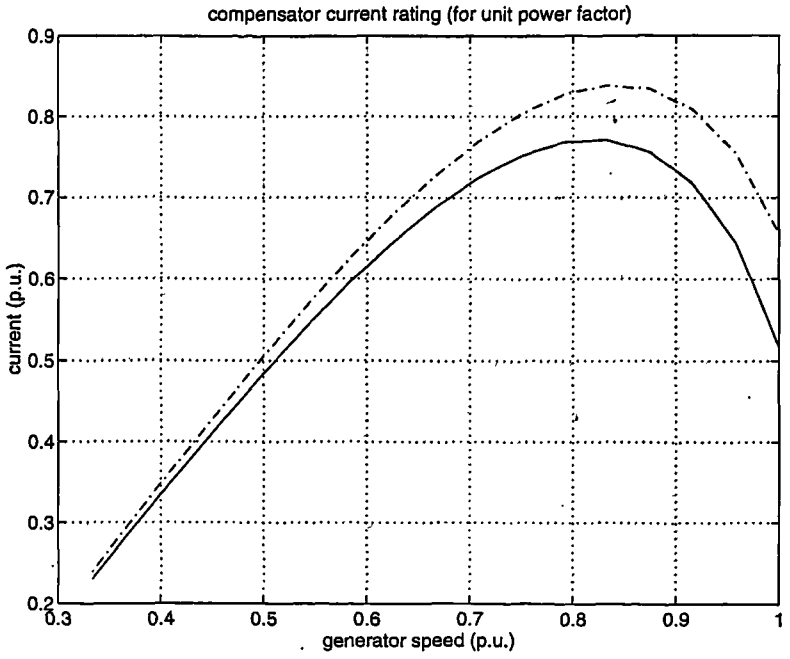

6-pulse.-.-.-.-.-.-.-.-.-.-.-.-.-.-.-.-.-.-.- - -

12-pulse ----------

Figure 10.10: Compensator current (RMS) curve (harmonic and reactive power compensation)

iii) Harmonic compensation and unity power factor operation with capacitor and active compensator

This scheme includes a fixed capacitor (0.5pu rating) and an active compensator. The resulting compensator current vs. generator speed curve is shown in figure 10.11. It shows that a significant rating reduction can be achieved for the active compensator at the expense of providing static capacitors. It is assumed, for the purpose of assessing the active compensator rating, that the capacitors contribute only to the reactive power. In

practice, static capacitors will have a beneficial affect in helping to absorb current harmonics.

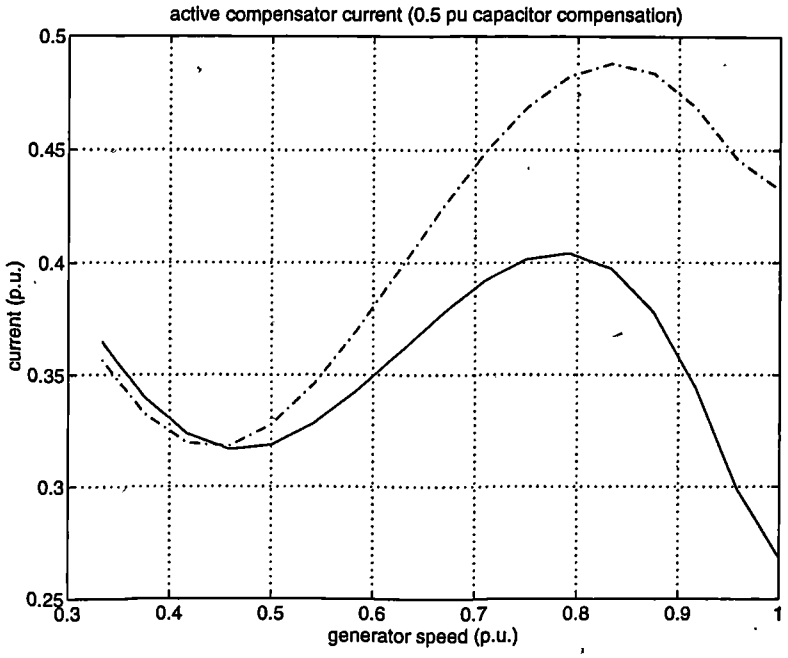

6-pulse .-

12-pulse ----------

Figure 10.11Compensator current (RMS) curve (capacitor combination)

10.4 Time Domain Simulation

10.4.1 Simulation model

PSPICE is used for this simulation study. The simulation model consists of:

1) generator-rectifier-DC link,
2) VSI active compensator
3) 6 pulse or 12 pulse SCR inverter,
4) ac grid system,
5) control signal generators for the SCR inverter and VSI active compensator.

The use of static capacitors has not been included and so the study corresponds to the worst case situation.

Generator-rectifier-dc link system: The smooth dc link voltage and current waveforms of PM generator-rectifier system allow the generator-rectifier system to be simulated by a dc current source for steady state performance analysis, the current source takes the current value for maximum power as illustrated by the curve of figure 5.12(e).

AC grid system: The AC grid is represented by a three-phase sinusoidal voltage source connected to the compensator ac output terminal through inductors. The inductance value corresponds to the commutation inductance (5%) and includes the leakage inductance of the transformer.

VSI based active compensator: The VSI model described in chapter 8 is used. The dc terminal is held at a constant voltage.

VSI active compensator driving signal generator: The switching signal generator includes a three phase sine waveform generator, which produces ideal system current, differential amplifiers for obtaining the current error, a triangular waveform generator and comparators which generate gate driving signals. The simulation model is shown in figure 10.12.

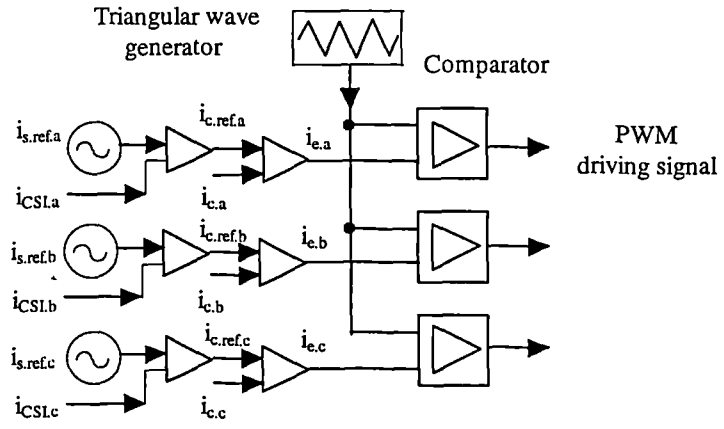

Figure 10.12Active compensator driving signal generator simulation model

SCR driving signal generator: Three pulse-type voltage sources are used to generate square waveforms which are used to synthesise three-level driving signals for the SCR inverter simulation model. A schematic diagram of the SCR signal generator is shown in figure 10.13.

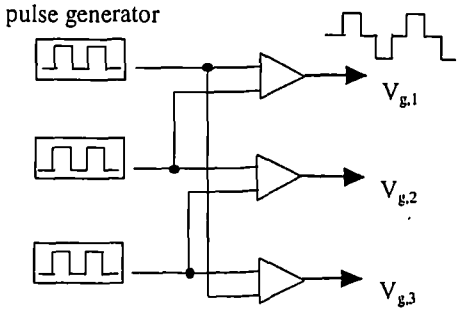

Figure 10.13 SCR CSI driving signal generator

SCR inverter system: The SCR inverter model is also constructed using the switching function representation and is shown in figure 10.14. The inverter model includes dependent current sources (G_1, G_2 and G_3) and dependent voltage sources (E_1, E_2 and E_3) which are controlled by signals from the SCR CSI driving signal generator with the expression: G_i: value={ $I_d \times V_{g,i}$ } and E_i: value={ $V_i \times V_{g,i}$ }; i=1,2,3.

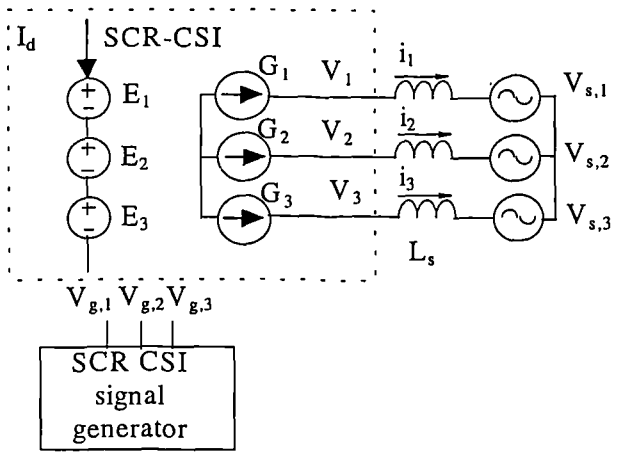

Figure 10.14 SCR-CSI grid interface simulation model

The overall simulation model system is shown in Figure 10.15.

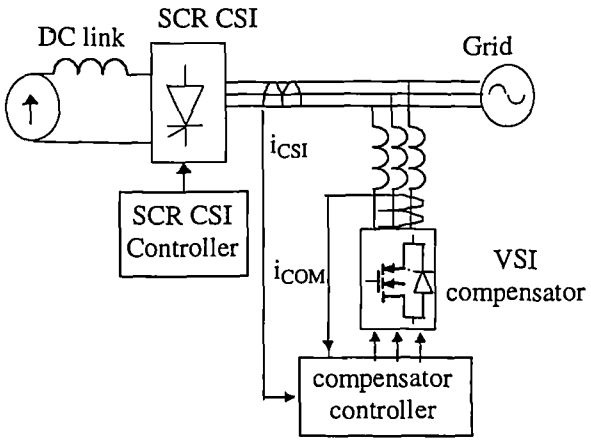

Figure 10.15: Schematic simulation system

10.4.2 Simulation results

Some typical results derived from the model described above are presented as follows.

The VSI of the active compensator operates at a switching frequency of 2.4kHz. Simulated waveforms and harmonic spectra of ac system current, i_{sys}, are shown in figure 10.16, 10.17, 10.18 and 10.19 for operating conditions:

- 6 pulse SCR CSI harmonic compensation only (figure 10.16),
- 6 pulse SCR CSI harmonic and reactive power compensation (figure 10.17),
- 12 pulse SCR CSI harmonic compensation only (figure 10.18),
- 12 pulse SCR CSI harmonic and reactive power compensation (figure 10.19).

Each of these figures give waveforms in the following sequence from top to bottom:

1. ac grid voltage
2. SCR inverter ac line current
3. Active compensator ac line current
4. Compensated system current

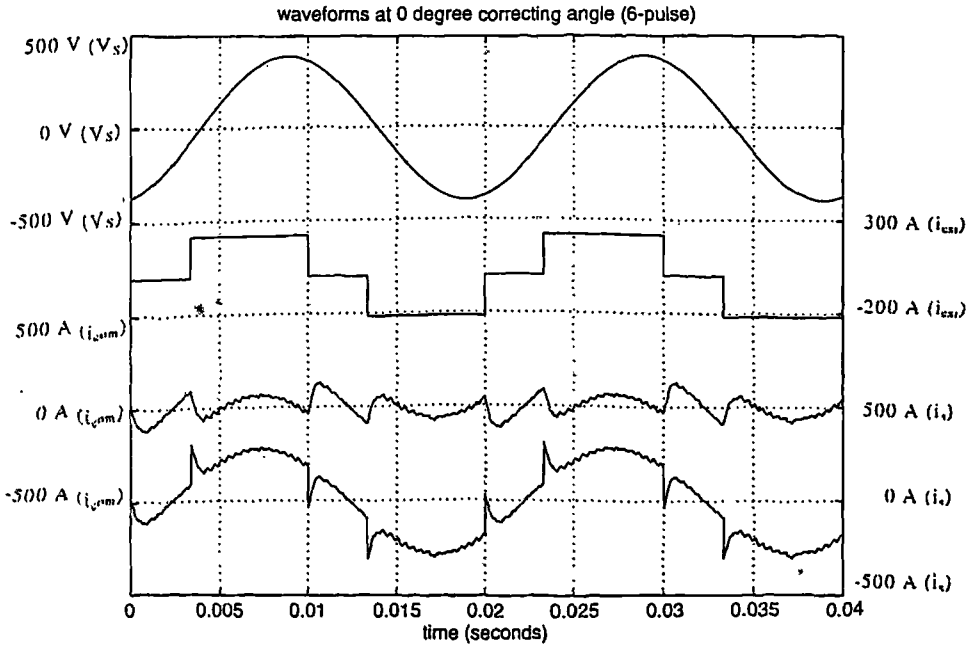

(a) waveforms

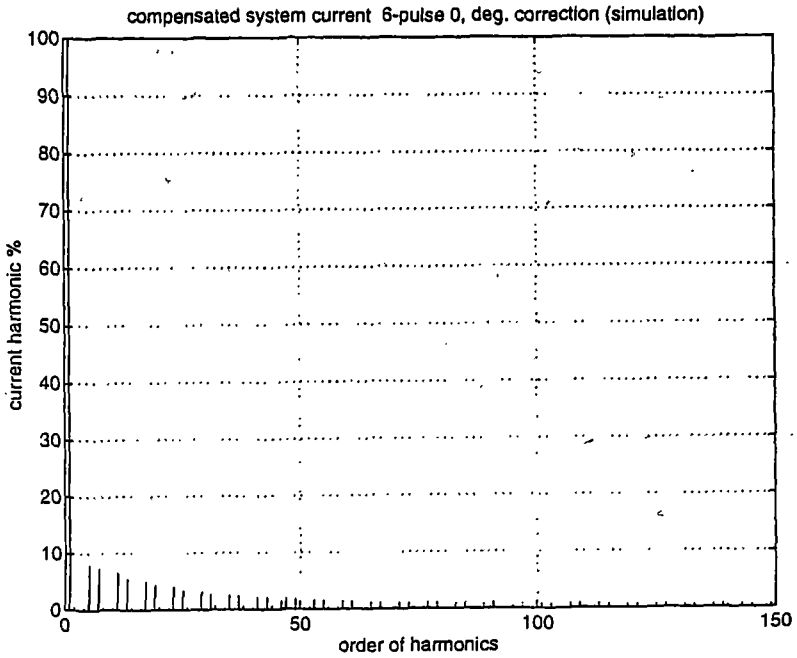

(b) compensated system current harmonic spectra

Figure 10.16 Active Compensated SCR-CSI (simulation 6-pulse correcting angle 0°)

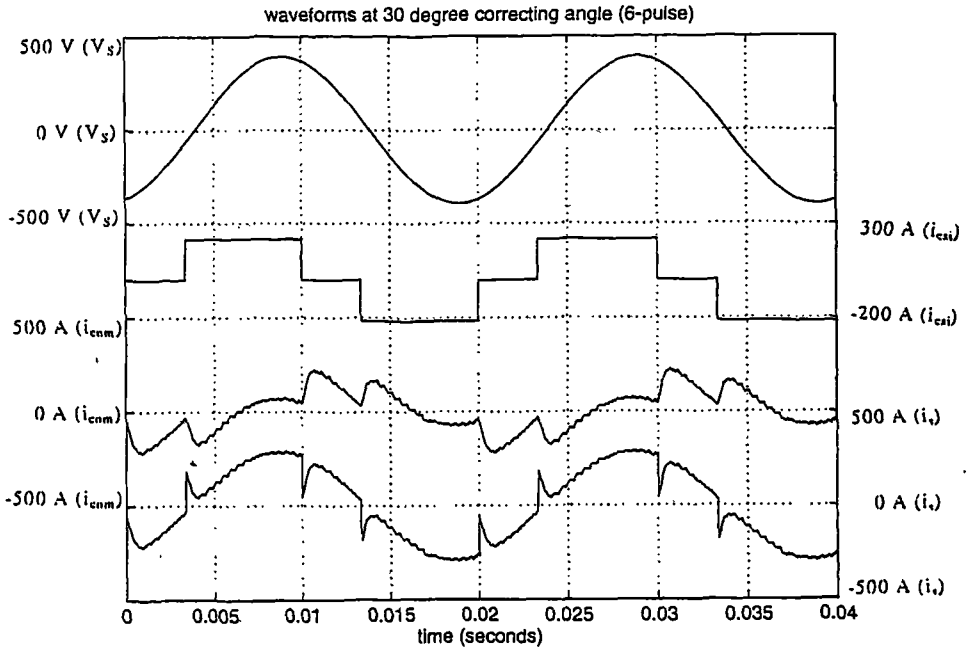

(a) waveforms

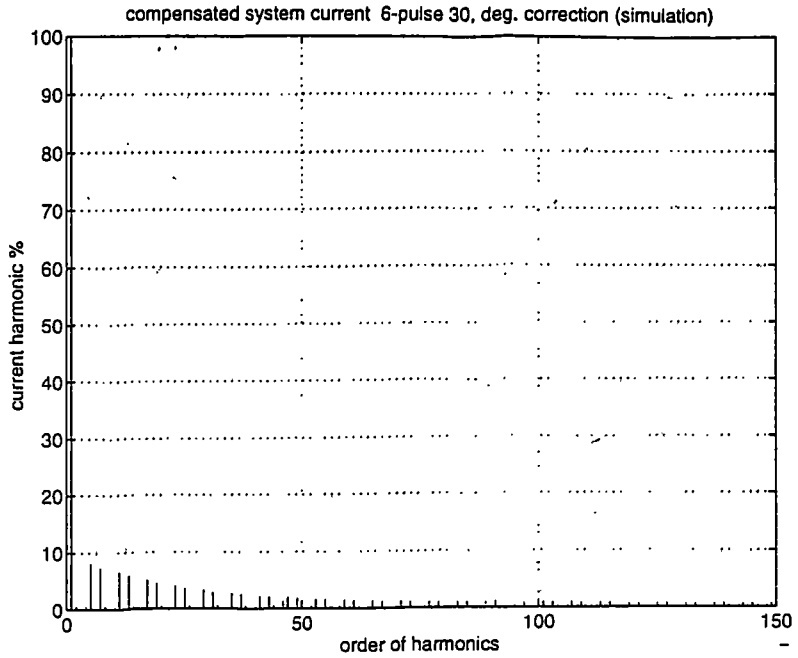

(b) compensated system current harmonic spectra.

Figure 10.17 Active Compensated SCR-CSI (simulation 6-pulse correcting angle 30°)

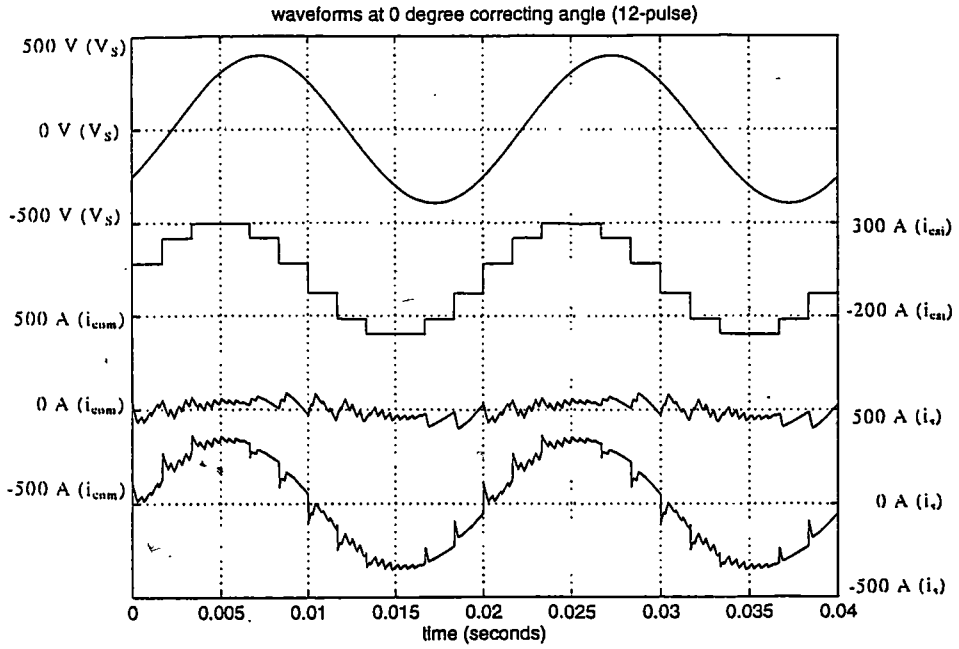

(a) waveforms

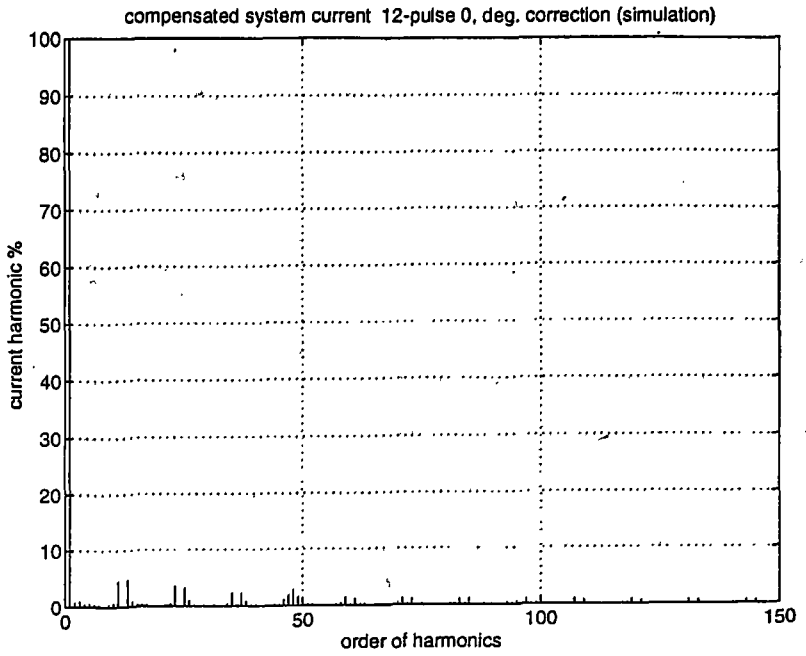

(b) compensated system current harmonic spectra

Figure 10.18 Active Compensated SCR-CSI (simulation 12-pulse correcting angle 0°)

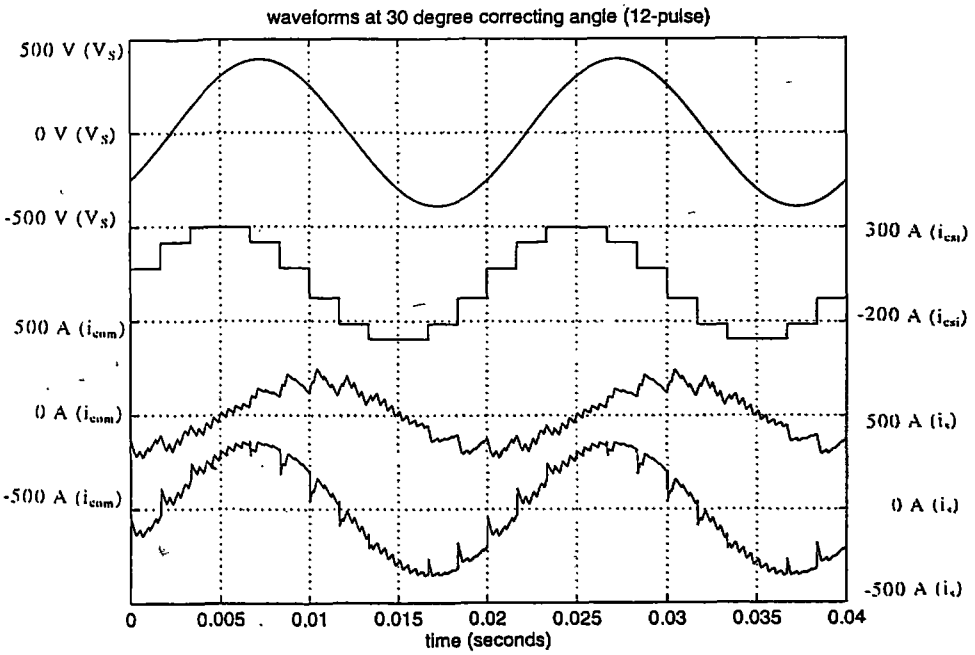

(a) waveforms

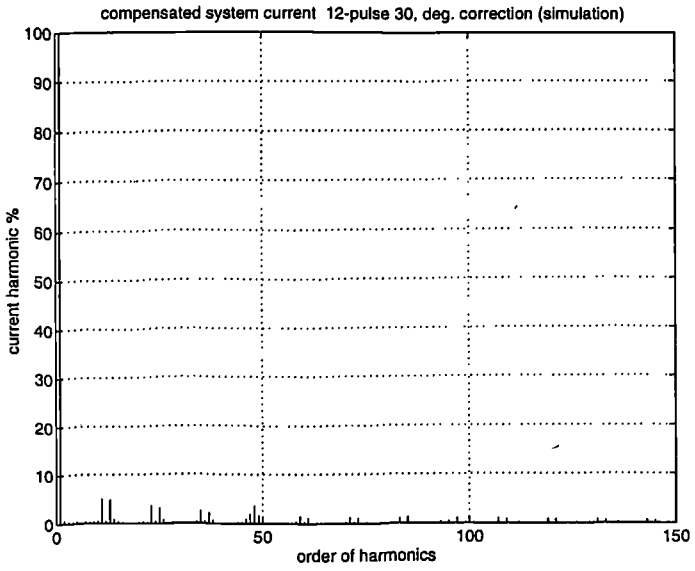

(b) compensated system current harmonic spectra

Figure 10.19 Active Compensated SCR-CSI (simulation 12-pulse correcting angle 30°)

10.5 Experimental Study

A laboratory model of the active compensated SCR-CSI interface system has been designed and built for experimental investigation. This section reports the experimental studies.

10.5.1 Experimental model

The laboratory model is shown schematically in figure 10.20. The main parts of the system include SCR inverter, VSI based active compensator, their associating driving circuits and control systems.

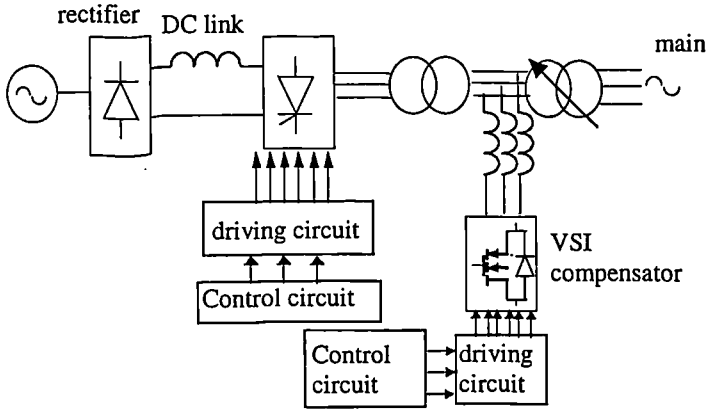

Figure 10.20 Block diagram of experimental system

The SCR inverter is constructed with thyristor modules (SKKT42B08D, V_{RRM}=800V and I_{ave}=40A) and may be configured for 6 or 12-pulse operation. The 12-pulse circuit configuration is shown in figure 10.21. The active compensator is a 6-pulse voltage source inverter used for VSI interface studies.

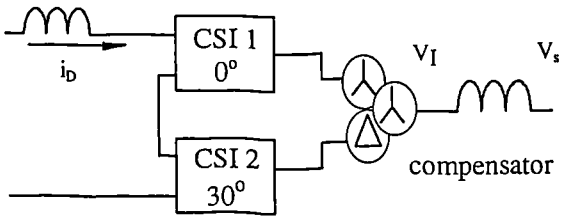

Figure 10.21 12-pulse SCR inverter configuration

Driving circuits: the active compensator VSI uses the IGBT driving circuit described in chapter 8. The SCR is a current driven device, the drive circuit designed and built for the model is shown in figure 10.22.

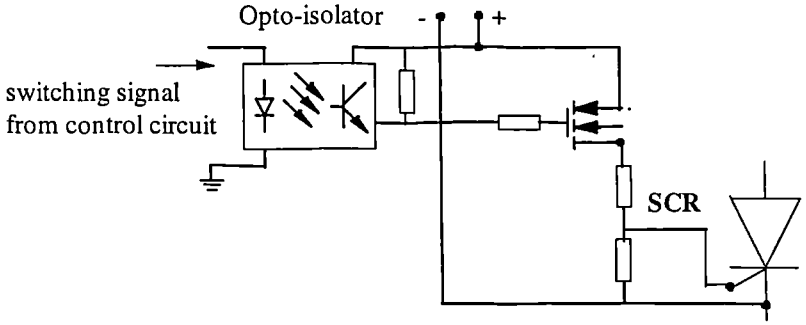

Figure 10.22 SCR driving circuit (experimental model)

The control system consists of two part: SCR-CSI firing angle control which regulates the delay angle with respect to ac grid voltage to control the real power transfer, and the active compensator PWM switching controller which switches the VSI active compensator to minimise harmonics and control reactive power.

The block diagram of SCR firing angle control circuit is shown in figure 10.23.

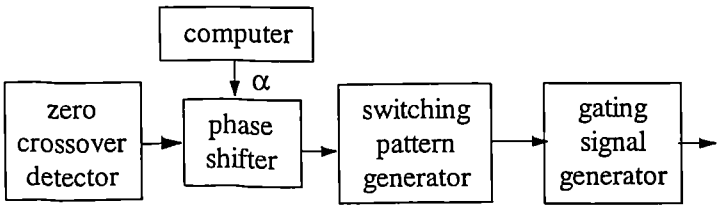

Figure 10.23 Block diagram of SCR-CSI control system (experimental model)

The zero crossover detector and phase shifter create a square wave signal which has a controllable phase angle and is synchronised with the grid voltage. The switching pattern generator produces switching signals with 120° conduction for 6 pulse or 12 pulse operation of SCR CSI. These signals are then converted into pulse trains for the gate drive circuits.

A block diagram of active compensator controller is shown in figure 10.24. The first block is an ideal waveform generator. It produces the reference sine wave, which can be controlled in magnitude and phase angle in response to variation of the ignition angle and current of SCR inverter and the demand value of the correcting angle, δ_c. Then the ideal system current waveform is compared with the SCR inverter current to produce a reference waveform for the active compensator which then is compared with real VSI compensator current to drive the PWM signal generator.

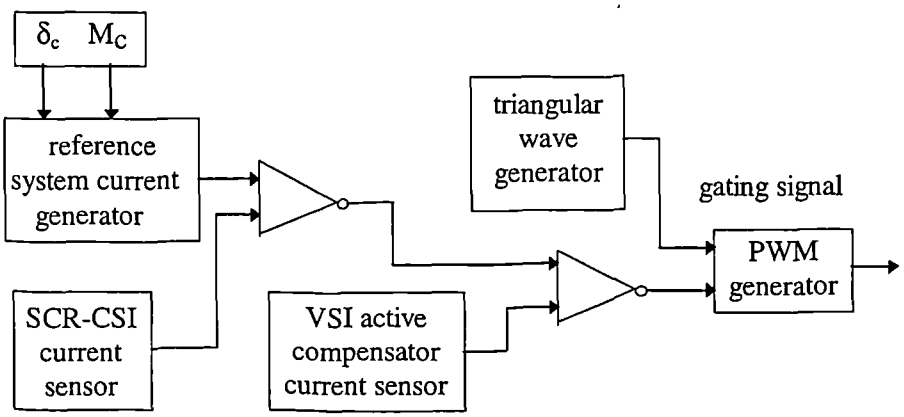

Figure 10.24 Block diagram of SPWM-VSI active compensator control system (experimental model)

As with the experimental models described in previous chapters, the computer is used as a controller to set and regulate the control variable (ignition angle, α, for CSI and correcting angle,δ_c and magnitude, M_c for the reference current waveform for the active compensator).

10.5.2 Experimental results

Some typical experimental waveforms and harmonic spectra are presented as follows: Figures 10.25 to 10.28 show waveforms for an extinction angle of 30° and both 6 and 12 pulse form CSI operation. The VSI switching frequency is 2.4 kHz. Operation both with and without reactive power compensation are illustrated.

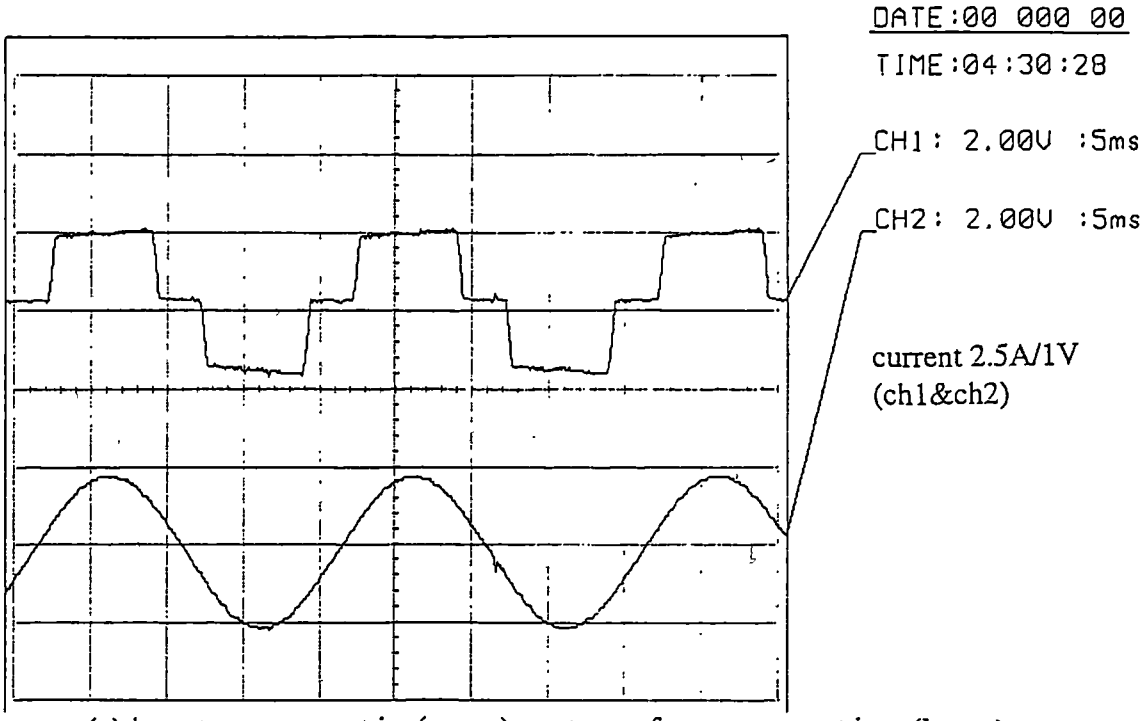

(a) inverter ac current i_{csi} (upper), system reference current $i_{s,ref}$ (lower)

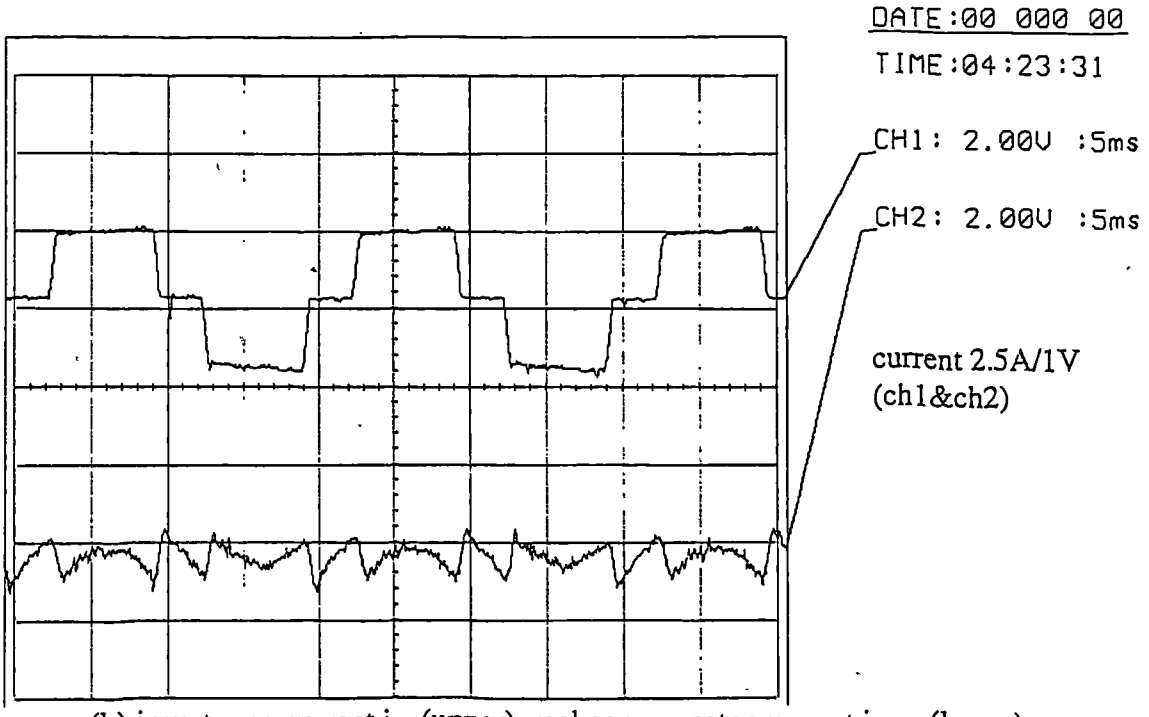

(b) inverter ac current i_{csi} (upper), real compensator current $i_{c,real}$ (lower)

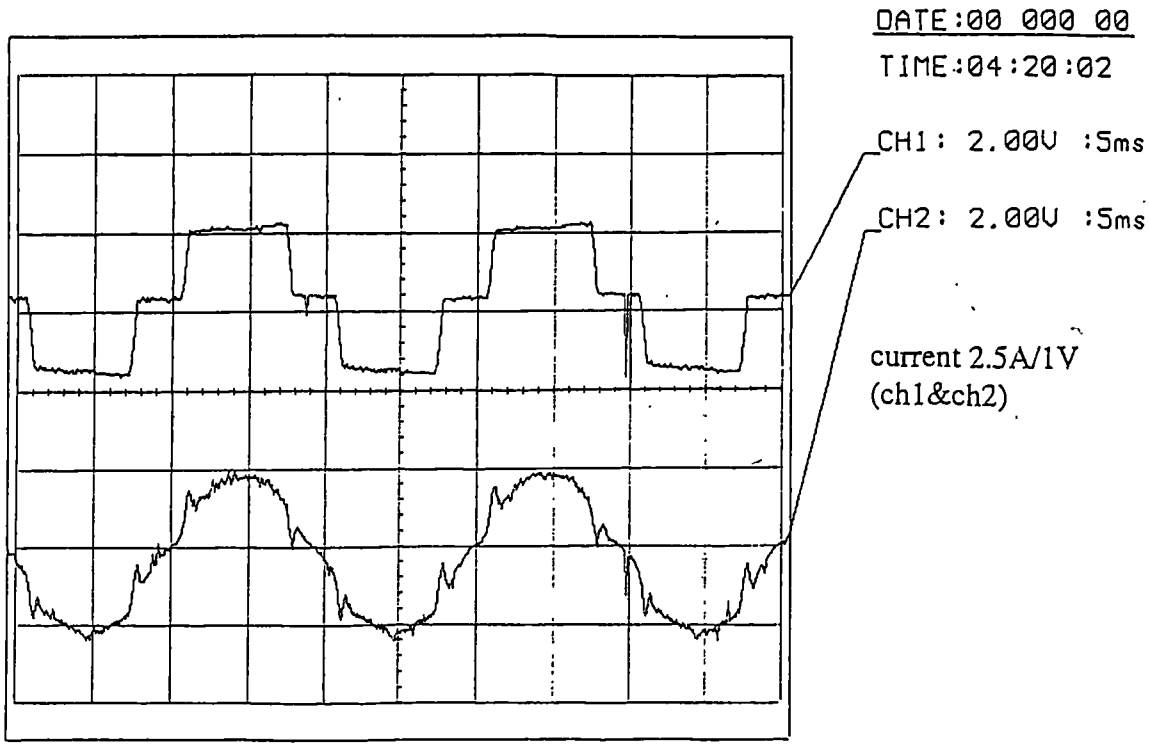

(c) inverter ac current i_{csi} (upper), real system current $i_{s,real}$ (lower)

Figure 10.25 Active compensated 6-pulse SCR-CSI waveform

(experimental, correcting angle 0°)

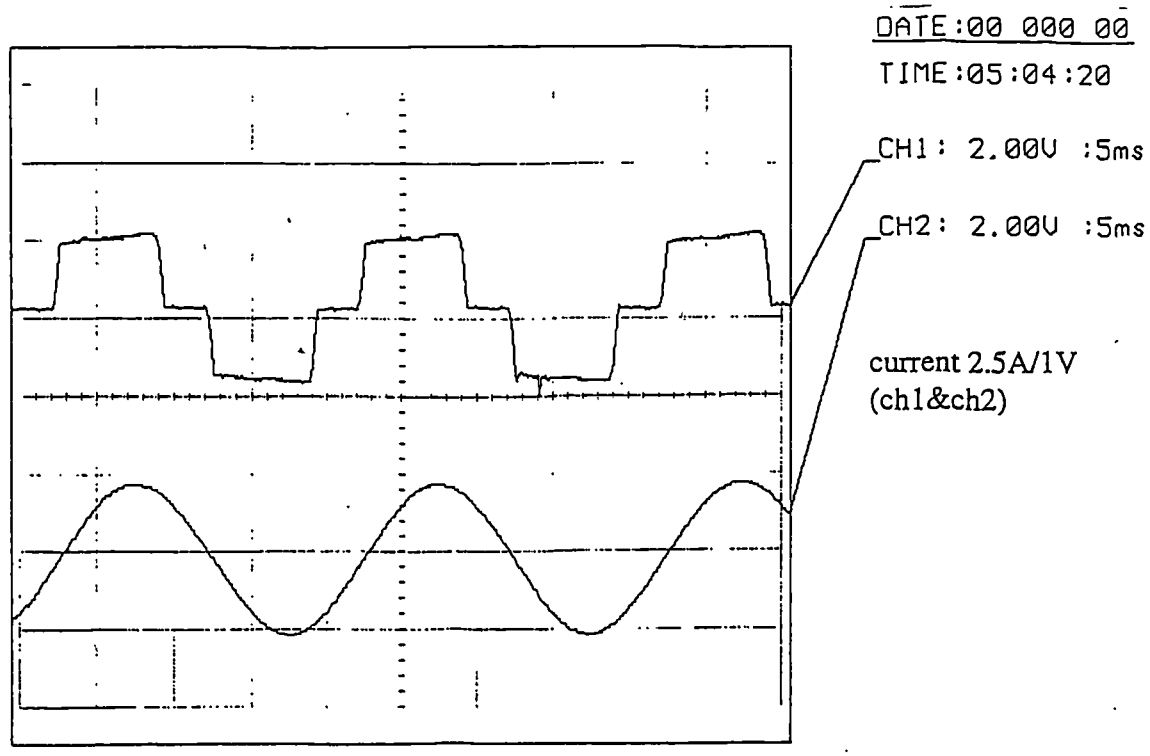

(a) inverter ac current i_{csi} (upper), system reference current $i_{s,ref}$ (lower)

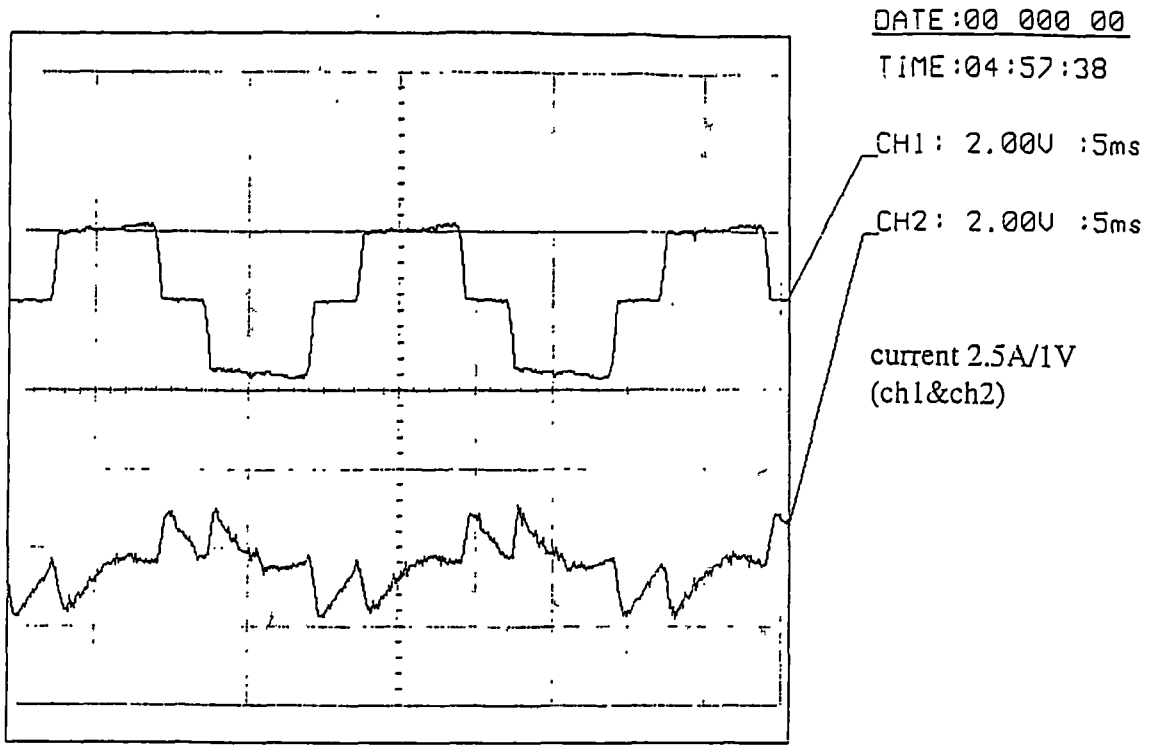

(b) inverter ac current i_{csi} (upper), real compensator current $i_{c,real}$ (lower)

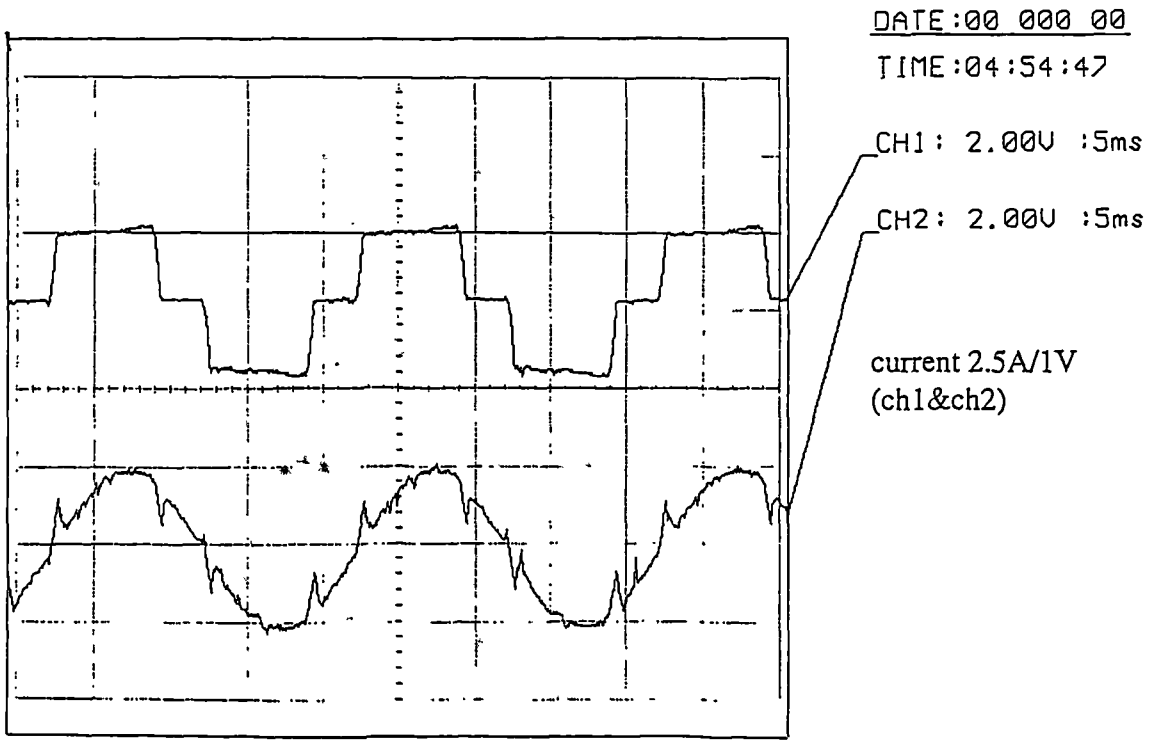

(c) inverter ac current i_{csi} (upper), real system current $i_{s,real}$ (lower)

Figure 10.26 Active compensated 6-pulse SCR-CSI waveform

(experimental, correcting angle 30°)

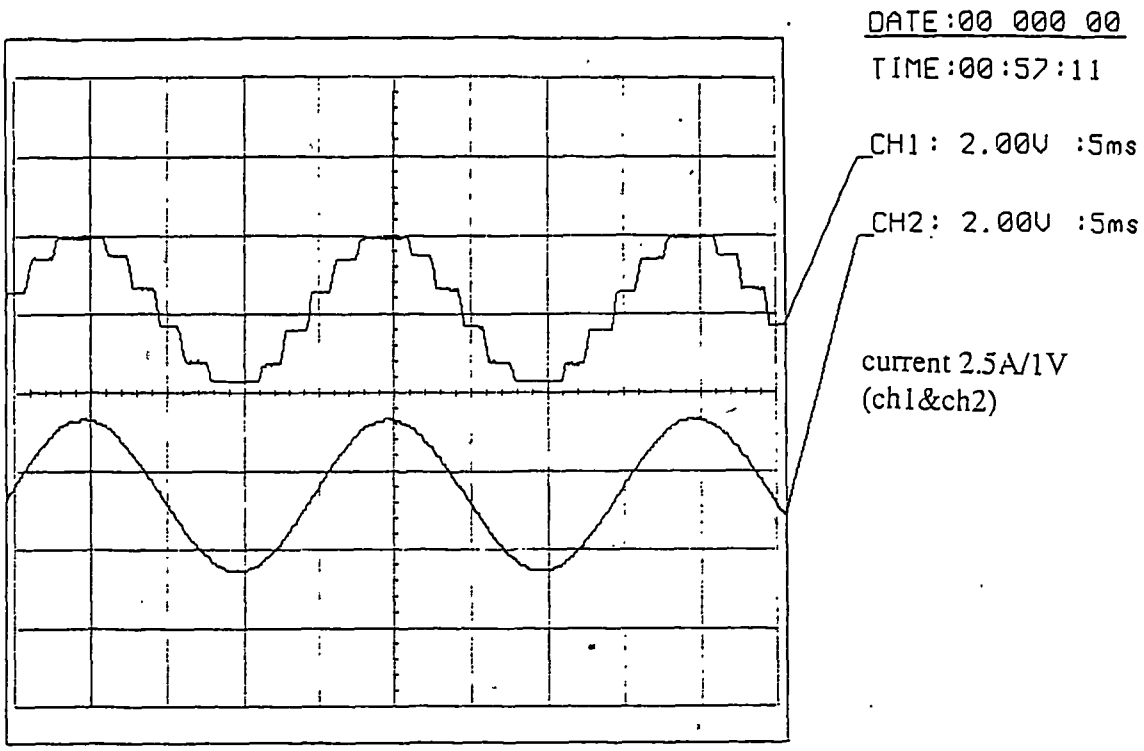

(a) inverter ac current i_{csi} (upper), system reference current $i_{s,ref}$ (lower)

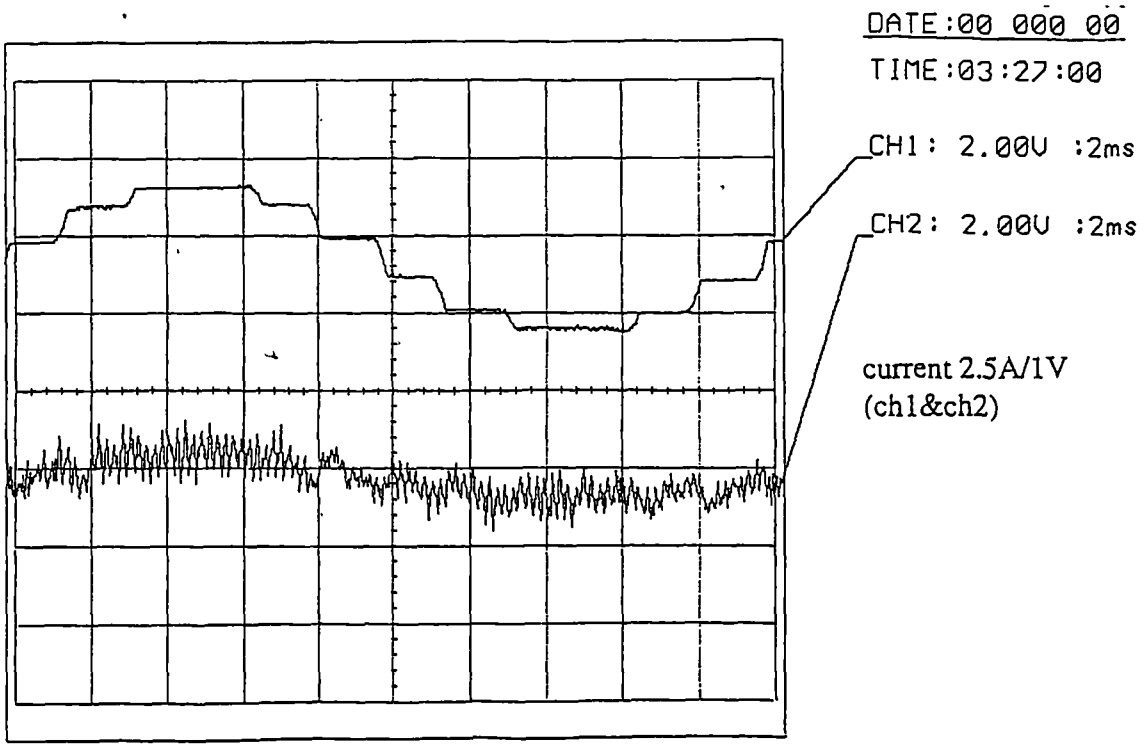

(b) inverter ac current i_{csi} (upper), real compensator current $i_{c,real}$ (lower)

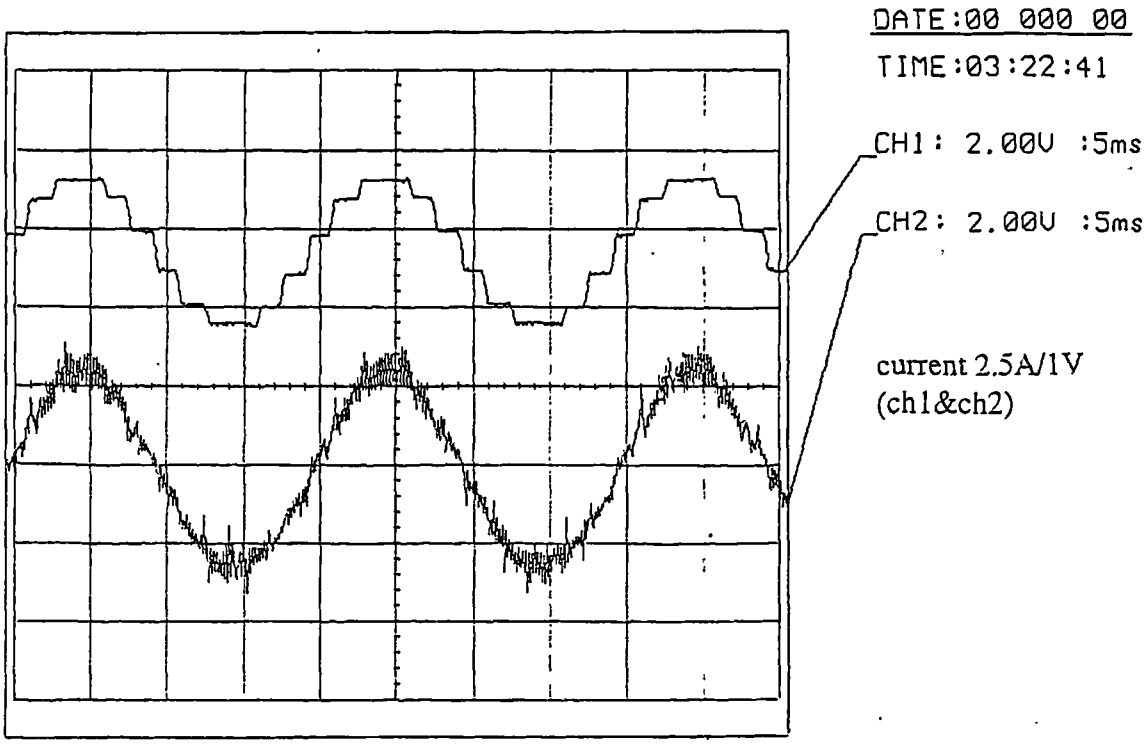

(c) inverter ac current i_{csi} (upper), real system current $i_{s,real}$ (lower)

Figure 10.27 Active compensated 12-pulse SCR-CSI waveform

(experimental, correcting angle 0°)

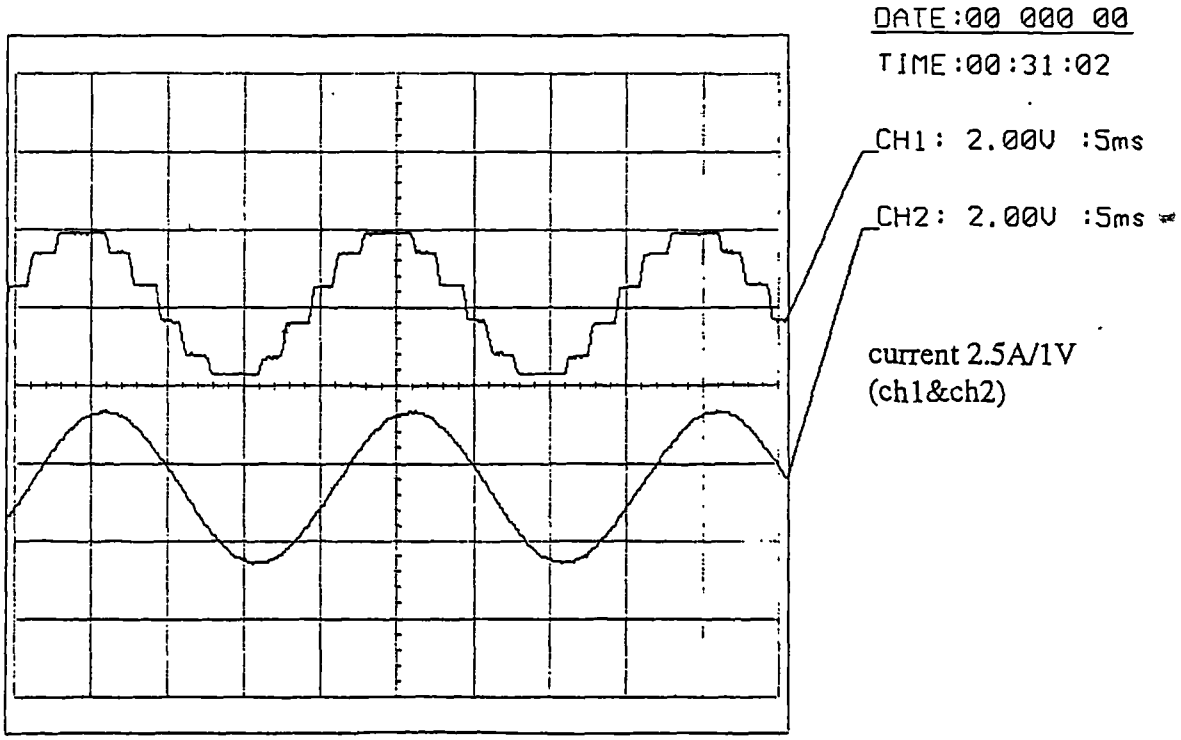

(a) inverter ac current i_{csi} (upper), system reference current $i_{s,ref}$ (lower)

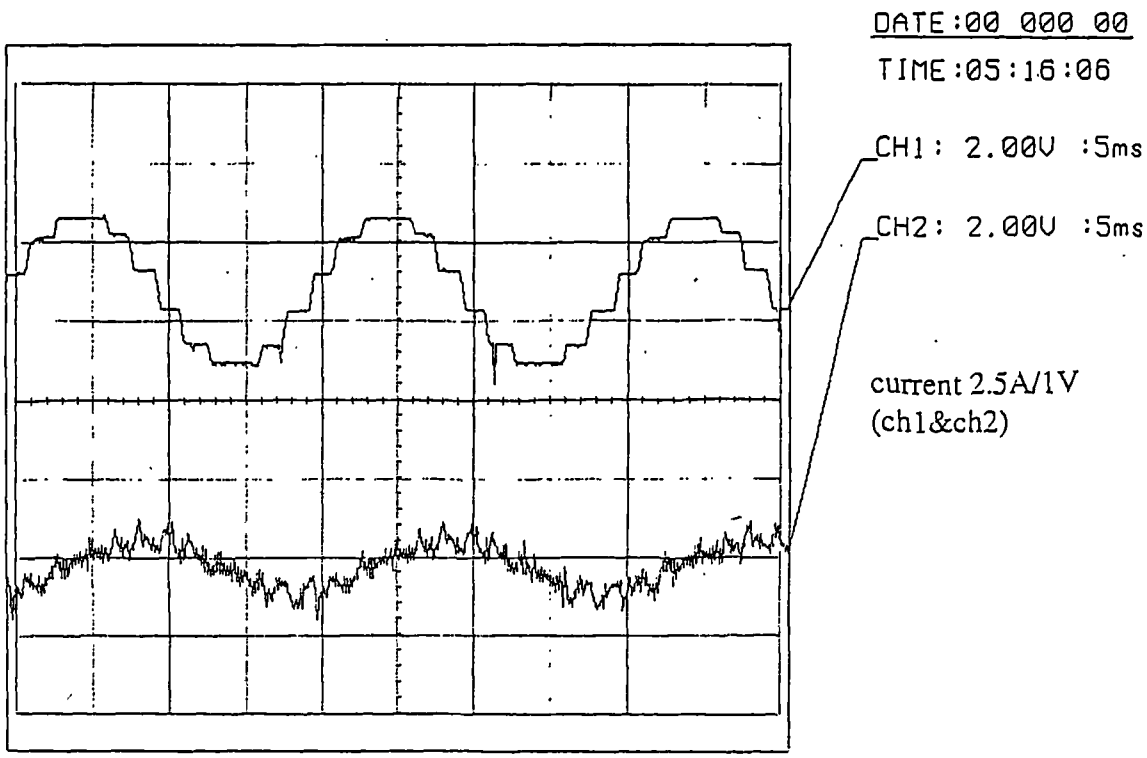

(b) inverter ac current i_{csi} (upper), real compensator current $i_{c,real}$ (lower)

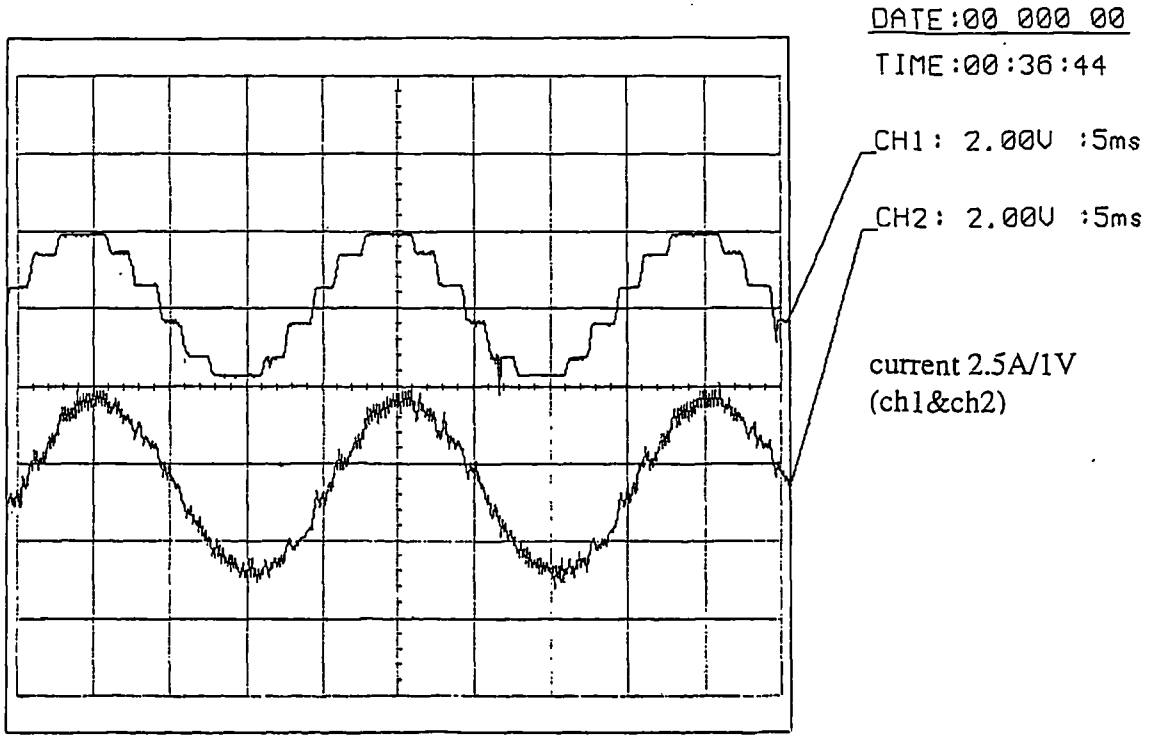

(c) inverter ac current i_{csi} (upper), real system current $i_{s,real}$ (lower)

Figure 10.28 Active compensated 12-pulse SCR-CSI waveform

(experimental, correcting angle 30°)

The harmonic spectra of 6 pulse and 12 pulse SCR inverter are shown in figure 10.29, and the compensated system harmonics spectra are shown in figure 10.30. The close agreement between the experimental, analytical and simulation results validates the models employed.

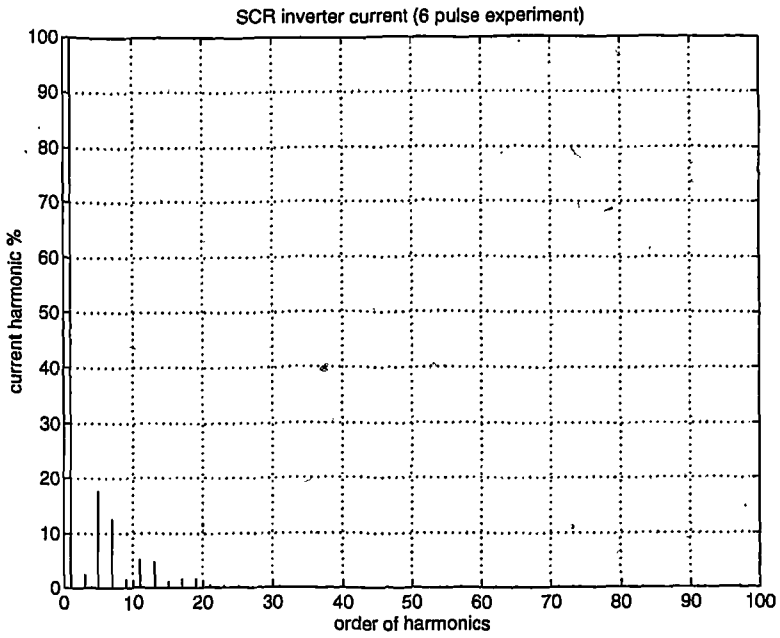

(a) 6-pulse SCR-CSI

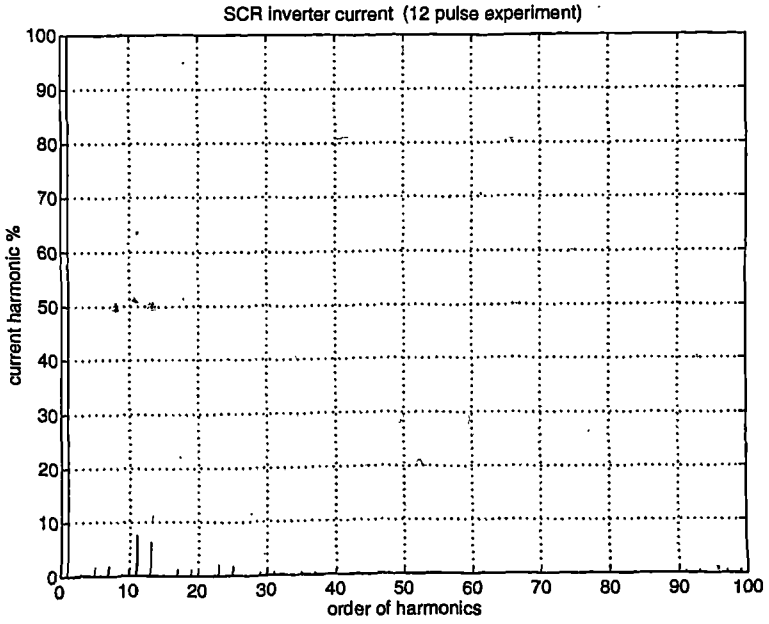

(b) 12-pulse SCR-CSI

Figure 10.29 SCR-CSI current harmonics spectra (experimental)

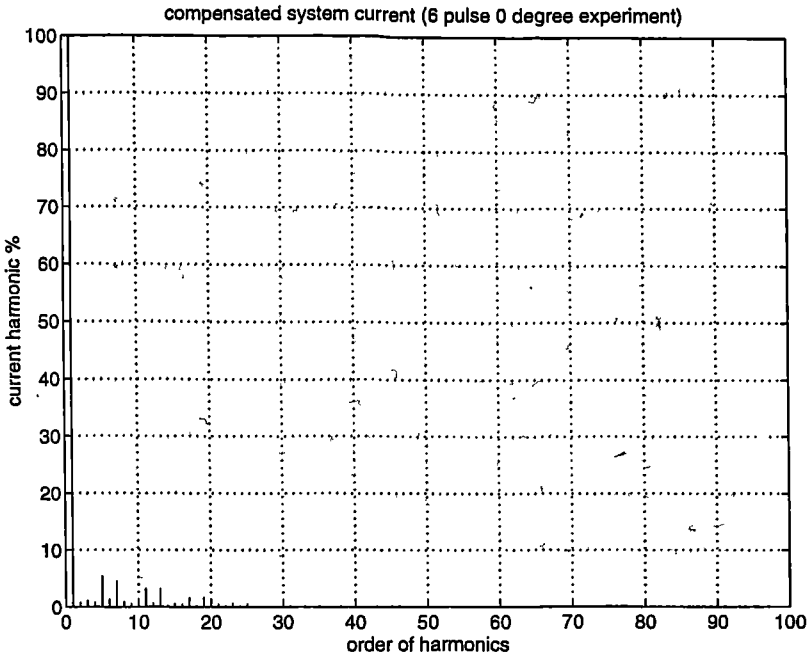

(a) 6-pulse SCR-CSI, correcting angle 0°

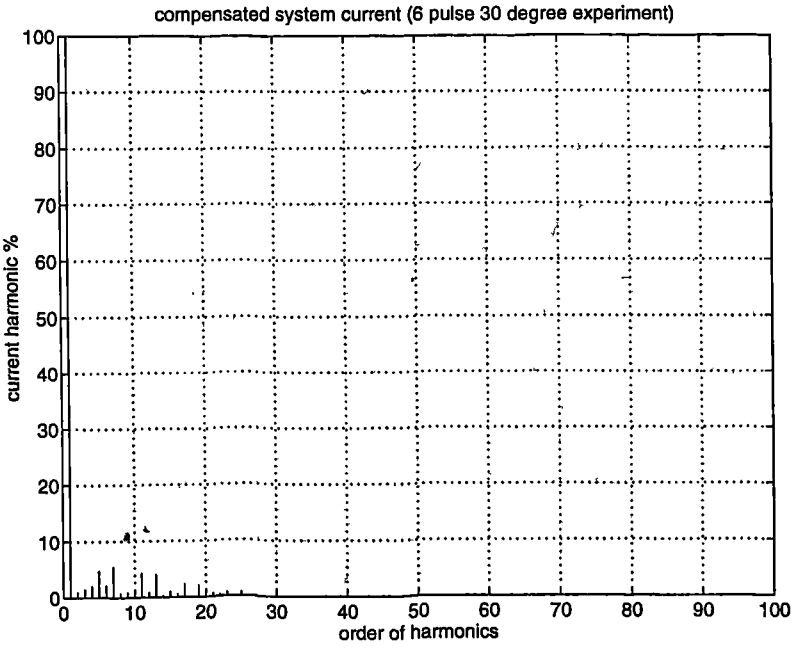

(b) 6-pulse SCR-CSI, correcting angle 30°

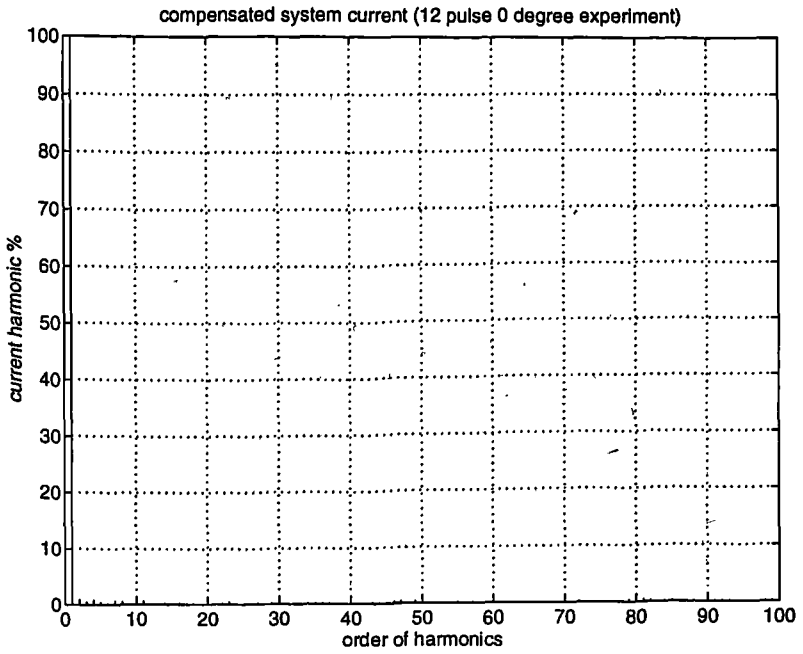

(c) 12-pulse SCR-CSI, correcting angle 0°

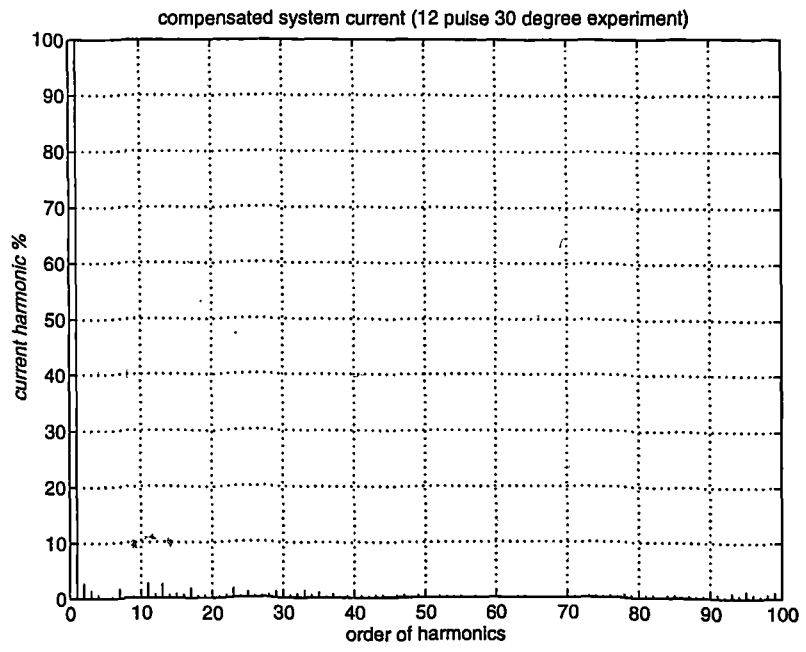

(d) 12-pulse SCR-CSI, correcting angle 30°

Figure 10.30 Compensated system current harmonic spectra (experimental)

10.6 Discussion

In practice, the active compensator can only provide an approximation to the ideal compensation current. The error can be reduced by increasing switching frequency. The

active compensator can also generate additional harmonics itself. However if the switching frequency is relatively high, the higher order voltage harmonics create little pollution in the inductive dominated power system and are easily filtered out. But high frequency switching leads to high power losses and a compromise between efficiency and pollution is required.

In principle, according to the instantaneous power theory, the active compensator requires no capacitor for energy storage, however, it is prudent to provide a capacitor to maintain the voltage of dc bus in order to force the current in the desired direction. A controllable rectifier could be connected with the dc capacitor to compensate voltage drop, losses within the active compensator and to help suppress voltage fluctuations.

A 6-pulse SCR inverter needs an active filter with about 30% of its rating for harmonic compensation, while the same active filter could be used for two 6-pulse SCR inverters if they are connected in a 12-pulse arrangement.

This type power converter is suitable for connection to a strong ac system. If no grid voltage is present at the inverter ac side, for example, in an isolated system, the naturally commutated SCR-CSI type interface can not transfer power into the system.

10.7 Conclusion

In this chapter, the actively-compensated SCR-CSI type power electronics interface has been discussed in detail.

The thyristor inverter has the advantage of low cost and high power capacity compared with the self-commutated inverter. However, the system interface performance, such as reactive power control and harmonic pollution requires a compensation system, especially for a variable dc link voltage case.

The active compensator based upon a voltage-stiff type inverter can be used to keep a sinusoidal current waveform injected into the grid and to make the system operate at a desired power factor. Therefore high quality power is delivered to the system.

The multi-pulse thyristor configuration can reduce the required compensator rating for the harmonic compensation.

The capacity of the active compensator can be reduced by sharing the reactive power compensation burden with a conventional power factor correction capacitor.

The discussed harmonic and reactive power compensation techniques can be used to upgrade existing SCR CSI power conversion systems at relatively low cost.

Chapter

11.

Comparisons of Inverter Options

Three inverter options have previously been discussed in detail, all of these inverters can transfer optimal power and provide controllable reactive power with satisfactory harmonic performance, however, their costs and efficiencies differ. This chapter addresses the semiconductor cost and power losses of these inverter options. Firstly, the power loss calculation method is described, then the cost and power losses of semiconductors are discussed on the basis of a 150kW wind power generation system example.

11.1 Semiconductor Power Losses Calculation

During a given time period, t, the energy dissipated in a semiconductor can be obtained with the following expression:

$$E = \int_0^t v_{ce}(i) \times i(t) dt \qquad (11.1)$$

where v_{ce} is the voltage across the semiconductor, i is the current carried by the semiconductor. The mean power dissipated may be obtained by multiplying the energy dissipation by frequency.

Equation 11.1 encompasses both conduction and switching (turn on, turn off, and recovery) losses. These power loss components during a power system cycle (T_s) may be calculated separately by taking account of the current waveforms, such as the one shown in figure 11.1.

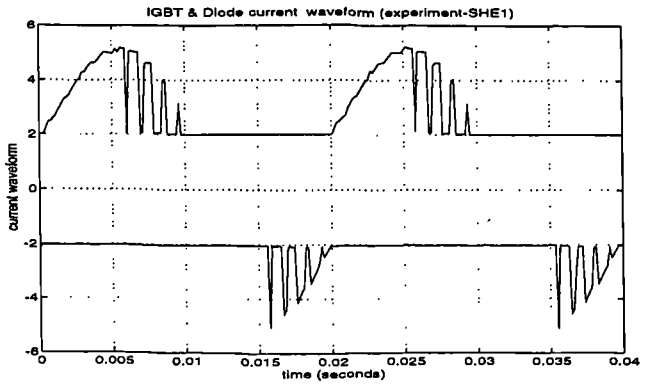

Figure 11.1: Current waveforms of semiconductors

(upper-IGBT, lower-diode)

Conduction energy losses

The instantaneous conduction power loss of a semiconductor is the product of the current through the semiconductor, i_C, and the on-state voltage drop, v_F, which may be expressed as a function of the conduction current. The conduction energy loss during the ith conduction period of a cycle, E_{Ci}, can be calculated by integrating the instantaneous power loss in that conduction period, t_{Ci}.

$$E_{Ci} = \int_0^{t_{ci}} v_F i_C dt$$

The total conduction energy losses (E_C) in one cycle can be found by summing over all the conduction periods in a cycle.

$$E_C = \sum_{i=0}^{n_c} E_{Ci} = \sum_{i=0}^{n_c} \int_0^{t_{ci}} v_F i_C dt$$

where n_c is the number of conduction periods during one cycle, T_S.

Switching energy losses

The switching energy loss includes turn-on, turn-off and reverse recovery energy ($E_{on,i}$, $E_{rr,i}$ and $E_{off,i}$) losses. The total switching energy loss is the sum of these components.

$$E_s = \sum_{i=0}^{n_{on}} \left(E_{on,i} + E_{rr,i}\right) + \sum_{i=0}^{n_{off}} E_{off,i}$$

where

n_{on} is the number of turn-ons during one cycle.

n_{off} is the number of turn-offs during one cycle.

$E_{on,i}$, $E_{rr,i}$ and $E_{off,i}$ of the semiconductors are dependent on switching current and voltage, and on gate driving conditions. They can be calculated by using current waveforms with energy loss curves from the data sheet. Alternatively, following simplified formulae give reasonable accuracy [18].

$$E_{on,i} = \int_0^{t_{ri}} v_{cc} i_{on,i} dt = \frac{1}{2} v_{cc} i_{on,i} t_{ri} = \frac{1}{2} v_{cc} i_{on,i} t_{rN} \frac{i_{on,i}}{I_{cN}}$$

$$E_{off,i} = \int_0^{t_{fi}} v_{cc} i_{off,i} dt = \frac{1}{2} v_{cc} i_{off,i} t_{fi}$$

$$E_{rr,i} = v_{cc} t_{rr} \left(0.35 I_{rrN} + 0.15 \frac{i_c}{I_{cN}} I_{rrN} + i_c \right)$$

Where $i_{on,i}$, $i_{off,i}$, and v_{cc} are turn-on, turn-off currents and switching voltage of the semiconductor, t_{ri}, and t_{fi} are the rise time and the fall time, t_{rN}, and t_{fN} are the rise time and the fall time at rated current condition, t_{rr}, and I_{rrN} are recovery time and rated recovery current for semiconductors in VSI. Then the total power losses of the semiconductors of a p-pulse inverter can be found by

$$P_{loss} = \frac{p}{T_s}(E_s + E_{cI} + E_{cd})$$

Basic operating condition for inverter comparison studies

For inverter option comparison studies of this chapter, the following conditions are adopted:

The stator coils of the modular PM generator are connected in multi-phase. A multi-phase diode rectifier system is used to produce a smooth voltage and current dc link. Power enhancement capacitors are connected to enable the optimal power to be transferred to the dc link, the dc power, voltage and current at the rectifier terminal are controlled to follow the curves shown in figure 5.12 by co-ordinating control of wind turbine and power inverter.

The investigated operation range is from 0.5 pu wind speed, $W_{0.5}$, (7.5 m/s) to rated wind speed, $W_{1.0}$, (15 m/s). It is assumed that the grid voltage is constant. The grid voltage and ac current at rated condition are used as the base values. The detailed operating conditions are given in Table 11.1.

Table 11.1 System operating conditions

wind speed	0.5 p.u. (7.5m/s)	1.0 p.u. (15m/s)
power (kW)	18.8	150
DC voltage V_{DC} (V)	241	600
DC current (A)	78	250

Based on the above operating condition, appropriate power semiconductors are chosen for the discussed power inverter options in turn. Using the power loss calculation methods described above, the power semiconductor power losses of these inverters are calculated. The detailed analysis and calculation results are presented in the following sections.

11.2 SPWM VSI System

The SPWM VSI system is sketched in figure 11.2, where the variables of interest are illustrated. The reactance between the inverter and grid (including transformer inductance) is 0.2 p.u and grid voltage is kept at 440V (line to line, RMS). The self-commutated SPWM inverter operates at unity power factor.

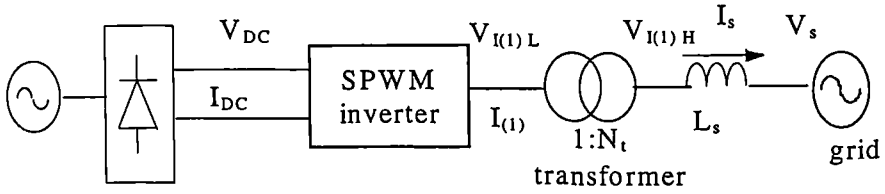

Figure 11.2 Schematic diagram of SPWM VSI

The calculated operating conditions are given in Table 11.2 for the given variation range of dc voltage and modulation ratio control strategy discussed in chapter 8, the inverter ac current is 586 A (rms) at rated wind speed. With the assumption of

sinusoidal waveform, the peak valve current would be 828A. The required semiconductors (IGBTs and diodes) cost about £1160 based on catalogue price.

Table 11.2 SPWM Inverter operating condition

wind speed	0.5 p.u. (7.5m/s)	1.0 p.u. (15m/s)
power angle (degree)	1.4	11.3
Grid ac current (unity power factor) (A)	24.6	196.8
inverter ac voltage $V_{I(1).H}$ (grid side), (V)	440	449
inverter ac voltage $V_{I(1).L}$ (inverter side), (V)	148 (M_a=1.0)	150.8 (M_a=0.41)
inverter ac current (A) rms	73 (peak 104)	586 (peak 828)

The power losses are calculated based on the simulation waveform and are presented in figure 11.3.

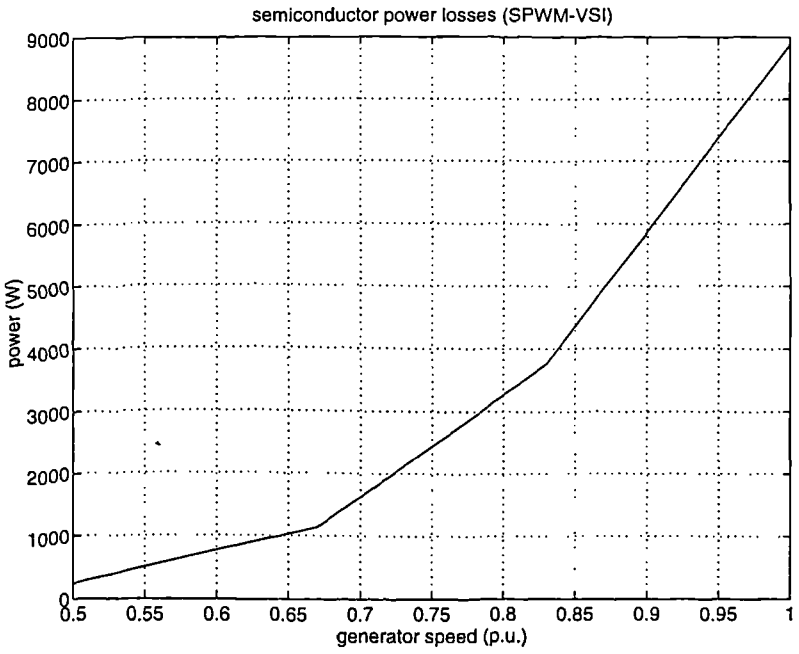

Figure 11.3 SPWM-VSI semiconductor power losses (unity displacement power factor)

11.3 DC/DC converter and VSI

The DC/DC converter and VSI system is sketched in figure 11.4 indicating the parameters of interest. The grid voltage and reactance between the inverter and grid (including transformer inductance) are the same as that of SPWM case (440V and 0.2 p.u). The VSI uses SHE switching to eliminate harmonics up to 25th and the DC/DC converter switches at 8 kHz.

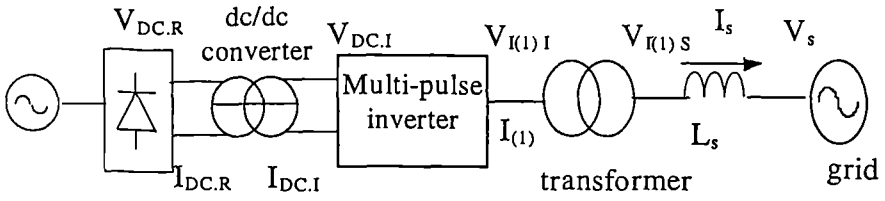

Figure 11.4 Schematic diagram of DC/DC converter-VSI

Table 11.3 lists some calculated results, the inverter peak ac current could be 266 A at rated wind speed. The semiconductors of this system (DC/DC converter and VSI) will cost about £620. The semiconductor power losses of this system are plotted in figure 11.5.

Table 11.3 DC/DC converter (boost) -VSI operating condition

wind speed	0.5 p.u. (7.5m/s)	1.0 p.u. (15m/s)
inverter side dc voltage $V_{DC.I}$ (V)	591	600
dc/dc converter ratio ($V_{DC.I}$ /$V_{DC.R}$)	2.5	1.0
inverter ac voltage $V_{I(1).I}$ (inverter side),	460	469
inverter ac current (A) rms	23.5 (peak 33.2)	188 (peak 266)

11.4 Thyristor Inverter and Active Compensator

The SCR-CSI converter and VSI compensator system is sketched in figure 11.6. The SCR inverter delivers the power form the dc link to the grid.

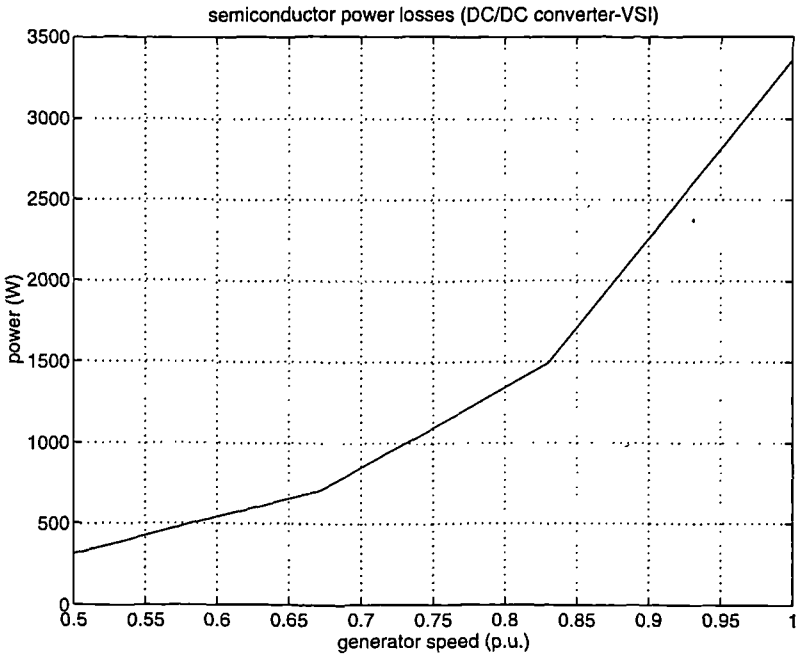

Figure 11.5 DC/DC converter-VSI semiconductor power losses (unity DPF)

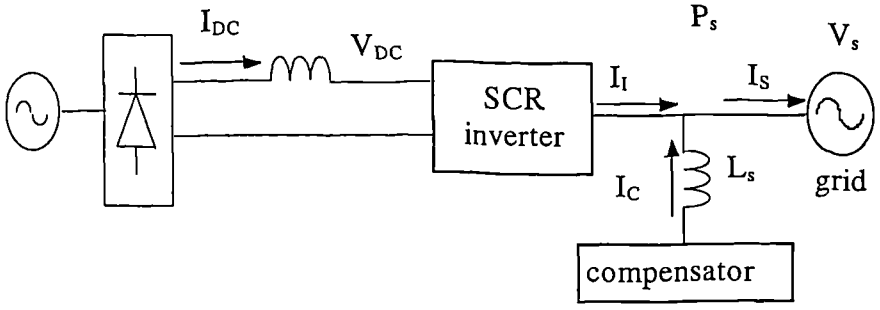

Figure 11.6 Schematic diagram of SCR-CSI VSI compensator

Assuming the SCR inverter is line commutated and configured in 12-pulse form, its operating conditions are calculated and listed in Table 11.4. The active compensator, a six pulse PWM IGBT inverter, switches at 2.4 kHz to keep the grid ac current, I_s, at unity power factor with a sinusoidal waveform. The semiconductors (12-pulse SCR CSI and 6-pulse VSI) cost about £540. The semiconductor power losses of the system are plotted in figure 11.7.

Table 11.4 Line commutated SCR inverter operating condition

wind speed	0.5 p.u. (7.5m/s)	1.0 p.u. (15m/s)
extinction angle γ (degree)	67	14
power factor	0.36	0.95
reactive power (kVAr)	47.0	51.2
SCR peak current (A) (120° conduction)	80	250

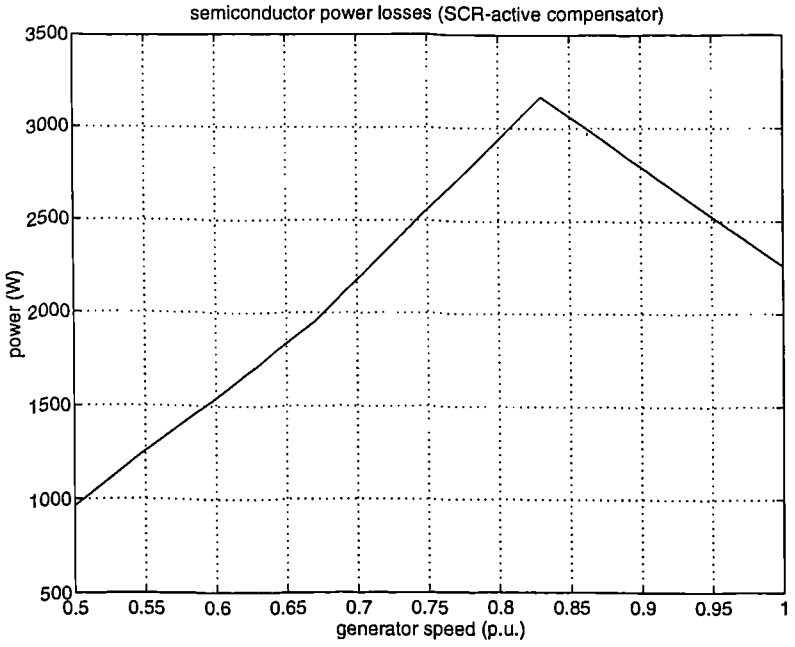

Figure 11.7 Semiconductor power loss of active compensated SCR system (unity DPF)

11.5 DC/AC Conversion Option Comparisions

The main features of the discussed DC/AC power conversion systems are given in Table 11.5.

Table 11.5. Main features comparisons of DC/AC conversion system

Inverter Options	SPWM-VSI	DC/DC-VSI	SCR & Compensator
complexity	low	medium	high
Semiconductor cost	high	low	low
available power level	medium	medium	high
limitation	none (strong/weak ac system.)	none (strong/weak ac system.)	strong ac system for commutation
efficiency	low	medium	high
Semiconductor utilisation	low	medium	high

The studies of this chapter show that although SPWM-VSI has the simplest circuit configuration, its poor device utilisation and high operation loss yield poor economic performance. The DC/DC converter-VSI system provides improved device utilisation, however, it should be noted that additional power losses and cost attributable to the reactors essential to its operation have not been included. The line-commutated SCR inverter and compensator system provides good semiconductor utilisation. The SCR inverter is a mature and reliable technology, therefore, high reliability can be expected. When combined with the capacitor reactive power compensation as discussed, the cost of active compensator VSI could be reduced. It is expected the SCR economical performance could become more significant at higher power rating, therefore, active compensated SCR inverter system is the recommended choice for high power wind energy conversion system in terms of the capital investment and efficiency. Some other technical aspects of note include:

SCR-CSI needs a strong ac system or other facilities to ensure the commutation whereas a self commutated VSI can operate independently. Therefore, SCR-CSI and compensator system is suitable for a strong AC system, while self-commutated VSI may be used for the weak or isolated systems.

The fast switching and gate turn off features of the self-commutated semiconductors and voltage type dc link result in the VSI possessing valuable control features. For example, the voltage source inverter can be switched off very rapidly as a means of circuit protection without any difficulty arising from stored energy. On the other hand, thyristor CSI can not be turned off by gate control and cutting off the dc current would generate large overvoltage.

During a power system fault, the self-commutated VSI (main inverter or active compensator) can lend support with voltage regulation and reactive power control abilities.

Power conversion system extension: The self-commutated VSI can be easily extended to combine with other renewable energy sources, solar etc. and to operate with stored dc energy from batteries.

11.6 Conclusions

This chapter has discussed the cost and efficiency issues of the DC/AC power converter options for grid interface of a variable-speed direct-drive modular PM generator.

Voltage controlled SPWM VSI has poor investment and efficiency performance, and is, therefore, not suitable for the addressed application.

DC/DC converter-VSI system may be used for medium level, weak or isolated systems.

SCR CSI-VSI compensator system is the most suitable for high ratings but requires a strong ac system.

Chapter

12.

Conclusions and Recommendation

12.1 Conclusions

This thesis has described the research work on developing the advanced wind energy conversion system: power electronics interfacing a variable speed direct drive modular permanent magnet generator. Main attention is paid on developing efficient and economical power electronic converters to transfer optimal power and to provide controllable reactive power with minimum harmonic pollution.

Variable speed operation of the modular PM generator

The modular permanent-magnet generator is a promising direct drive generator for variable speed wind energy conversion system. Some attractive features include light weight, simple structural parts using plate or beams, standard magnet blocks, simple stator laminations, common rotor and stator modules for all specifications, ease of assembly of magnetised rotor with stator and simple cooling.

The variable speed operation could simplify the grid connection by eliminating the damping and synchronism equipment. Also a poly-phase modular generator system where each stator coil forms one phase winding could simplify the generator winding connection. The variable speed operation could also benefit the machine design since there exists further design freedom when the frequency is not tied to that of the grid.

An AC/DC/AC power electronic conversion system is the most suitable type of grid interface.

AC/DC power conversion

The cheap and reliable diode rectifier can be used for AC/DC power conversion. Without any control circuit involved, the diode rectifier can operate at high efficiency. The output of the poly phase generator can be conveniently rectified to generate a high quality DC link. The DC link ripple is small due to the large number of phases. The poly-phase rectifier can be connected into various configurations which have no significant influence on the power output though the dc voltage and current may be different.

The internal impedance of the stator coil significantly effects the power output and could limit the power delivery capability of the modular PM generator-rectifier, especially at high frequency. However, with the proposed power enhancement technique, capacitors connected at the rectifier ac terminals can compensate and increase the power capacity. The power enhancement technique can be applied to the various stator coil circuit configurations with equal effect.

Using the ac capacitor connection, the power-frequency characteristics of the generator and rectifier can be controlled to match the wind power characteristics and to enable the maximum power to be captured from the wind.

DC/AC power conversion

With PM generator and diode rectifier system, the power control is set at the grid inverter. Two type of DC/AC converters, Voltage Source Inverter (VSI) and Current Source Inverter (CSI), are discussed. The comparison of self commutated VSI and self commutated CSI indicates the VSI is more attractive if self commutated devices are used.

The operation of the grid connected VSI powered from a dc link with varying voltage is analysed. The results shows that the optimal power transfer and reactive power regulation can be realised by controlling the fundamental ac voltage magnitude and power angle. Such control strategies are presented.

The performance of the VSI in a power network has been studied. It shows that the power system operating condition could be improved by appropriate control of the VSI. The controller could be embedded in a Supervisory Control And Data Acquisition (SCADA) system at a power network control centre.

The power characteristics of line commutated SCR inverter are discussed and means of optimal power transfer control are proposed. The performance of a SCR-CSI interfaced wind farm in a power network has been studied. The line commutated SCR inverter has the advantage of being economical, reliable and suitable for high power application, but the reactive power needs to be compensated.

System Harmonics

Based on the proposed control strategies, the general harmonic performance of inverters (VSI and CSI) are investigated. The six-pulse square wave converters cannot be directly used for the grid interface due to their poor harmonic performance. Harmonic reduction methods are discussed and the resultant harmonic performances of the potential inverter systems are presented.

Inverter Option Studies

The following DC/AC converter systems have been investigated in detail by analysis, simulation and experiment.

- Sinusoidal pulse width modulation voltage source inverter, SPWM-VSI.
- DC/DC converter-VSI with selective harmonic elimination switching or multi-pulse circuit.
- Line commutated SCR-CSI with VSI active compensator.

The operation and control of these system are addressed in detail, the technical feasibility has been established. The economic issues, the semiconductor cost and power losses are also studied.

These inverters can delivers the optimal real power captured from the wind to the grid, generate the desired reactive power and have satisfactory harmonic performance.

The studies have shown that SPWM VSI can be implemented as a basic six pulse inverter to control the ac voltage fundamental component and phase angle, therefore transfer optimal power with a controllable power factor and satisfactory harmonic performance. The simple structure is an attractive aspect of this type of interface, but, the low semiconductor utilisation is a serious drawback. The studies indicate that SPWM VSI is technically feasible but has low efficiency and high cost.

In DC/DC converter-VSI power conversion system, the magnitude of the inverter ac voltage fundamental component can be controlled by a high switching frequency DC/DC converter, which gives a higher VSI switch utilisation factor than SPWM VSI. Freeing the VSI from voltage control duty allows more efficient harmonic minimisation methods, such as selective harmonic elimination and multi-pulse inverter techniques, to be easily implemented.

The SCR inverter is a mature and reliable technology and has the advantage of low cost and high power capacity compared with the self-commutated VSI. However, for satisfactory system interface performance in terms of reactive power control and harmonic pollution a compensation system is required, especially for the variable dc link voltage case. The active compensator based on a PWM VSI can be used to keep a sinusoidal current waveform injected into the grid and to make the system operate at a desired power factor. Therefore high quality power is delivered to the system. The multi-pulse SCR configuration can reduce the required compensator rating for harmonic compensation. The capacity of the active compensator can be reduced by sharing the reactive power compensation burden with a conventional power factor correction capacitor. The proposed compensation techniques can also be used to upgrade existing SCR power conversion systems. The economical advantage of active compensated SCR-CSI system will become significant for high power units.

DC/DC converter-VSI system can be used for medium power output to weak or isolated power systems.

SCR-CSI and VSI compensator system is suitable for the high power rating power converter but requires a strong ac system.

12.2 Recommendation

The wind energy industry is moving rapidly toward the adoption of variable speed systems for reduced noise, increased energy capture, and for better economy. The project has developed such an advanced wind energy conversion system with a direct drive generator. The results of analytical, numerical analysis, simulation and small-scale laboratory studies have demonstrated the performance of several alternative systems. It is recommended that a prototype be constructed for industrial appraisal.

12.3 A Note on Further Work

In this thesis, the voltage controlled VSI type power electronic interfaces have been presented in detail (chapter 5, 8 and 9), and the current controlled VSI (CC-VSI) has been used as the active compensator in chapter 10. However, with the same circuit (DC/DC converter-VSI) in chapter 9, the DC/DC converter could be controlled to keep a constant DC voltage at VSI terminal, then the VSI could be operated under the current control scheme to transfer the optimal power and regulate reactive power compensation with the minimised harmonics. Such a system has been also studied in detail by the author and has been reported in a separate paper [91].

References

1. Akagi, H., Nabae, A., Atoh, S., "Control Strategy of Active Power Filter Using Multiple Voltage-Source PWM Converters", IEEE Transactions on Industry Applications, Vol. IA-22, No. 3, May/June 1986, pp. 460-465.
2. Akagi, H., Tsukamoto, Y., Nabae, A., "Analysis and Design of an Active Power Filter Using Quad-Series Voltage Source PWM", IEEE Transactions on Industry Applications, Vol. 26, No. 1, January/February 1990, pp. 93-98.
3. Ammasaigounden, N., Subbiah, M., "Microprocessor-Based Voltage Controller for Wind-Driven Induction Generators", IEEE Trans. Ind. Electron., Vol. 37, No. 6, December 1990, pp. 531-537
4. Arrilaga, J., Watson, D.B., "Static Power Conversion from Self-Excited Induction Generators", Proc. IEE, Vol. 125, No. 8, August 1978, pp. 743-746
5. Arrillaga, J., Arnold, C.P., "Computer Analysis of Power Systems", John Wiley & Sons,Inc.,1990.
6. Bailey, R. L., "Solar-Electrics research and development", Ann Arbor Science Publishers, Inc., 1980
7. Barton, R.S., Lucas, W.C., "Development of the 7.3 MW MOD-5A Wind-Turbine Generator System", IEE Proc., Vol. 130, Pt. A, No. 9, Dec. 1983, pp. 537-554
8. Benesh, A.H., "The Benesh Wind Turbine", SED-Vol. 12, 11th ASME Wind Energy Symposium, ASME 1992, pp.153-154
9. Binns, K.J., Low, T.S., "Performance and application of multistacked imbricated Permanent-Magnet Generators", IEE Proc-B Electric Power Applications, vol 130, No 6, 1983, pp. 407-414.
10. Bird, B.M., King, K.G., Pedder, D.A., " An Introduction to Power Electronics" ,John Wiley & Sons, Inc.,1993.
11. Boost, M., Ziogas, P.D., "State-of-the Art PWM Techniques: A Critical Evaluation", IEEE Power Electronics Specialists Conference, 1986, pp. 425-433.

12.Bose, B.K., "Introduction to Power Electronics", *Modern Power Electronics-Evolution, Technology, and Applications* Edited by Bose, B.K. the Institute of Electrical and Electronics Engineers, Inc. 1992.

13.British Wind Energy Association, "Wind Energy for the Eighties", Peter Peregrinus Ltd, England. 1982.

14.Brod, D.M., Novotny, D.W., "Current Control of VSI-PWM Inverters", IEEE Trans. on Industry Applications, Vol. IA-21, No. 4, May/June 1985, pp. 562-567.

15.Brune, C.B., Spee R., Wallace, A.K., "Experimental Evaluation of a Variable-Speed, Doubly-Fed Wind-Power Generation System", IEEE Trans. Industry Appl., Vol. 30, No. 3, May/June 1994, pp. 648-655.

16.Cúk S., "Basics of Switched-mode power conversion: topologies, magnetics, and control " Power conversion International 1981.

17.Cadirci, I., Ermis, M., "Double-output induction generator operating at subsynchronous and supersynchronous speeds: steady-state performance optimisation and wind-energy recovery", IEE Proc.-B, Electric Power Appl., Vol. 139, No. 5, September 1992, pp. 429-442

18.Casanellas, F., "Losses in PWM inverters using IGBTs", IEE Proc- Electric Power Applications, vol. 141, No. 5, September 1994.

19.Cavallini, A., Montanari, G. C., "Compensation Strategies for Shunt Active-Filter Control". IEEE Transactions on Power Electronics, Vol. 9, No. 6, November 1994, pp. 587-593.

20.Chen, Z., Spooner, E., "Power Converter Options For Variable Speed Wind Turbines", UPEC'96, Crete, Greece, September, 1996. Vol.1, pp 318-321.

21.Chen, Z., Spooner, E., "A DC To AC Converter With Thyristor Inverter and Active Compensation", IEE International conference PEVD'96, Conference publication No. 429, 1996, 1-6.

22.Chen, Z., Spooner, E., "A Modular, Permanent-Magnet Generator for Variable speed Wind Turbines", IEE International conference EMD'95, conference publication No. 412, 1995, 453-457.

23.Chen, Z., Spooner, E., "A Solid-State Synchronous Voltage Source With Low Harmonic Distortion", IEE International conference DPG'96, conference publication No. 419, 1996, 158-163.

24.Chen, Z., Spooner, E., "Grid Interface For A Variable-Speed, Permanent-Magnet, Wind Turbine Generator", International Conference On Electric Machine ICEM'96, Vigo, Spain, 1996.

25.Chen, Z., Tennakoon, S.B., "A Technique for the Reduction of Harmonic Distortion and Power Losses in Advanced Static VAR Compensators", IEEE Conference APEC'95, Dallas, Texas, USA, March, 1995.

26.Chen, Z., Tennakoon, S.B., "Harmonic Filter Considerations for Voltage Source Inverter Based Advanced Static Var Compensator ", UPEC'92, Bath ,UK September.

27.Cromack, D.E., Oscar, D., "Design Optimization of Small Wind Turbines for Low Wind Regimes", Trans. of the ASME, Vol. 106, August 1984, pp. 347-350.

28.De Doncker, R.W., Demirci, O., Arthur, S., Temple, V. A., "Characteristics of GTO's and High-Voltage MCT's in High-Power Soft-Switching Converters", IEEE Trans. on Industry Applications, Vol. 30, No. 6, November/December 1994.

29.Depart of Trade and Industry, "Wind energy" , Technology status report 001, May 1993.

30.Diamantaras, K., "Wind Energy in the European Market", Wind Energy Conversion, Proc. of the 1994 Sixteenth MWEA Wind Energy Conference, June 1994, pp. 9-12.

31.Divan, D.M., " The Resonant DC Link Converter - A New Concept in Static Power Conversion ", IEEE Trans. Ind. Appl.,vol. 25, No. 2, March/April 1989, pp 317.

32.Divan, D.M., Skibinaki, G., "Zero-Switching-Loss Inverters for High-Power Applications ", IEEE Trans. Ind. Appl.,vol. 25, No. 4, July/August 1989, pp 634.

33.Donlon, J., Motto, E., Majumdar, G., Mori, S., Taylor, W., Xu, R., "A New Converter/Inverter System for Windpower Generation Utilizing a New 600 Amp, 1200 Volt Intelligent IGBT Power Module", Conference Record of the 1994 IEEE IAS Industry Applications Society Annual Meeting, pp. 1031-1042.

34.EI-Sharkawi, N.A., Venkata, S.S., Vadari, S.V., Chen, M.L., Butler, N.G., Yinger, R.W., "Development and Field Testing of an Adaptive Power Factor Controller", IEEE Trans. Energy Conversion, Vol. EC-2, No.2, No. 4, Dec. 1987, pp.520-525.

35.Ermis, M., Ertan, H.B., Akpinar, E., Ulgut, F., "Autonomous Wind Energy Conversion System with A Simple Controller for Maximum-Power Transfer", IEE Proc.-B,. Vol. 139, No. 5, September 1992, pp. 421-428.

36.Ermis, M., Ertan, H.B., Demirekler, M., Saribatir, B.M., Uctug, Y., Sezer, M.E., Cadirci, I., "Various induction generator schemes for wind-electricity generation", Electric Power Research, 23 (1992) pp. 71-83.

37.Ernst, J., "Control of a Variable Speed Wind Energy Converter with a Synchronous Generator and a D.C. Link Converter", Proc. of European Wind Energy Conference, Oct. 1984, pp. 606-611.

38.Fuchs, E.F., Fardoun, A.A., Carlin, P.W., Erickson, R.W., "Permanent-Magnet Machines for Operation with Large Speed Variations", Proc. of Windpower 1992, Seattle, Washington, Oct. 1992.

39. Fuchs, E. F., "Electronically commutated variable-speed, permanent-magnet drive train for wind power plants", IEEE Power Engineering Review, December 1992, pp 7-8.

40.Fuchs, E.F., Carlin, P.W., "An Electronically Commutated Permanent-Magnet Generator with Flux Weakening Voltage Control", SED-Vol. 12, 11th ASME Wind Energy Symposium, ASME 1992, pp.151

41.Ghandakly, A.A., Sbeiti, Z.H., "A Digital Optimal Controller for VSCF Wind Generators", IEEE 1991.

42.Goodfellow, D., Smith, G.A., "Control Strategies for Variable-Speed Wind Energy Recovery", pp. 219-228.

43.Gourieres, D. LE, " Wind Power Plants", Pergamon press Ltd., England. 1982.

44.Patel, H., Hoft, R.G., "Generalized Techniques of Harmonic Elimination and Voltage Control in Thyristor Inverters: Part I--Harmonic Elimination," IEEE Transactions on Industry Applications, Vol. IA-9, No. 3, May/June 1973.

45.Patel, H., Hoft, R.G., "Generalized Techniques of Harmonic Elimination and Voltage Control in Thyristor Inverters: Part II--Voltage Control Techniques ," IEEE Transactions on Industry Applications, Vol. IA-10, No. 5, September/October 1974.

46.Hayashi, Y., Sato, N., Takahashi, K., "A Novel Control of a Current-Source Active Filter for ac Power System Harmonic Compensation", IEEE Transactions on Industry Applications, Vol. 27, No. 2, March/April 1990, pp. 380-387.

47.Hendler, J., Flowers, W., Bell, A., "Windmill Tip-Speed Ratio Regulation Using an Impedance-Matching Control System", Trans. of the ASME, Vol. 107, Nov. 1985, pp. 326-334.

48.Hilloowala, R.M., Sharaf, A.M., " A Utility Interactive Wind Energy Conversion Scheme with an Asynchronous DC Link Using a Supplementary Control Loop", IEEE Trans. Energy Conversion, Vol. 9, No. 3, Sept. 1994.

49. Hindmarsh, J "Electrical machines and their applications" 4th Edition Pergamon Press 1977.

50.Holz, J., "Pulse width Modulation--A Survey", IEEE Transactions on Industrial Electronics, Vol. 39, No. 5, Dec. 1992, pp. 410-420.

51. IEE Conference Publication Number 202, "Small and Special Electrical Machines" 1981.

52.Pitel, J., Talukdar, S. N., Wood, P., "Characterisation of Programmed-Waveform Pulse width Modulation," ," IEEE Transactions on Industry Applications, Vol. IA-16, No. 5, September/October 1980.

53.Johnson, G.L., " Wind Energy Systems", Prentice-hall, INC., Englewood Cliffs, N.J. USA.

54.Jones, R., Smith, G. A., "High Quality Mains Power From Variable-Speed Wind Turbines", Renewable Energy, 17-19 Nov. 1993, Conference Publication No. 385, IEE, 1993, pp. 202-206.

55.Kassakian, J. G., Schlecht, M. F., Verghese, G. C., "Principles of Power Electronics", Addison-Wesley Publishing company, Inc. 1991.

56.Key, T.S., "Evaluation of Grid-Connected Inverter Power Systems: The Utility Interface", IEEE Trans. Industry Appl., Vol.IA-20, No. 4, July/Aug. 1984, pp. 735-741.

57.Kheraluwala, M.H., Divan, D.M., "Delta Modulation Strategies for Resonant Link Inverters", IEEE Trans. Power Electronics, vol. 5, No. 2, April 1990 pp 220.

58.Kimbark, E.W., "Direct Current Transmission", Volume I, John Wiley & Sons Inc. 1971.

59.Lindley, D., "Wind Energy - Current Status in the UK", Wind Energy Conversion, Proc. of the 1994 Sixteenth MWEA Wind Energy Conference, June 1994, pp. 1-8.

60.Lowe, J.E., Wiesner, W., "Status of Boeing Wind-Turbine Systems", IEE Proc., Vol. 130, Pt. A, No. 9, Dec. 1983, pp. 531-536.

61.Mets, V., Hermansson, O., "Status and Experience with the 2 MW WTS 75 at Nasudden, Gotland", IEE Proc., Vol. 130, Pt. A, No. 9, Dec. 1983, pp. 542-549.

62.Milborrow, D.J., "Wind and Cluster Research: Past, Present and Future", IEE Proc., Vol. 130, Pt. A, No. 9, Dec. 1983, pp. 566-573.

63. Miller, T.J.E., "Brushless Permanent-Magnet and Reluctance Motor Drives", Clarendon Press Oxford, 1989.

64. Mohan, N., Undeland, T. M., Robbins, W. P., "Power Electronics: Converters, Applications and Design", Second edition, John Wiley & Sons, Inc., 1995.

65.Musgrove, P.J., "Wind Energy Conversion - an Introduction", IEE Proc., Vol. 130, Pt. A, No. 9, Dec. 1983, pp. 506-516.

66. Nagataka Seki, Hiroshi Uchino, "Which is better at high power reactive power compensation system, high PWM frequency or multiple connection?", Conf. Record 1994, IEEE Industry Application Society, pp 946-953.

67.Natarajan, K., Sharaf, A.M., Sivakumar, S., Naganathan, S., "Modelling and Control Design for Wind Energy Power Conversion Scheme Using Self-Excited Induction Generator", IEEE Trans. Energy Conversion, Vol. EC-2, No. 3, Sept. 1987.

68.Nayar, C.V., Perahia, J., Thomas, F., Phillips, S.J., Pryor, T., James, W.L., "Investigation of capacitor-Excited Induction Generators and Permanent Magnet Alternators for Small Scale Wind Power Generation", Renewable Energy Vol. 1, No. 3/4, 1991, pp. 381-388.

69.Norgaard, P., "Limitation in Variable Speed Operation of Stall Regulated Wind Turbines", Wind Energy Conversion, Proc. of the 1994 Sixteenth MWEA Wind Energy Conference, June 1994, pp.55-59.

70.Paradopoulos, M., Parathanasslou, S., Tegopoulos, J., "Comparison of Variable Speed Wind Turbine Generators Schemes" Proc. of ICEM 1994, pp. 73-78.

71.Ramakumar, R., "Wind Energy Systems-1992 Summer Meeting Panel Session on Developments in Wind-Electric Conversion System Technology", IEEE Power Engineering Review, December 1992, pp. 6-9.

72.Rashid, M.H., "Power Electronics: Circuits, Devices, and Applications", Prentice-Hall, Inc., 1988.

73.Round, S. D., Duke, R. M., "Real-Time Optimization of an Active Filter's Performance", IEEE Transactions on Industry Applications, Vol. 41, No. 3, June 1994, pp. 278-284.

74.Salameh, Z., Wang, S., "Microprocessor Control of Double Output Induction Generator-Part I: Inverter Firing Circuit", IEEE Trans. Energy Conversion, Vol, 4, No. 2, June 1989, pp. 172-176.

75.Salameh, Z.M., Kazda, L.F., "Analysis of the System State Performance of the Double Output Induction Generator", IEEE Trans. Energy Conversion, Vol. EC-1, No. 1, March 1986, pp. 26-32.

76.Salazar, L., Joos, G., "PSPICE Simulation of Three-Phase Inverters by Means of Switching Functions", IEEE Transactions on Power Electronics, Vol. 9, No. 1, Jan. 1994, pp. 35-42.

77. Seguier, G., "Power Electronic Converters", translated by Griffin, E. North Oxford academic Publishers Ltd 1986.

78. Sen, P.C., "Principles of Electric machine and power electronics", John Wiley & sons Inc. 1989.

79.Soderholm, L.H., "Interfacing Small Wind Systems to Rural Power Distribution Systems", IEEE Trans. Industry Appl., Vol.IA-20, No. 2, March/April 1984, pp. 439-442.

80. Spooner E., Chalmers, B.J., "'TORUS': A slotless, toroidal-stator, Permanent-Magnet Generator", IEE Proc-B Electric Power Applications, vol 139, No 6, November 1992, pp 497-498.

81. Spooner E., Williamson, A.C., Thomson L., "Direct-Drive, Grid-connected, Modular Permanent-Magnet Generators", British Wind Energy Assoc. Conference, Stirling, June, 1994.

82.Spooner, E., Williamson, A.C., "Direct-coupled, permanent-magnet generators for wind turbine applications", IEE Proc.-B, Electric Power Applications, vol. 143, No. 1, January, 1996, pp 1-8.

83.Spooner, E., Williamson, A. C., "Modular design of permanent-magnet generators for wind turbines", Accepted for IEE Proc-B Electric Power Applications.

84.Steinbuch, M., "Optimal Multivariable Control of a Wind Turbine with Variable Speed", Wind Engineering Vol. 11, No. 3, 1987, pp. 153-163.

85.Tang, Y., Xu, L., "A Flexible Active and Reactive Power Control Strategy for a Variable Speed Constant Frequency Generating System", IEEE Trans. Power Electron., Vol. 10, No. 4, July 1995, pp. 472-478.

86.Templin, R.J., Rangi, R.S., "Vertical-Axis Wind Turbine Development in Canada", IEE Proc., Vol. 130, Pt. A, No. 9, Dec. 1983, pp. 555-561.

87.Thomas, R.J., Phadke, A.G., Pottle, C., "Operational Characteristics of a Large Wind-Farm Utility-System with a Controllable AC/DC/AC/Interface", IEEE Trans. Power Systems, Vol, 3, No. 1, Feb. 1988, pp. 220-225.

88.Tomas, R. J., Wang, X., "The Control of Large Wind-Farm-Induced Voltage Fluctuations" IEEE Trans. on Energy Conversion, Vol. EC-2, No. 1, March 1987, pp 1-8.

89.Tsisovits, A.J., "Dynamics of an Isolated Power System Supplied from Diesel and Wind", IEE Proc., Vol. 130, Pt. A, No. 9, Dec. 1983, pp. 587-595.

90.Warne, D.F., Calnan, P.G., " Generation of electricity from the wind", Proc. IEE, vol. 124, No.11R, November 1977, IEE Reviews.

91.Chen, Z., Spooner, E., "Grid Interface For Renewable Energy Sources", to be presented, 2nd International Power electronics and motion control conference (IPEMC'97), November, 1997, Hangzhou, CHINA.

Appendix

A

Equivalent Circuit of A Simple AC Circuit with Capacitor Connection

The equivalent EMF, E_{eq}, and internal impedance, Z_{eq}, of figure A.1 could be found by using the *Thevenin's Theorem.*

The equivalent EMF is equal to the open circuit voltage:

$$V_c = \frac{\frac{1}{j\omega C_{ac}}}{R_g + j\omega L_g + \frac{1}{j\omega C_{ac}}} E_g = \frac{E_g}{1-\omega^2 L_g C_{ac} + j\omega C_{ac} R_g} \tag{A.1}$$

the equivalent impedance:

$$Z_{eq} = \frac{(R_g + j\omega L_g)\frac{1}{j\omega C_{ac}}}{R_g + j\omega L_g + \frac{1}{j\omega C_{ac}}} = \frac{(R_g + j\omega L_g)}{1-\omega^2 L_g C_{ac} + j\omega C_{ac} R_g} \tag{A.2}$$

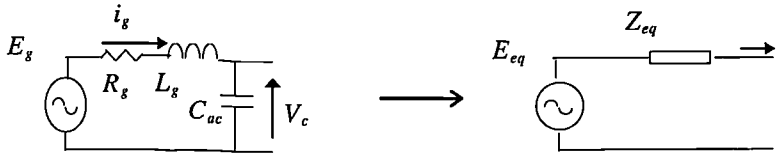

Figure. A.1 *Thevenin* equivalent circuit

let $$K_c = \frac{1}{1-\omega^2 L_g C_{ac} + jR_g \omega C_{ac}} \tag{A.3}$$

Therefore, E_{eq} and Z_{eq} are

$$E_{eq} = K_c E_g \tag{A.4}$$

$$Z_{eq} = K_c Z_g \tag{A.5}$$

where $Z_g = R_g + j\omega L_g$

Appendix

B

Maximum load power with respect to connected capacitor

In the capacitor connected circuit shown in figure 4.2, the load power is

$$P_{load(c)} = \frac{\left|E_g\right|^2 R_{load}}{\left|\frac{R_{load}}{K_c} + Z_g\right|^2} = \frac{\left|E_g\right|^2 R_{load}}{\left|R_{load}((1-\omega^2 L_g C_{ac}) + jR_g \omega C_{ac}) + R_g + j\omega L_g\right|^2}$$

$$= \frac{\left|E_g\right|^2 R_{load}}{\left|R_{load}(1-\omega^2 L_g C_{ac}) + R_g + j\omega(R_{load} R_g C_{ac} + L_g)\right|^2}$$

$$= \frac{\left|E_g\right|^2 R_{load}}{\left(R_{load}(1-\omega^2 L_g C_{ac}) + R_g\right)^2 + \omega^2 (R_{load} R_g C_{ac} + L_g)^2} \qquad \text{(B.1)}$$

where $E_g = \omega E_{gb}$

E_{gb} is constant.

To find C_{ac} which makes $P_{load(c)}$ reach its maximum for a fixed load and frequency, let

$$\frac{\partial P_{load(c)}}{\partial C_{ac}} = 0 \qquad \text{(B.2)}$$

we have

$$\frac{\partial P_{load(c)}}{\partial C_{ac}} = \frac{\partial}{\partial C_{ac}} \left(\frac{\left|E_{gb}\right|^2 \omega^2 R_{load}}{\left(R_{load}(1-\omega^2 L_g C_{ac}) + R_g\right)^2 + \omega^2 (R_{load} R_g C_{ac} + L_g)^2} \right)$$

let

$$f_2 = \left(R_{load}(1-\omega^2 L_g C_{ac}) + R_g\right)^2 + \left(\omega(R_{load} R_g C_{ac} + L_g)\right)^2$$

$$f_3 = \left|E_{gb}\right|^2 \omega^2 R_{load}$$

$$\frac{\partial P_{load(c)}}{\partial C_{ac}} = \frac{f_3' f_2 - f_3 f_2'}{f_2^2}$$

since $f_3' = 0$, the condition of $\frac{\partial P_{load(c)}}{\partial C_{ac}} = 0$ changes into $f_2' = 0$ so

$$\frac{\partial f_2}{\partial C_{ac}} = 2\Big(R_{load}(1-\omega^2 L_g C_{ac}) + R_g\Big)(-\omega^2 L_g R_{load}) + 2\Big(\omega(R_{load} R_g C_{ac} + L_g)\Big)(R_g \omega R_{load})$$

$$0 = \Big(R_{load}(1-\omega^2 L_g C_{ac}) + R_g\Big)(-L_g) + (R_{load} R_g C_{ac} + L_g) R_g$$

therefore

$$(-L_g + \omega^2 L_g^2 C_{ac} + R_g^2 C_{ac}) = 0$$

$$C_{ac} = \frac{L_g}{\omega^2 L_g{}^2 + R_g{}^2} \qquad \text{(B.3)}$$

To substitute equation (B.3) into equation (B.1), we have the maximum power with respect to the capacitance, $P_{load(c).max.c}$:

$$P_{load(c).\max.c} = \frac{\left|E_{gb}\right|^2 \omega^2 R_{load}}{\left(R_{load}(1-\omega^2 \frac{L_g^2}{\omega^2 L_g{}^2 + R_g{}^2}) + R_g\right)^2 + \omega^2 (R_{load} R_g \frac{L_g}{\omega^2 L_g{}^2 + R_g{}^2} + L_g)^2}$$

$$= \frac{\left|E_{gb}\right|^2 \omega^2 R_{load}(\omega^2 L_g^2 + R_g^2)}{\left(R_{load} R_g + \omega^2 L_g^2 + R_g^2\right)^2} \qquad \text{(B.4)}$$

Appendix

C

Maximum load power with respect to EMF frequency

To find ω which makes $P_{load(c)}$ reach its maximum for the circuit shown in figure 4.2 under a fixed load and capacitance, let

$$\frac{\partial P_{load(c)}}{\partial \omega} = 0 \tag{C.1}$$

using (B.1), we have

$$\frac{\partial P_{load(c)}}{\partial \omega} = \frac{\partial}{\partial \omega}\left(\frac{\left|E_{gb}\right|^2 \omega^2 R_{load}}{\left(R_{load}(1-\omega^2 L_g C_{ac})+R_g\right)^2 + \omega^2 (R_{load} R_g C_{ac} + L_g)^2} \right)$$

$$= \frac{2\omega R_{load}\left|E_{gb}\right|^2}{\left(R_{load}(1-\omega^2 L_g C_{ac})+R_g\right)^2 + \omega^2 (R_{load} R_g C_{ac} + L_g)^2} -$$

$$\frac{\left|E_{gb}\right|^2 \omega^2 R_{load}\left[-4\left[\left(R_{load}(1-\omega^2 L_g C_{ac})+R_g\right)\right] R_{load}\omega C_{ac} L_g + 2\omega (R_{load} R_g C_{ac} + L_g)^2\right]}{\left(\left(R_{load}(1-\omega^2 L_g C_{ac})+R_g\right)^2 + \omega^2 (R_{load} R_g C_{ac} + L_g)^2\right)^2}$$

$$= \left(\frac{-2\left|E_{gb}\right|^2 \omega R_{load}(R_{load}^2 + 2R_{load}R_g - R_{load}^2\omega^4 L_g^2 C_{ac}^2 + R_g^2)}{\left(R_{load}^2 - 2R_{load}^2\omega^2 L_g C_{ac} + 2R_{load}R_g + R_{load}^2\omega^4 L_g^2 C_{ac}^2 + R_g^2 + \omega^2 L_g^2 + R_{load}^2\omega^2 R_g^2 C_{ac}^2\right)^2} \right)$$

Let the nominator of the above equation equal to zero, we have

$(R_{load}^2 + 2R_{load}R_g - R_{load}^2\omega^4 L_g^2 C_{ac}^2 + R_g^2) = 0$

there are four roots for the ω:

$$\omega 1 = \frac{1}{\left[\sqrt{R_{load}}(\sqrt{C_{ac}}\sqrt{L_g})\right]}\sqrt{-R_{load} - R_g}$$

$$\omega 2 = \frac{-1}{\left[\sqrt{R_{load}}(\sqrt{C_{ac}}\sqrt{L_g})\right]}\sqrt{-R_{load} - R_g} \qquad (C.2)$$

$$\omega 3 = \frac{-1}{\left[\sqrt{R_{load}}(\sqrt{C_{ac}}\sqrt{L_g})\right]}\sqrt{R_{load} + R_g}$$

$$\omega 4 = \frac{1}{\left[\sqrt{R_{load}}(\sqrt{C_{ac}}\sqrt{L_g})\right]}\sqrt{R_{load} + R_g}$$

only ω_4 is meaningful in the studied case. Therefore

$$\omega = \frac{1}{\left[\sqrt{R_{load}}(\sqrt{C_{ac}}\sqrt{L_g})\right]}\sqrt{R_{load} + R_g} \qquad (C.3)$$

The relation maximum power frequency and the capacitance calculation frequency

If capacitance is calculated using frequency of ω_f, $C_{ac} = \frac{L_g}{\omega_f^2 L_g^{\,2} + R_g^{\,2}}$

then $\omega = \frac{1}{\left[\sqrt{R_{load}}(\sqrt{C_{ac}}\sqrt{L_g})\right]}\sqrt{R_{load} + R_g}$

$$= \frac{\sqrt{R_{load} + R_g}}{\sqrt{R_{load}}}\sqrt{\omega_f^2 + R_g^{\,2} / L_g^{\,2}} \qquad (C.4)$$

Clearly $\omega \geq \omega_f$, therefore that the maximum power with varying frequency will occurs at a frequency higher then capacitance calculation frequency, ω_f.

The maximum power with respect to the varying frequency

To substitute equation (C.3) into equation (B.1), we have the maximum power with respect to the frequency, $P_{load(c).max.f}$:

$P_{load(c).\max.f}$ =

$$\frac{\left|E_{gb}\right|^2 (R_{load}+R_{g)}R_{load}}{\left(R_{load}L_gC_{ac}\right)\left[\left[R_{load}\left(1-\frac{1}{R_{load}}(R_{load}+R_g)\right)+R_g\right]^2+\frac{(R_{load}R_gC_{ac}+L_g)^2}{\left(R_{load}L_gC_{ac}\right)}(R_{load}+R_g)\right]}$$

$$=\frac{R_{load}\left|E_{gb}\right|^2}{(R_{load}R_gC_{ac}+L_g)^2} \qquad \text{(C.5)}$$

If the equation (C.4) is substituted into equation (B.5),

$$P_{load(c).\max.f}=\frac{R_{load}\left|E_{gb}\right|^2\left[\omega_f^2L_g^2+R_g^2\right]^2}{L_g^2\left[\omega_f^2L_g^2+R_g^2+R_{load}R_g\right]^2} \qquad \text{(C.6)}$$